



UNIVERSITÀ
DEGLI STUDI
FIRENZE

IMPROVEMENT OF PIEZOCONE TEST INTERPRETATION FOR PARTIAL DRAINAGE CONDITIONS AND FOR TRANSITIONAL SOILS

Dissertation

submitted to and approved by the

Department of Architecture, Civil Engineering and Environmental Sciences
University of Braunschweig – Institute of Technology

and the

Department of Civil and Environmental Engineering
University of Florence

in candidacy for the degree of a

Doktor-Ingenieurin (Dr.-Ing.) /

Dottore di Ricerca in Civil and Environmental Engineering^{*)}

by

Ilaria Giusti

born 7 August, 1979

from Pisa, Italy

Submitted on 25 August, 2017

Oral examination on 9 November, 2017

Professorial advisors

Prof. Diego C.F. Lo Presti, University of Pisa

Prof. Joachim Stahlmann, Technische Universität Braunschweig

Prof. Andrew J. Whittle, Massachusetts Institute of Technology

2018

^{*)} Either the German or the Italian form of the title may be used.

1. Summary

Baligh first proposed the piezocone in 1981 as a means of improving the identification of soil stratigraphy. Today piezocone soundings are widely employed in geotechnical engineering practice using a standardized geometry jacked into the ground at a standard rate of 2 cm/s (ISSMGE IRTP, 1999; ASTM, 2007). These tests are ideal for the identification of the major lithologic variations and the reconstruction of the stratigraphic profile, thanks to measurement reliability, possibility to investigate a soil volume greater than that of a laboratory sample and possibility of getting continuous records. Though current piezocone test procedures are able to identify sand and clay layers, interpretation is much more complex in soils of intermediate permeability due to partial consolidation that can occur ahead of the advancing tip. Furthermore, standard approaches of piezocone interpretation only consider either fully saturated or completely dry conditions, whereas in reality a vadose zone of unsaturated soils most often exists above the ground water table. The difficulty in applying classification charts in partially saturated soils, especially fine-grained soils, is due to the soil suction which modifies the effective stress state leading to an overestimate of soil grain size (Lo Presti et al., 2009). For this reason, the interpretation of piezocone tests in partially saturated soils is still an open issue. In order to investigate the influence of partial drainage during penetration the instrument of repeating the tests changing the penetration rate is widely used. However, to date most of the experimental studies conducted with this purpose have been carried out on kaolin clay inside a centrifuge (Finnie and Randolph, 1994, House et al., 2001, Randolph and Hope, 2004; Schneider et al., 2007, Lehane et al., 2009; Mahmoodzadeh and Randolph, 2014). Few studies have been carried out on natural clay (Chung et al., 2006) or mixed soils (Kim et al., 2008; Schneider et al., 2007).

The present study shows the results of experimental analyses of field cone penetration tests as well as calibration chamber mini-piezocone tests on soils of intermediate permeability (silts, clayey and sandy silts). The penetration rate varied across over three orders of magnitude to provide information on partially drained and undrained tip resistance, excess pore water pressure and friction sleeve. Whilst previous experimental researches essentially focused on tip resistance and pore water pressure measurements, it is worthwhile underlying that the present study is one of the first experimental studies that explored the effect of penetration rate on sleeve friction measurements. As the penetration rate is reduced, moving from the undrained conditions to the fully drained conditions, friction sleeve systematically decreases, together with the expected results in terms of increasing tip resistance and decreasing excess porewater pressure. The obtained experimental database of penetration measurements on intermediate soils can be added to the previous worldwide collected data to develop a new general interpretation procedure for cone tests in transitional soils.

Besides, numerical analyses have been carried out by using the Finite Element Method. To the author's knowledge there are only two relevant researches on partially drained penetration simulated with FEM analyses (Yi et al., 2012; Mahmoodzadeh et al., 2014). For the present study, the Updated Lagrangian technique has been adopted to simulate the large strain penetration process. Both the Modified Cam Clay constitutive model and the Mohr Coulomb model have been used to compare numerical simulation results with, respectively, the experimental results on kaolin clay (Randolph and Hope, 2004; Schneider et al., 2007) and those obtained with the present study.

The problem of piezocone miss-interpretation in case of transitional soils, such as loose silt mixture has been dealt with an empirical methodology, based on the calibration of the Soil Behaviour Type index using soil characteristics inferred from reference boreholes.

Moreover, a new approach has been proposed to overcome miss-interpretation of piezocone test results for soil layers belonging to vadose zones in which the effective stress state is controlled by suction. This procedure allows for the correction of the Soil Behaviour Type (SBT) index, in order to allocate correctly the investigated soils inside SBT classification charts (Robertson, 1990). In addition to that, the applied method has suggested a procedure, based on piezocone measurements, to estimate the effective stress state in the case of a homogeneous soil layer in which a vadose zone above the water table is present.

2. Contents

1. Summary	2
2. Contents	4
3. Introduction	6
4. Thesis outline	10
5. Cone Penetration Test in partially drained conditions	11
6. In-situ experimental activities	25
6.1 Identification and characterisation of dredged sediments	25
6.1.1 Experimental activities at Livorno Port Area (Italy).....	26
6.1.1.1 Laboratory tests	28
6.1.1.2 Piezocone tests with different penetration rates	31
6.1.1.3 Analyses of piezocone test results.....	44
6.2 Identification and characterisation of alluvial soil deposits in Pisa delta area	51
6.2.1 Effects of sleeve diameter on f_s measurements.....	62
6.3 Identification and characterisation of alluvial soil deposits	67
6.4 Conclusions	70
7. Calibration chamber tests	71
7.1 Equipment description	71
7.2 Selected material	77
7.2.1 Preliminary estimation of non-dimensional velocity range	79
7.2.2 Consolidation and mechanical characteristics of the selected soil.....	95
7.3 Specimen preparation procedure.....	101
7.4 Cone Penetration tests	103
7.5 Cone Penetration test results	104
7.6 Analysis of Cone Penetration test results	107
7.6.1 S1 series	107
7.6.2 S2 series	109
7.6.3 Dissipation tests	112
7.6.4 Normalised tip resistance and excess pore water pressure versus normalised penetration rate.....	118
7.6.5 Proposed f_s/σ'_v versus V expression.....	124
7.7 Conclusions	125

8.	Numerical modelling of piezocone penetration	127
8.1.1	Adaptivity technique	127
8.1.2	Model characteristics	128
8.1.3	Modified Cam Clay model results	129
8.1.4	Numerical simulation of Calibration Chamber tests	140
8.1.5	Conclusions	154
9.	Use of CPT for soil profiling in transitional soils	155
9.1	Re-interpretation of CPTU at Broni	156
9.1.1	Cone Penetration tests	159
9.1.2	THE MK MODEL	164
9.1.3	CPTu interpretation	165
9.2	Specific- empirical calibration of <i>I_c</i> values from borehole evidences	169
9.2.1	Empirical <i>I_c</i> correction	172
9.3	Conclusions	175
10.	Estimation of preconsolidation stress based on piezocone test results.....	176
10.1.1	Verification of applicability of several empirical correlations available in literature to the over-consolidation ratio estimation.....	176
10.1.2	Estimation of the effective in situ stress and preconsolidation stress for soil layers above the water table	181
11.	Conclusions	184
12.	Appendix	188
13.	List of figures	193
14.	List of tables	201
15.	References	202

3. Introduction

The Brundtland report (1987) and the Rio Conference (1992) have defined the concept of sustainable development: sustainable development is not a fixed state of harmony, but rather a process of change in which the exploitation of resources, the direction of investments, the orientation of technological development, and institutional change are made consistent with future as well as present needs. This concept goes through all scientific, social and economic disciplines and stresses the necessity to look for efficiency, equity and ecological integrity in the use of resources. The technical-scientific knowledge plays a leading role in supporting public institutions for a sustainable territorial planning and development. In particular, engineering knowledge is called to deal with some fundamental questions like environment's protection against natural disasters and impact of human activity, and waste management. The study of these issues can be tackled with the support of geotechnical engineering.

Geotechnical Engineering is a branch of Civil Engineering. The theoretical background of Geotechnical Engineering is usually based on the following:

- Continuum mechanics
- Hydraulics of porous media

As far as the continuum mechanics is concerned, it is worthwhile to underline the difficulties in defining a general constitutive law for geomaterials because of the anisotropic-elasto-plastic-viscous behaviour of those types of materials. More importantly, since geomaterials are essentially generated by spontaneous processes, the experimental determination of their mechanical and hydraulic characteristics is crucial and represents a huge research topic.

Geotechnical engineering avails of laboratory and in situ testing to study geomaterials mechanical behaviour. Among these, the penetration tests, CPT and CPTu test, are economical methodologies to get continuous measurements of some soil parameters. The Cone Penetration Test consists of pushing an instrumented cone tip into the ground at a constant rate. During the test, the pressure required for tip penetration (q_c) and the adhesion force between the sleeve, placed above the tip, and the soil (f_s) are measured. In case of piezocone test (CPTu), the pore water pressure is also measured during penetration (Figure 1). Baligh first proposed the piezocone in 1981 as a means of improving the identification of soil stratigraphy. Today piezocone soundings are widely employed in geotechnical engineering practice using a standardized geometry jacked into the ground at a standard rate of 2 cm/s (ISSMGE IRTP, 1999; ASTM, 2007).

These tests are ideal for the identification of the major lithologic variations and the reconstruction of the stratigraphic profile, distinguishing between low permeability clays, which are sheared in an 'undrained' mode (i.e., with no migration of pore water within the soil and excess pore pressures develop around the advancing penetrometer), and high permeability

sands, where drained shearing occurs (i.e., shearing with no excess pore pressures). This capability is due to measurement reliability, possibility to investigate a soil volume greater than the one of a laboratory sample and possibility of getting continuous records. Furthermore, common applications include the soil engineering parameters evaluation such as stress state, stress history, strength characteristics and stiffness.

As highlighted by Mayne (2010), the research efforts on CPT can be summarized into three main areas:

1. Tests procedures
2. Interpretation methodologies
3. Improved equipment

The present study deals with the above areas, in particular:

1. Whilst current piezocone tests procedures are able to identify sand and clay layers, the interpretation is much more difficult in the case of soils of intermediate permeability. In fact, cone tests are generally conducted at a standard rate of 20 mm/s and the common cone diameter is 35.7 mm (area of 1000 mm²). At this rate and for this diameter, tests in clay soils can be considered fully undrained and tests in sands can be considered fully drained, whereas in the case of intermediate soils the test may be partially drained depending on the coefficient of consolidation c_v (Finnie and Randolph, 1994; Randolph and Hope, 2004). For this reason, it is much more difficult for intermediate soils to identify soil type with conventional classification charts (Lo Presti et al., 2010; Schneider et al. (2008); DeJong and Randolph (2012); Schneider et al. (2012)). Many researchers studied the effects of changing the penetration rate during the test as a way to find the demarcation of drainage boundaries corresponding to undrained, partially drained and drained regions. In order to investigate potential improvements in the use and interpretation of piezocone tests for soils of intermediate permeability, experimental activities and numerical analyses have been carried out. As far as experimental activities are concerned, the results from in situ tests and calibration chamber tests are presented. In both cases a laboratory characterisation of the soils, which are object of the study, has been done. Numerical analyses have focused on the mechanics of partially drained penetration simulating the large strain penetration processes by using finite element methods.

2. In practice, the stratigraphic profile is usually obtained using empirical correlation and classification charts such as Begemann (1965), Schmertmann (1978) and Searle (1979) for CPT and Robertson et al. (1986), Senneset et al. (1989), Robertson (1990), Eslami and Fellenius (1997, 2000) for CPTu. The main limit of empirical correlations is related to the difficulty in being applied in different contexts: the correlations were determined on particular geological and geotechnical conditions, which might be different from the soils characteristics to be

investigated. With this respect, stratigraphic soil profiles inferred from CPT can be validated against those obtained from reference boreholes.

Besides, the standard approaches only consider either fully saturated or completely dry conditions, whereas in reality a vadose zone of unsaturated soils most often exists above the ground water table. The difficulty to apply classification charts in partially saturated soils, especially fine soils, is due to the soil suction which modifies the effective stress state, leading to an overestimate of soil grain size (Lo Presti et al. 2009). On this topic some research activities have been carried out by Brazilian Universities and Oklahoma Department of Transportation. Another important aspect concerns the applicability of penetration tests in “unusual soils” like “underconsolidated” dredged sediments.

The standard means of interpretation of CPT data use deterministic expressions that have been derived from empirical, statistical or analytical models. These models have been calibrated in most cases with site specific databases. The verification of the applicability of several empirical correlations available in literature to the over-consolidation ratio estimation are also studied.

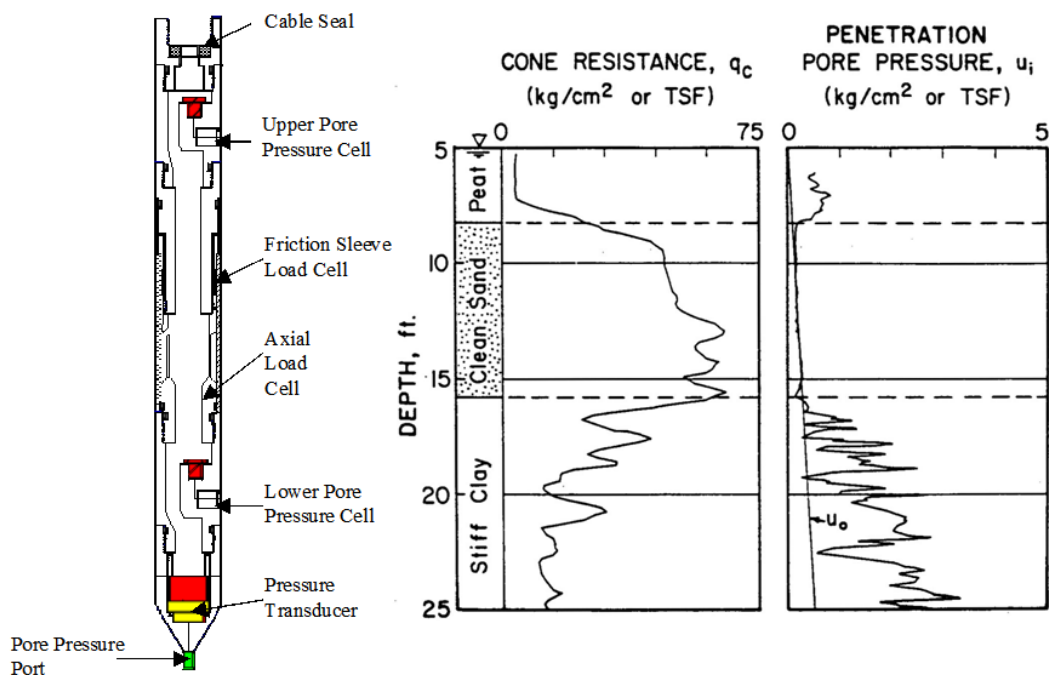


Figure 1: Interpretation of stratigraphy from tip resistance and penetration pore pressures. Piezocone with tip pore pressure transducer (left, Zeeb et al., 1997); Penetration data in layered soil (right).

3. As far as the equipment is concerned, several aspects have been studied. In particular, in order to investigate a large range of drainage conditions during penetration, a mini-piezocone, developed by Pagani Geotechnical Equipment, has been adopted. Both in-situ and calibration chamber tests have been conducted. The diameter of the cone is 16 mm (2 cm² the cone area), whereas the sleeve area is 10 cm². In the case of in-situ tests, mini-piezocone measurements have been compared with standard piezocone measurements (d= 35.7 mm – 10 cm²). Pore-water

pressure is measured through a slot filter placed at cone shoulder. The slot filter saturation fluid is a silicone grease. The use of grease as a saturation fluid was first proposed by Elmgren (1995) and Larsson (1995), subsequently, its reliability have been testified from various studies. With this respect, results of an accurate calibration procedure of pore water pressure measurements are presented.

Furthermore, the influence of sleeve diameter on friction measurements of a standard piezocone has been evaluated. Several tests have been carried out, using three different sizes of the sleeve without changing the conical tip. The ASTM standard (D 5778-12) specifies the tolerances for the cone tip and sleeve dimensions, in particular, the cone tip diameter is required to be between 35.3 and 36.0 mm, measure of 35.7 mm; while the sleeve diameter has to be equal to the cone diameter or greater, with a tolerance within the range 0.0 mm - 0.35 mm. A Pagani Geotechnical Equipment piezocone has been used, with a cone tip diameter of 35.7 mm for all the tests, and three different sleeve diameters: 35.8 mm, 35.9 mm and 36.0 mm. Three tests have been conducted for each sleeve. Results are compared with the study conducted by Holtrigter et al. (2014).

4. Thesis outline

The thesis is organized as follows. After an initial introduction of the previous chapter, Chapter 5 describes the main issues and previous researches related to cone penetration tests in partially drained conditions. In particular results from previous experimental activities and numerical analyses are explored. Chapter 6 presents results from in situ piezocone tests conducted with different penetration rates and different piezocone diameters. Tests have been conducted on under-consolidated dredged sediments within a storage basin of the Port of Livorno (Italy), on alluvial soil deposits in Pisa and Lucca (Italy). Furthermore, laboratory characterisation of the soils investigated is presented. As far as the tests conducted in Pisa, an additional study on the influence of the sleeve diameter on side friction measurements is shown.

Chapter 7 describes the calibration chamber tests equipment, the analyses and the results. The laboratory tests carried out in order to select an appropriate material for the tests are described in this chapter, as well as the tests conducted on the selected material, in order to obtain consolidation and mechanical characteristics. Finite Element analyses of penetration tests under partially drained conditions are illustrated in Chapter 8. Analyses are carried out with Abaqus (2016) by using the Updated Lagrangian technique to preserve mesh quality during the simulation. Experimental data on normally consolidated kaolin clay (Randolph and Hope, 2004; Schneider et al., 2007) are reproduced using the Modified Cam Clay model to simulate the soil constitutive behaviour. In addition to that, an attempt to reproduce the calibration chamber test results is made using the Mohr Coulomb model.

Chapter 9 shows an approach that could be used in case of erroneous Soil Behaviour Type classification of soil layers belonging to the vadose zone. The proposed method consists in properly correcting the vertical effective stress in order to take into account the effects of suction. Furthermore, an empirical correction of the Soil Behaviour Type Index is provided in order to get a more realistic soil profiling of loose silt mixtures, in particular Serchio River levee system (Italy) and dredged sediments of the Livorno port area (Italy).

Chapter 10 deals with the possibility of estimating the preconsolidation stress and the overconsolidation ratio from piezocone tests. In the first part, the applicability of several correlations available in literature, to the estimation of the overconsolidation ratio from piezocone measurements, is investigated. In particular, thanks to the large amount of piezocone tests conducted in Pisa, the available correlations to infer overconsolidation values with depth are compared with the overconsolidation profile result of the huge amount of laboratory tests conducted in this area. In the second part, a new approach is proposed to establish overconsolidation profile in the particular case of soil layers saturated by capillarity.

General conclusions and remarks are presented in Chapter 11.

5. Cone Penetration Test in partially drained conditions

The current interpretation of stratigraphy relies on empirical classification charts (e.g., Robertson et al., 1986; Senneset et al., 1989; Robertson, 1991), and semi-empirical correlations for estimating shear strength, consolidation and permeability properties of the soils (e.g., Wroth, 1984; Baligh, 1986a, b; Teh&Houlsby, 1991). While current piezocone test procedures are able to identify sand and clay layers, interpretation is much more complex in soils of intermediate permeability. In this case, partial drainage of pore water occurs during penetration and affects the shear strength that can be mobilised in the surrounding soil (Figure 2). For this reason, it is much more difficult for intermediate soils to identify soil type with conventional classification charts (Ramsey, 2010; Lo Presti et al., 2010).

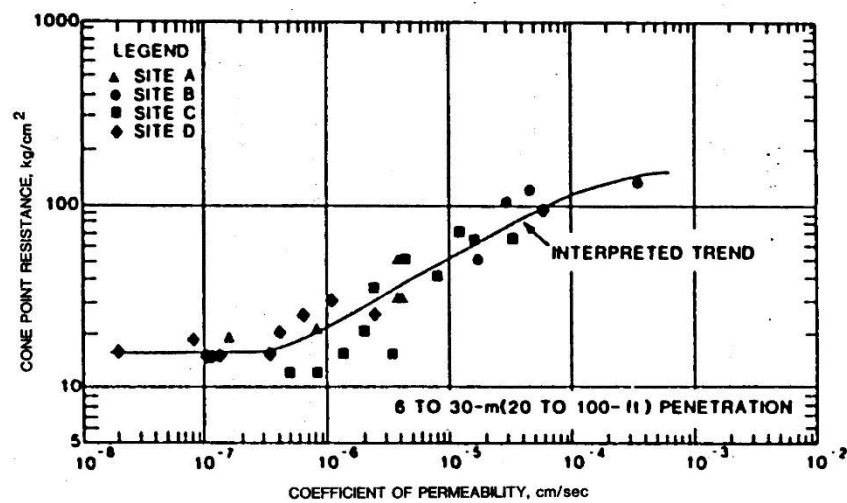


Figure 2: Effects of partial drainage on measurements of piezocone tip resistance in silts (McNeilan & Bugno, 1985).

As a matter of fact, the interpretation of penetration tests for soil profiling is based on the analogy between penetration tests and drilled piles behaviour. The cone resistance can be interpreted as base unit bearing capacity and the sleeve friction as side unit bearing capacity of drilled piles. In the case of granular soils, and drained conditions, the following relationships hold:

$$q_t = N_{\gamma q} \cdot \sigma'_{v0}$$

$$f_s = K \cdot \tan \delta \cdot \sigma'_{v0}$$

Where $q_t = q_c + (1 - a_n) \cdot u_2$ is the total cone tip resistance corrected for unequal end area (Lunne et al.; 1997); a_n = net area ratio of the penetrometer (a_n is not usually defined in advance but is best found by calibration of cone in a pressure chamber); $N_{\gamma q}$ = cone factor, σ'_{v0} = effective geostatic vertical stress, δ = soil cone friction, K = coefficient of earth pressure. With realistic values of the bearing capacity factor, of K and of $\tan \delta$, f_s/q_t is between 0.2 and 2% and quite constant.

For fine grained soils in undrained conditions, the following relations hold:

$$q_t = N_c \cdot s_u + \sigma_{v0}$$

$$f_s = a \cdot s_u$$

where N_c = bearing capacity factor in undrained conditions, s_u = undrained shear strength. In this case f_s/q_t is greater than 2% and varies significantly with depth.

During penetration tests, in the case of granular soils, the pore water pressure is comparable to hydrostatic pore pressure because of drained conditions, whereas for fine grained soils the pore water pressure during the test can be much higher than hydrostatic pore pressure.

For intermediate soils, such as clayey sands and silts, silty clays and silts, under standard conditions, the penetration with partial drainage is more likely. Therefore, it is not possible to apply the above considerations and it is more difficult to interpret test results. Penetration resistance in normally consolidated soils can increase 2-4 times moving from the undrained to the fully drained conditions, therefore the assessment of drainage conditions during penetration has significant importance on the assessment of geotechnical parameters.

The influence of penetration rate on penetration resistance and excess pore water pressure has been studied by: Finnie and Randolph (1994), House et al. (2001), Randolph and Hope (2004), Chung et al. (2006); Kim et al. (2008); Schneider et al. (2007); Schneider et al. (2008); Lehane et al. (2009); Dejong and Randolph (2012); Mahmoodzadeh and Randolph (2014). Most of these studies have been performed with centrifuge tests on normally consolidated kaolin clay. The behaviour of natural clay has been studied by Chung (2006) while Schneider et al. (2007) carried out centrifuge tests on silica flour and bentonite slurry. Furthermore Schneider et al. (2007) considered the effects of overconsolidation on clay and silty clay behaviour. Kim et al. (2008) carried out tests on saturated clayey soils both in a calibration chamber and in the field. The variation of tip resistance can be described through two main physical aspects: viscous effects that are predominant at high rates, and consolidation effects that influence tip resistance in the range between the undrained conditions and the completely drained conditions (at very low penetration rates). There is a penetration rate at which the combination of these two phenomena leads to a minimum tip resistance (Craig, 1995). Since drainage conditions depends on the diameter of the tip, the penetration rate and the consolidation characteristics of the soil, Finnie and Randolph (1994) introduced the non-dimensional velocity V to define the degree of partial consolidation:

$$V = \frac{vd}{c_v}$$

where v is the cone velocity, d the cone diameter and c_v is the coefficient of consolidation. This parameter is the most common parameter used in literature to describe the changes in tip resistance within the range of penetration rates in which the consolidation phenomena is predominant. Randolph and Hope (2004) developed a series of piezocone tests at different

penetration rates in normally consolidated kaolin clay in a geotechnical centrifuge. They used both model cone and T-bar penetrometers (Figure 3). Data obtained from penetration tests were plotted in the typical form showed in Figure 3 and Figure 4. The effect of cone penetration rate on the excess pore pressure ratio, B_q , is shown in Figure 4.

B_q is defined as:

$$B_q = \frac{\Delta u}{q_{cnet}}$$

q_{cnet} is obtained by subtracting the vertical overburden pressure, σ_{v0} , from the total cone resistance. The transition from the undrained value of 0.57 to the drained value of zero occurs between V values of 30 and 0.3.

Figure 3 shows the effect of cone penetration rate on cone and T-bar resistance, where $q_{cnetref}$ and $q_{T-barref}$ are the average undrained resistances. As the penetration rate is reduced the penetration resistance first decreases due to reduced viscous effects and then increases as partial consolidation occurs ahead of the advancing tip. Fully drained conditions and pore water pressure equal to hydrostatic values are reached for V values between 0.1 and 0.3.

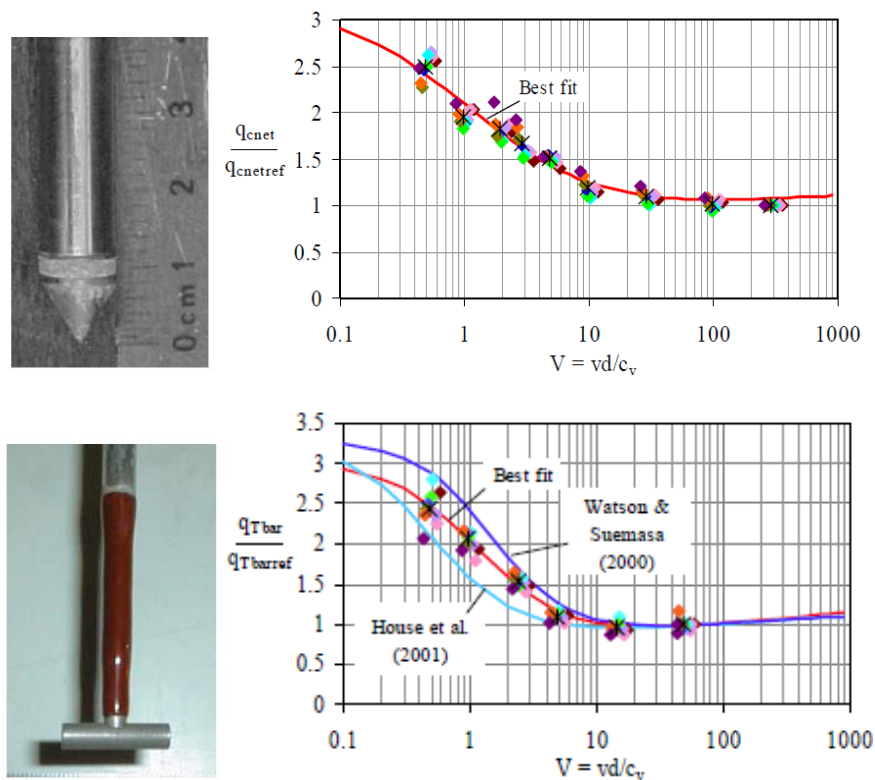


Figure 3: Normalised cone and T-bar resistance variation with normalised velocity (Randolph & Hope 2004)

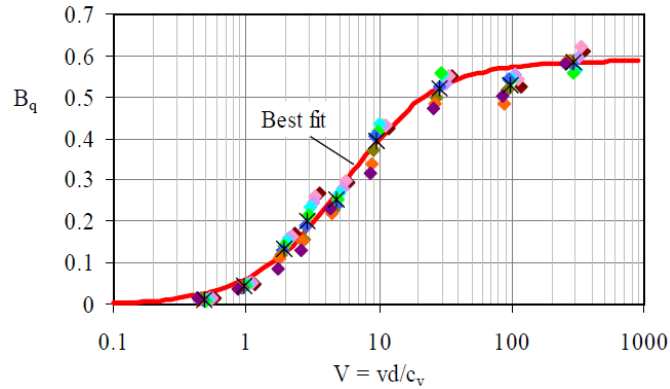


Figure 4: Variation of excess pore pressures ratio (B_q) with cone velocity (Randolph and Hope, 2004)

The so called “backbone” curve can be used to assess whether a given penetration test in a particular soil is partially drained or not. They proposed the following hyperbolic function to fit the experimental results, where a , b , c and m are constants:

$$\frac{q}{\sigma'_v} = \left[a + \frac{b}{1 + cV} \right]$$

At high velocities, beyond the minimum value, it is expected that the penetration resistance is a function of the strain rate and hence of the ratio between the penetration rate and the diameter of the tip. Lehane et al. (2009) extended the study made by Randolph and Hope (2004) investigating the effects of penetration rate in a wider velocity range. The effects of viscosity have been added to the previous expression, proposing the following (Figure 5):

$$\frac{q}{\sigma'_v} = \left[a + \frac{b}{1 + cV} \right] \left[\frac{v/d}{(v/d)_{ref}} \right]^m$$

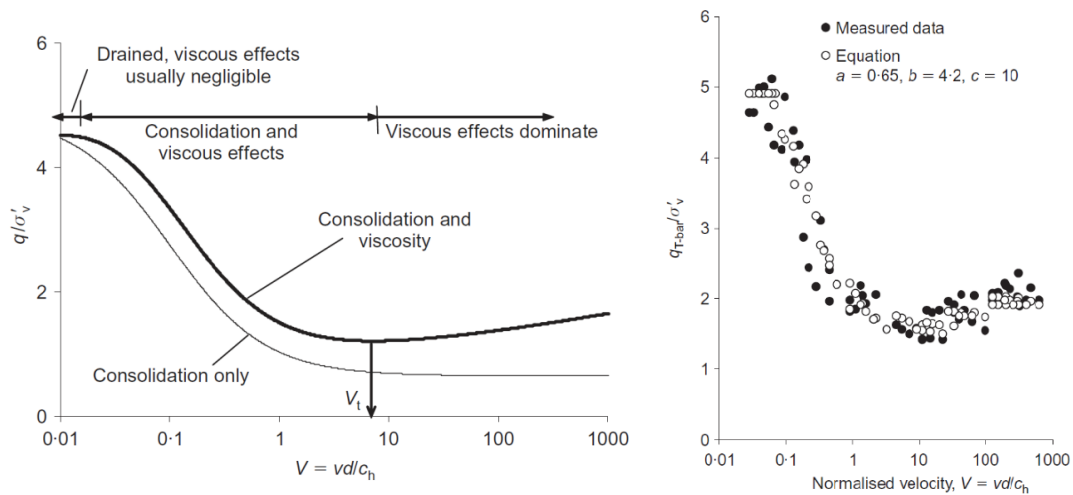


Figure 5: Variation of tip resistance with cone velocity in kaolin clay: Illustration of form of proposed equation (left); Comparison between T-bar data on normally consolidated kaolin clay and equation data using best-fit parameters $a=0.65$, $b=4.2$, $c=10$ (Lehane et al.,2009)

Viscous rate effects occur when v/d exceeds $(v/d)_{ref}$. The transitional velocity V_t can be evaluated as follows:

$$V_t \approx \frac{b}{acm} \text{ for } m < 0.1$$

Schneider et al. (2007) studied the effects of different penetration rates on piezocone measurements in a beam centrifuge for normally consolidated and overconsolidated clay and silty clay. They plotted the results in terms of the ratio between the net cone resistance and the vertical yield effective stress, as suggested by Mayne (1986), since for undrained penetration in clay this ratio is more unique than the ratio between tip resistance and vertical effective stress. The shape of the backbone curves is different for the four types of material investigated: there are differences in the width and position of the range of V in which partially drained penetration occurs, and in the ratio between the drained and the undrained measured tip resistance (Figure 6). As far as the normally consolidated kaolin is concerned, the ratio between the drained and the undrained value is around 2, whereas a value of 4 is measured in the case of lightly overconsolidated silica flour and bentonite slurry (LOC SFB). According to their results the fully drained conditions occur for V values lower than 0.04 for NC kaolin and 0.3 for LOC SFB. Undrained tip resistance is obtained for V higher than 100 for NC kaolin and 2 for LOC SFB. At the same time, they observed similar trends for the overconsolidated kaolin and the heavily overconsolidated silica flour and bentonite slurry. For all the investigated materials, minimum cone resistance is obtained for V around 100. Differences in porewater pressure measurements can be observed in Figure 7, where measurements are plotted on $\Delta u_2 / \sigma'_{v0} - V$ and $Bq-V$ spaces. As far as the $\Delta u_2 / \sigma'_{v0} - V$ plot is concerned, NC and HOC kaolin curves have the same trend, but over-consolidation ratio influences excess porewater pressure measurements under undrained conditions: a higher OCR value leads to higher $\Delta u_2 / \sigma'_{v0}$. Approximately zero values are obtained for V equal to 0.1. They observed that this value does not correspond to the maximum tip resistance measurement for NC kaolin, which occurs for $V=0.04$, showing that porewater pressure measurements at cone shoulder and tip resistance are not directly correlated. A completely different trend characterises the silica flour and bentonite slurry behaviour: after a first increase with normalised velocity, $\Delta u_2 / \sigma'_{v0}$ decreases for V values higher than 10, reaching negative values for V higher than 100. For LOC SFB this reduction in excess pore water pressure measurements is not followed by significant changes in measured tip resistance, while, in the case of NC kaolin, almost constant trend is observed for both tip resistance and excess pore water pressure measurements as the non-dimensional velocity exceeds 100. The combination of octahedral and shear excess pore water pressure generated during the penetration have different influences on tip resistance and pore water pressure measurements as the rate changes.

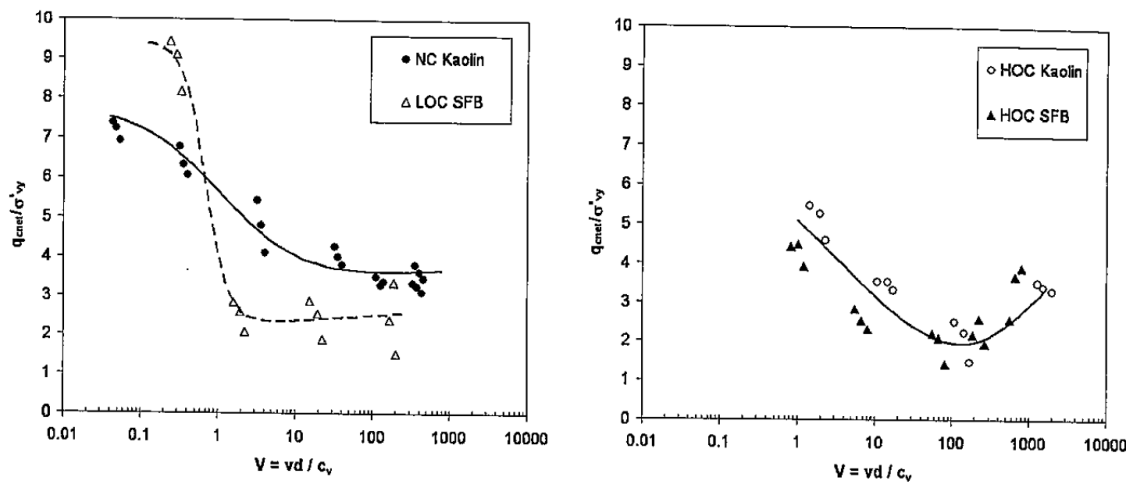


Figure 6: Influence of normalised penetration on normalised tip resistance for nearly normally consolidated soils (left) and overconsolidated soils (right). NC Kaolin: normally consolidated Kaolin; LOC SFB: lightly overconsolidated silica flour and bentonite slurry; HOC Kaolin: overconsolidated Kaolin; HOC SFB: heavily overconsolidated silica flour and bentonite slurry (Schneider et al., 2007).

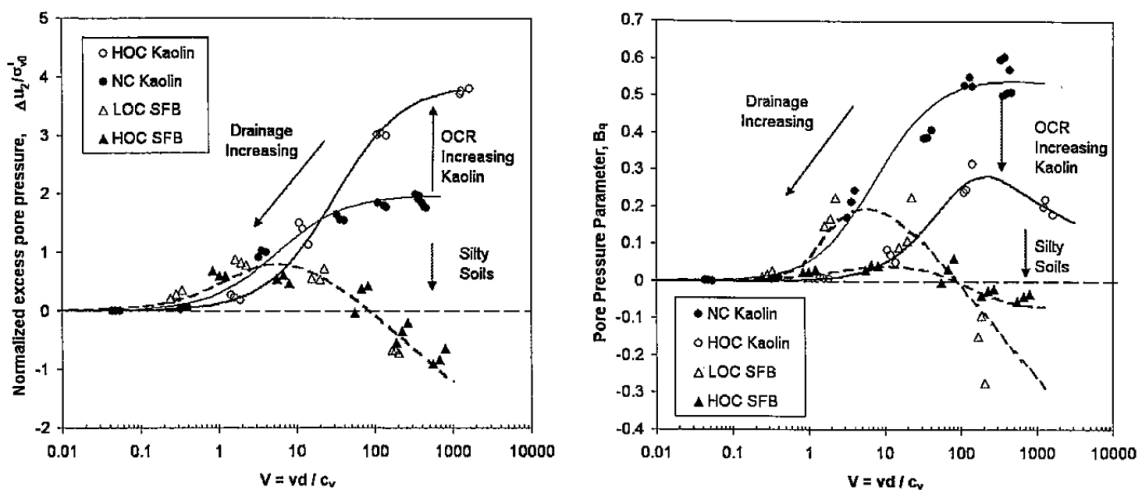


Figure 7: Influence of normalised velocity on normalised excess pore water pressure and pore pressure parameter B_q . NC Kaolin: normally consolidated Kaolin; LOC SFB: lightly overconsolidated silica flour and bentonite slurry; HOC Kaolin: overconsolidated Kaolin; HOC SFB: heavily overconsolidated silica flour and bentonite slurry (Schneider et al., 2007)

Schneider et al. (2008; 2012) proposed a framework for classifying soils, using piezocone tests, with variable rate penetration tests that “provide additional levels of information, which cannot be achieved with dissipation testing”. They investigated the effects of overconsolidation and partial consolidation on the Robertson (1991) classification chart. Increasing OCR and increasing degree of consolidation around the tip have the same effects on Robertson (1991) classification chart, in particular, Q increases and B_q decreases. This trend has been observed for different kind of soils: normally consolidated clay and lightly overconsolidated clay, silts

and dense fine sands. In order to separate partial consolidation and OCR effects they proposed to plot results on a $\Delta u_2 / \sigma'_{v0} - Q$ chart. Where the parameters are defined as follows:

$$Q = \frac{q_t - \sigma_{v0}}{\sigma'_{v0}} = \frac{q_{cnet}}{\sigma'_{v0}}; \quad \Delta u_2 = u_2 - u_0$$

Where $q_t = q_c + (1 - a_n) \cdot u_2$ is the corrected total cone resistance, σ'_{v0} is the vertical effective stress, σ_{v0} is the total vertical stress, u_2 is the measured pore water pressure at cone shoulder and u_0 is the hydrostatic pore pressure. They used the term q_{cnet} to distinguish results from cone measurements from those obtain for the T-bar tip (as Randolph and Hope, 2004).

The outcome of this classification is that the influence of OCR during undrained penetration in clays and the influence of partial consolidation have opposite trends. They introduced a new classification chart, very different from the existing charts, as shown in Figure 8. The proposed simple algorithm allows for the subdivision in three main soil groups: drained, undrained or partially drained conditions during the penetration test. Transitional soils are clearly defined within the proposed charts, but it is highlighted that standard design correlations have low reliability, if applied, and, in addition to that, they suggested adding different source of information, such as dissipation tests and variable rate penetration tests, when transitional soils are identified.

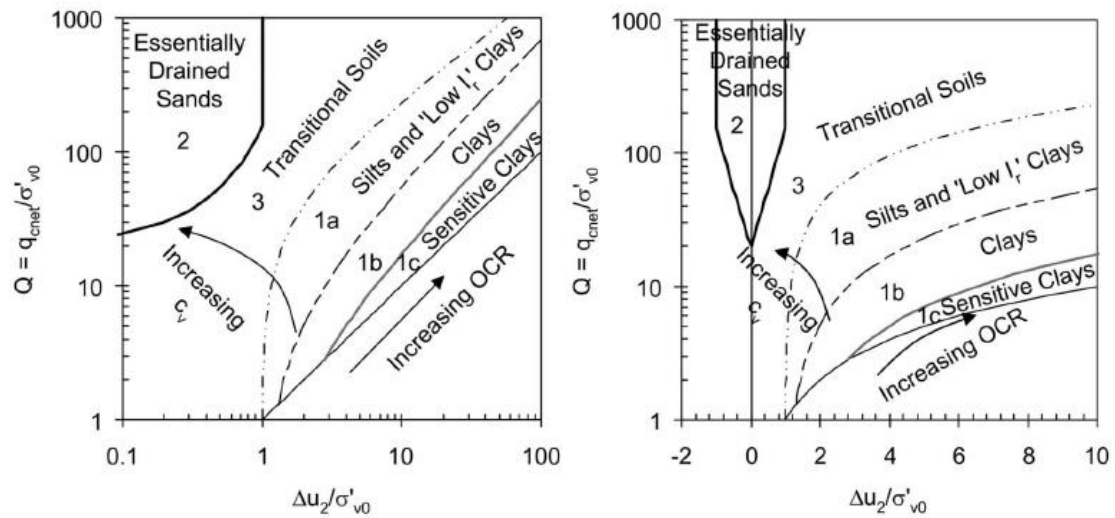


Figure 8: Classification charts proposed by Schneider et al. (2008) in two different plotting formats.

Schneider et al. (2012) introduced a new chart that included f_s measurements (Figure 9). Data are plotted in a Q-F chart, where:

$$Q = \frac{q_t - \sigma_{v0}}{\sigma'_{v0}} = \frac{q_n}{\sigma'_{v0}}; \quad F(\%) = \frac{f_s}{q_t - \sigma_{v0}} \cdot 100 = \frac{f_s}{q_n} \cdot 100$$

They assumed the same definition of soil classes as for the Schneider et al. (2008) classification charts. This additional instrument can be useful if high quality pore water pressure measurements are not available.

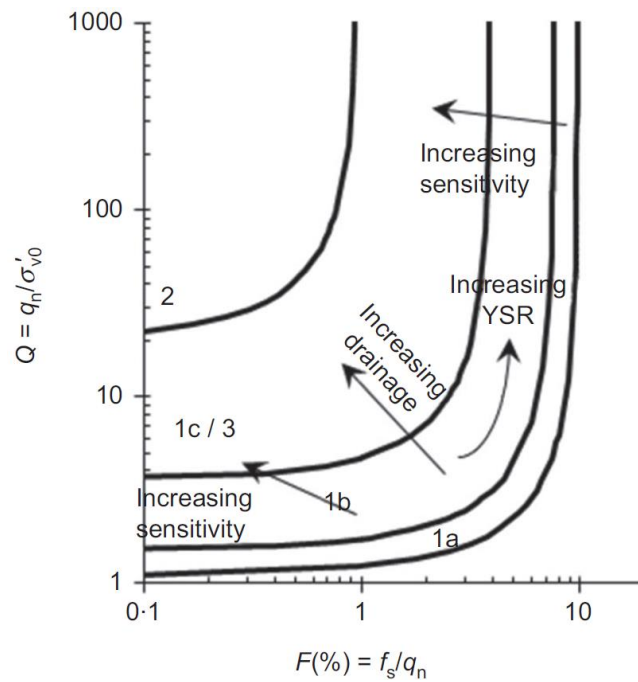


Figure 9: Additional classification chart proposed by Schneider et al. (2012).

Kim et al. (2008) carried out piezocone tests both in a calibration chamber and in the field, analysing the effects of penetration rate on clayey silt and silty clay as well as sand-clay mixtures. The transition between the undrained conditions and partially drained conditions in terms of tip resistance occurs for V values between 4 and 10 for the in situ measurements. For the material studied in the calibration chamber, consisting of two different samples obtained mixing kaolin clay (25% and 18% by weight) and Jumun sand (75% and 82%), the transition between the partially drained and fully undrained conditions occurs for V equal to 10. In this case the ratio between the drained and the undrained tip resistance is approximately 3-4. Fully drained conditions occurs at $V=0.05$ where it is possible to observe stabilization of tip resistance and complete dissipation of excess porewater pressure. For both in situ tests and calibration chamber tests, they observed differences in transition limits for the undrained region between the qt/σ'_v-V plot and the $\Delta\tau/\Delta\tau_{max}-V$ plot. In particular, for calibration chamber tests, whereas tip resistance reaches the lower value for $V=1$, maximum values of excess porewater pressure are obtained from $V=10$. They explained the shift in boundaries with the combination of decreasing tip resistance, while approaching the undrained region, and increasing viscous effects that can be present.

A key parameter for assessing the drainage boundaries in terms of non-dimensional velocity V , in the form proposed first by Finnie and Randolph (1994), is the coefficient of consolidation.

As highlighted by many researches (Sully et al. 1988; Levadoux et al. 1980; Robertson et al., 1986) pore water pressure distribution around a penetrating cone is a function of the stress-strain behaviour of soil. Pore water pressure generation is a function of soil properties such as sensitivity, stiffness, plasticity index, cementation and overconsolidation ratio.

Robertson et al. (1986) have presented field data on the distribution of normalised pore pressures around a penetrating cone. The total dynamic pore pressure, u , is normalised with respect to the hydrostatic pore pressure, u_0 , at test's depth. The variation in the normalised pore pressure, u/u_0 , for various soil types is shown in Figure 10.

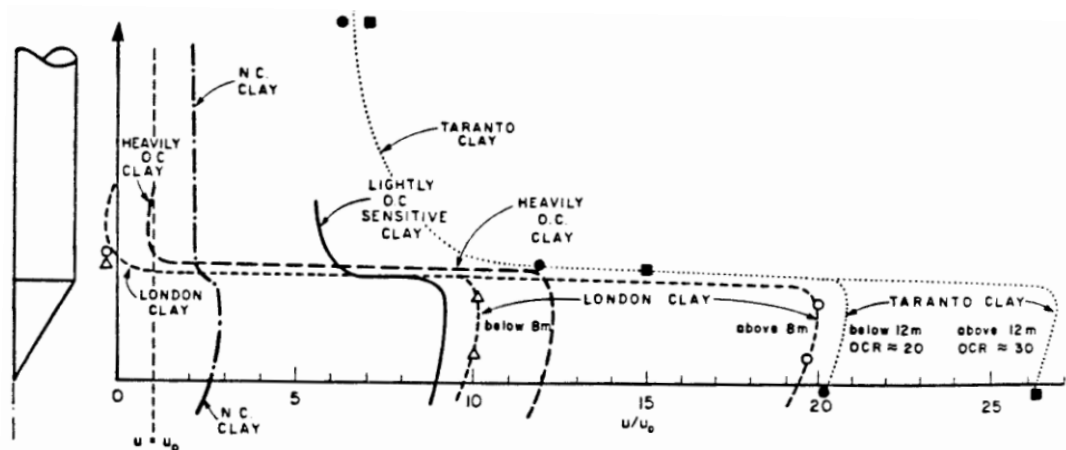


Figure 10: Conceptual pore pressure distribution in saturated clays during CPTu based on field measurements (after Robertson et al. 1986)

The pore pressure measured on the tip or face of the cone is always higher than that measured behind the cone and the difference between the normalised pore pressure measured on the tip of the cone and the one measured at the base of it increases as the overconsolidation ratio increases. The pore water pressure measured at the tip or along the face of the cone is positive and increases as the overconsolidation ratio increases. However, behind the tip the pressure may become negative in relation with the overconsolidation level.

Excess pore pressure measurements at the cone shoulder (u_2 position) can be divided in two components, the octahedral and the shear induced excess pore pressure (Wroth, 1984; Baligh, 1986; Mayne and Bachus, 1988):

$$u_2 = u_0 + \Delta u_{2,oct} + \Delta u_{2,shear}$$

According to Burns and Mayne (1998) there is a thin zone very closed to the penetrometer where the response is affected by shear induced pore pressure, whereas the dimensions of the zone, where octahedral excess pore pressure is predominant, can be much greater than the cone diameter, depending on the rigidity index value. Negative shear induced pore water pressure is more significant for overconsolidated clays and sandy silts. Outside of the zone where shear behaviour is predominant, octahedral excess pore water pressures are predominant and the total

excess pore water pressure is usually positive and assumes high values. This behaviour is confirmed by several “nonstandard” dissipation curves where the measured excess pore water pressure, initially negative, gradually increases to equalise the positive pore pressure that are present in the zone outside the shear region (Figure 11).

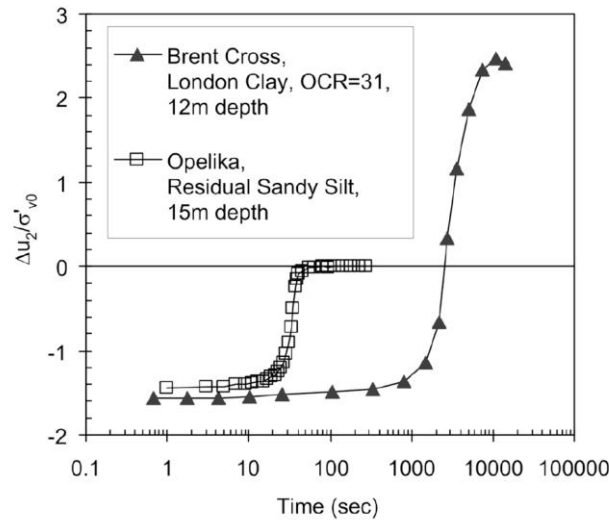


Figure 11: Example of non-standard dissipation curves for overconsolidated clay and sandy silt (Schneider, 2008)

The dissipation test is an important instrument to characterise soil consolidation parameters and it consists of measuring pore water pressure over time once the tip is halted at a certain depth during a penetration test. Teh and Houlsby (1991) analysed cone penetration test in clay by the use of the strain path method and considering the clay as a homogeneous elastic perfectly plastic material obeying the von Mises yield criterion. They proposed an interpretation method for dissipation tests that is widely used in geotechnical engineering practice, when the test is conducted under undrained condition and the shape of the dissipation curve overlaps the theoretical one. The dissipation response is mostly influenced by the overconsolidation ratio and the partial consolidation during the previous penetration. Sully et al. (1999) proposed a framework to interpret dissipation tests in overconsolidated fine grained soils, subdividing the various non-standard dissipation responses in main classes and proposing plot corrections. (logarithmic time and square root time). DeJong and Randolph (2012) explored the influence of partial consolidation during cone penetration on pore pressure measurements. Pore water pressure measurements during penetration are highly influenced by drainage conditions. They studied the response of normally consolidate kaolin clay under different drainage conditions and numerical analyses made by Silva et al. (2006) based on cavity expansion theory applied to NC kaolin clay. In practice, usually, dissipation measurements are normalised with respect to the maximum, initial, pore water pressure value. Utilising this method, as the penetration rate is reduced, moving from undrained penetration to drained penetration, dissipation curves move

to the right in a $\frac{\Delta u}{\Delta u_{max}} - Time$ plot, causing an increase in the necessary time to the 50% dissipation of initial pore water pressure. Therefore, the interpretation of dissipation tests that are carried out during partial drainage conditions and using the standard method proposed by Teh & Houlsby (1991), leads to an under-estimation of the horizontal coefficient of consolidation. This effect is more evident as the phenomenon of partial consolidation increases, reaching differences of one order of magnitude. DeJong and Randolph (2012) proposed a method to correct the estimation of t_{50} to be introduced in the Teh and Houlsby solution. The practical formula is recommended when t_{50} is less than about 100s; in this range partial consolidation during penetration, if not considered, leads to unacceptable differences between the estimation of the coefficient of consolidation and the corrected value.

Mahmoodzadeh and Randolph (2012) investigated the effects of partial consolidation on dissipation tests carried out on kaolin clay under centrifuge conditions. Different tip shapes have been used, the piezoball (with two different position of pore measurements) and the piezocone. Despite the shape of the cone and the pore measurement positions lead to different shapes of the dissipation curves, partial drainage conditions during the penetration has the same consequences in all different cases, increasing the time necessary for a given degree of pore pressure dissipation.

Numerical analysis of the cone penetration process has been conducted the strain path method (Levadoux and Baligh, 1980; Teh and Houlsby, 1991), the cavity expansion method (Salgado et al. 1997; Yu, 2004), the finite element and finite difference method, the material point method. Most of these analyses assumed either fully drained or undrained conditions and the effect of consolidation is still an open issue. Both Bearing Capacity and Cavity Expansion Theory treat cone resistance as a collapse load problem. At the same time, the penetration of the cone in a homogeneous and isotropic material can be interpreted as a steady state process. In the steady state approach, the penetration process is treated as a steady flow of soil passing the fixed cone penetrometer. The Strain Path Method is the first example of the steady state approach. Analysing the undrained penetration problem in clay, Baligh (1986) observed that, due to the severe kinematic constraints that exist in deep penetration problems, soil deformation and strains are independent of the shearing resistance of soil and can be determined with reasonably accuracy based only on kinematic considerations and boundary conditions. Baligh originally defined a "Simple Pile" geometry that is generated by a single spherical source inserted in a uniform flow (Baligh, 1985). The following figure illustrates the contour of octahedral strain and strain rate of a penetrometer with radius equal to 1.78 cm and penetration rate of 2 cm/s.

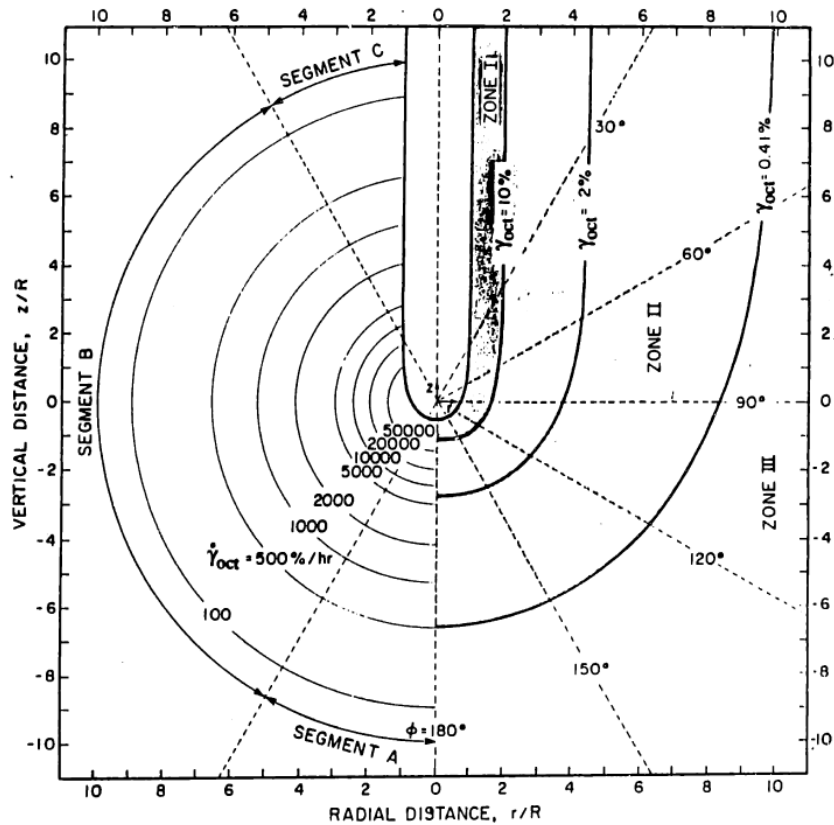


Figure 12: Shear strains during Simple Pile penetration (Baligh, 1985)

It can be seen that steady penetration causes very high strain rates around the tip. Three different modes of shearing can be defined:

- Segment A is defined by $150^\circ < \phi < 180^\circ$, in this region the principal mode of shearing is the triaxial mode
- Segment B, $30^\circ < \phi < 150^\circ$, is the most difficult region because of rotation of principal strain directions and reversal of individual strain components
- Segment C, $0^\circ < \phi < 30^\circ$, where conditions are similar to the expansion of a cylindrical cavity are recovered.

The complete analysis of the simple pile geometry by the use of strain path method is highly complex. Elghaib (1989) developed a simplified predictive framework based on the strain path method for conditions along the centerline of the simple pile penetrometer, in this case:

- The mode of shearing of soil elements is restricted to triaxial compression
- The strain paths for elements approaching the pile tip involve monotonically increasing strain rates and strain components magnitudes
- Close to the pile centerline there are only small gradients of the field variables in the radial direction, hence realistic solutions can be obtained by considering only the conditions of vertical equilibrium

With these simplifications, it is possible to obtain closed form solutions along the centerline for the simple pile geometry and analytical expressions can be developed to predict tip measurements (resistance and pore pressures) from a given set of soil properties. The framework also permits partial drainage to be incorporated in the analysis as a function of consolidation characteristics of the soil.

Levadoux and Baligh have evaluated the theoretical distribution of excess pore pressure around a penetrating cone for normally consolidated to slightly over-consolidated clays. Good agreement was obtained with field results in Boston Blue Clay.

In principal, numerical techniques, in particular the Finite Element Method, can allow a more complete solution of the penetration problem, by taking into account the penetrometer geometry, interface properties and soil constitutive behaviours. A large-strain finite element formulation is needed.

Yi et al. (2012) adopted extensively the Finite Element Method to examine cone penetration response in a homogeneous elastic-perfectly plastic soil obeying to the Drucker-Prager yield criterion, spanning from fully drained to fully undrained conditions. Their model assumed a smooth soil/cone interface. They carried out coupled-consolidation analyses, taking into account for large deformation and finite sliding effects. In particular, the Updated Lagrangian technique has been adopted. The parametric study explored the effects of several parameters on tip resistance changes due to different drainage conditions during penetration. Several backbone curves have been established considering different values of: friction angle, ratio between the shear modulus and the initial mean effective stress ($G/p' =$ modulus ratio). Penetration rates range is between 0.000001 mm/s and 1 mm/s. They observed that changes in friction angle, maintaining a constant value of the modulus ratio, produce little changes in the backbone curves. At the same time, changes in the modulus ratio have significant influence on the shape of the backbone curve end in particular in the ratio between the maximum tip resistance, corresponding to the drained conditions, and the minimum tip resistance, q_{ref} , obtained for fully drained condition. They proposed an expression to evaluate the resistance ratio ($q_{drained}/q_{ref}$) as a function of modulus ratio. For the explored range of modulus ratio (17.5-140), and fixed value of friction angle, the resistance ratio varies between 1.6 and 4.2. Furthermore, the obtained backbone curves can be well described with the expression proposed by Randolph and Hope (2004):

$$\frac{q_{cnet}}{q_{ref}} = 1 + \frac{b}{1 + cV^m}$$

Where $\frac{q_{cnet}}{q_{ref}}$ = ratio between net tip resistance and undrained tip resistance; b, c and m are constant to be evaluated. The parameter b can be estimated through the following expression:

$$b = \frac{q_{drained}}{q_{ref}} - 1 = 0.022 \frac{G}{p'} + 0.331$$

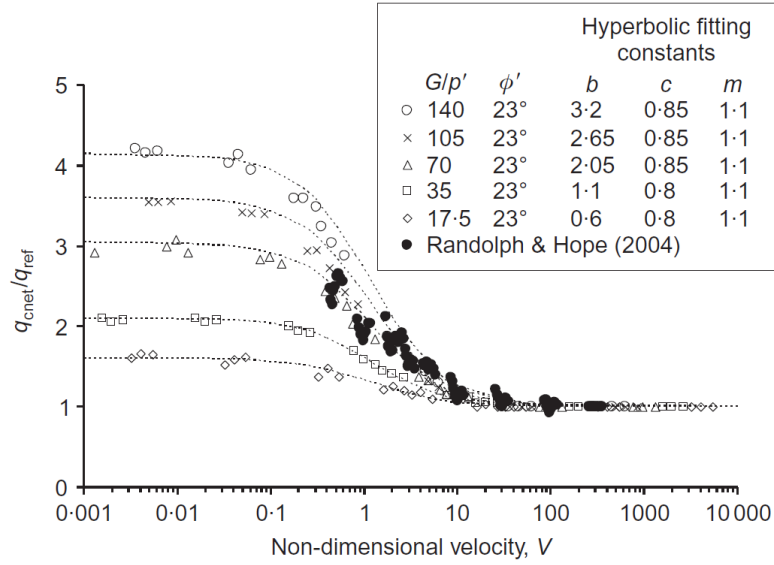


Figure 13: Symbols - Normalised cone resistance against non-dimensional velocity from numerical simulations for different values of the G/p' ratio (Yi et al., 2012). Dotted lines - Backbone curves obtained with the expression proposed by Randolph and Hope (2004), the respective parameters are shown in the legend. Full dots - Experimental data on normally consolidated kaolin clay (Randolph and Hope, 2004).

Another important application of Finite Element Method to this topic consists in the study carried out by Mahmoodzadeh et al. (2014). They carried out a parametric study, by using the Modified Cam Clay constitutive model for the soil, to analyse the effects of various parameters on dissipation curves. They compared the results obtained with the Modified Small Strain FE method proposed by Mahutka et al. (2006) and the Large Deformation FE approach based on frequent remeshing. Frequent remeshing is necessary to overcome the problem of excessive distortion of mesh elements during penetration. The influence of many parameters has been investigated, in particular: rigidity index, slopes of the compression and swelling line, initial stress anisotropy, overconsolidation ratio and partial drainage during penetration. With the introduction of an “operative” coefficient of consolidation and a specific expression of the normalised dissipation time proposed by Teh & Houlsby (1991) it is possible to obtain a unified normalised dissipation curve. The proposed expression takes into account the fact that the dissipation response is related to the combination of both plastic deformation near the piezocone and unloading further away (Fahey & Lee Goh, 1995):

$$c_h = \frac{3(1-\nu)(1+e)p'k}{1+\nu \kappa^\alpha \lambda^{1-\alpha} \gamma_w}$$

Also, they linked the operative coefficient of consolidation defined above to the vertical coefficient of consolidation inferred from oedometer tests:

$$c_h = \frac{3(1-\nu)}{1+\nu} \left(\frac{\lambda}{\kappa}\right)^\alpha c_v$$

6. In-situ experimental activities

In this section, several aspects related to the importance of drainage conditions on piezocone measurements are studied. In situ piezocone tests have been executed on three different kinds of intermediate materials: the dredged sediments of the Livorno Port area (Italy), the alluvial deposits situated in the delta area of Arno River (Pisa, Italy) and in Lucca (Italy).

6.1 Identification and characterisation of dredged sediments

In recent years there has been a great proliferation of artificial basins for the storage of dredged sediments associated with port development, both in Italy and worldwide. There is now great interest in utilising the same storage basins for a range of urban infrastructure projects and this requires an accurate assessment of the stratigraphy and state of consolidation within the dredged sediments.

An excellent example concerns the Port of Livorno, where the designated 40 hectares storage basin has been filled with dredged sediments (a total volume of 1.7Mm³) since 2000. The storage basins are typically capped with low permeability materials to prevent the spread of contaminants from within the sediments into the overlying water column, and the sediments are allowed to consolidate under their own self-weight, a process which can take place over many years. Many consolidation techniques are available depending on the nature of the sediments. Considering the huge investigation area, CPTu test represents an important instrument to identify the soil type and the spatial variability, as it is an economical and expeditious method. As previously mentioned, conventional classification charts and interpretation techniques are not suitable for special soils like dredged sediments.

The research project investigates the use of piezocone penetration devices to characterise 'underconsolidated' sediments.

A laboratory characterisation and in situ testing of dredged sediments from the port of Livorno has been carried out. The in-situ tests use a Pagani penetrometer system (TG 63-200) with a seismic piezocone (thrust capacity is 200kN). Tests are performed with penetration rates ranging from 0.5 cm/s to 5 cm/s. Because dredged sediments may contain some pollutants the basin is impermeable and the process of consolidation is difficult.

6.1.1 Experimental activities at Livorno Port Area (Italy)

Several experimental activities have been carried out at the port of Livorno within the basin for the storage of dredged sediments (Figure 14). The basin is located inside a bigger area used as storage for dredged sediments. The top surface covers 40 hectares and is subdivided in 14 basins. The basins are delimited by embankments. The filling process started in 2000. Dredged sediments came from several locations and had various granulometric characteristics. The contents of the basin are isolated from the marine subsoil with an impermeable membrane to prevent contamination of the surrounding soils due to the possible presence of pollutants. The total capacity has been saturated and the Livorno Port Authority is planning to extend the existing railway on the area of the basin object of this study.



Figure 14: Basin for the storage of dredged sediments object of this study (Livorno Port).

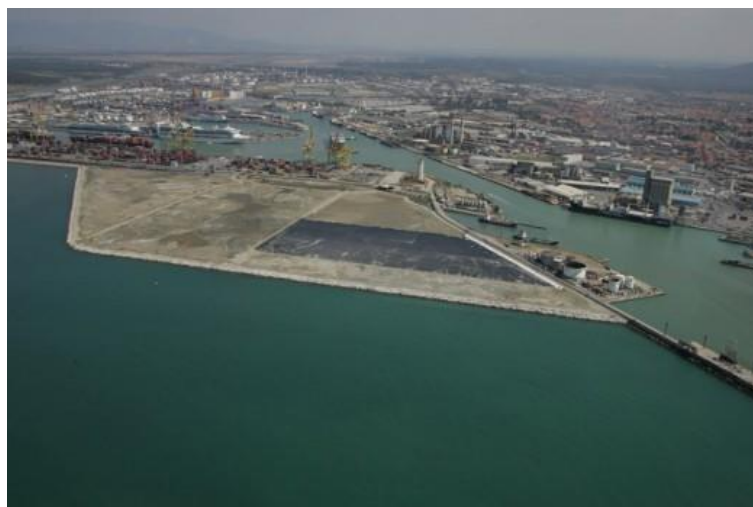


Figure 15: View of the Livorno Port area used for the storage of dredged sediments.

Tests' results from a previous survey in the basin are available. Two main types of material have been selected from the previous test's results: the first material is silt (ML or MH according to the USCS classification), whereas the second material is silty-sand (SM according to the USCS classification).

During this survey two locations within the basin have been chosen (hereafter indicated as "North" and "South") as showed in Figure 16. For each location, the following activities have been done:

- extraction of one block sample (depth 1-1.5 m)
- CPTu test at standard rate of 2 cm/s
- CPTu test at a rate of 0.8 cm/s
- CPTu test at a rate of 4.8 cm/s
- dissipation test for each CPTu test
- extraction of Osterberg samples (depth 1.6-3 m)

The following laboratory tests have been carried out:

- Soil classification
- Incremental loading oedometer test
- Oedometer test with constant rate of strain (5 mm/min)
- Triaxial test TxCIU (50, 100, 200 kPa)
- Resonant column test (20, 50, 100 kPa)



Figure 16: Location of the geotechnical soundings and CPTu tests.

6.1.1.1 Laboratory tests

Osterberg samples and block samples have been extracted at a distance from piezocone tests of around 1.5-2 meters. Block samples (C1 and C2) have been extracted at a depth between 1 and 1.5 meters, Osterberg samples (P1, P2, P3) between 1.6 and 3 meters.



Figure 17: Block sample and Osterberg sample (“North” location).

Figure 18 and Figure 19 show the grain size distribution of the samples. Table 1 and Table 2 summarise the samples characteristics and the classification parameters: grain size distribution, natural water content (w_n), Atterberg's limits (Liquid Limit, Plastic Limit, Plasticity Index), Unified Soil Classification System (ASTM 2487) and Massachusetts Institute of Technology classification system (MIT classification) based on grain size distribution. In addition, the results obtained from incremental loading oedometer tests are displayed in Table 3. In particular, the soil from block samples exhibits a certain overconsolidation (over-consolidated ratio, OCR, between 2.5 and 4), whereas the soil from Osterberg samples shows OCR values lower than 1.9 for all the specimens. Table 3 shows compressibility and hydraulic conductivity parameters, these data are necessary to estimate consolidation properties in order to establish drainage conditions during the piezocone tests. The obtained constrained modulus, M , at the in-situ vertical effective stress, is equal to 1 MPa for all the specimens. The coefficient of consolidation has been evaluated with Casagrande's method, values are between $2.3 \cdot 10^{-8}$ and $6.5 \cdot 10^{-8} \text{ m}^2/\text{s}$. Therefore, the evaluated hydraulic conductivity:

$$k = \frac{c_v \cdot \gamma_w}{M}$$

where: γ_w is the water unit weight, c_v is the coefficient of consolidation, M is the constrained modulus is between $2.3 \cdot 10^{-10} \text{ m/s}$ and $6.4 \cdot 10^{-10} \text{ m/s}$. The constrained modulus is evaluated for each loading step with the following expression:

$$M = \frac{1}{\frac{\partial \epsilon}{\partial \sigma'_v}}$$

Triaxial tests results are summarised in Table 4 where strength parameters are displayed. The specimens don't show dilatant behaviour, the friction angle for Osterberg samples is around

34.5°, whereas for block samples is between 32.3° and 34.5°. The interpretation envelope leads to a cohesion equal to zero for all the triaxial tests. This is reasonable since the soil can be considered normally consolidated or slightly overconsolidated.

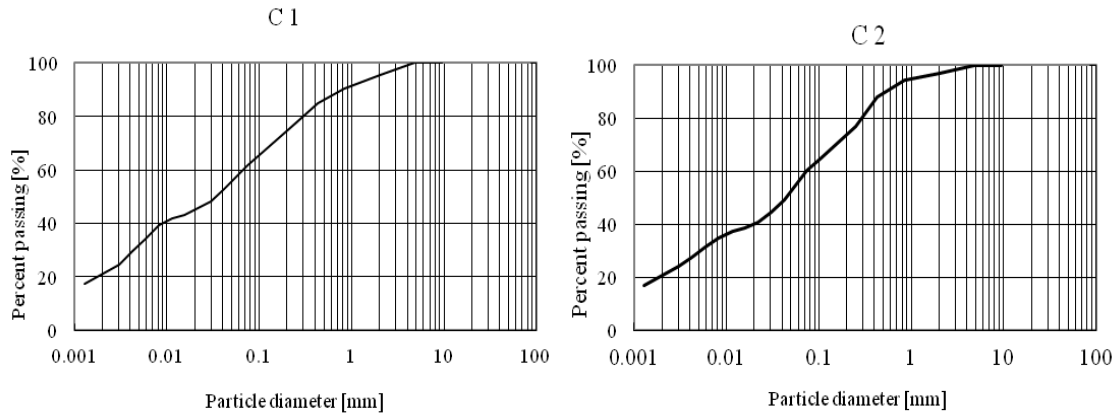


Figure 18: Grain size distribution from block samples C1 and C2.

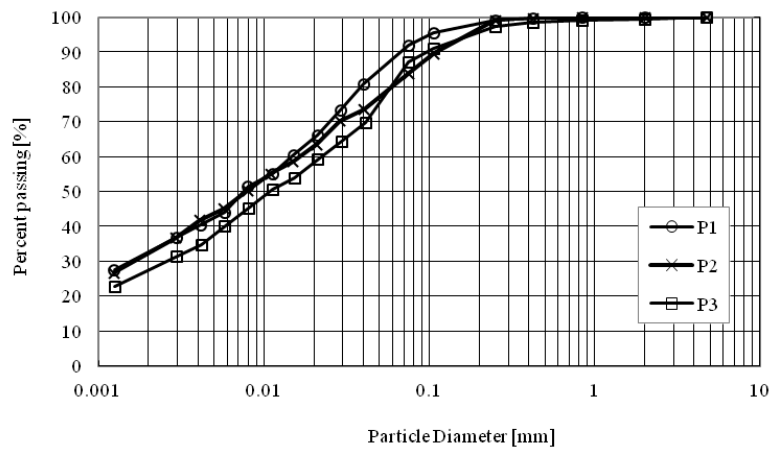


Figure 19: Grain size distribution for Osterberg samples P1 (=O1), P2 (=O2) and P3 (=O3).

Sample	Depth		Wn (%)	Grain size distribution				Atterberg's limits			USCS-ASTM
	from (m)	to (m)		Gravel (%)	Sand (%)	Silt (%)	Clay (%)	LL (%)	PL (%)	PI (%)	
C1	1	1.3	29.1	5	37	37	21	40	23	17	SM Silty Sand
C2	1.2	1.5	47.27	3	41.5	35.5	20	33	20	13	SM Silty Sand
O1	1.6	2.2	44.68	0	10	57	33	45	24	21	CL Lean Clay
O2	2	2.5	42.72	0	17	50	33	41	21	20	CL Lean Clay
O3	2.5	3	40.01	0	15	57	28	38	21	17	CL Lean Clay

Table 1: USCS Classification for the block samples (C1 and C2) and the Osterberg samples (O1, O2, O3).

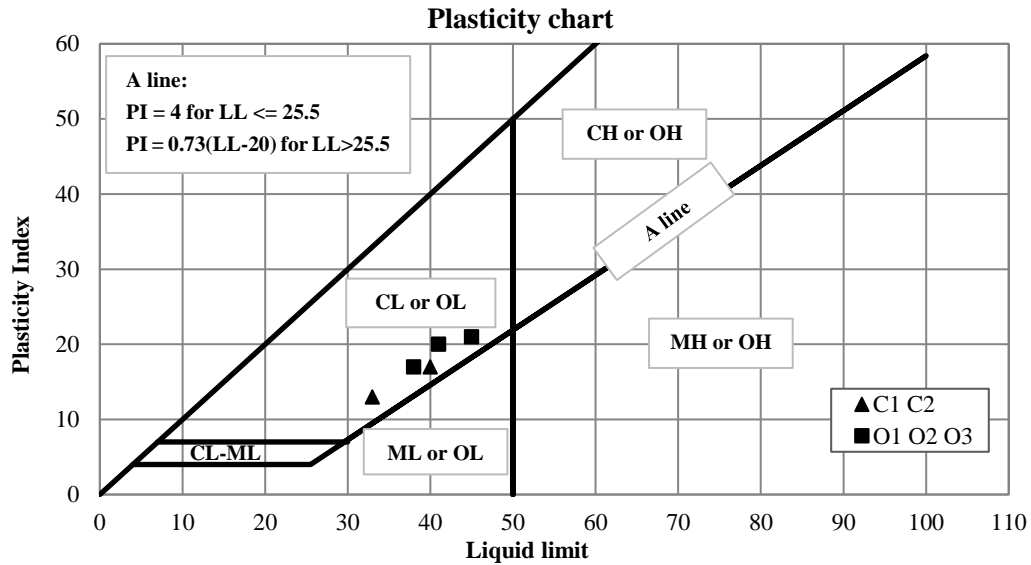


Figure 20: USCS Classification chart, for block samples (C1, C2) and Osterberg samples (O1, O2, O3).

Sample	Depth		W _n (%)	Grain size distribution				MIT Classification
	from (m)	to (m)		Gravel(%)	Sand (%)	Silt (%)	Clay (%)	
C1	1	1.3	29.1	5	37	37	21	Sand with silt
C2	1.2	1.5	47.27	3	41.5	35.5	20	Sand with silt
O1	1.6	2.2	44.68	0	10	57	33	Silt with clay
O2	2	2.5	42.72	0	17	50	33	Silt with clay
O3	2.5	3	40.01	0	15	57	28	Silt with clay

Table 2: MIT Classification for the block samples (C1 and C2) and the Osterberg samples (O1, O2, O3).

Sample	Depth		γ (kN/m ³)	e ₀ Initial void ratio	σ'_p (kPa)	σ'_{v0} (kPa)	OCR	k (m/s)	M (MPa)	c _v (m ² /s)
	from (m)	to (m)								
C1	1	1.3	18.03	0.906	92	23.44	3.93	3.29E-10	1	3.35E-08
C2	1.2	1.5	16.99	1.306	65	25.49	2.55	2.26E-10	1	2.30E-08
O1	1.6	2.2	17.54	1.225	43	32.21	1.33	5.86E-10	1	5.97E-08
O2	2	2.5	17.7	1.174	26	34.93	NA	4.24E-10	1	4.32E-08
O3	2.5	3	18.75	0.972	79	42.03	1.88	6.4E-10	1	6.52E-08

Table 3: Parameters inferred from Oedometer tests (Incremental Loading Oedometer test).

Sample	Depth		ϕ'	c'
	from (m)	to (m)		
C1	1	1.3	34.5°	0
C2	1.2	1.5	34.5°	0
O1	1.6	2.2	32.5°	0
O2	2	2.5	34.5°	0
O3	2.5	3	32.35°	0

Table 4: Strength parameters inferred from triaxial tests, TxCIU tests.

6.1.1.2 Piezocone tests with different penetration rates

Piezocone tests have been conducted by means of a standard piezocone. The standard piezocone has a projected tip area of 10 cm². More details are plotted in the following figure.

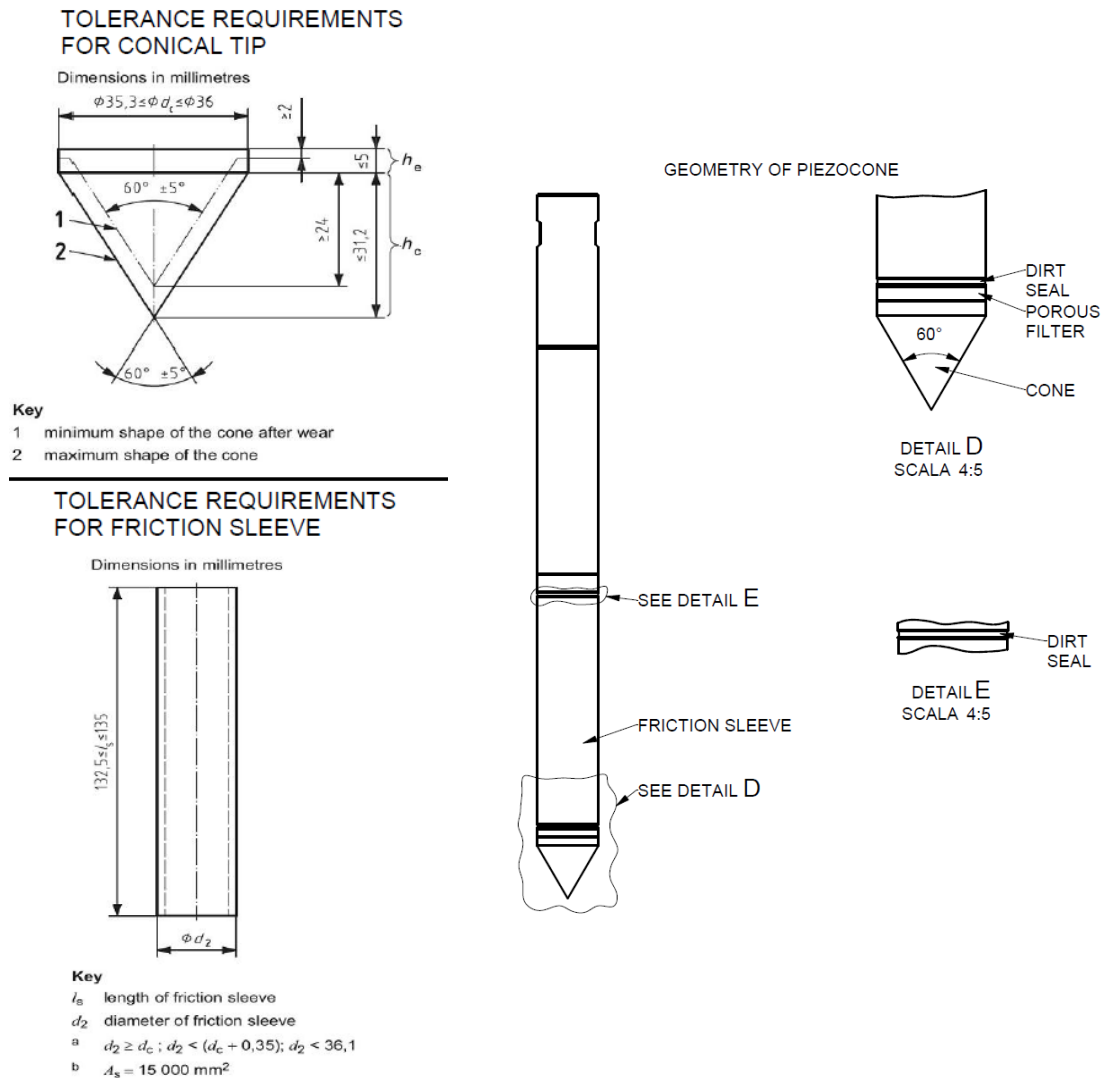


Figure 21: Piezocone characteristics (Pagani Geotechnical Equipment).

Piezocone tests have been carried out up to a depth of approximately 4.5 meters in order to prevent the lower membrane damaging. The distance between the tests at the same location is approximately 50 cm. Tests are conducted with three different penetration rates: 0.8 cm/s, 2 cm/s, 4.8 cm/s. The range of penetration rates depends on the thrust system available for the tests, a 13.5 kW hydraulic engine that does not allow for a further rate reduction.

From Figure 25 to Figure 30, the piezocone results are plotted in terms of the total tip resistance, the sleeve friction and the pore water pressure. The water table is positioned at a depth of 1.55 m.

Figure 22 and Figure 23 show Soil Behaviour Type (SBT) classification obtained for the tests conducted at the South and the North location, respectively. SBT classification is made through

the use of the classification charts proposed by Robertson (1990). The following normalised quantities have to be evaluated:

$$Q = \frac{q_t - \sigma_{v0}}{\sigma'_{v0}}; \quad F = \frac{f_s}{q_t - \sigma_{v0}} \cdot 100; \quad B_q = \frac{u_2 - u_0}{q_t - \sigma_{v0}}$$

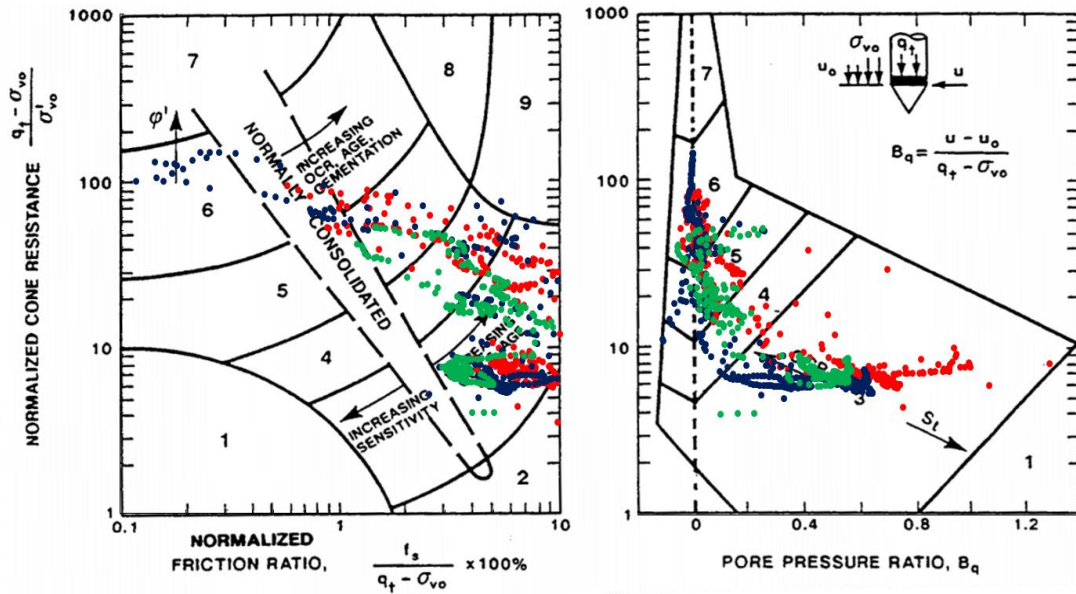


Figure 22: Soil Behaviour Type classification charts proposed by Robertson (1990). CPTu tests conducted at South location ((0.8 cm/s- blue dots, 2 cm/s- green dots, 4.8 cm/s- red dots).

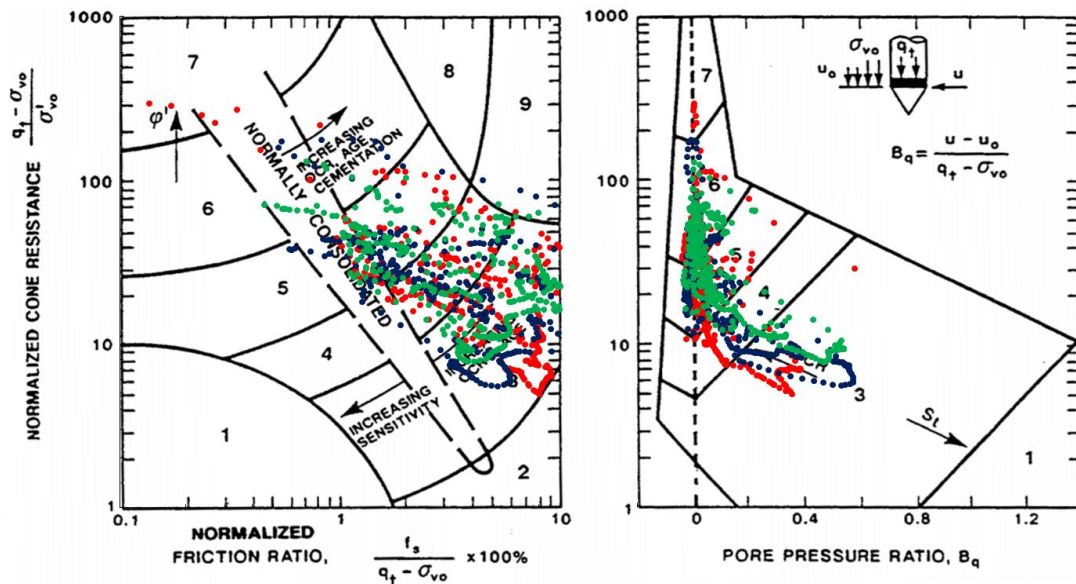


Figure 23: Soil Behaviour Type classification charts proposed by Robertson (1990). CPTu tests conducted at North location ((0.8 cm/s- blue dots, 2 cm/s- green dots, 4.8 cm/s- red dots).

The class numbers correspond to:

- 1: sensitive, fine grained
- 2: organic soil-peat
- 3: clays-clays to silty clay

- 4: silt mixtures-clayey silt to silty clay
- 5: sand mixtures-silty sand to sandy silt
- 6: sands- clean sand to silty sand
- 7: gravelly sand to sand
- 8: very stiff sand to clayey sand (heavily overconsolidated or cemented)
- 9: very stiff, fine grained (heavily overconsolidated or cemented)

The evaluation of the Soil Behaviour Type Index is made with the iterative method proposed by Robertson and Wride (1998):

$$I_c = \sqrt{(3.47 - \log Q_{tn})^2 + (\log F + 1.22)^2}$$

$$Q_{tn} = \left(\frac{q_t - \sigma_{v0}}{\sigma_{atm}} \right) \left(\frac{\sigma_{atm}}{\sigma'_{v0}} \right)^n$$

$$n = 0.381 \cdot I_c + 0.05 \cdot \left(\frac{\sigma'_{v0}}{\sigma_{atm}} \right) - 0.15$$

The following table shows the correspondence between I_c values and SBT classes defined by Robertson (1990).

Soil classification (SBTn)	Zone number (Robertson SBT 1990)	SBT Index values
Organic soils: peats	2	$I_c > 3.60$
Clays: silty clay to clay	3	$2.95 < I_c < 3.60$
Silt Mixtures: clayey silt to silty clay	4	$2.60 < I_c < 2.95$
Sand Mixtures: silty sand to sandy silt	5	$2.05 < I_c < 2.60$
Sands: clean sand to silty sand	6	$1.31 < I_c < 2.05$
Gravelly sand to dense sand	7	$I_c < 1.31$

Early classification methods directly based on measurement of tip and sleeve resistance have been proposed by Schmertmann (1978) and Douglas and Olsen (1981). The most popular classification system, based on tip resistance q_t and Friction Ratio, has been proposed by Robertson et al. in 1986. Friction ratio is evaluated as follows:

$$R_f(\%) = \frac{f_s}{q_t} \cdot 100$$

The advantage of this method is the chance of evaluating soil types immediately during the test, since it does not require the evaluation of normalised parameters. The chart by Robertson et al. (1986) has 12 soil types, whereas the chart by Robertson (1990) uses normalised parameters and has 9 soil types. The following table shows the Soil Behaviour Type classes from Robertson (1986). Figure 24 and Figure 25 show the results obtained for the tests conducted at the North and South location. The chart on the right has been proposed by Robertson in 2010.

Zone	Soil Behaviour Type
1	Sensitive fine grained
2	Organic material
3	Clay
4	Silty clay to clay
5	Clayey silt to silty clay
6	Sandy silt to clayey silt
7	Silty sand to sandy silt
8	Sand to silty sand
9	Sand
10	Gravelly sand to sand
11	Very stiff fine grained (Overconsolidated or cemented)
12	Sand to clayey sand (Overconsolidated or cemented)

Table 5: Soil Behaviour Type classes proposed by Robertson et al. 1986.

Common SBT description	SBT zone	SBTn zone
	Robertson et al. 1986	Robertson 1990
Sensitive fine grained	1	1
Clay - Organic soil	2	2
Clays: clay to silty clay	3	3
Silt mixtures: Clayey silt and silty clay	4 & 5	4
Sand mixtures: Silty sand to sandy silt	6 & 7	5
Sands: clean sands to silty sands	8	6
Dense sand to gravelly sand	9 & 10	7
Stiff sand to clayey sand - Overconsolidated or cemented	12	8
Stiff fine grained - Overconsolidated or cemented	11	9

Table 6: Robertson (1986) SBT classes and respective Robertson (1990) SBTn classes, as proposed by Robertson (2010).

This chart is an update of the previous Robertson (1986), the number of classes has been reduced to match Robertson (1990) SBTn zones. The classification is made in terms of dimensionless cone resistance, (qt/p_a) , where p_a is the atmospheric pressure, and R_f . In this case a log scale is used on both axes. When vertical effective stress has little influence on piezocone measurements, the normalised classification proposed by Robertson (1990) and the non-normalised classification proposed by Robertson (2010) give almost the same results. All the classification charts identified soils belonging to classes 3 to 6. At south location, the profile is more homogeneous and the investigated soil predominantly belongs to zone number 3. The most important differences between the classification chart Robertson-1990 and Robertson-

1986/2010 is that in the second case organic materials, zone number 2, are present. This is clearly visible in Figure 31 and 32 where the SBT and SBTn stratigraphic profiles are compared for the South and North locations. Ic values evaluated for the SBT classification are moved to the right with respect to the Ic values of the SBTn classification.

In the next section, the comparison of the different classification systems is made for a homogeneous layer identified in the stratigraphic profile at North and South location.

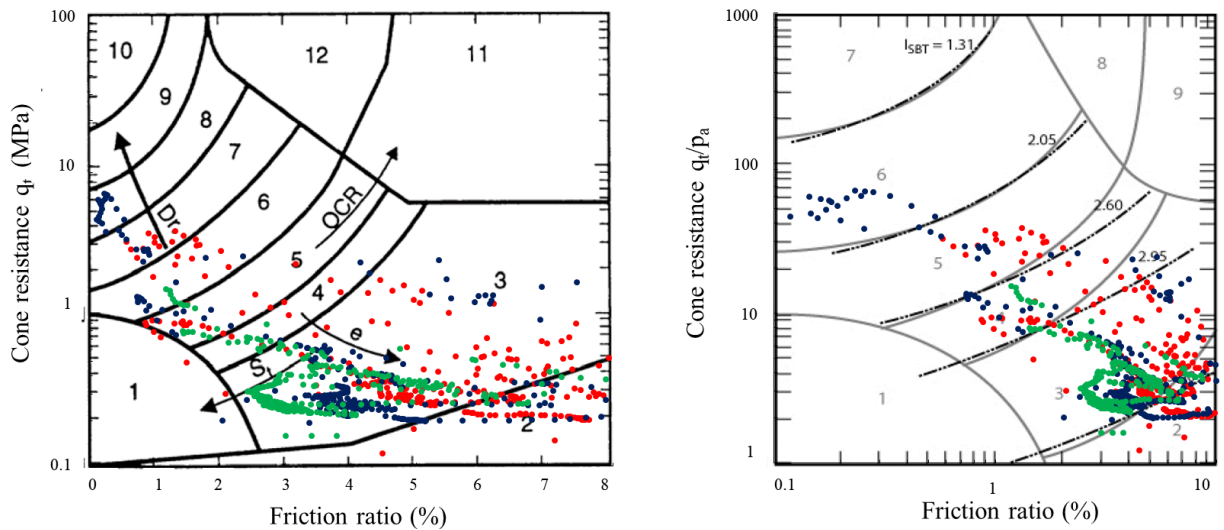


Figure 24: SBT classification following Robertson (1986), chart on the left, and Robertson (2010), chart on the right. Data from different penetration tests conducted at South location (red dots=4.8 cm/s, green dots=2 cm/s, blue dots=0.8 cm/s).

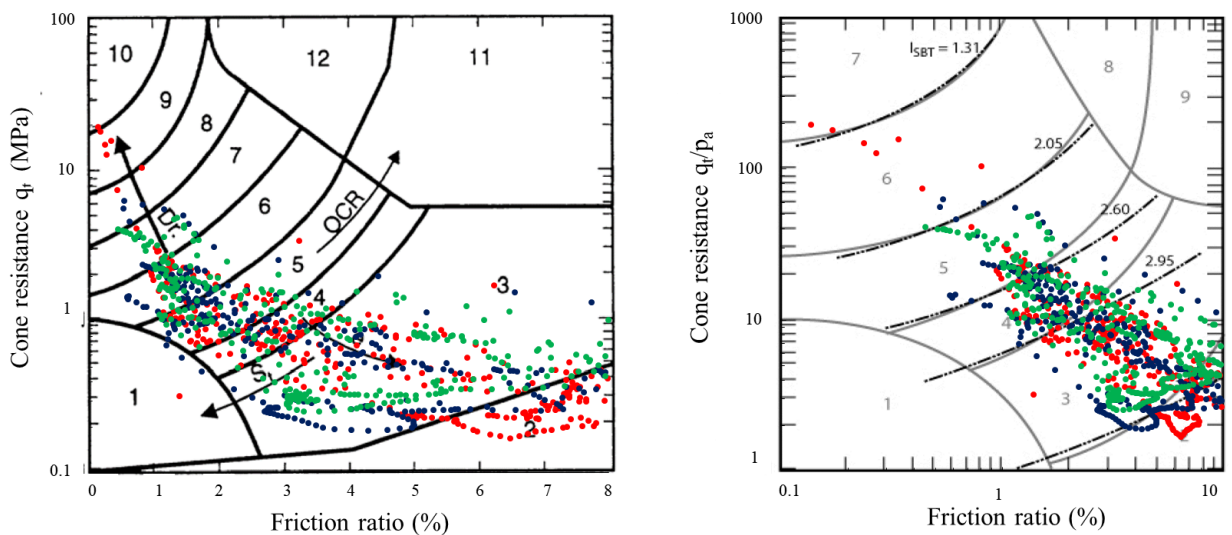


Figure 25: SBT classification following Robertson (1986), chart on the left, and Robertson (2010), chart on the right. Data from different penetration tests conducted at North location (red dots=4.8 cm/s, green dots=2 cm/s, blue dots=0.8 cm/s).

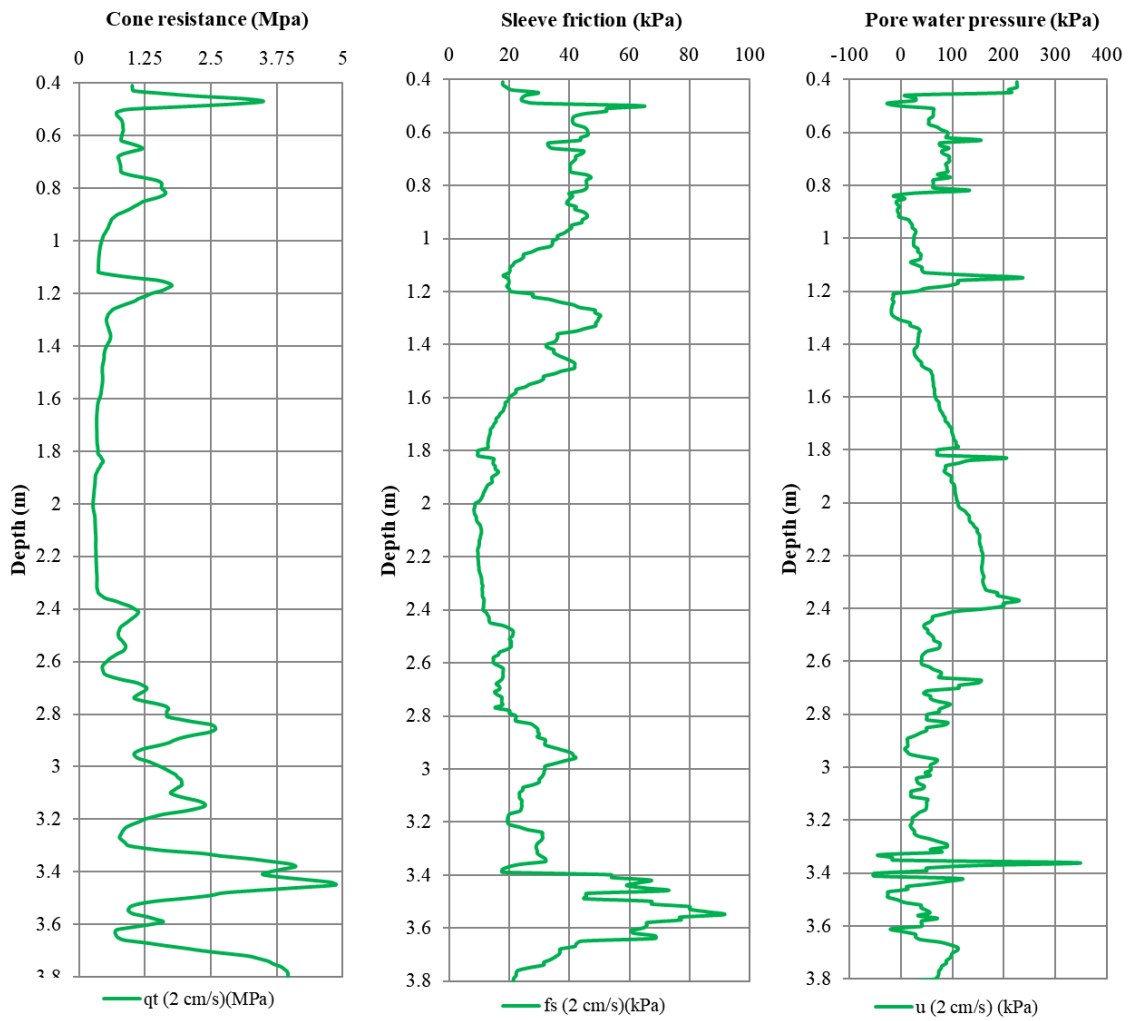


Figure 26: Piezocone test results, site “North”, penetration rate=2 cm/s.

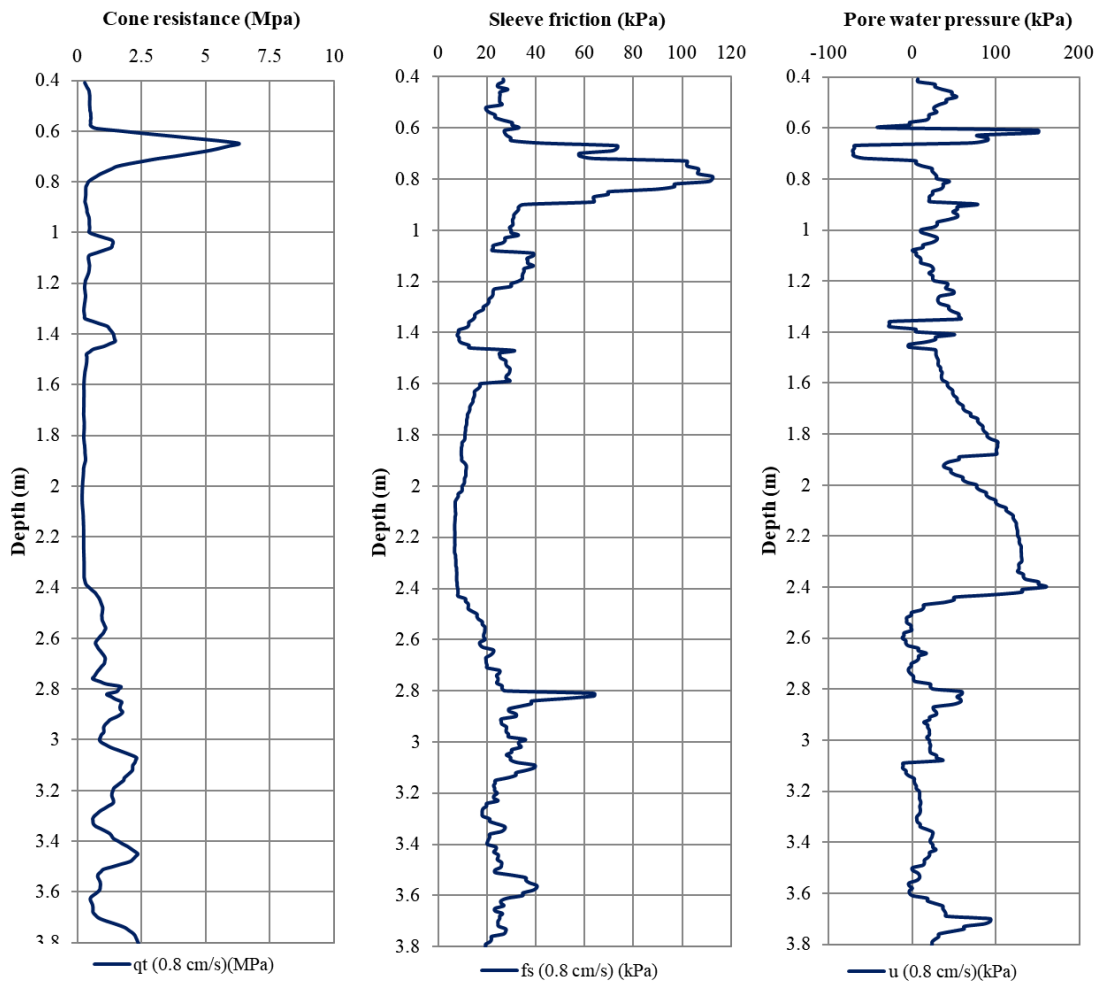


Figure 27: Piezocone test results, site “North”, penetration rate=0.8 cm/s

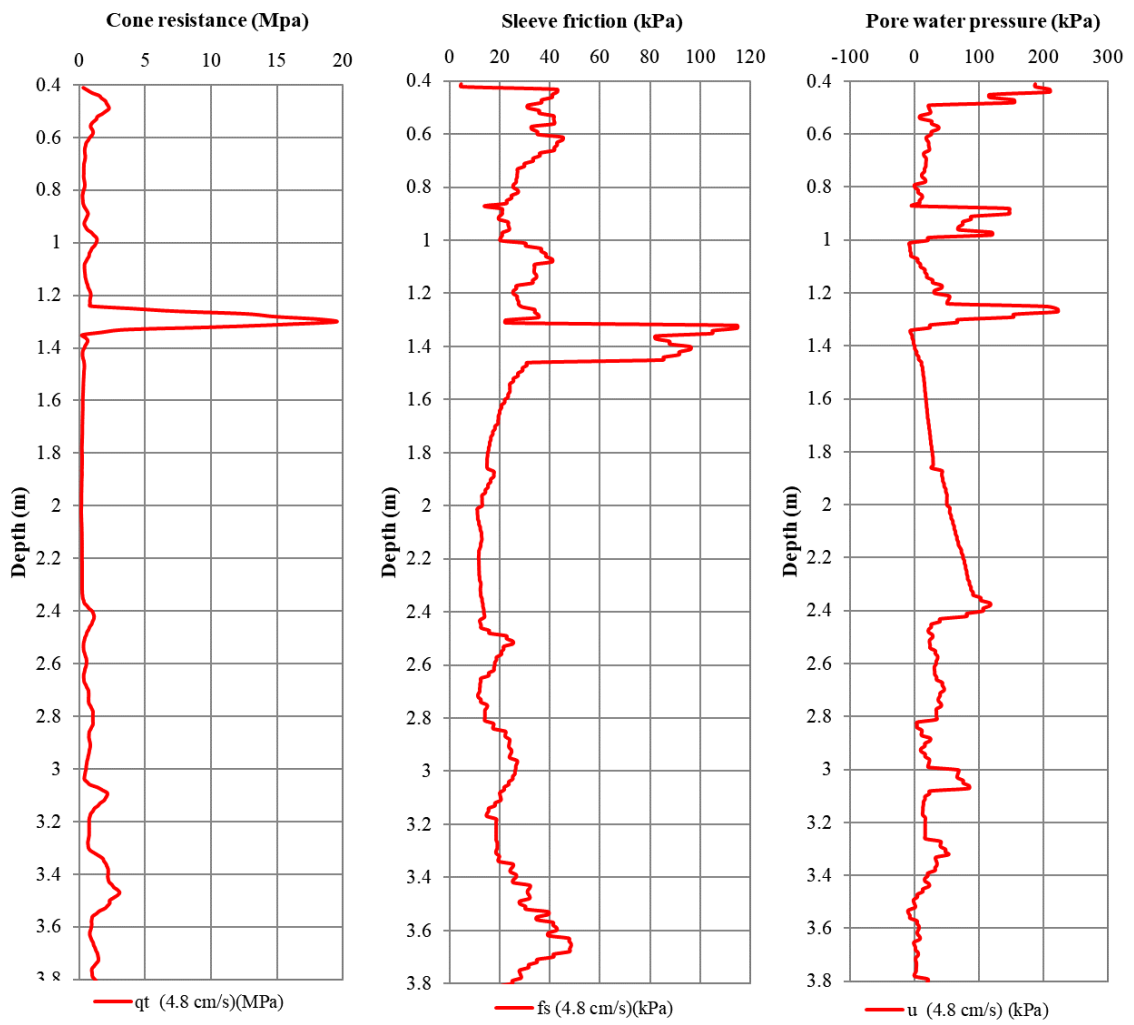


Figure 28: Piezocone test results, site “North”, penetration rate=4.8 cm/s.

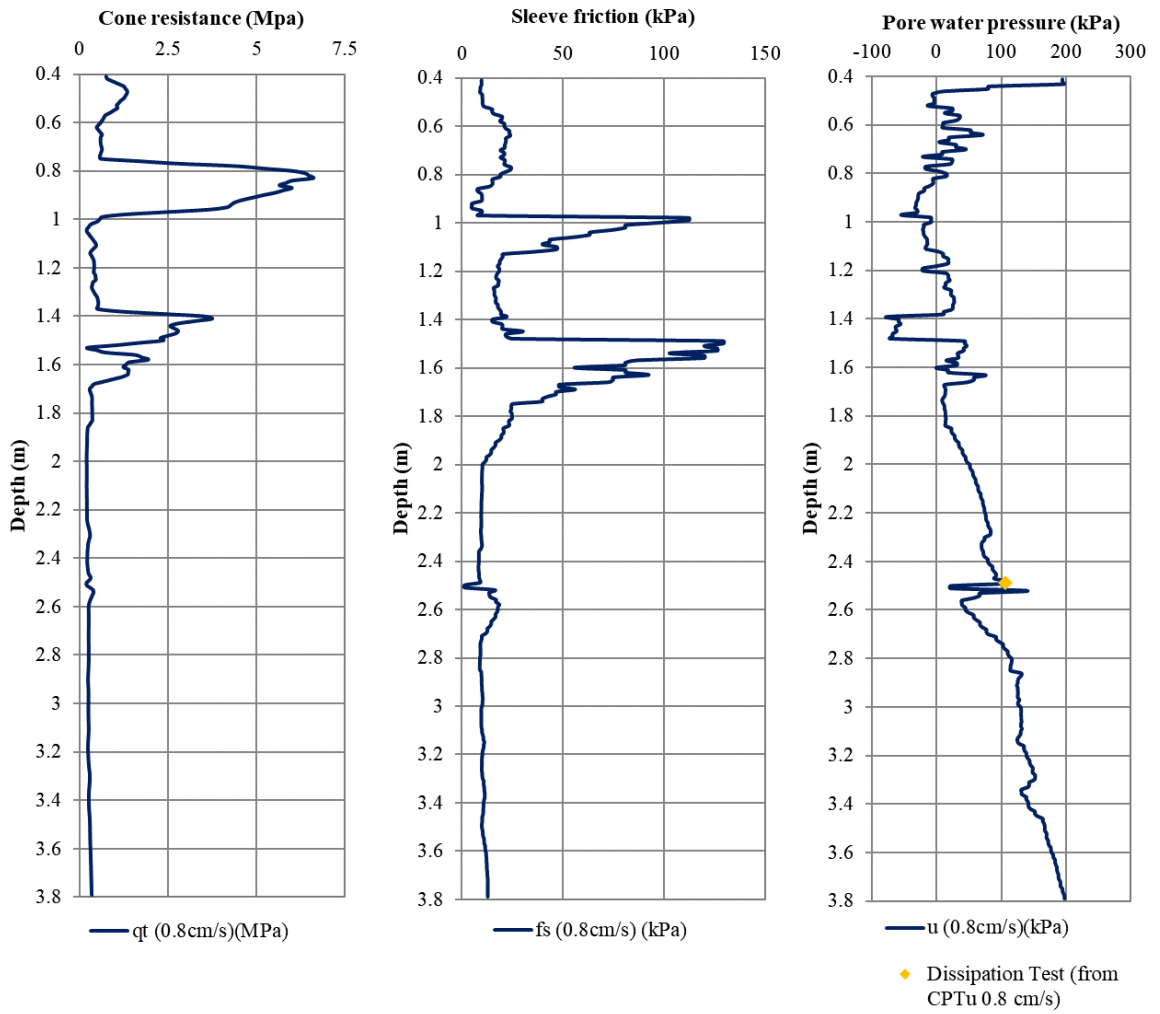


Figure 29: Piezocone test results, site “South”, penetration rate=0.8 cm/s.

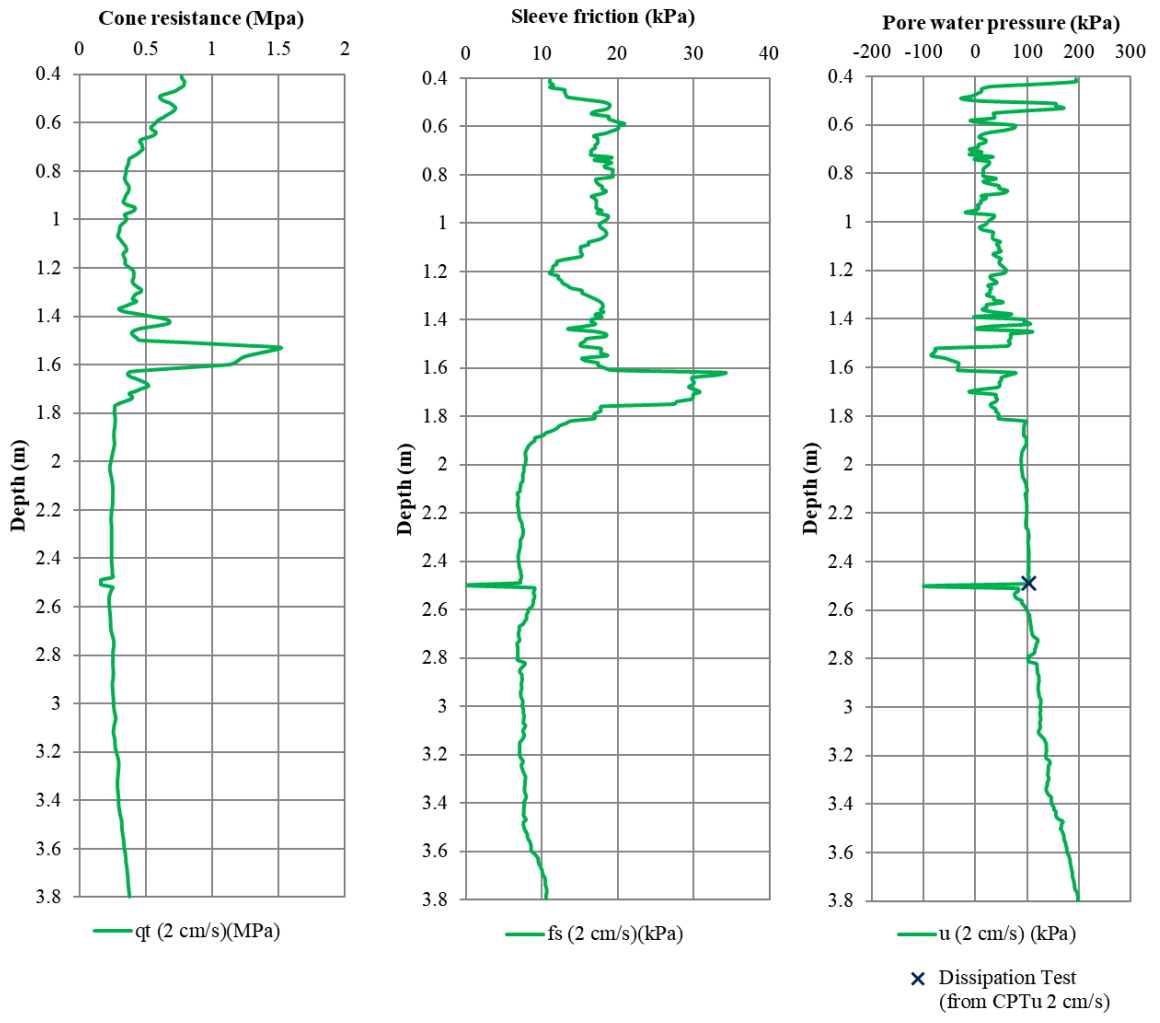


Figure 30: Piezocone test results, site "South", penetration rate=2 cm/s.

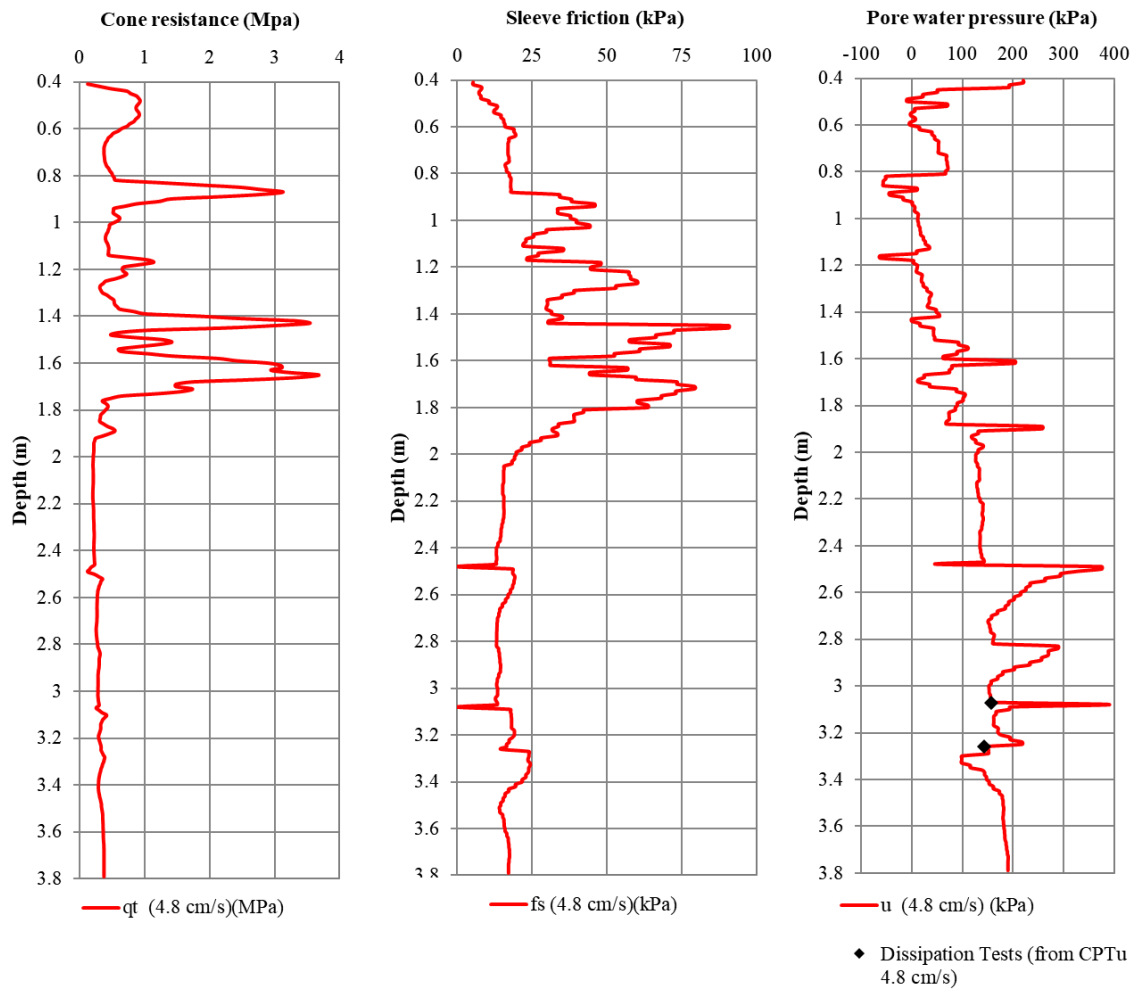


Figure 31: Piezocone test results, site “South”, penetration rate=4.8 cm/s.

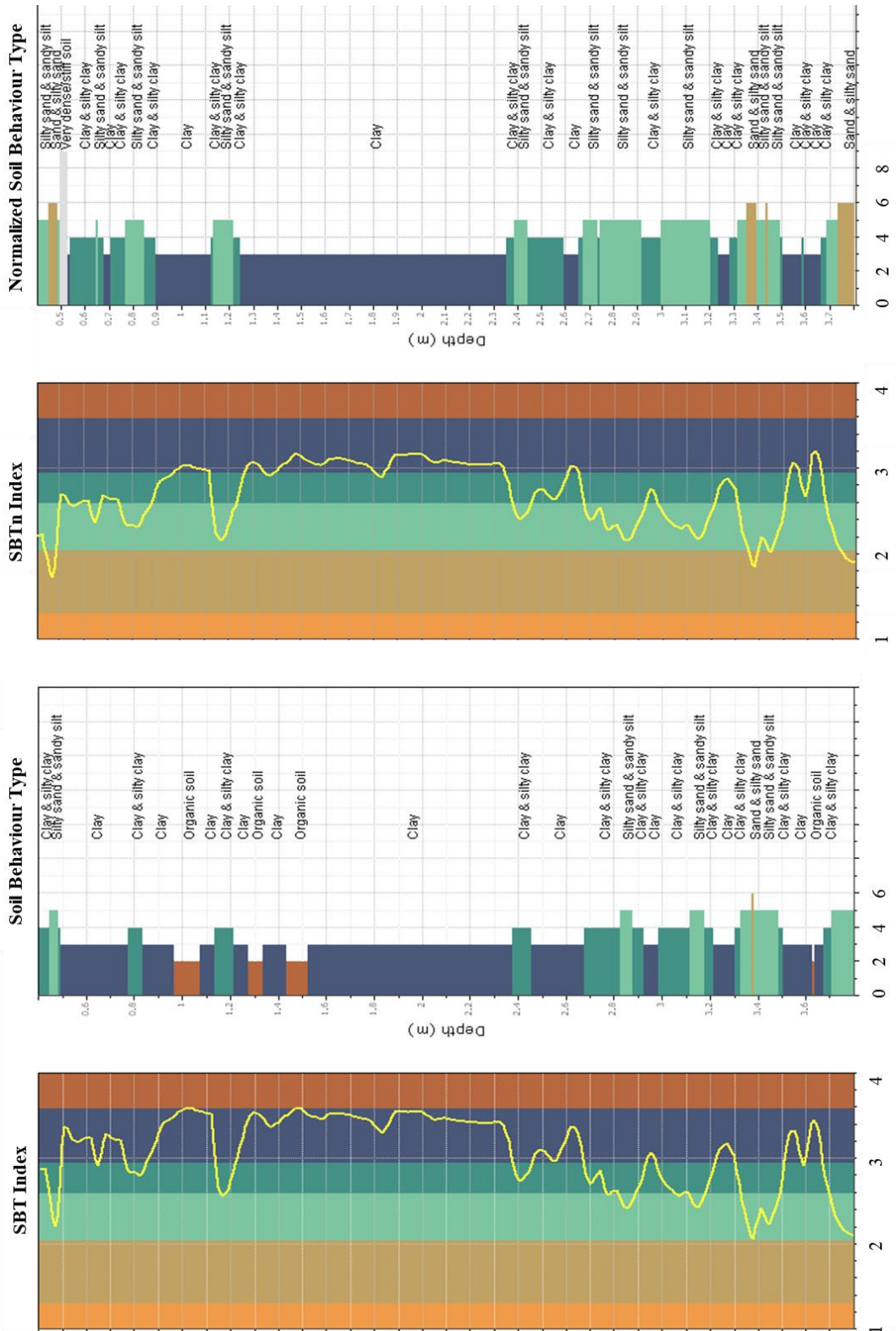


Figure 32: SBTn Classification (Robertson 1990) and SBT Classification (Robertson, 2010) at site "North" for the standard penetration rate $v=2$ cm/s.

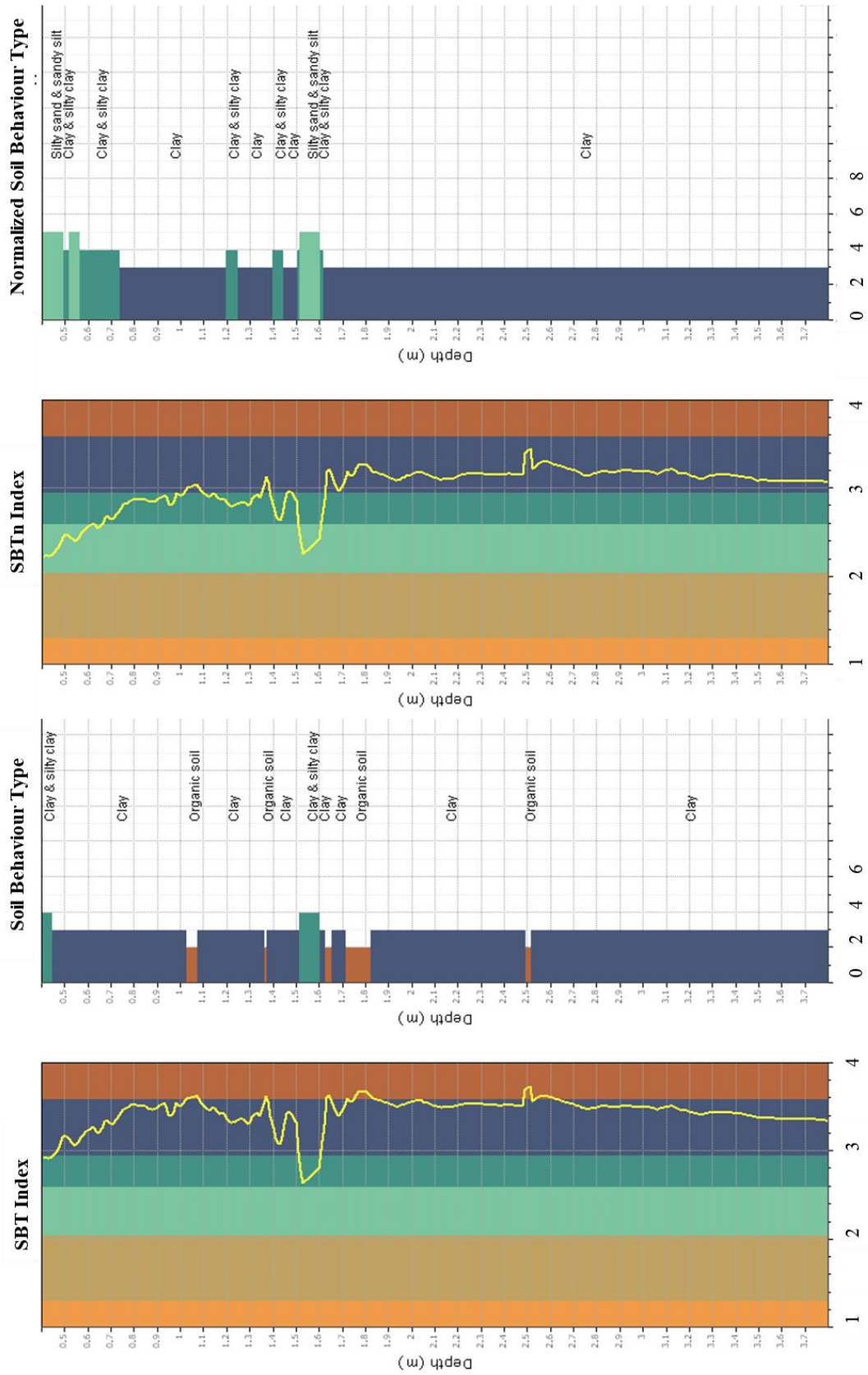


Figure 33: SBTn Classification (Robertson 1990) and SBT Classification (Robertson, 2010) at site “South” for the standard penetration rate $v=2$ cm/s.

6.1.1.3 Analyses of piezocone test results

The interpretation of CPTu tests for “special soils” like dredged sediments has to be inferred, as a general rule, with reference to near boreholes.

In particular in this case the SBT classification identifies the following layers:

- A first superficial layer, very heterogeneous, characterised by I_c values between 2.60 and 3.60 (clays and silt mixture), with the presence of thin layers of sand and silty sand (I_c values between 1.31 and 2.05);
- A second clay layer, between 1.2 and 2.4 meters at North location, and 1.5m and 3.8 m at South location, interbedded with layers of very soft soils or sands;
- A third deeper layer at the North location, very heterogeneous, with the presence of silt mixtures and sand mixtures (I_c values between 2.05 and 2.95)

The SBTn classification results for the second layer are in contrast with the classification carried out on the extracted samples. The Osterberg samples have been extracted from the layer described by the SBT classification as “clay”, but the laboratory classification identifies the soil as “silt with clay”. This is most probably due to the low penetration resistance recorded in this layer.

The presence of a superficial vadose zone and the high heterogeneity of the soils in this first layer, lead to a difficult comparison between the tests conducted at different penetration rates.

The diagrams below displayed show the comparison of the CPTu test results between 1.5 and 2.4 meters for the North location and between 1.8 and 3.8 meters for the South location (“silt with clay” layer). The position of the dissipation tests is also showed.

Looking at the site South results (Figure 35) we can observe that as the penetration rate increases pore water pressure increases. We also observe differences in f_s values, whereas differences in penetration resistance are negligible. The same trend can be recognized in Figure 33 where measured data, between 2 and 3.6 meters, are plotted against the penetration rate.

The SBTn (Robertson,1990) and SBT (Robertson, 1986 and 2010) classification is showed in Figure 35 and Figure 36: data are grouped inside the zone number 3 (clay to silty clay), in the first case, and zone number 2 and 3 (clays and organic material), in the second case. Differences due to penetration rate are especially pronounced in the Robertson (1986) chart, where data are displayed along a horizontal line due to little changes in tip resistance and higher differences in friction ratio.

The differences in q_t , f_s and u profiles for the three tests carried out at site North are shown in Figure 38 (depth of 1.5 and 2.4 m) and Figure 40 (depth of 2.4 and 4 m). Figure 38 and Figure 40 show the average values in the range 1.6-2.3 m and 2.4-3.2 m. In this case the obtained results show different profiles that are not consistent with those due to penetration rate changes inside the partially drained range. The observed changes in q_t , f_s and u profiles can suggest that

the middle rate of 2 cm/s represents the balance between consolidation effects and viscous effects.

SBT and SBTn classification charts between 1.6 and 2.3 meters characterize the soil as belonging to zones 3 and 2 as far as the Robertson (1986) and (2010) classification is concerned (Figure 42). In the case of Robertson (1990), data plot inside the zone 3 in the Q-F chart, while in the Q-Bq plot data are located inside zone 3 and 4 (Figure 41). Therefore, the Q-Bq plot represent the most reliable instrument, since correctly identify soil classification.

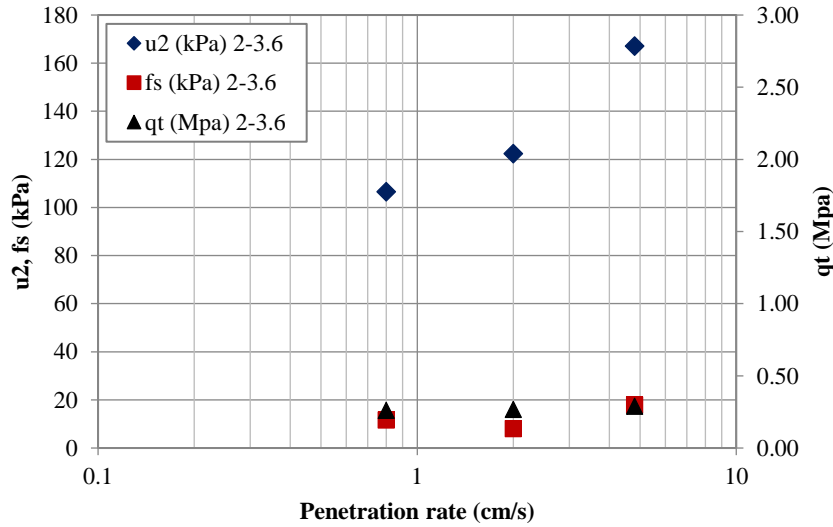


Figure 34: Comparison of CPTu measurements, tip resistance, pore water pressure and friction sleeve, over penetration rate, for the soil layer between 2 and 3.6 meters – south location.

The coefficient of consolidation has been evaluated from dissipation tests as well as oedometer tests. Dissipation tests have been interpreted following the model proposed by Teh and Houlsby (1991), identifying the elapsed time corresponding to the 50% dissipation of the excess pore water pressure generated during penetration:

$$c_{vh} = \frac{T_{50} \cdot a_c^2 \cdot \sqrt{I_r}}{t_{50}}$$

where: a_c is the probe radius, $I_r = \frac{G}{s_u}$ is the rigidity index of the soil, t_{50} is the elapsed time corresponding to the 50% of excess pore water pressure dissipation and $T_{50} = 0.245$ is the time factor corresponding to the 50% of dissipation for u_2 measurements. The rigidity index has been evaluated from triaxial tests and is equal to 45.

The coefficient of consolidation inferred from the dissipation tests is around $8.7 \cdot 10^{-8} \text{ m}^2/\text{s}$. The estimates of the vertical coefficient of consolidation from Osterberg samples, using the Casagrande's method, are equal to $6.5 \cdot 10^{-8} \text{ m}^2/\text{s}$ and $7.4 \cdot 10^{-9} \text{ m}^2/\text{s}$.

The non-dimensional velocity, V , can be evaluated as:

$$V = \frac{v \cdot d}{c_v}$$

For v values of 0.8, 2 and 4.8 cm/s and a standard piezocone, V is in all the cases much higher than 1000. Therefore, tests are on the right side of the transitional velocity between partially drained and undrained conditions and what we are observing is probably due to viscous effects.

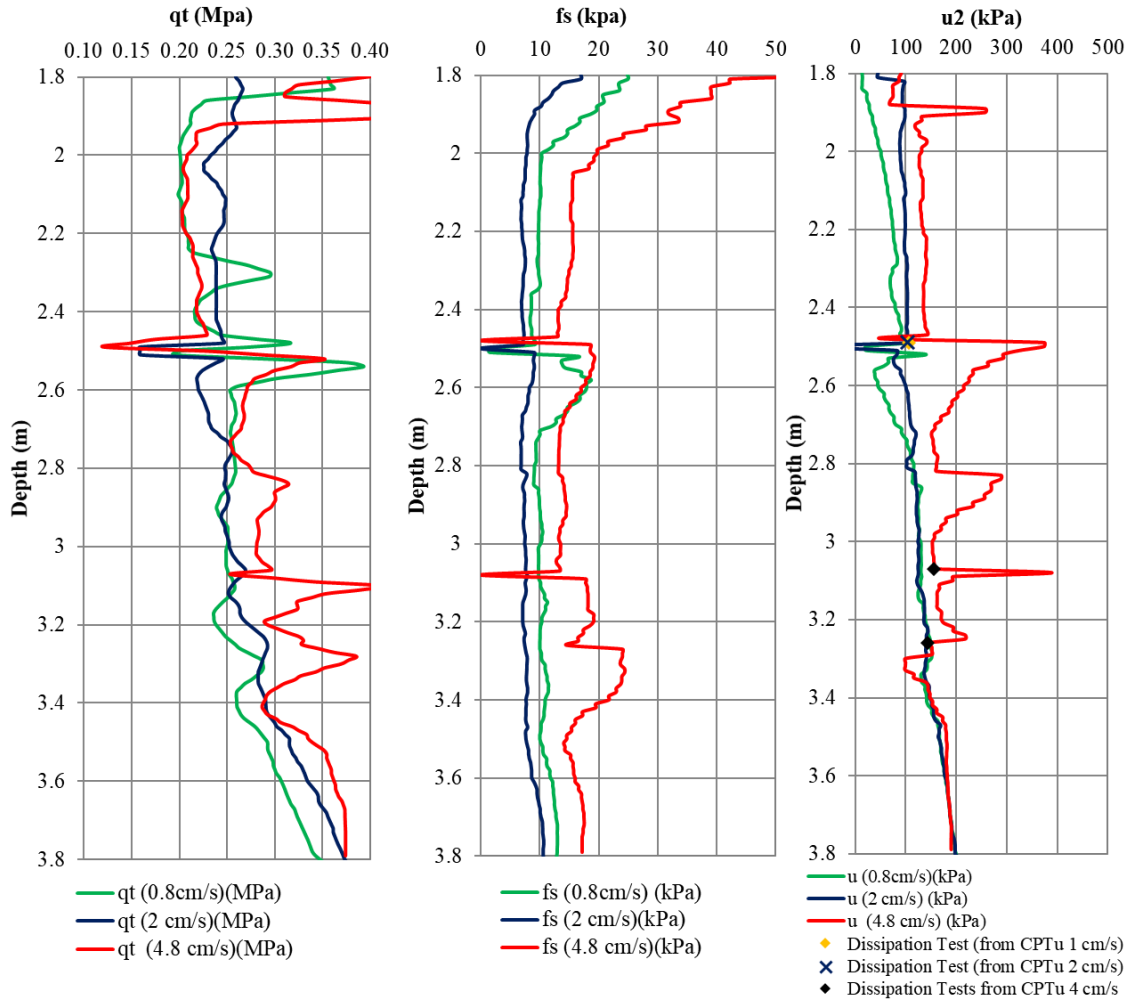


Figure 35: CPTu results at south location for three different rates (0.8 cm/s, 2 cm/s, 4.8 cm/s) and position of dissipation tests.

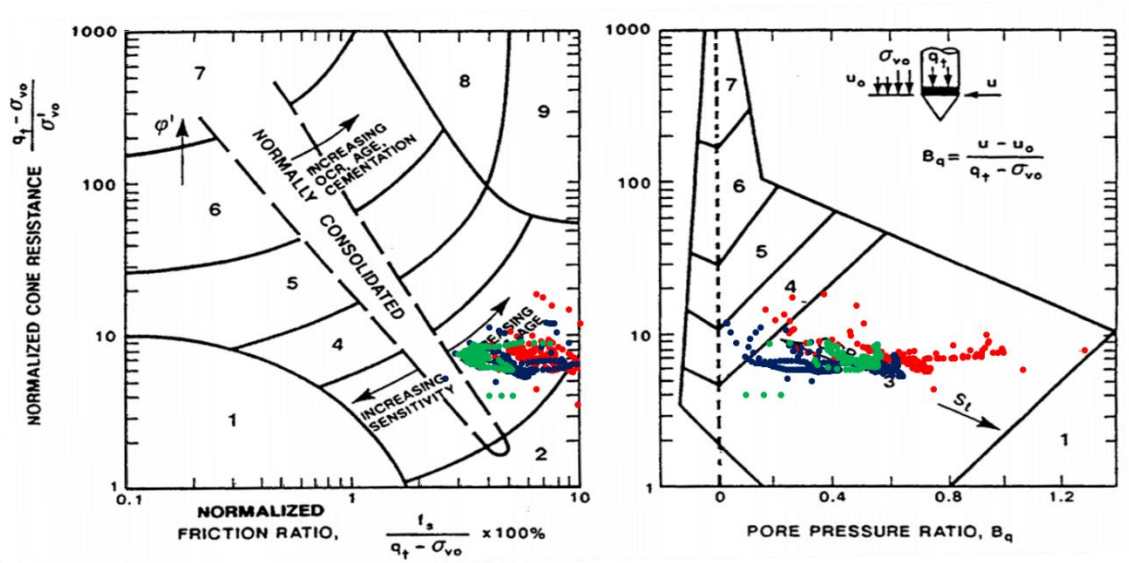


Figure 36: Robertson (1990) SBTn classes for soil layer between 1.8 m and 3.8 m, south location.

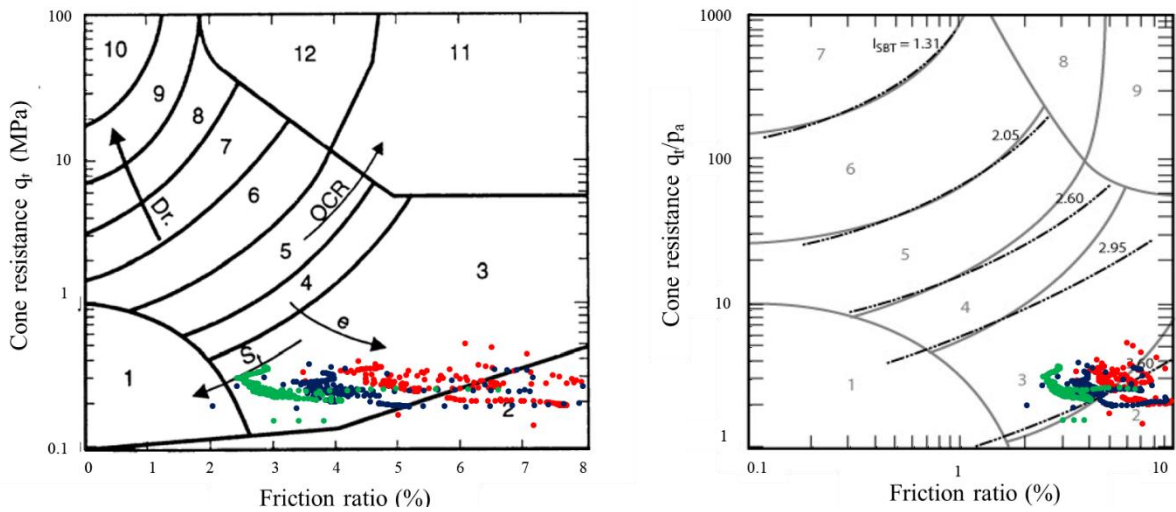


Figure 37: Robertson (1986) and Robertson (2010) SBT classes for soil layer between 1.8 m and 3.8 m, south location.

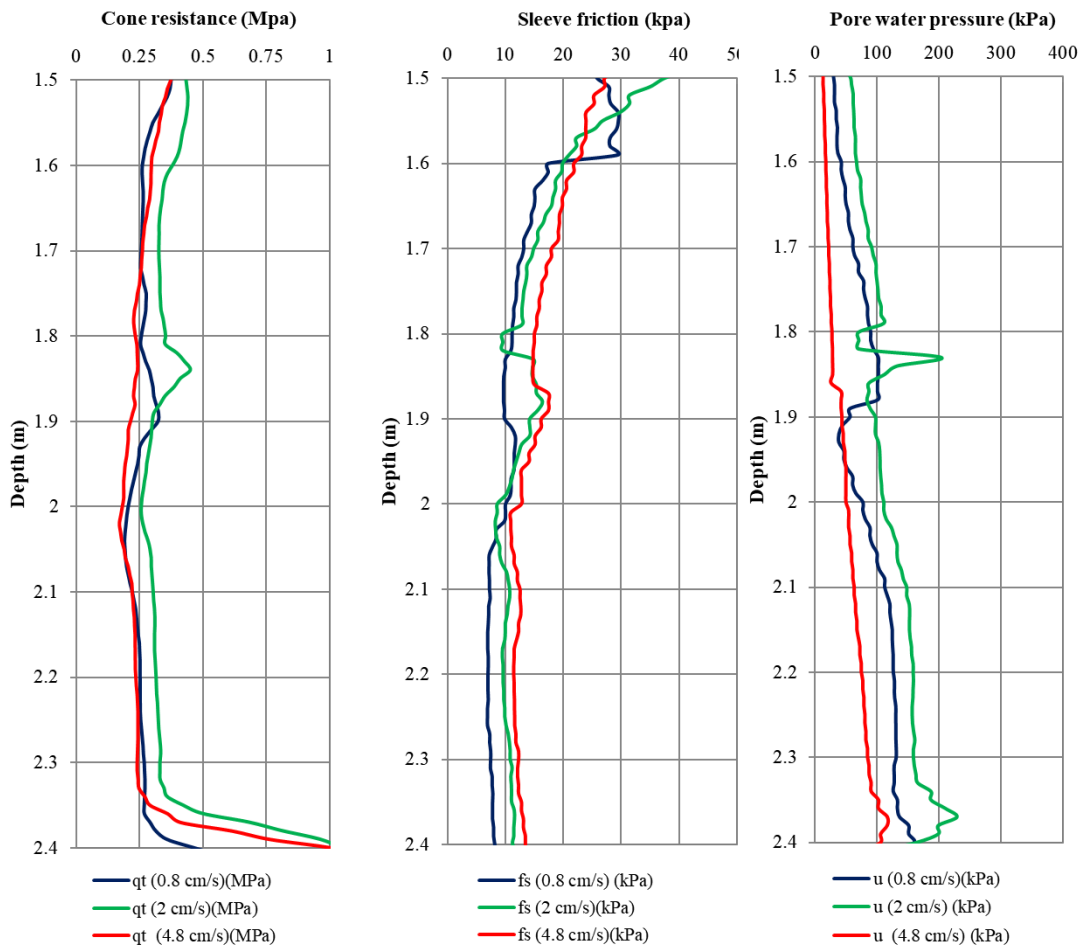


Figure 38: CPTu results in the north location (depth 1.5 m- 2.4 m) for three different rates (0.8 cm/s - green line, 2 cm/s-blue line, 4 cm/s-red line).

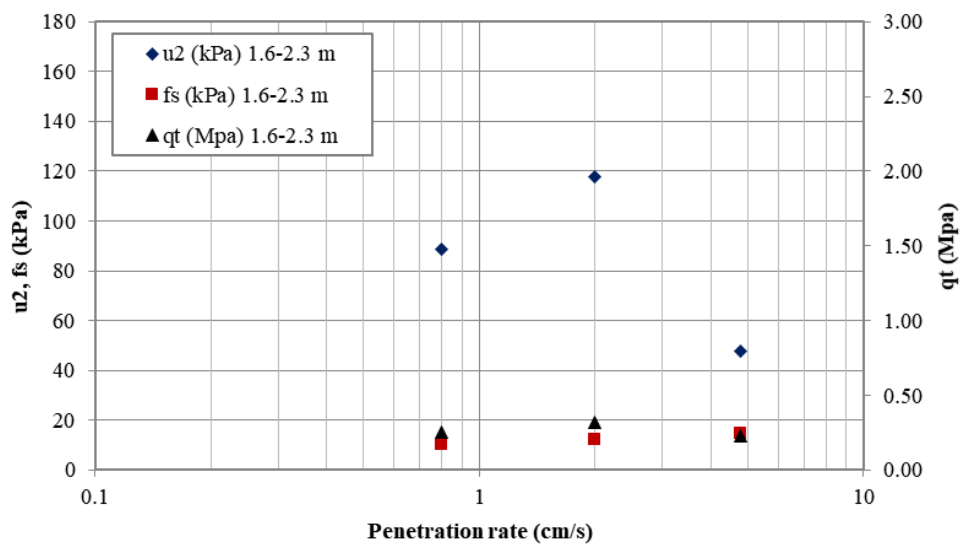


Figure 39: Average values of tip resistance, side friction and pore water pressure between 1.6 and 2.3 meters, north location, over penetration rate.

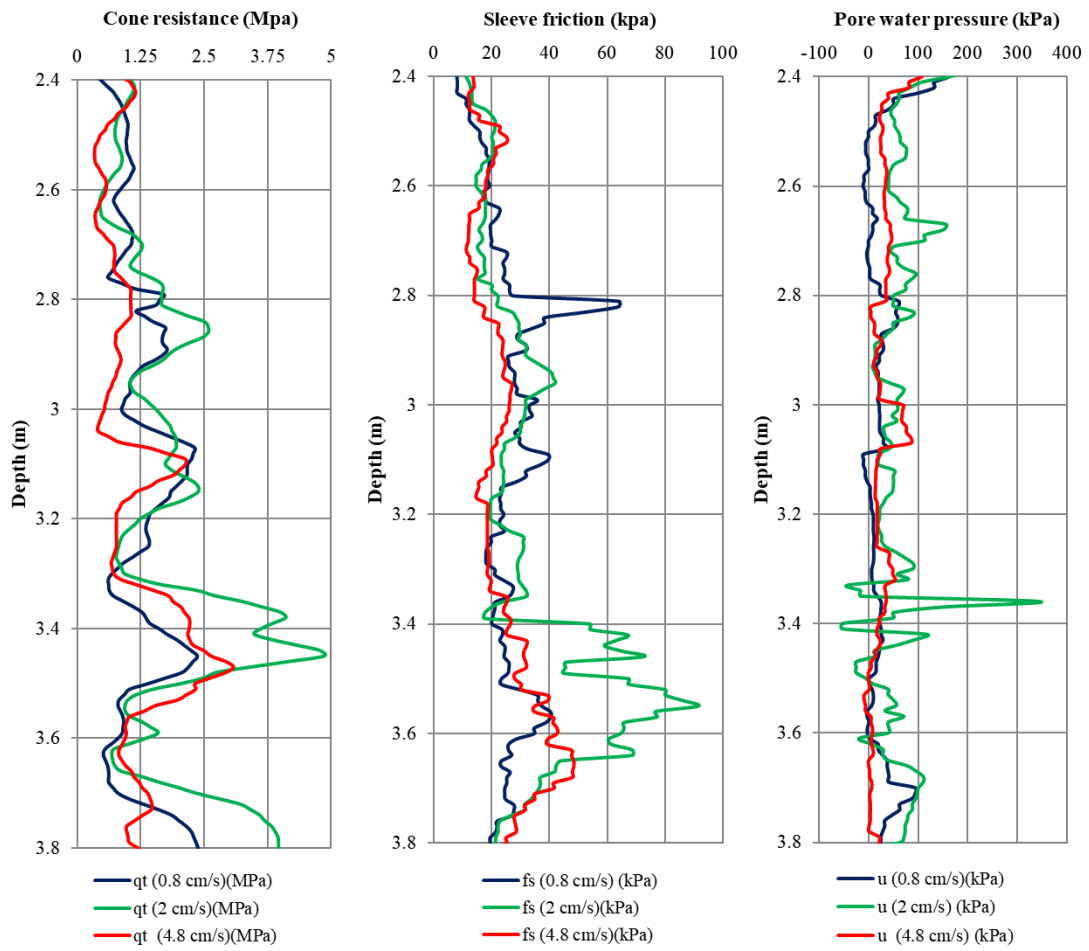


Figure 40: CPTu results at north location for three different penetration rates (depth 2.4 m- 3.8 m).

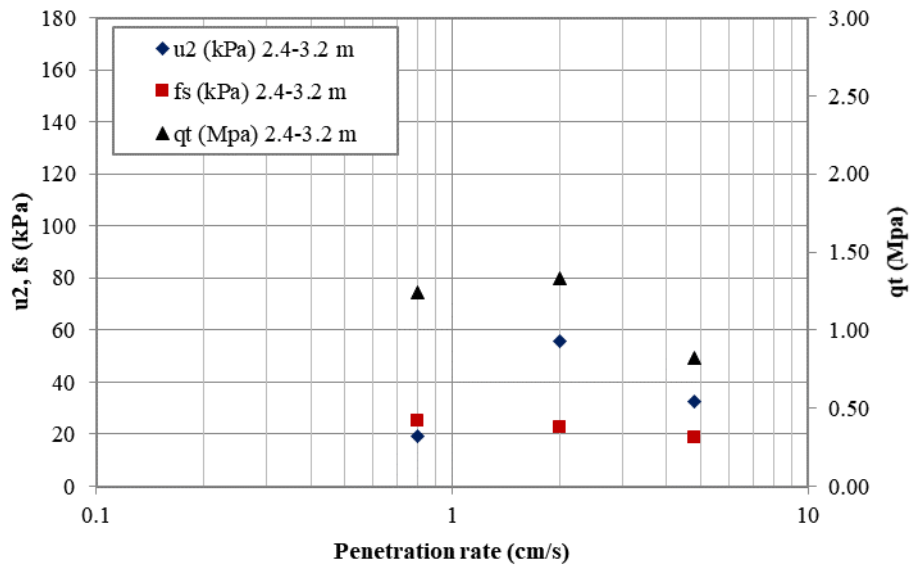


Figure 41: Average values of tip resistance, side friction and pore water pressure between 2.4 and 3.2 meters, north location, over penetration rate.

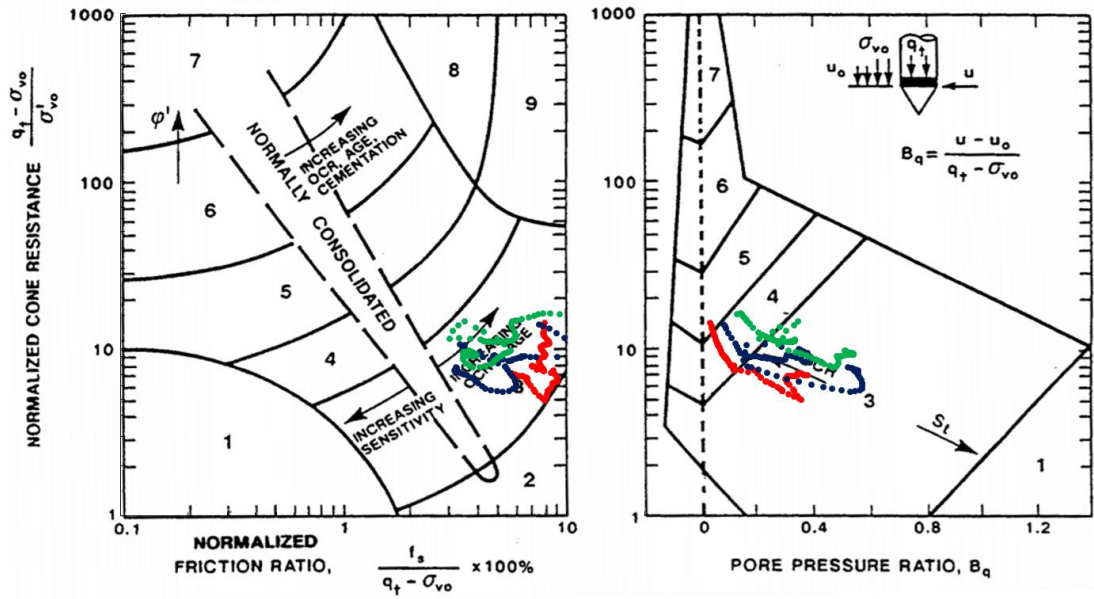


Figure 42: Robertson (1990) SBTn classes for soil layer between 1.6 m and 2.3 m, north location.

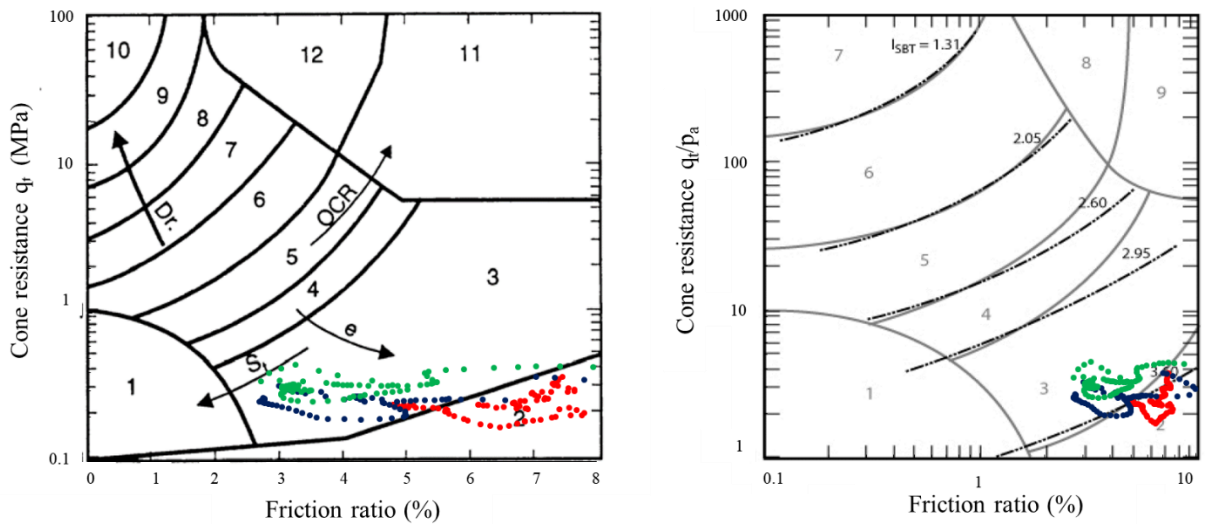


Figure 43: Robertson (1986) and Robertson (2010) SBT classes for soil layer between 1.6 m and 2.3 m, north location.

6.2 Identification and characterisation of alluvial soil deposits in Pisa delta area

The subsoil of Pisa belongs to the alluvial (Holocene-Pleistocene) deposits of the Arno River. The first 60 m are characterised by the following profile (Lo Presti et al., 2003):

- Horizon A: upper variable deposits from 3 to 10 meters, consisting of silt, clay and sand of various thickness. The main characteristic of this horizon is that the sediments have been deposit in an estuarine environment, in salty water;
- Horizon B: clayey deposits from 10 to 40 m, subdivided in four sub-layers:
 - High plasticity marine clay. It is a soft sensitive clay called Pancone clay,
 - Intermediate clay and sand layers, similar to the deposit of Horizon A,
 - Soft clay similar to Pancone;
- Horizon C: lower sand deposits from 40 to 60 m, consists of eolian sands with inter-layers of silt and clay.

The CPTu tests have been carried out in Pisa in the “Porta a Mare” district, up to a depth of 6.5 meters. The stratigraphic profile, inferred from a reference borehole, up to 7.8 meters coincides with the “Horizon A” typical of the Pisa area. It is characterised by a first layer of sandy silt from 1 to 3 meters, a second layer of silty clay from 3 to 5 meters and a third layer of clay from 5 to 7 meters. Below this layer sand is present from 6.8 m to 7.8 meters (Grey sands).

The tests have been conducted using a standard piezocone and a mini-piezocone (Figure 68) with a projected tip area of 2 cm², whereas the standard projected tip area is 10 cm². This device allows reducing the value of the non-dimensional velocity, V , not only with the reduction of the penetration rate, but also thanks to a reduced tip diameter. More details on this device will be given in the following chapter.

Tests have been conducted by following the scheme showed in Figure 51: nine CPTu tests conducted at two different penetration rates (0.5 and 2 cm/s).

Dissipation tests have been carried out too.

The distance between each test is around 50 cm. The limits of the penetration rate range are due to two factors: the first is the thrust system used in common practice (13.5 kW hydraulic engine) that influences the lower limit; the second is the possibility of instability phenomena of the rods (more slender in the case of a mini-penetrometer) and the possible damaging of the tip. In fact, a passing hole has been carried out for each test, to cross a first thin layer of 40 cm of man-made ground. For this reason, it was possible to have penetration rates up to 2 cm/s.

Besides, two more penetration tests with a standard piezocone and a standard penetration rate have been conducted. Figure 44, Figure 45 and Figure 46 show the results of the tests conducted with the minipiezocone at 0.5 cm/s. Figure 47, Figure 48 and Figure 48 show the results of the tests conducted with the minipiezocone at 2 cm/s.

Figure 49 shows the results of the standard piezocone test at 2 cm/s and the SBTn classification profile.

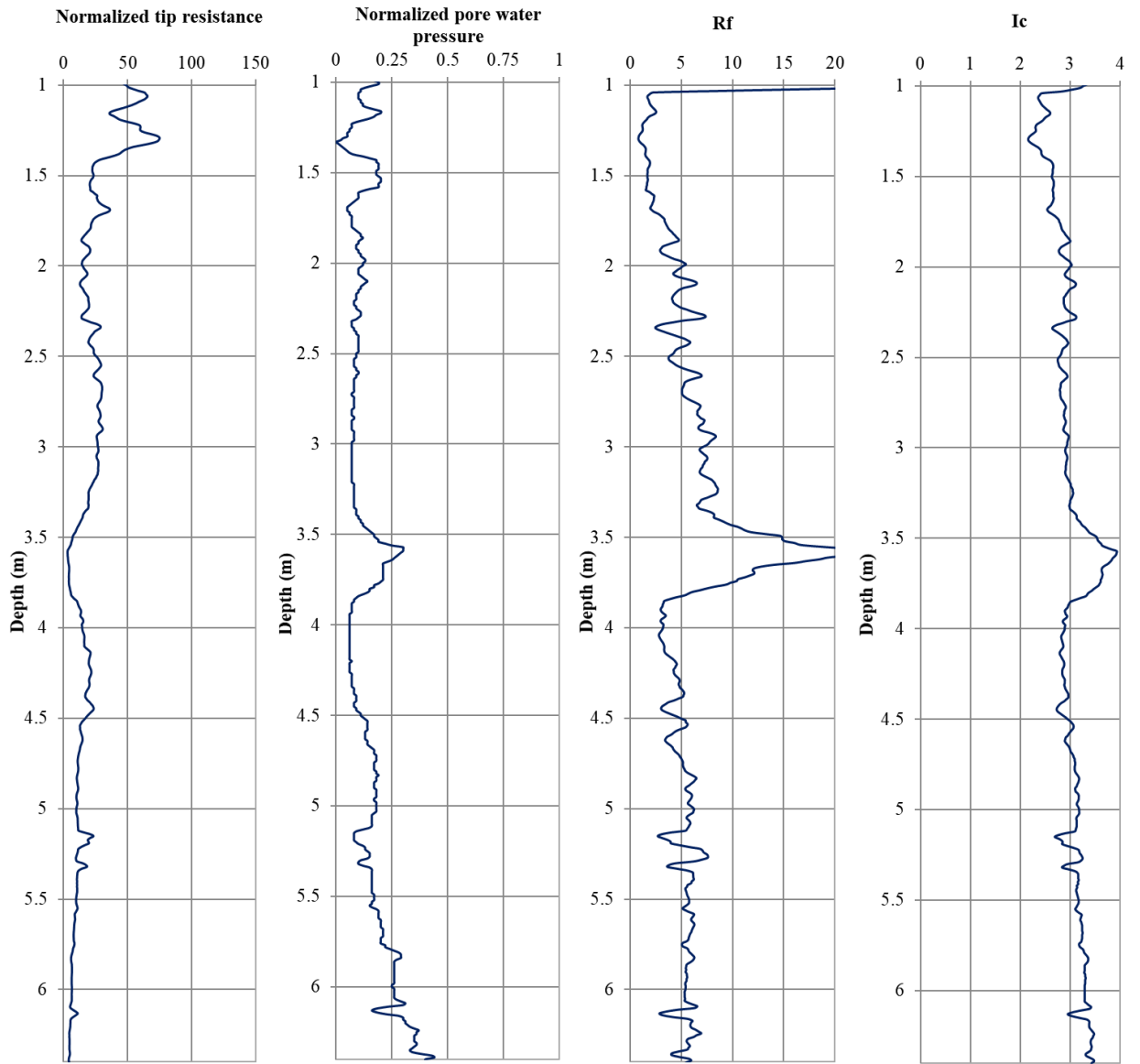


Figure 44: CPT1, minipiezocone at 0.5 cm/s.

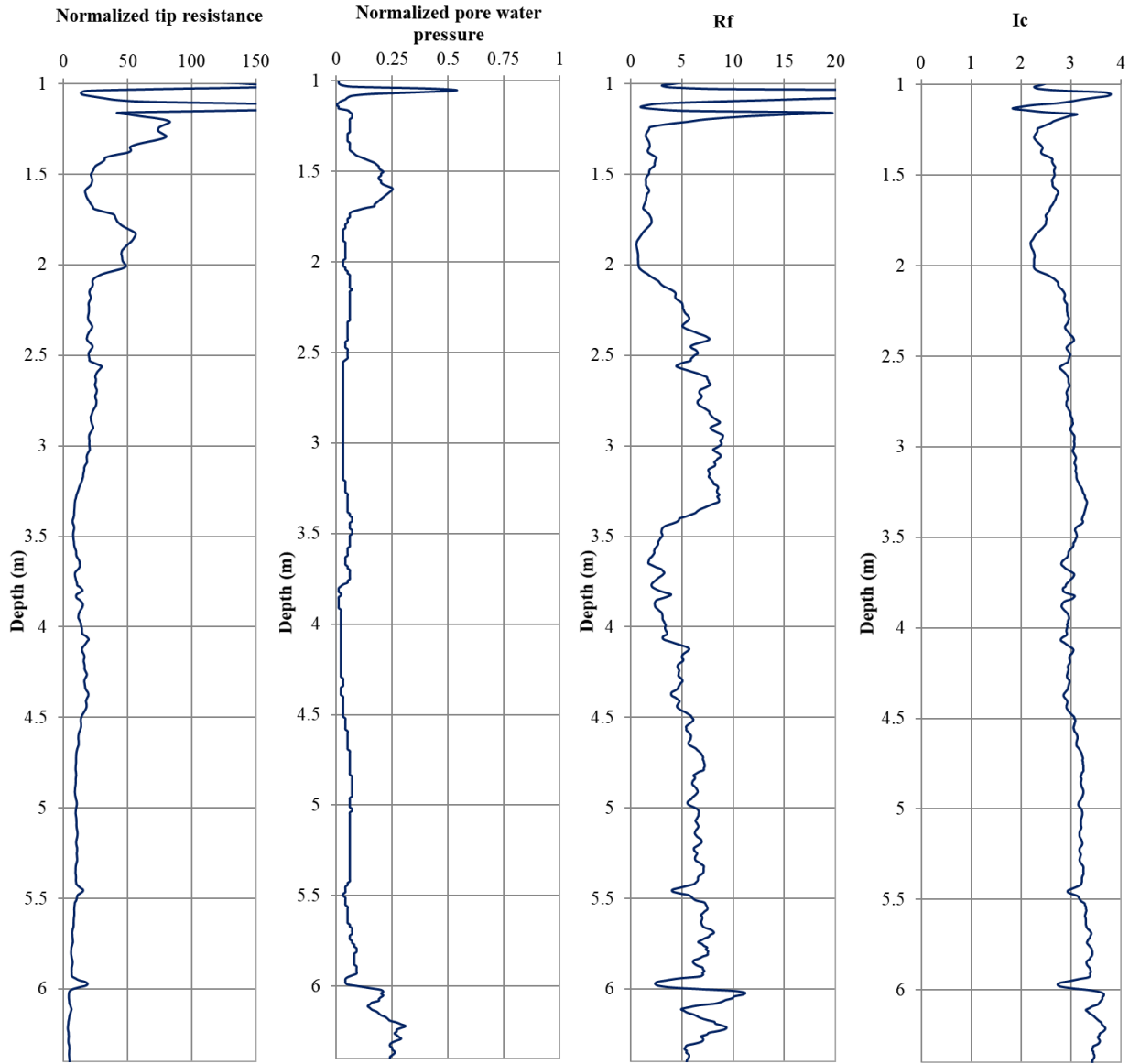


Figure 45: CPT2, minipiezocone at 0.5 cm/s.

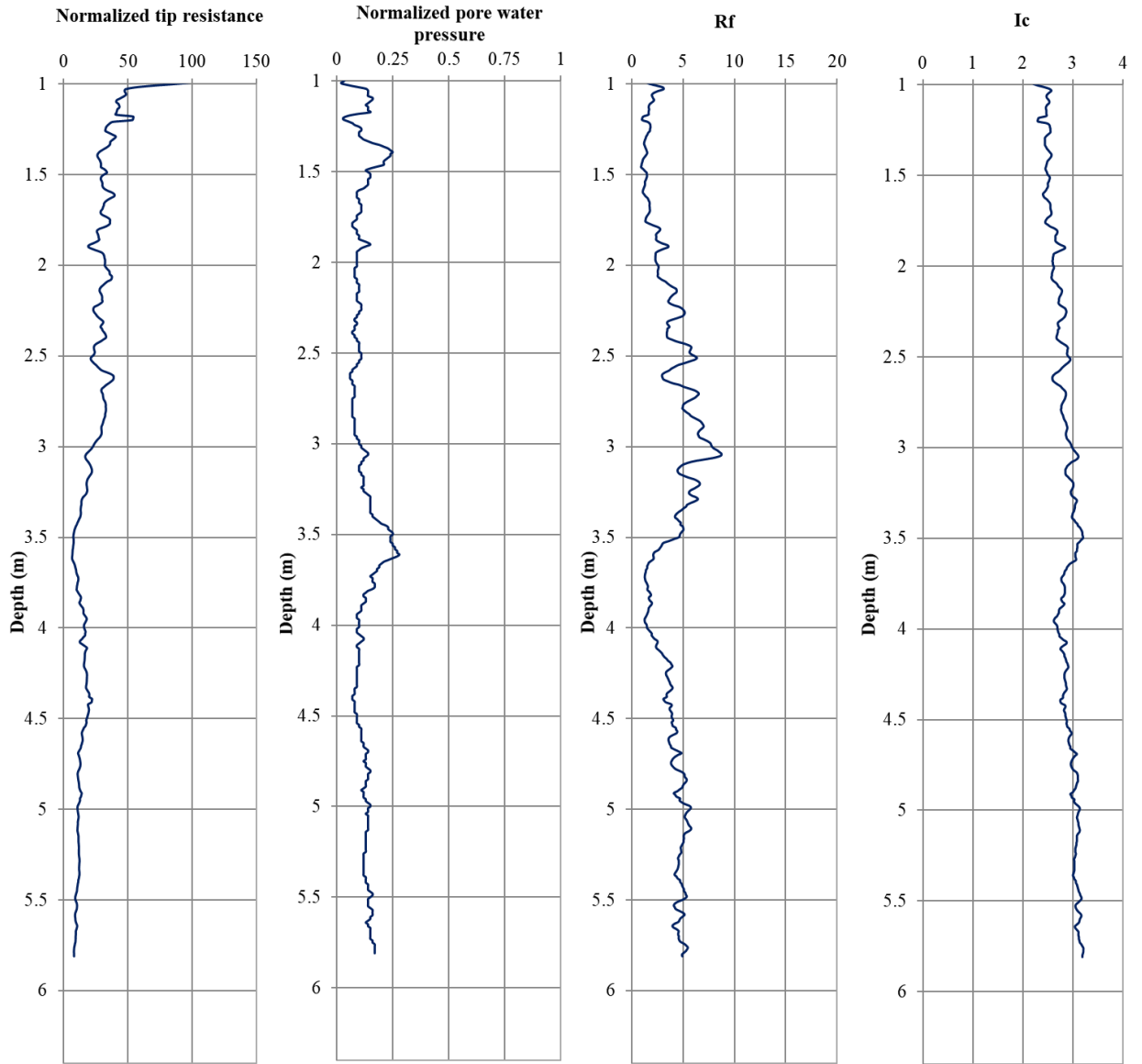


Figure 46: CPT9, minipiezocone at 0.5 cm/s.

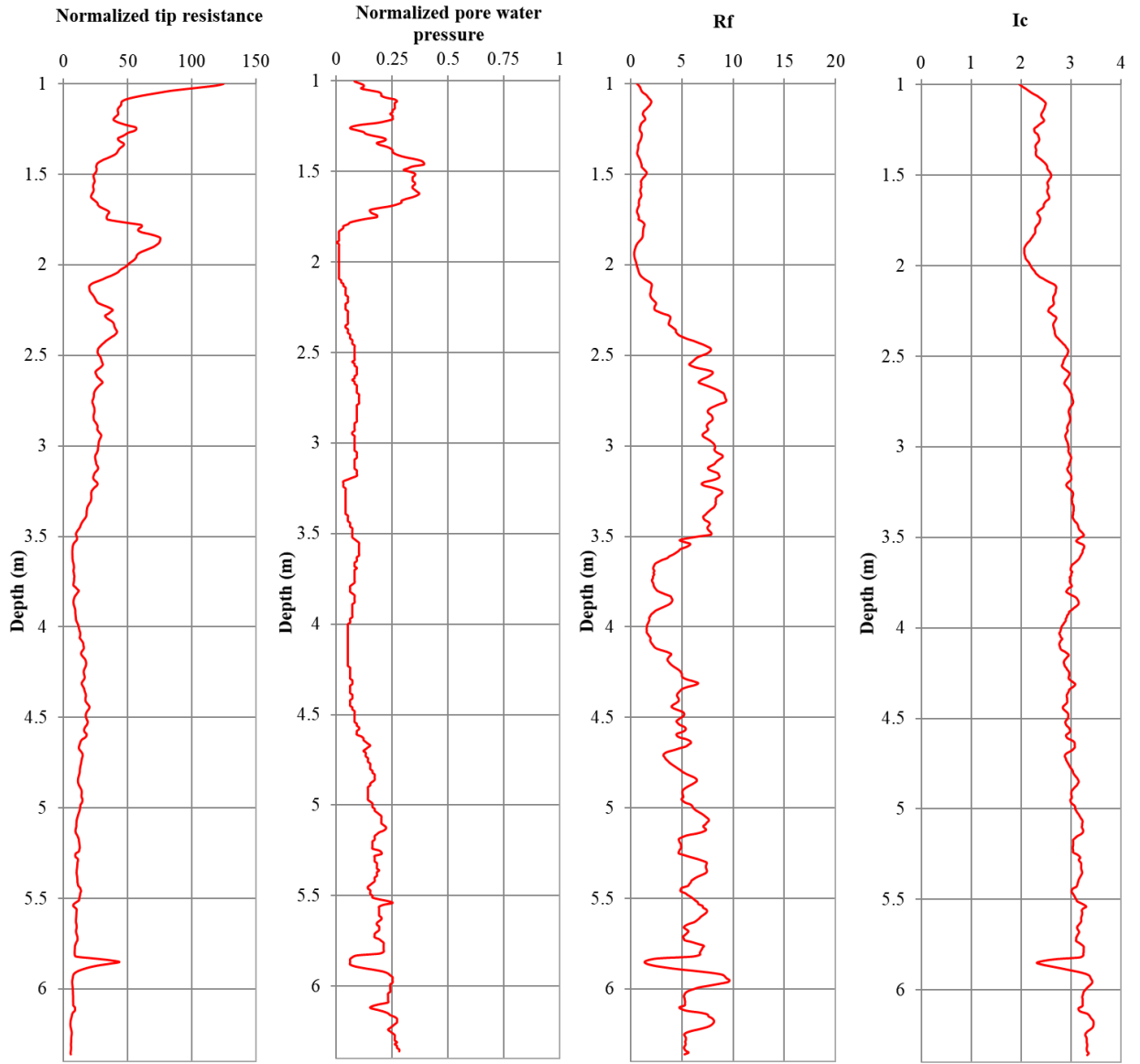


Figure 47: CPT6, minipiezocone at 2 cm/s.

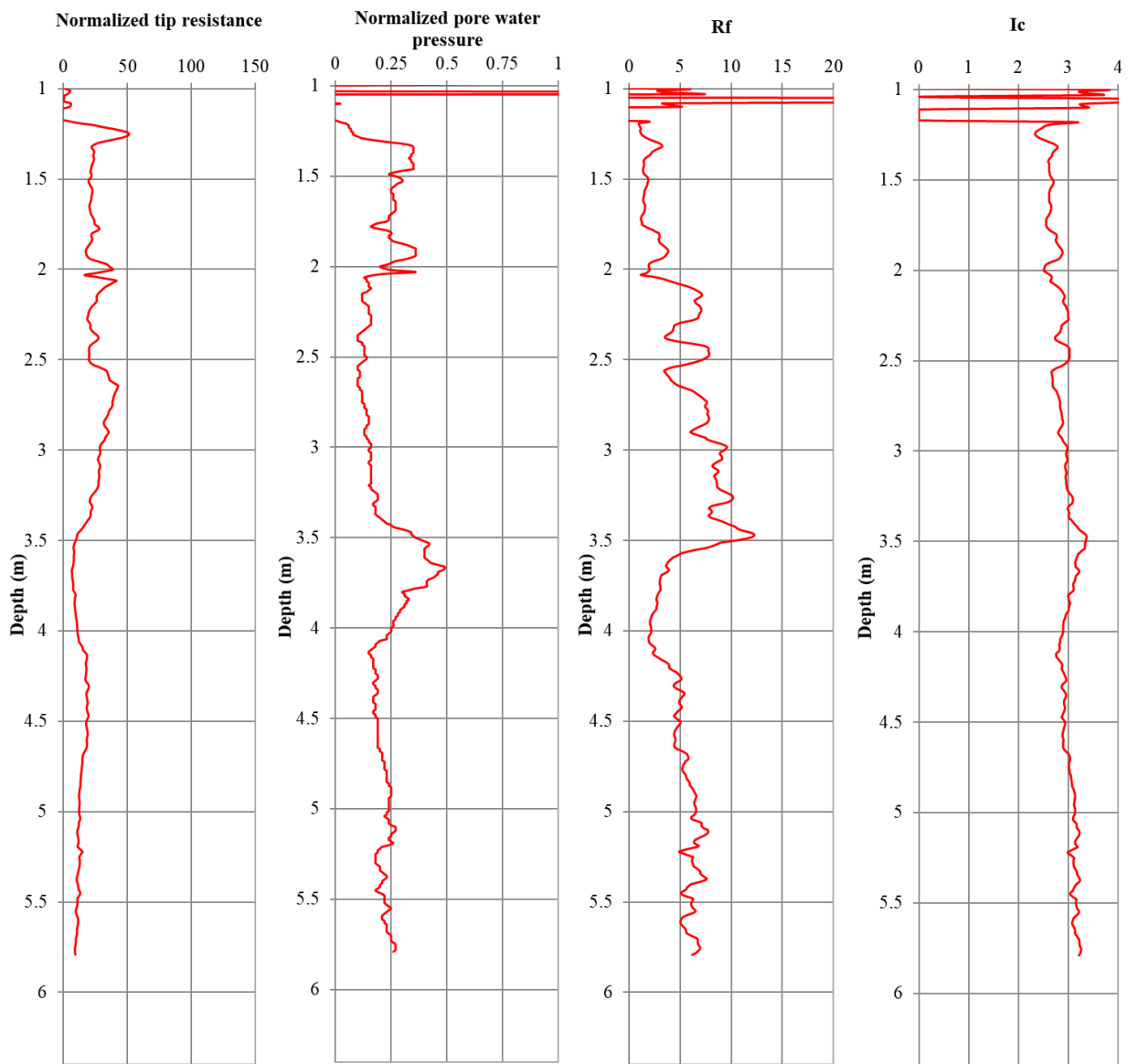


Figure 48: CPT8, minipiezcone at 2 cm/s.

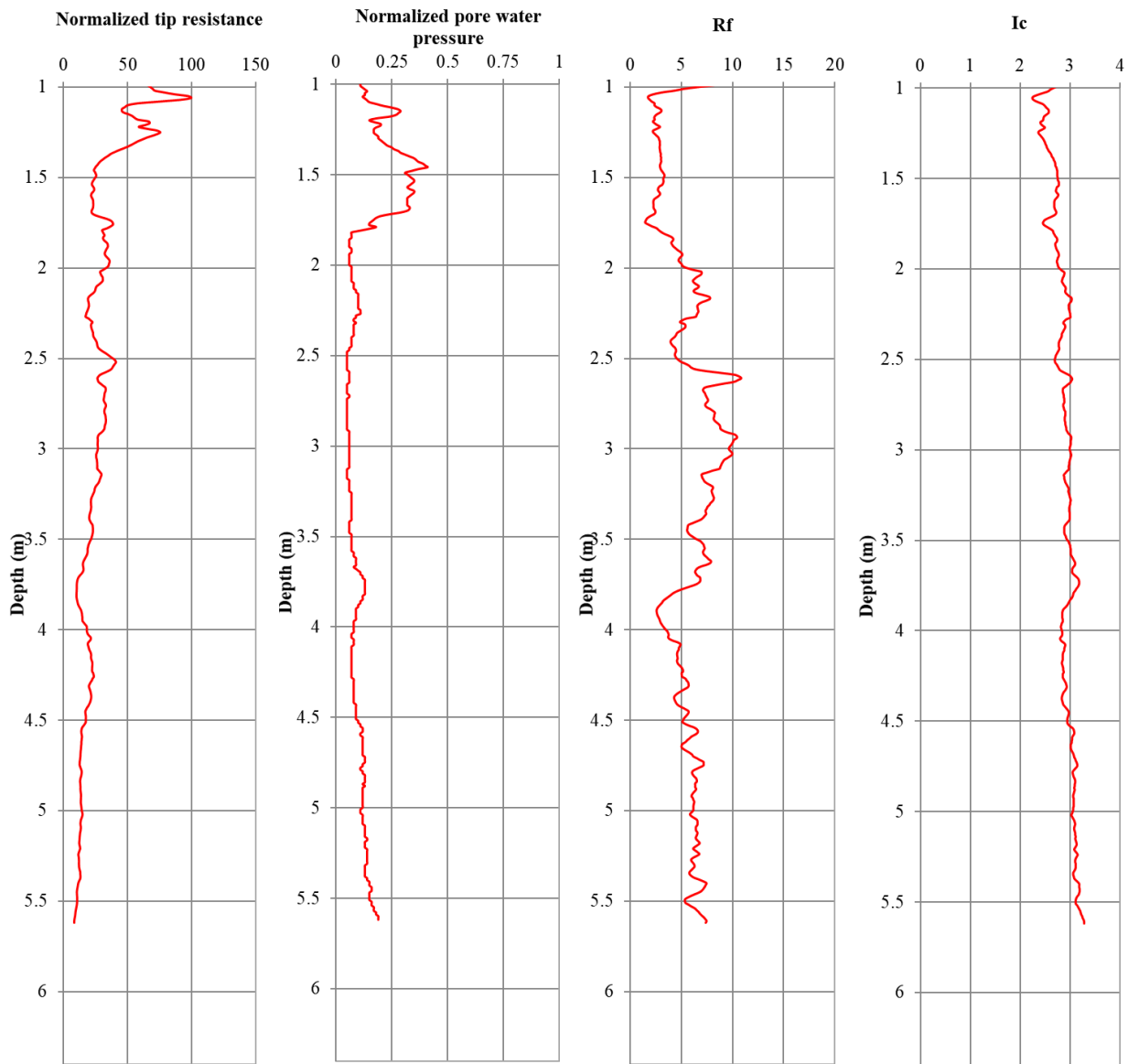


Figure 49: CPT5, minipiezcone at 2 cm/s.

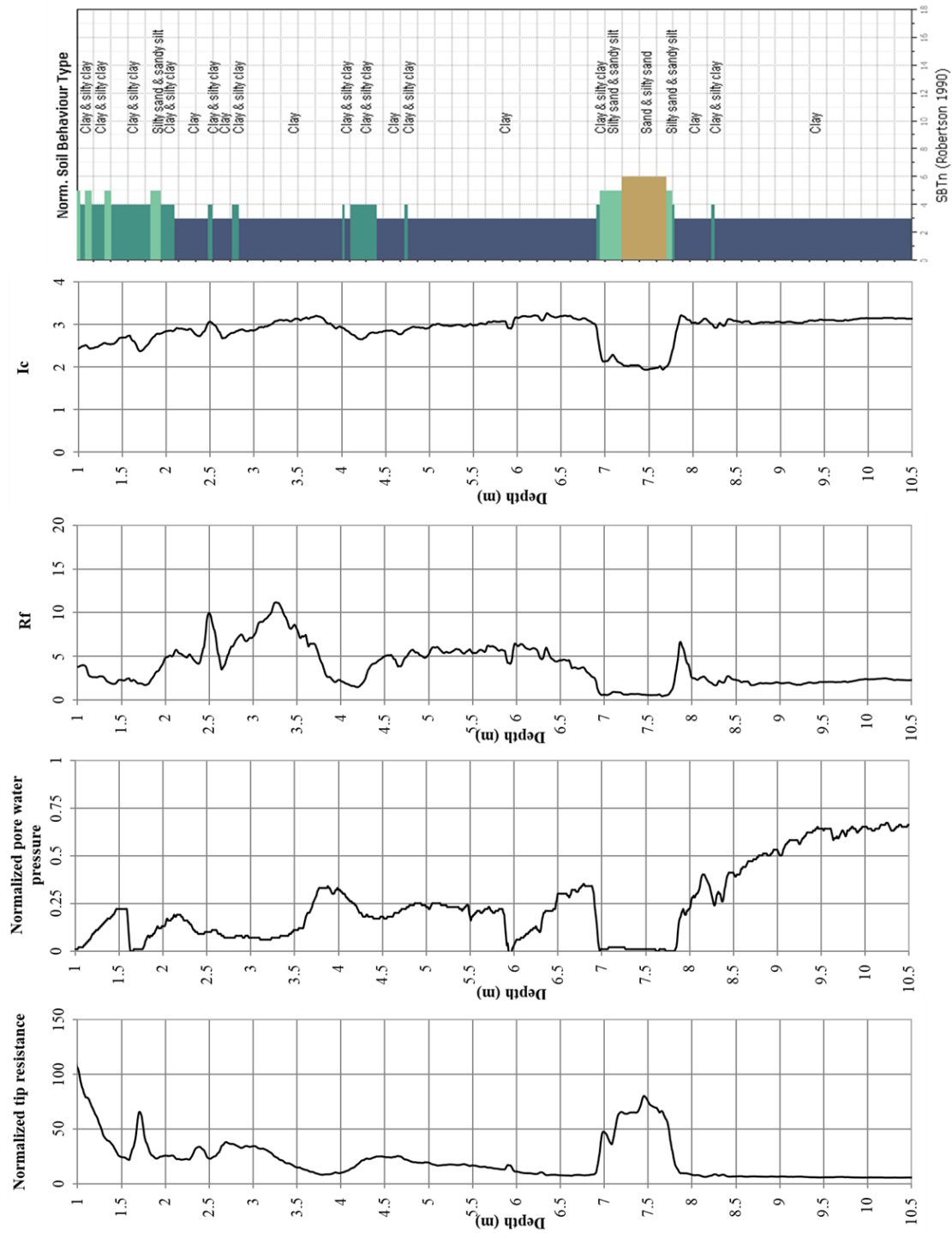


Figure 50: Standard piezocone test at 2 cm/s.

The SBT classification by Robertson (1990) is able to reproduce the stratigraphic profile, recognising correctly the sequence of silts and clays. Data plot in SBTn zone 3 (clay to silty clay), 4 (Silt mixtures), 5 and 6 (Sand mixtures and sands) (Figure 53). Figure 52 and Figure 53 show the comparison between the test conducted at the standard rate and the test conducted at 0.5 cm/s: it is possible to observe an average reduction of the measured pore water pressure

as the penetration rate is reduced. Furthermore, no significant differences are visible from the friction ratio chart, and the difference in the normalised tip resistance cannot be linked to the penetration rate changes.

Dissipation tests have been used to estimate the coefficient of consolidation of the soil.

Classification charts have been calibrated considering standard procedure and equipment. Changing one of these parameters can produce an erroneous soil class identification. Even though the classification chart proposed by Robertson (1990) well describes the stratigraphic profile, evaluated parameters cannot be considered reliable since the influence of drainage conditions on the measured data is unknown. The same consideration can be made for dissipation curves data. As mentioned previously, increasing partial drainage during the penetration leads to an overestimation of the time at which the 50% of initial pore water pressure is dissipated. An additional information can be achieved, plotting the data on the Schneider et al. (2008) classification chart.

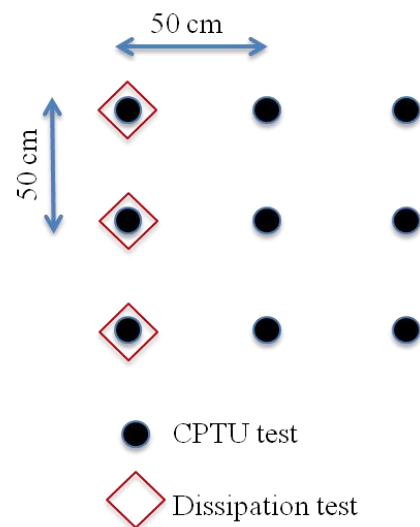


Figure 51: Scheme of the tests conducted in Pisa, nine CPTu at two different penetration rates (0.5 and 2 cm/s), and three dissipation tests.

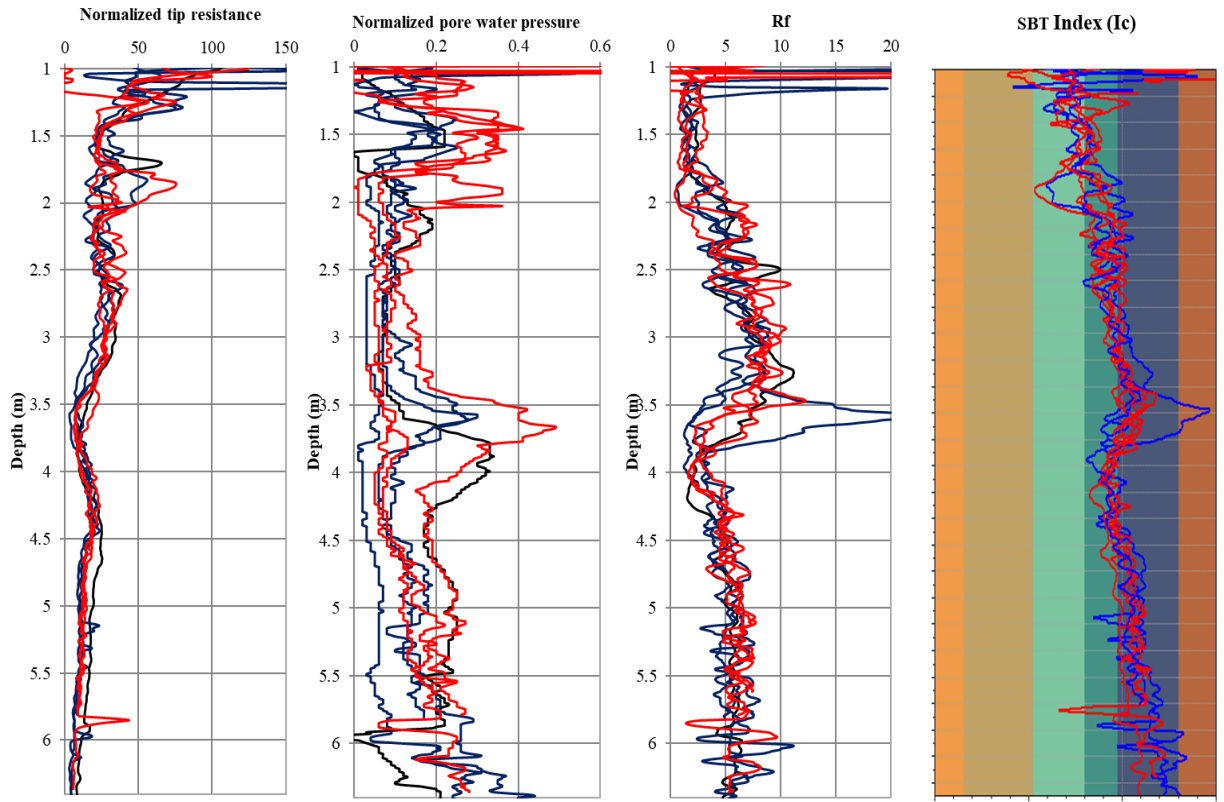


Figure 52: CPTu results (in terms of normalised parameters, Robertson 1990) from tests conducted with the minipiezocone at 2 cm/s (red) and 0.5cm/s (blue) in Pisa. The standard cone test is also plotted (black line).

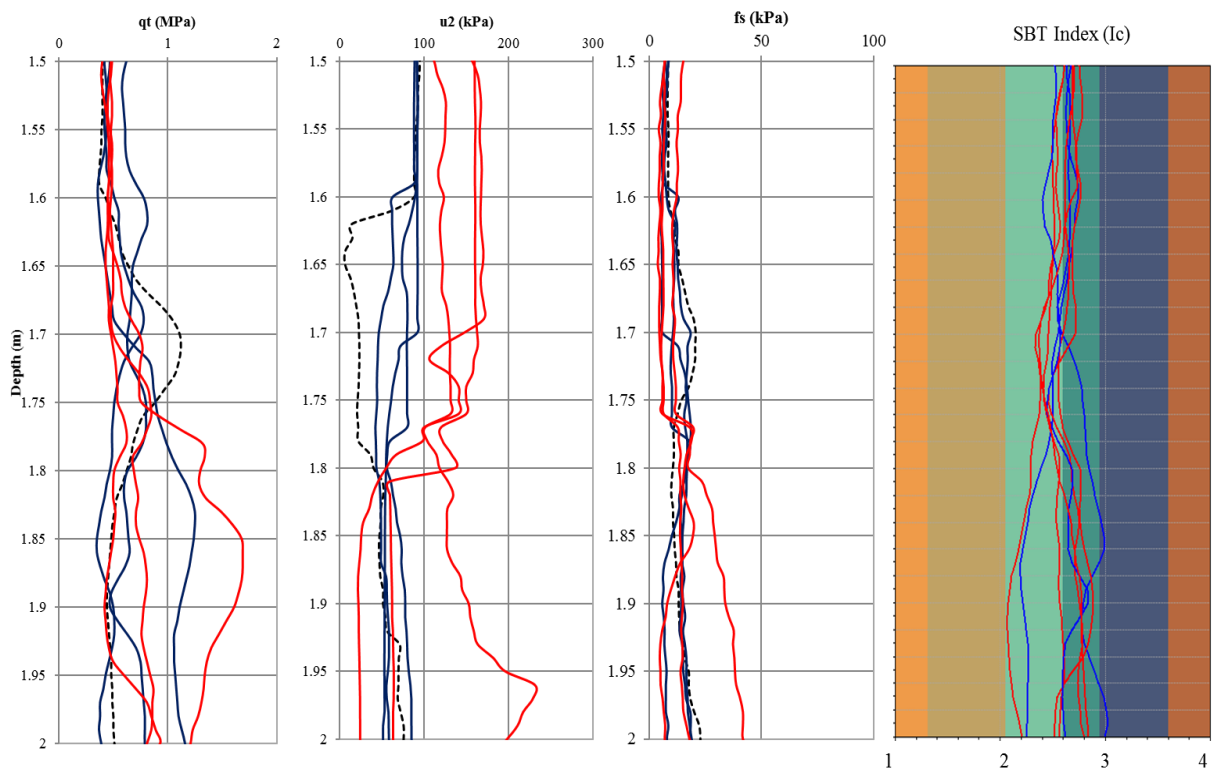


Figure 53: CPTu results (in terms of normalised parameters, Robertson 1990) from tests conducted with the minipiezocone at 2 cm/s (red) and 0.5cm/s (blue) in Pisa (1 m - 2 m depth).

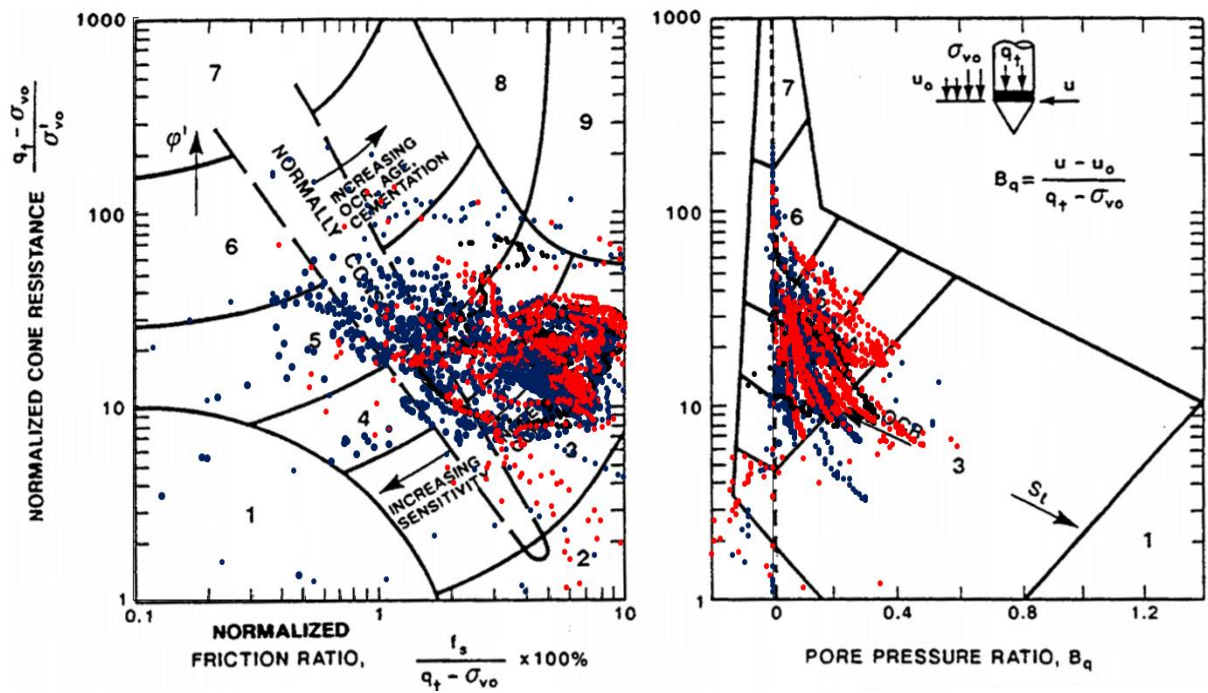


Figure 54: Normalised CPT soil behaviour type chart, as proposed by Robertson (1990). Soil types: 1, sensitive, fine grained; 2, peats; 3, silty clay to clay; 4, clayey silt to silty clay; 5, silty sand to sandy silt; 6, clean sand to silty sand; 7, gravelly sand to dense sand; 8, very stiff sand to clayey sand (heavily overconsolidated or cemented); 9, very stiff, fine grained (heavily overconsolidated or cemented). OCR, overconsolidation ratio; ϕ' , friction angle.

6.2.1 Effects of sleeve diameter on f_s measurements

The sleeve friction measurement is considered from many authors the least reliable, due to the highest variation of the three measurements, obtained during CPTu tests (Tiggelmann & Beukema, 2008, Lunne, 2010). Following Lunne and Anderson (2007) the main causes of the lack of accuracy in f_s measurements are the followings:

- Pore pressure effects on the ends of the sleeve
- Tolerance in dimensions between the cone and sleeve
- Surface roughness of the sleeve
- Load cell design and calibration

Holtrigter et al. (2014) studied the effect of the tolerance between cone and sleeve diameters carrying out several penetration tests with different sleeve diameters. They used the same piezocone for all the tests and therefore the other three aforementioned possible causes can be considered negligible. The tests have been carried out in three different sites, two sand sites in Christchurch and one clay site in Auckland. They used a cone tip diameter of 35.7 mm and five different sleeve diameters: 35.6 mm, 35.7 mm, 35.85 mm, 36.05 mm, and 36.15 mm. They noticed that the sleeve friction values progressively increase with increasing sleeve diameter (Figure 55). These effects are more evident in the case of stiff clays and dense sands. They considered the following main causes:

- End resistance on the edge of the sleeve nearer the cone tip (Figure 56)
- Increased friction along the sleeve due to increased volume of displacement

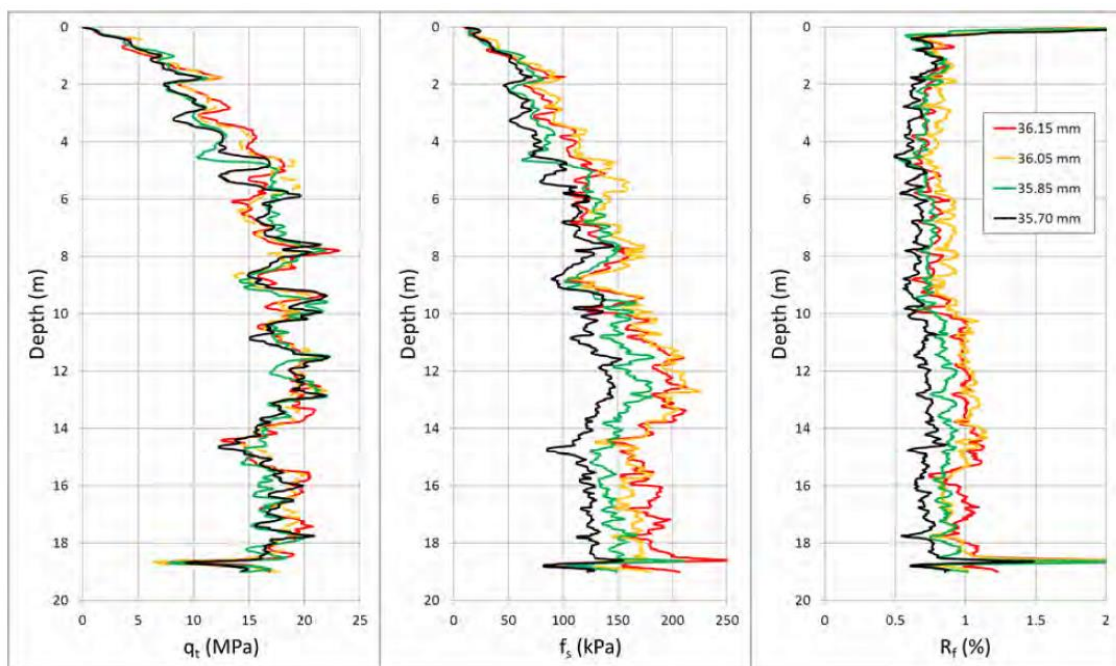


Figure 55 : Tests results from Christchurch (Holtrigter et al., 2014).

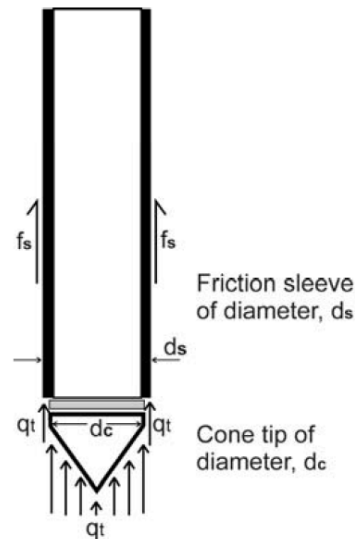


Figure 56: End resistance effect on oversize friction sleeve (Holtrigter et al., 2014).

In order to evaluate the influence of sleeve diameter on f_s measurements for soil of intermediate permeability, side-by-side CPTu tests have been conducted in Pisa (Italy), with 3 different sleeve diameters. The ASTM standard (D 5778-12) specifies the tolerances for the cone tip and sleeve dimensions:

- The cone tip diameter is required to be between 35.3 and 36.0 mm, measure of 35.7 mm
- The sleeve diameter has to be equal to the cone diameter or greater, with a tolerance within the range 0.0 mm - 0.35 mm

A Pagani Geotechnical Equipment piezocone has been used, with a cone tip diameter of 35.7 mm for all the tests, and three different sleeve diameters: 35.8 mm, 35.9 mm and 36.0 mm. Three tests have been conducted for each diameter. The nine tests follow a square scheme of 1m side, with 1 test at each corner, 1 in the middle of each side and 1 at the center of the square. The results of the measured data are shown in the following figures. The first three diagrams show results of tests conducted with different sleeve diameter along the same line (CPTu1, CPTu2 and CPTu3 series of tests). The second three diagrams show the overlay of the measurements obtained for the same sleeve diameter.

It is possible to observe that for this kind of materials there are no effects of the different sleeve diameter on f_s measurements, the variability of f_s measurements using different friction sleeve diameters has the same order of magnitude of the one obtained for the three tests conducted with the same diameter.

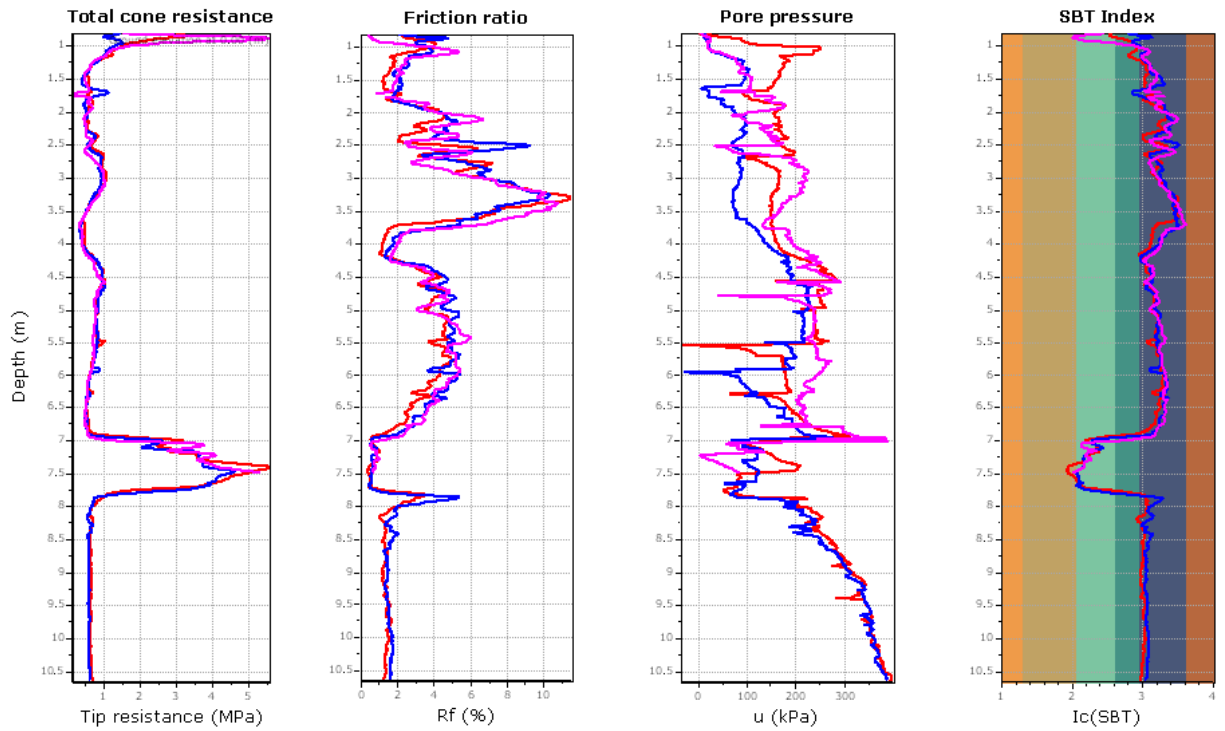


Figure 57: CPTu1 series, tests with different sleeve diameter along the same line, distance between tests 50 cm (Geologismiki,2007).

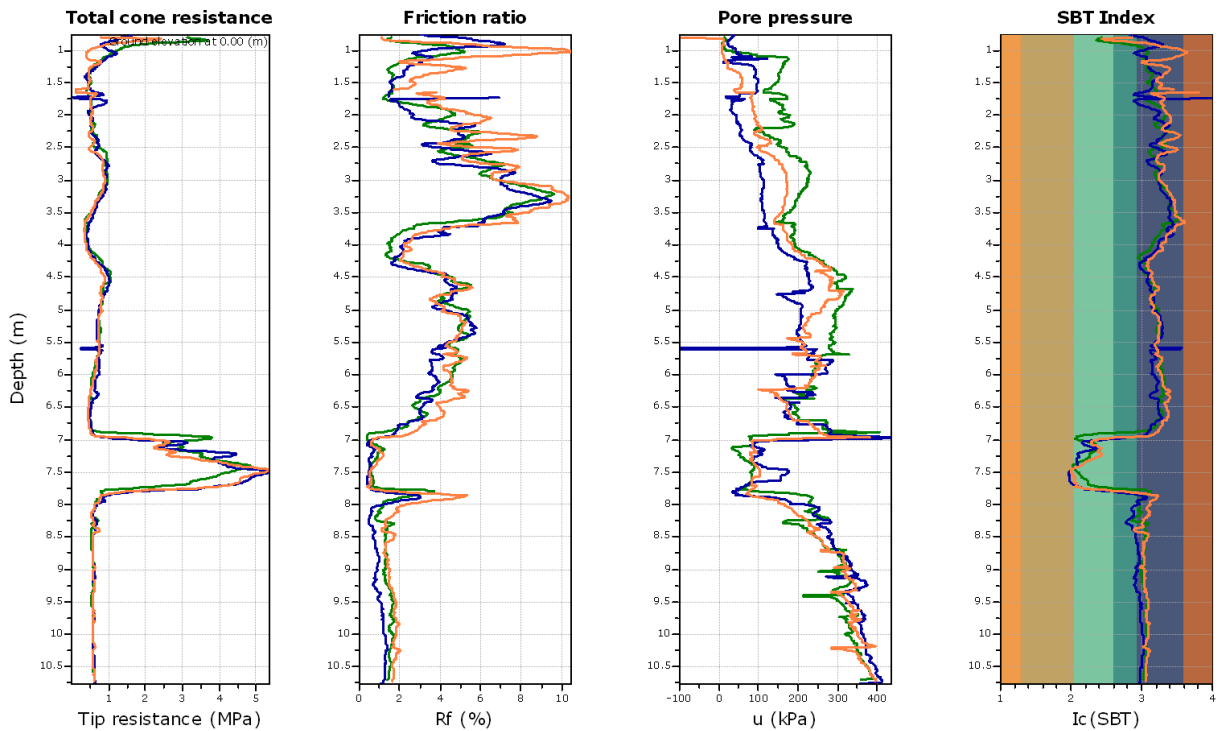


Figure 58: CPTu2 series, tests with different sleeve diameter along the same line, distance between tests 50 cm (Geologismiki,2007).

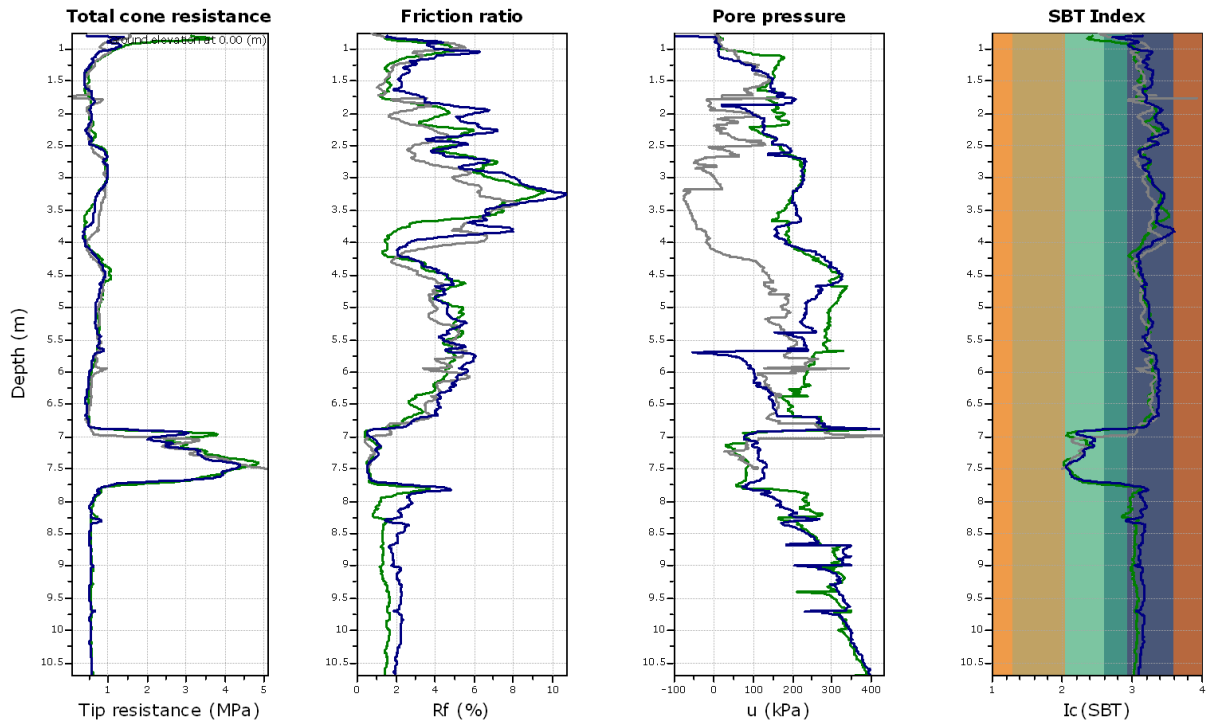


Figure 59: CPTu3 series, tests with different sleeve diameter along the same line, distance between tests 50 cm (Geologismiki,2007).

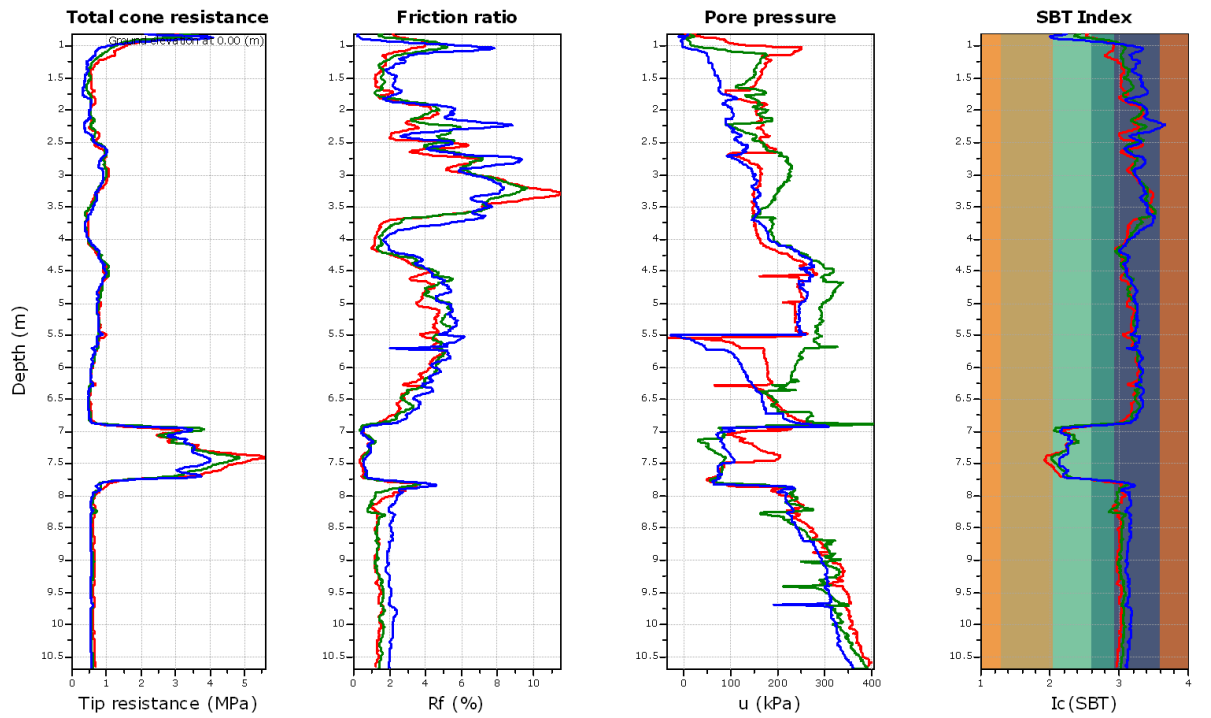


Figure 60: comparison of tests results for the same sleeve diameter, equal to 35.8 mm, distance between tests 50 cm (Geologismiki,2007).

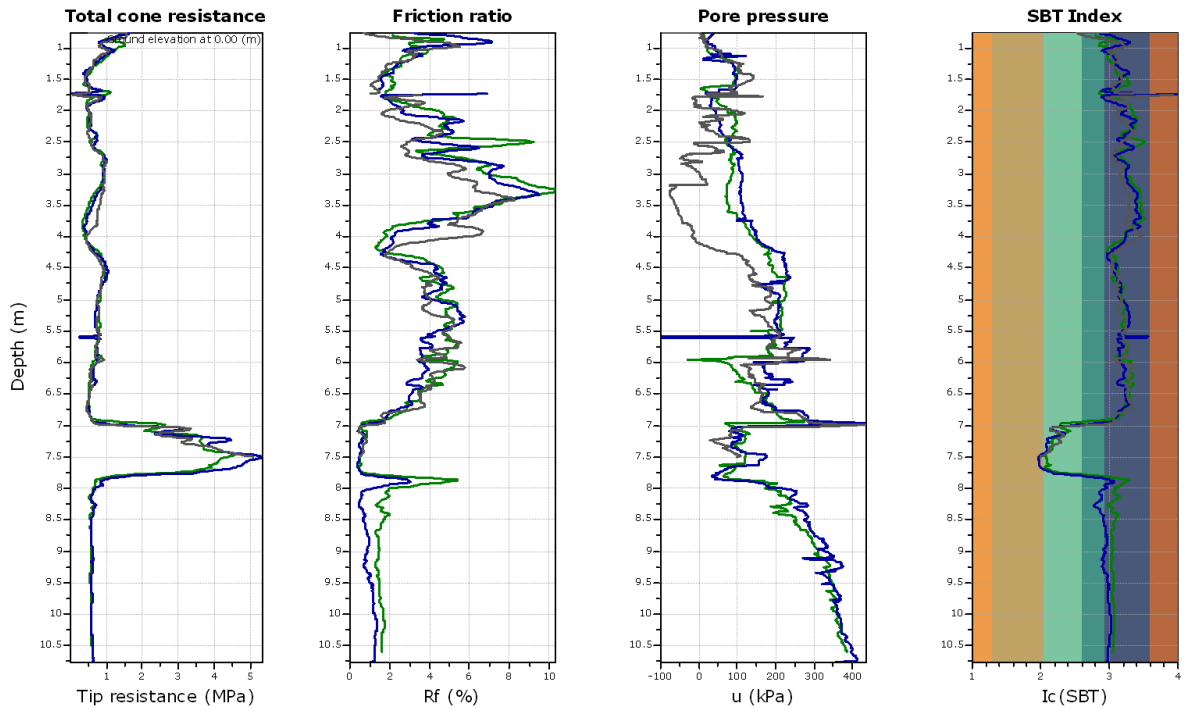


Figure 61: comparison of tests results for the same sleeve diameter, equal to 35.9 mm, distance between tests 50 cm (Geologismiki,2007).

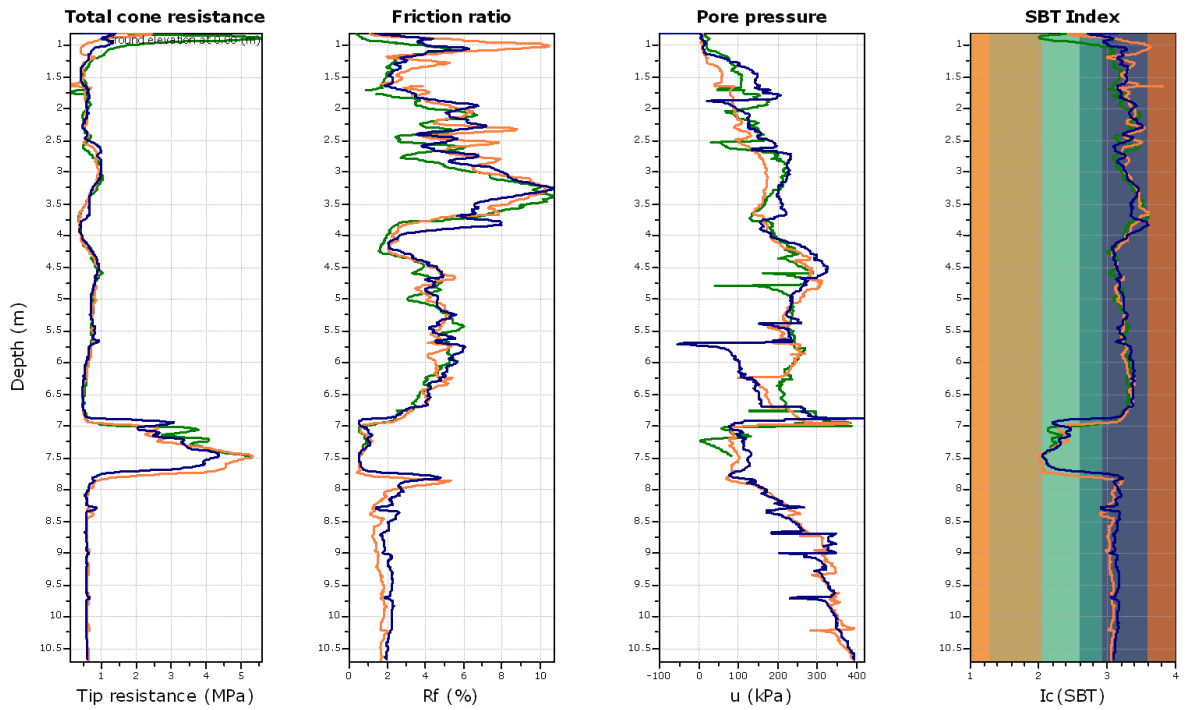


Figure 62: comparison of tests results for the same sleeve diameter, equal to 36.0 mm, distance between tests 50 cm (Geologismiki,2007).

6.3 Identification and characterisation of alluvial soil deposits

Piezocone tests have been conducted on alluvial deposits that are present in the Serchio River valley in S. Angelo (Lucca, Italy). The applied procedure is the same as the analyses carried out in Pisa. The minipiezocone has been used, as well as a standard piezocone. The maximum depth reached during the tests is 7 meters. The subsoil is characterised by alluvial deposits. A borehole has been conducted near the piezocone test location. The soil layers, between zero and seven meters depth, are classified as silty sands and clayey silts. In particular, two samples have been extracted in the investigated area. The first sample at a depth between 1.5 and 2.0 meters, the second sample between 3.0 and 3.5 meters. The granulometric composition for the upper sample is: 74.3% silt, 17.2% clay and 8.5% sand. The lower sample is composed as follows: 60.4% silt, 20.4% clay and 19.2% sand. According to the USCS classification system (ASTM, 2487), both samples belong to the CL (Lean Clay) class. The ground water table is 0.5 meters below the surface.

Figure 63 shows the results of two tests conducted at the standard rate (orange and red solid lines), two tests conducted at the minimum rate of 0.5 cm/s (light green and green solid lines) and one test conducted at the standard rate with a standard piezocone (conical tip area equal to 10 cm²). Tip resistance, pore water pressure measurements and sleeve friction are plotted with depth, together with the Soil Behaviour Type Index. Soil Behaviour Type Classification (SBTn, normalised Soil Behaviour Type) has been made on the basis of Robertson (1990) charts and the evaluation of the SBTn Index, I_c , following Robertson and Wride (1998):

$$I_c = \sqrt{(3.47 - \log Q_{tn})^2 + (\log F + 1.22)^2}$$

$$Q_{tn} = \left(\frac{q_t - \sigma_{v0}}{\sigma_{atm}} \right) \left(\frac{\sigma_{atm}}{\sigma'_{v0}} \right)^n ;$$

$$F = \frac{f_s}{q_t - \sigma_{v0}} \cdot 100;$$

$$n = 0.381 \cdot I_c + 0.05 \cdot \left(\frac{\sigma'_{v0}}{\sigma_{atm}} \right) - 0.15$$

Soil classification (SBTn)	Zone number (Robertson SBTn 1990)	SBTn Index values
Organic soils: peats	2	$I_c > 3.60$
Clays: silty clay to clay	3	$2.95 < I_c < 3.60$
Silt Mixtures: clayey silt to silty clay	4	$2.60 < I_c < 2.95$
Sand Mixtures: silty sand to sandy silt	5	$2.05 < I_c < 2.60$
Sands: clean sand to silty sand	6	$1.31 < I_c < 2.05$
Gravelly sand to dense sand	7	$I_c < 1.31$

Table 7: Definition of soil classification (Robertson, 1990) from the Soil Classification Index (Robertson and Wride, 1998).

Figure 64 shows the results on the normalised classification charts proposed (Robertson, 1990). Data on the Q-Bq chart cross the same class zones and it is not possible to distinguish the results obtained for different penetration rates. Observing the Q-Fr chart, data from different penetration rate tests plot on the same zones, in particular, classes 3 and 4. It is worthwhile to notice that the results from different penetration rates are clearly distinguished in the upper part of the chart. The plots move to the right of the chart as the penetration rate and the diameter of the tip increases, i.e. the non-dimensional velocity increases. This part of the chart corresponds to the data obtained between 0.5 and 1.5 meters depth. In fact, in this part of CPTu measurements profile, there is a clear increase in sleeve friction with penetration rate and tip diameter, whereas changes in tip resistance and pore water pressure are non-consistent with changes in drainage conditions due to different penetration rates. In particular, pore water pressure measurements of the test conducted with the standard cone and the standard penetration rate are lower than those obtained with the minipiezocone tests at 0.5 cm/s and 2 cm/s. Furthermore, changes in tip resistance are almost negligible and it is not possible to recognise different behaviours linked to applied different penetration rates.

Therefore, for the present case, as far as the soil layer between 0.5 and 1.5 meters is concerned, sleeve friction measurements are more sensitive to changes in penetration rates, resulting in a very clear increase as the penetration rate and/or tip diameter increases.

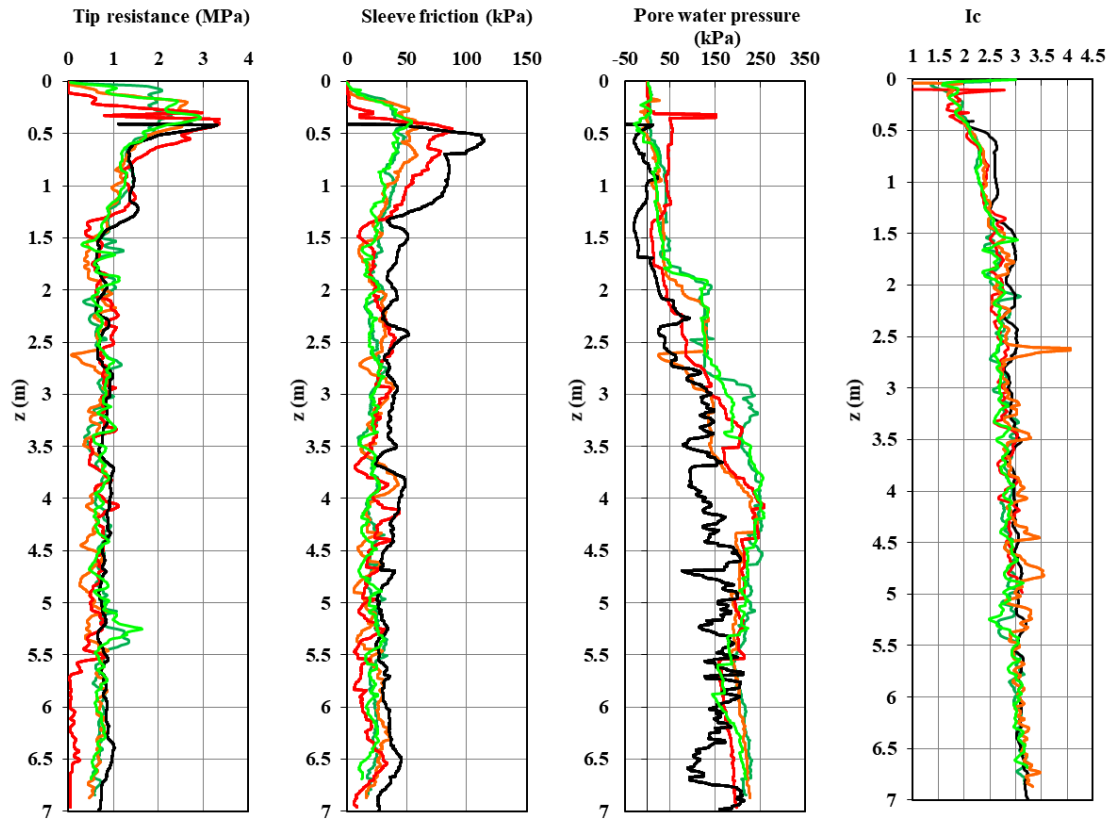


Figure 63: Comparison of CPTu tests results for the site located in Lucca (color legend: black=standard rate and standard piezocone; orange and red= 2 cm/s; light green and dark green= 0.5 cm/s).

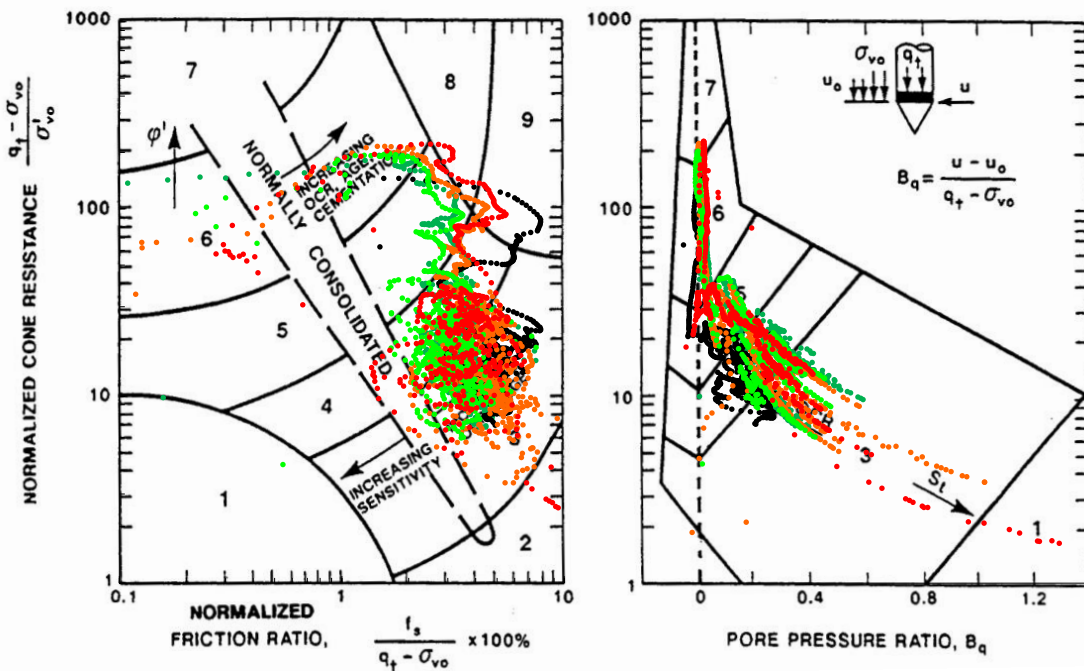


Figure 64: Normalised CPT soil behaviour type chart, as proposed by Robertson (1990). Soil types: 1, sensitive, fine grained; 2, peats; 3, silty clay to clay; 4, clayey silt to silty clay; 5, silty sand to sandy silt; 6, clean sand to silty sand; 7, gravelly sand to dense sand; 8, very stiff sand to clayey sand (heavily overconsolidated or cemented); 9, very stiff, fine grained (heavily overconsolidated or cemented). OCR, overconsolidation ratio; ϕ' , friction angle.

6.4 Conclusions

The chapter has described in-situ piezocone tests executed on three different kinds of intermediate materials: the dredged sediments of the Livorno Port area (Italy), the alluvial deposits situated in the delta area of Arno River (Pisa, Italy) and in Lucca (Italy). The chapter presents major principles from the test data showing the effect of different penetration rates on soil key parameters. The effect of penetration rate on sleeve friction is of particular interest. Moreover, the reliability of sleeve friction measurements has been shown, in relationship to minor variations of sleeve diameter.

The chapter presents a large body of data, both raw and interpreted data, making use of different approaches, such as alternative classification charts for piezocone data proposed by Robertson and by Schneider et al..

The nature of field tests is that trends in the measured data, such as arising from varying the cone penetration rate, may sometimes be obscured by natural variations in ground conditions from one test to another. This necessitates both careful planning of the tests, such as a grid of relatively closely spaced tests, but also careful interpretation to separate out natural variations from those due to deliberate changes in the test conditions.

Due to the aforementioned reasons, additional experimental activities have been developed using a calibration chamber, as described in the following chapter. The available device includes an electric engine used as thrust system that allows the penetration rate of the mini-piezocone to be considerably reduced covering a wider range of penetration rates, with respect to the one adopted for the in-situ tests analysed in the present chapter.

7. Calibration chamber tests

In order to investigate the influence of partial drainage during penetration the instrument of repeating the tests changing the penetration rate is widely used. However, most of the experimental studies on the influence of penetration rate on piezocone test results have been carried out inside a beam centrifuge on kaolin clay (Finnie and Randolph, 1994, House et al., 2001, Randolph and Hope, 2004, Schneider et al., 2007, Lehane et al., 2009; Mahmoodzadeh and Randolph, 2014). Few studies have been carried out on natural clay (Chung et al., 2006) or mixed soils (Kim et al., 2008; Schneider et al., 2007). The present chapter shows the results of experimental analyses of calibration chamber mini-penetrometer tests on soils of intermediate permeability (sandy-clayey silts). The penetration rate was varied by over three orders of magnitude to provide information on partially drained and undrained tip resistance, excess pore water pressure and friction sleeve.

The chamber is located in Calendasco (Piacenza, Italy) at the Pagani Geotechnical Equipment factory. The available device allows the penetration rate of the mini-piezocone to be considerably reduced thanks to an electric engine used as thrust system. The mini-piezocone can move horizontally in all directions, covering the entire chamber top surface. The material adopted for the tests has been compacted at two different water contents. The selection of the suitable material and compaction characteristics has been done with a preliminary laboratory test campaign described in the following paragraph.

7.1 Equipment description

The equipment is made up of a cubic chamber, a thrust system, a data acquisition system, an electric motor and a mini-piezocone. The chamber is made of steel, except for the frontal side where glass is present. It has 1.5 m side. The internal volume is divided in two sections from a steel wall, kept in the correct position thanks to steel rods. The chamber is accessible from the top. The internal surface of the chamber has been covered with geotextile. On the bottom, an irrigation pipe is positioned under a steel grille. The irrigation pipe allows for the saturation of the sample (Figure 65).

After the complete filling of the chamber, the reaction frame applies the pressure on the top of the specimen. Four load cells control the applied pressure of 10 kPa on the total top surface. Due to their geometric dimensions and mechanical characteristics of the material, the sidewalls of the chamber can be considered as a rigid constraint that does not allow for lateral displacements when the vertical load is applied on the top surface of the soil. A K_0 stress condition therefore can be considered present inside the chamber. The K_0 value has been evaluated from the expression proposed by (Mayne and Kulhawy, 1982):

$$K_0 = \frac{\sigma'_{h0}}{\sigma'_{v0}} = (1 - \sin \varphi) OCR^{\sin \varphi}$$



Figure 65: Frontal view of the steel chamber, particles of the internal partition and the irrigation pipe on the bottom of the chamber.

The actuator consists of a 1.0 kW direct current brushless electric motor. The electric motor allows for a very stable penetration rate control, at high and low values. In particular between 0.006 cm/s and 4.5 cm/s.

On the soil top layer, a distributed load is applied thanks to 4 load cells and a reaction frame fixed to the chamber structure. The load is applied by means of a steel plate that covers the entire top surface. The plate has several holes to provide access for the cone penetrometer.

The tests have been conducted with a mini-penetrometer (Figure 68). The penetrometer has a 2 cm² projected tip area, whereas the standard cone has a 10 cm² projected tip area. This device allows for reducing the value of the non-dimensional velocity, V , not only with the reduction of the penetration rate, but also thanks to a reduced tip diameter.

The cone apex angle is 60°. The friction sleeve area is 50 cm². During the test, it is possible to measure the tip resistance and the adhesion force thanks to two groups of strain-gauges positioned under the sleeve: the advanced group measures the tip resistance, the second group measures both tip resistance and friction force so that the f_s value is obtained from the difference between the two measured values. In addition to that, the pore water pressure during penetration is measured through the slot filter, thanks to a pressure sensor placed inside the main body of the penetrometer.



Figure 66: The pressure on the top layer is applied using four load cells and a reaction frame fixed to the chamber structure.

Details of measurement characteristics of tip resistance, side friction and pore water pressure are displayed in Table 8. The pore water pressure is measured by the use of silicone grease (very fluid, NLGI 00) as the slot filter saturation fluid. The use of grease as a saturation fluid was first proposed by Elmgren (1995) and Larsson (1995), and various comparisons have testified its reliability. In addition, a calibration procedure was performed at Pagani Geotechnical Equipment (PC – Italy). Figure 69 shows the piezocone calibration test which was conducted in a specially devised calibration chamber: the upper diagram shows the relationship between the applied loads and readings during loading and unloading, whereas the lower diagram shows the calculated error, expressed as a percentage of the maximum applied pressure, during both the loading and unloading processes. It is possible to observe that there is a very good agreement between the measurements and applied pressures, with the absence of a threshold value, below which the transducer inside the cone would not be able to measure changes in the external pressure. Besides, no relevant hysteresis loop can be observed.

The penetration depth was measured by use of a depth encoding system and all data during the test were recorded running a data acquisition system. The Control Panel and the Data Acquisition System are shown in Figure 70.



Figure 67: Brushless electric motor (upper part of the image).

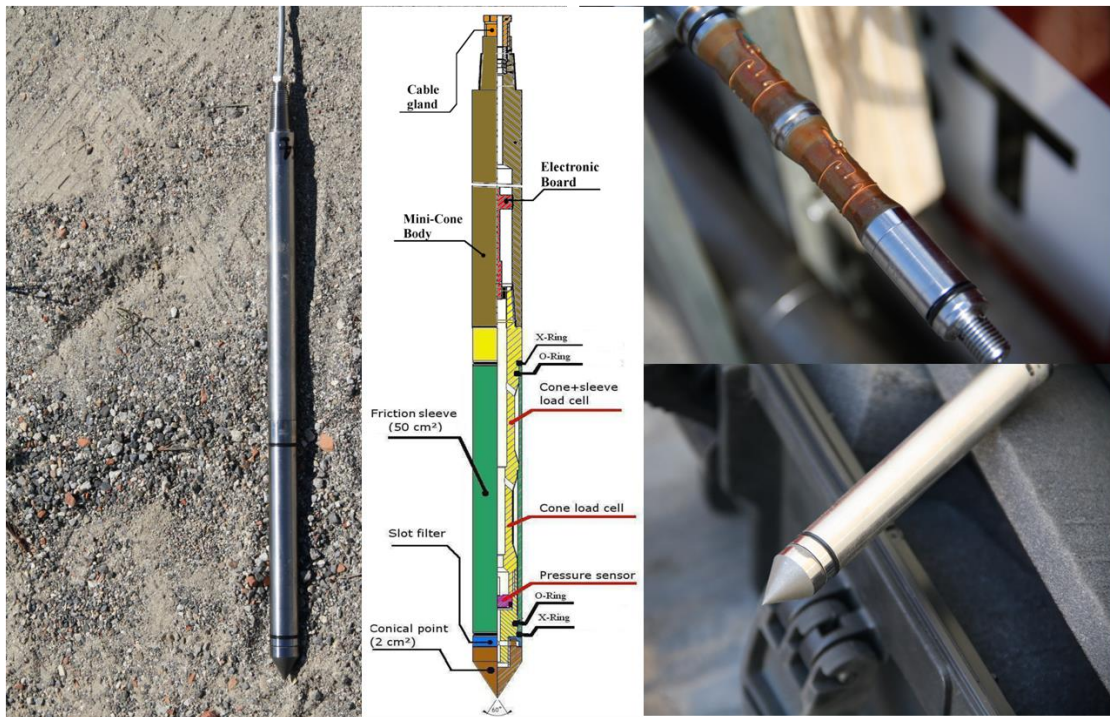


Figure 68: The mini-piezcone produced by Pagani Geotechnical Equipment.

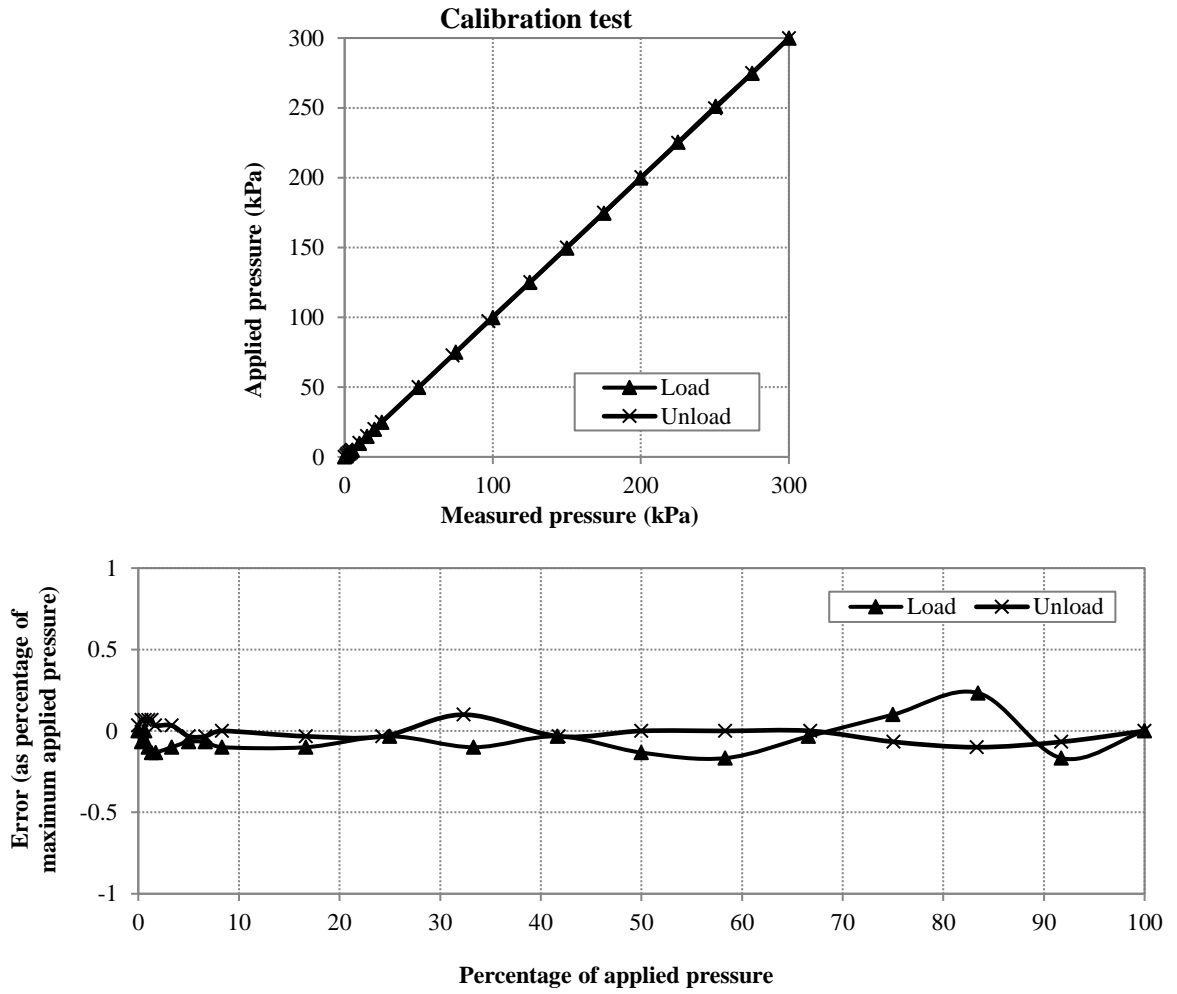


Figure 69: Calibration test for the slot filter.

Sensor	Full scale	Resolution	Precision
Tip resistance	30 MPa	24 bit	0.005 MPa
Friction force	500 kPa	24 bit	0.04 kPa
Pore Water Pressure	2500 kPa	24 bit	0.04 kPa

Table 8: Piezocone measurements details.

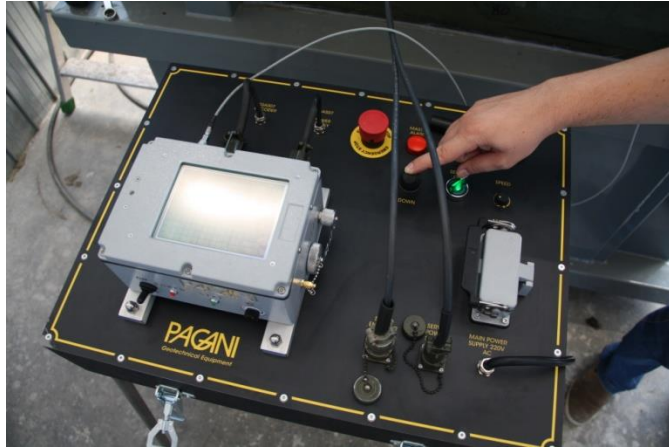


Figure 70: Control Panel and Data Acquisition System.

7.2 Selected material

In order to choose a proper material, a laboratory tests campaign has been conducted at the Geotechnical Laboratory of the University of Pisa. In particular, the following tests have been carried out:

- Classification (Grain size distribution, Atterberg's limits, G_s determination)
- Modified Proctor tests with the construction of the compaction curve (Figure 73)
- Incremental loading oedometer tests, conducted for each point of the compaction curve
- Direct measurements of the hydraulic conductivity, in particular, one measurement for each step of the oedometer tests
- Triaxial tests, isotropically consolidated undrained tests (TxCIU)
- Resonant column tests

Test procedures are aimed at identifying the material to be used for the analysis in the cube chamber. The soil comes from the alluvial deposits of the Po River. Figure 71 shows the particle size distribution of the selected material: 45% of silt, 30 % of sand and 25% of clay. The specific gravity value at 20°C, G_s , is 2.72.

Figure 73 shows the compaction curve obtained through the Modified Proctor procedure. The maximum dry density is 1.92 kg/dm³ and the optimum water content is approximately 11.9 %.

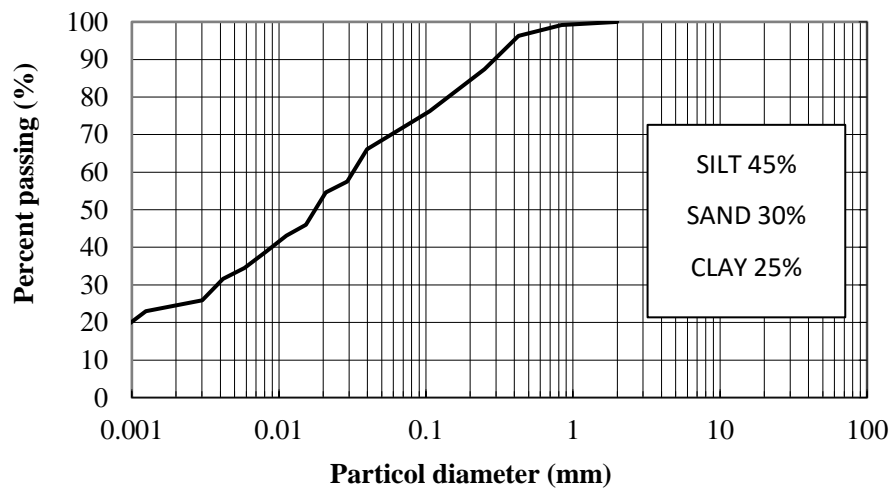


Figure 71: Particle size distribution.

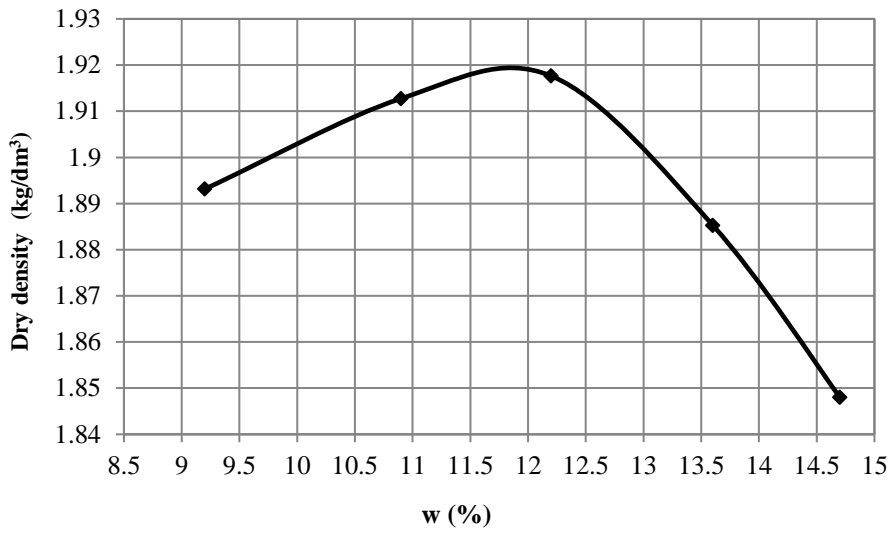
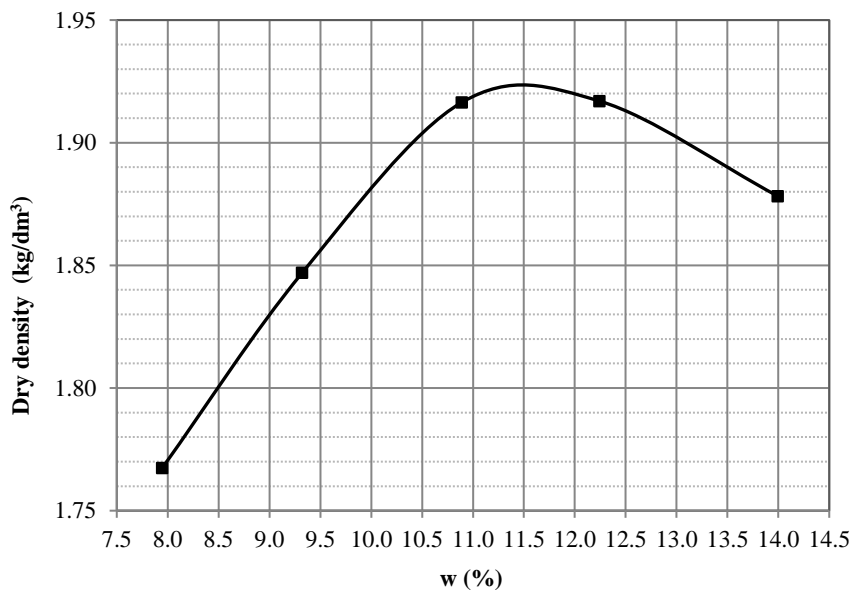


Figure 72: Compaction curve (Modified Proctor procedure).



Modified Proctor test						
	Sample 1	Sample 2	Sample 3	Sample 4	Sample 5	Optimum
Dry density (kg/dm ³)	1.767	1.847	1.916	1.917	1.878	1.924
Water content (%)	7.9	9.3	10.9	12.2	14.0	11.5

Figure 73: Compaction curve of the studied material (Modified Proctor).

7.2.1 Preliminary estimation of non-dimensional velocity range

Preliminary tests have been carried out in order to estimate the possible range of the non-dimensional velocity within the calibration chamber. Since the penetration rates and the diameter of the cone are fixed, the key value is the coefficient of consolidation of the material inserted in the chamber.

Direct measurements of hydraulic conductivity have been carried out and then compared with the estimations inferred from the Taylor's method during incremental loading oedometer tests. Data presented in this section are the results of tests on a material extracted from the same site of the soil used inside the calibration chamber, but with some different characteristics. The particle size distribution is characterised as follows: 47% of silt, 42% of sand and 11% of clay. The specific gravity value at 20°C, G_s , is 2.74.

Figure 73 shows the compaction curve obtained by means of the Modified Proctor procedure. The maximum dry density is 1.924 kg/dm³ and the optimum water content is circa 11.5%.

An Incremental Loading oedometer test has been conducted on specimens extracted from each Proctor sample (i.e. each water content value) used to build up the compaction curve. The maximum applied vertical load is 3200 kPa, subsequently 4 unloading steps are executed.

Vertical displacement data have been used to estimate the coefficient of consolidation at the average vertical effective stress of each loading step. Figure 74 shows vertical displacement versus time for the loading step between 200 kPa and 400 kPa, Sample 1 (see Figure 73). This trend is typical for all the samples of the present material and for all the loading steps. As shown in the figure, in order to estimate the coefficient of consolidation the Taylor's method has been applied. During each loading step, the bottom drainage line is closed and only upward drainage is allowed. This procedure extends the drainage length of the sample so that more accurate c_v values can be obtained.

In addition, during each oedometer test, the direct measurement of the hydraulic conductivity has been done after each loading step. The first step corresponds to a value of the vertical effective stress equal to 12.5 kPa, whereas the last step (n. 9) corresponds to 3200 kPa. Each loading step lasts 24 hours.

The saturated coefficient of hydraulic conductivity has been inferred from variable head tests. As shown in Figure 75, the standard oedometer test device has been opportunely modified in order to add the elements necessary to generate a vertical water flow inside the specimen and to measure hydraulic head changes over time.

The hydraulic load is applied at the bottom of the oedometer cell through the lower porous filter. The water can flow only through the soil sample thanks to o-rings positioned between the two metal rings and between the outer metal ring and the base of the oedometer cell. A graduate glass burette is available and it is possible to appreciate a water height variation as small as 0.5

mm, corresponding to a volume variation of 48 mm^3 . The average cross section of the burette has been measured before the tests. The hydraulic circuit is saturated with distilled water before the first loading step of the oedometer test. At the end of each loading step, the burette is filled with distilled water reaching an initial head of around 50 cm. The hydraulic head, initial and the following values, is evaluated with respect to the water level inside the oedometer cell. During the permeability test, the variation of time of the water level inside the burette is manually recorded, at least once every hour. At the same time, the variation of the height of the specimen and the ambient temperature are measured. During the test, water height recorded values (logarithmic scale) are plotted against time. This diagram allows for the determination of a stationary condition. Once the stationary condition is reached, the test is interrupted. The saturated hydraulic conductivity, k , is computed for the last, at least three, meaning values. The final estimation is the average value.

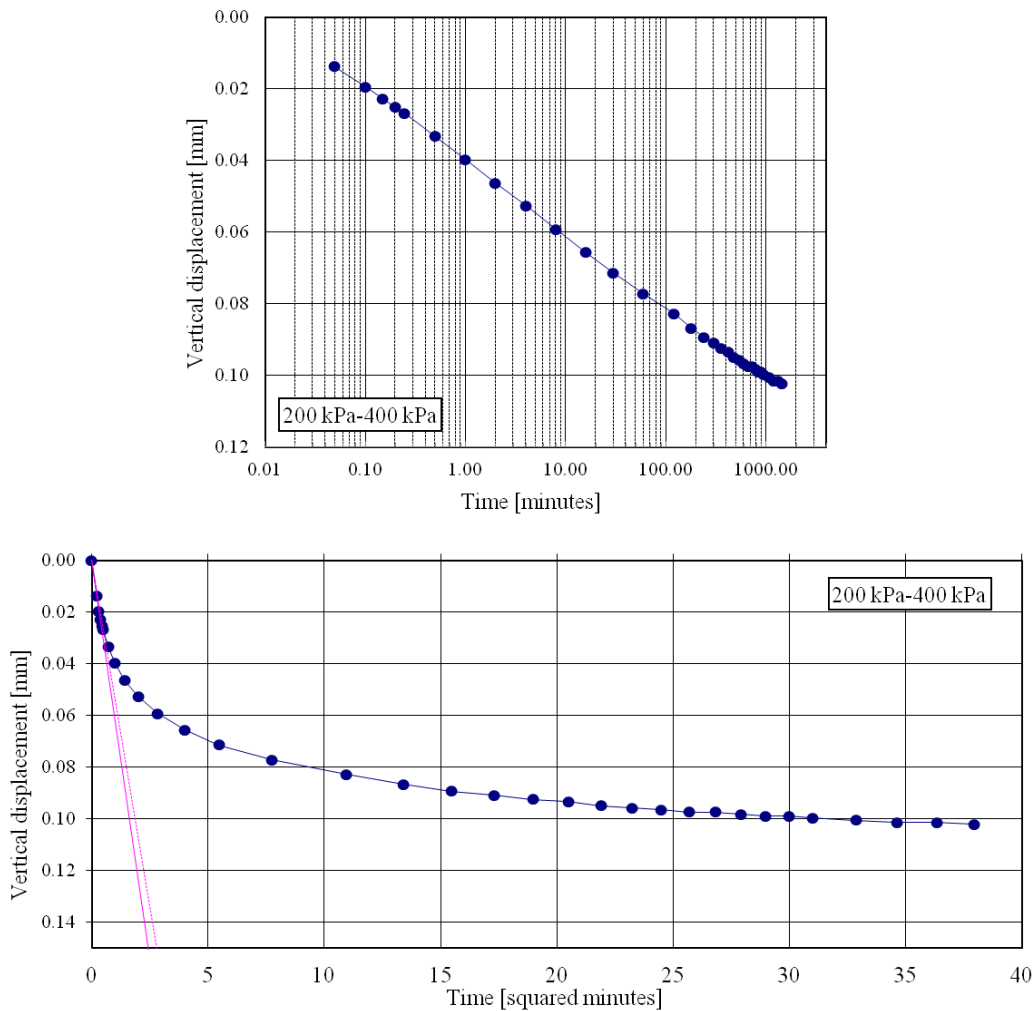


Figure 74: Vertical displacement vs time for the loading step between 200 kPa and 400 kPa, Sample 1.

The saturated hydraulic conductivity is computed with the following expression:

$$k = \frac{a \cdot L}{A \cdot (\Delta t)} \cdot 2.302 \cdot \log_{10} \frac{H_0}{H_1}$$

where: a is the burette cross section area, L is the current specimen height, A is the specimen cross section area, H_0 is the head reference value (at the beginning of the stationary condition), H_1 is the head value, Δt is the elapsed time between H_0 and H_1 . At least three different estimations for k are obtained from three different H_1 values. The average value is then computed. Table 9 summarises test results.

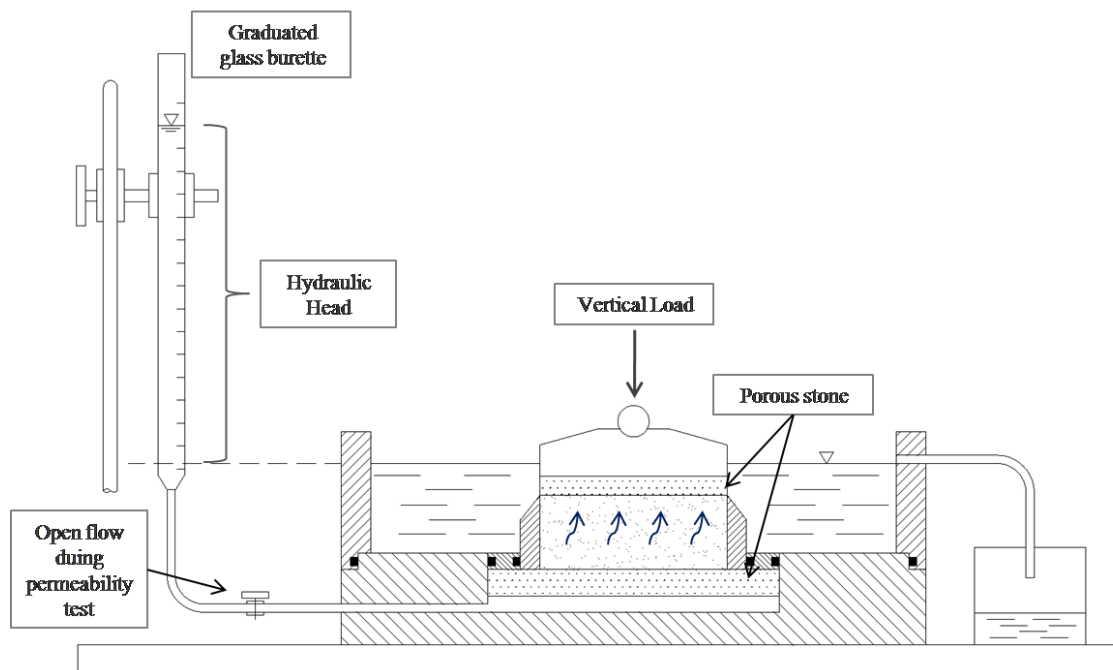


Figure 75: Variable head test device added to the standard incremental loading oedometer test device.

Once the permeability test is terminated, the hydraulic circuit that connect the burette with the oedometer cell, is closed and the oedometer test continues with the following loading step. Figure 76, Figure 77, Figure 78, Figure 79 and Figure 80 show the results of the variable head permeability tests conducted for each sample and for each loading step. These results are then compared with the estimation of the saturated hydraulic conductivity computed from the evaluation of the coefficient of consolidation (Taylor's method):

$$k = \frac{c_v \cdot \gamma_w}{M}$$

where: γ_w is the water unit weight, c_v is the coefficient of consolidation, M is the constrained modulus, both estimated from the current loading step of the oedometer test.

The differences between the two estimations can be between zero and about one order of magnitude. Observing the results, it is not possible to establish a general rule of the difference between the direct evaluation and the Taylor's estimation.

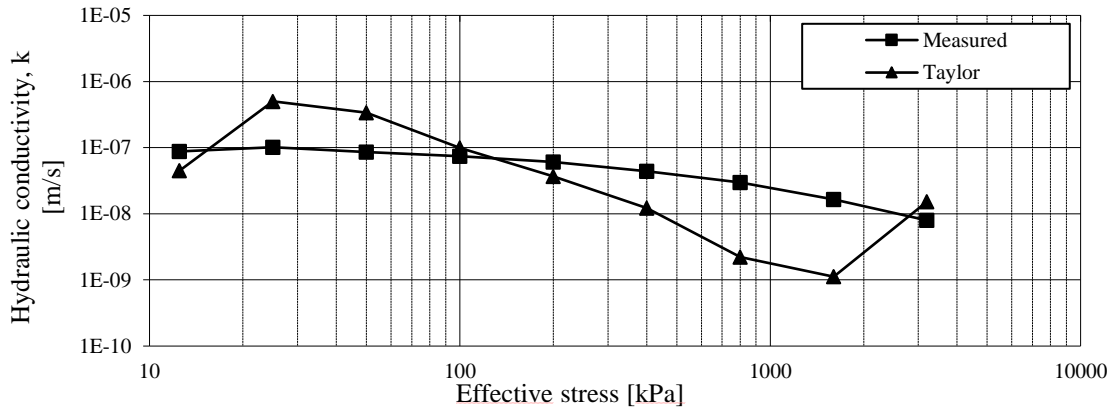


Figure 76: Sample 1 - Comparison between hydraulic conductivity measured data and estimated data from coefficient of consolidation values.

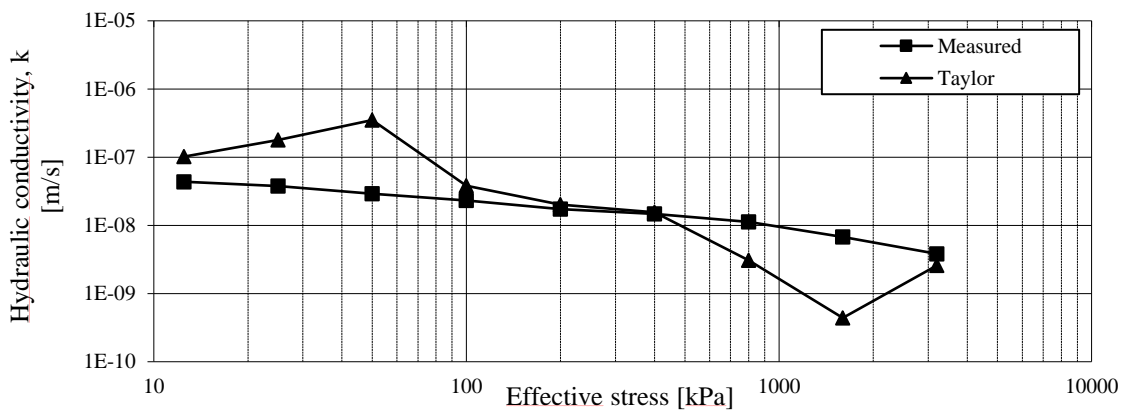


Figure 77: Sample 2 - Comparison between hydraulic conductivity measured data and estimated data from coefficient of consolidation values.

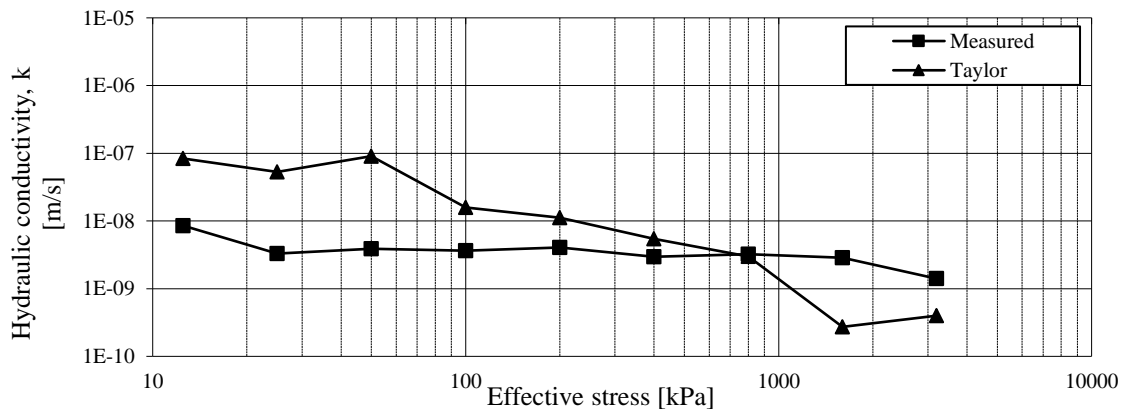


Figure 78: Sample 3 - Comparison between hydraulic conductivity measured data and estimated data from coefficient of consolidation values.

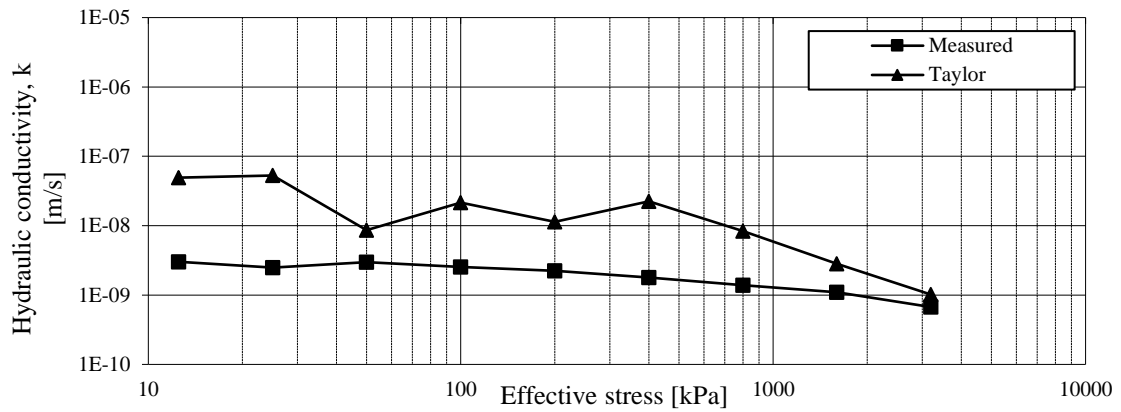


Figure 79: Sample 4 - Comparison between hydraulic conductivity measured data and estimated data from coefficient of consolidation values.

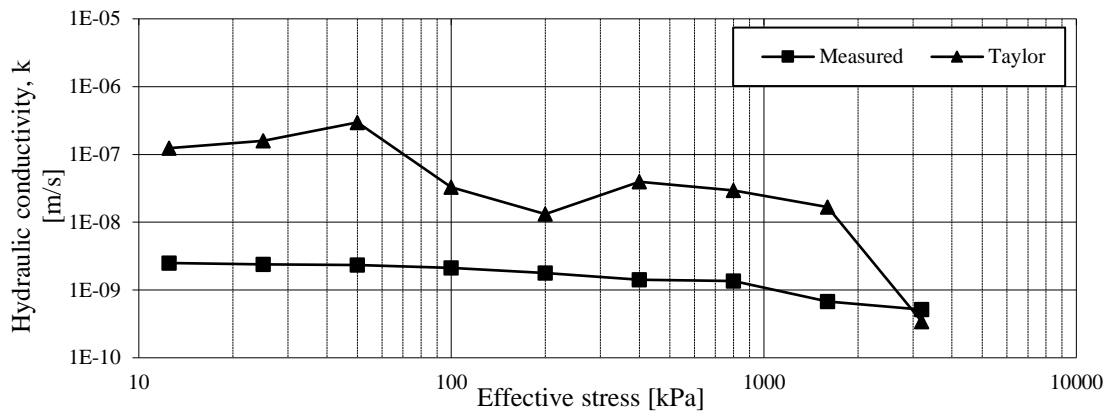


Figure 80: Sample 5 - Comparison between hydraulic conductivity measured data and estimated data from coefficient of consolidation values.

	Vertical effective stress (kPa)	Sample 1	Sample 2	Sample 3	Sample 4	Sample 5
		Proctor water content w (%)				
		7.9	9.3	10.9	12.2	14
Hydraulic conductivity direct measurements k (m/s)	12.5	8.8E-08	4.4E-08	8.5E-09	2.5E-09	3.0E-09
	25.0	1.0E-07	3.8E-08	3.3E-09	2.4E-09	2.5E-09
	50.0	8.6E-08	2.9E-08	3.9E-09	2.3E-09	3.0E-09
	100.0	7.4E-08	2.3E-08	3.6E-09	2.1E-09	2.5E-09
	200.0	6.1E-08	1.7E-08	4.1E-09	1.8E-09	2.2E-09
	400.0	4.4E-08	1.5E-08	3.0E-09	1.4E-09	1.8E-09
	800.0	3.0E-08	1.1E-08	3.2E-09	1.4E-09	1.4E-09
	1600.0	1.7E-08	6.8E-09	2.8E-09	6.8E-10	1.1E-09
	3200.0	8.0E-09	3.8E-09	1.4E-09	5.1E-10	6.7E-10

Table 9: Direct measurements of hydraulic conductivity

Permeability test results have been analysed to study the influence of compaction characteristics, in terms of degree of saturation and dry density at the end of the compaction process, on permeability characteristics and, therefore, consolidation characteristics of compacted soils. Figure 81 shows the influence of S_r at the end of compaction on measured hydraulic conductivity. It is assumed that after the first loading step and the subsequent water flow, the specimen can be considered fully saturated.

The measured k values range between 10^{-8} and 10^{-10} . As expected, for each soil specimen, lower values are obtained for high levels of applied vertical effective stress. The first three samples have water content smaller than the optimum, whereas the second two samples have a water content higher than the optimum. The first two samples, with respectively w equal to 7.9% and 9.3% are characterised by higher values of hydraulic conductivity, whereas the samples with higher water content values have lower k values of about an order of magnitude. The solid line in Figure 81 expresses the correlation between saturated hydraulic conductivity and degree of saturation at the end of compaction, this curve has been obtained following the studies conducted by Tatsuoka (2015) on the characteristics of compacted soils controlled by the degree of saturation at the end of compaction. The curve is obtained knowing the grading characteristics (in terms of D_{30} or D_{50}) and the values of degree of saturation and dry density obtained during the compaction test. The coefficient of saturated hydraulic conductivity, k , of compacted soil, is controlled by ρ_d and S_r at the end of compaction, similarly as the strength and deformation characteristics. Figure 83 shows the relationship between k (logarithmic scale) under saturated condition and S_r during compaction of the sieved core material (SCM) of Miboro dam, compacted at different compaction energy levels (1Ec= ASTM-698-78 Standard Proctor; 4.5Ec=ASTM D-1557-78 Modified Proctor). It is possible to observe a systematic and simple trend; following Tatsuoka, the scatter in k values for fixed S_r is due mostly to the variation of dry density among the data. The effects of ρ_d on k values are visible in Figure 84 where k values are plotted against ρ_d for different S_r values. Tatsuoka observed that the slope of the data for different S_r values is almost the same, that is the reason why the data was fitted by the following equation:

$$\log k = \log f_k(S_r) + 5.02 \left(1.872 - \frac{\rho_d}{\rho_w} \right)$$

where k is in cm/s, $f_k(S_r)$ is the k value when $\rho_d = [\rho_{d_{max}}]_{1Ec} = 1.872 \text{ g/cm}^3$

Figure 85 shows the relation between $f_k(S_r)$ and S_r at the end of compaction. It can be seen that the relation is rather unique and independent from the compaction energy levels. Plus, it is possible to observe that $f_k(S_r)$ is constant for $S_r < 60\%$ and it decreases at a constant slope as S_r increases. Tatsuoka repeated the same analysis for 8 different kinds of soil around Miboro dam and then for a wide variety of soil types. He observed that it was possible to describe the

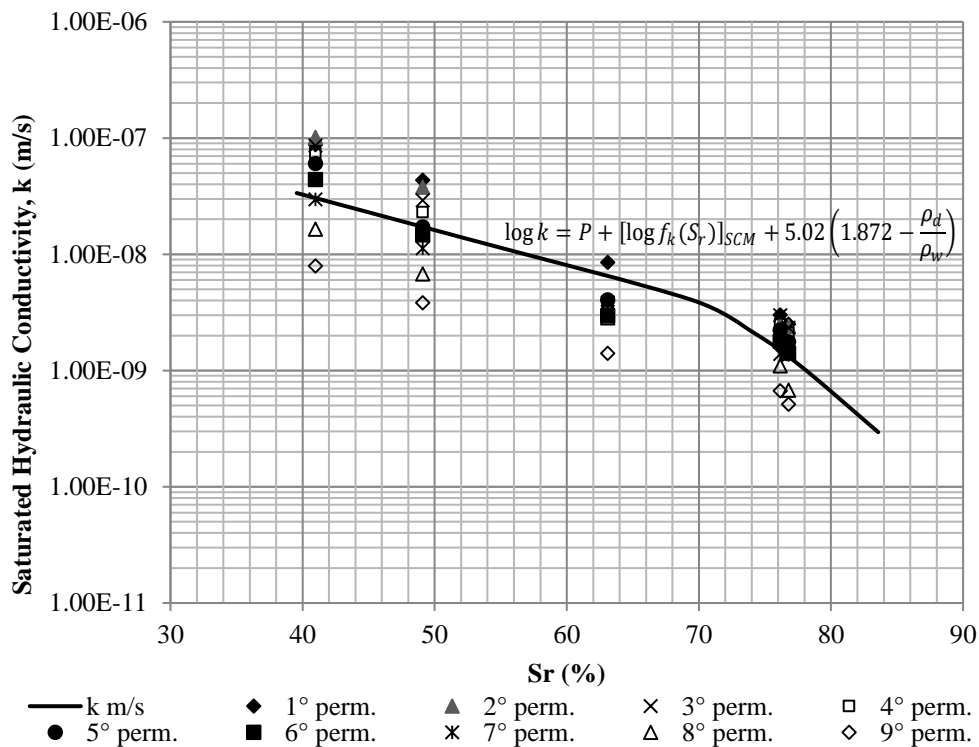
data with the same curve $f_k(S_r)$ on condition that the relationship took into account particle size effects. So, he introduced the parameter P (P=0 for SCM) described in Figure 87. P values are plotted against the ratio between D_{50} and $[D_{50}]_{SCM}=0.854$ mm or D_{30} and $[D_{30}]_{SCM}=0.356$ mm.

For any kind of soil an approximated estimate of k values can be obtained, from given ρ_d and S_r values, with the following relation (Tatsuoka,2015):

$$\log k = P + [\log f_k(S_r)]_{SCM} + 5.02 \left(1.872 - \frac{\rho_d}{\rho_w} \right)$$

where $[\log f_k(S_r)]_{SCM}$ is obtained from Figure 85 by substituting the value of S_r , P is obtained from Figure 87 by substituting D_{50} or D_{30} from the particle size distribution.

As shown in Figure 81 the direct measurements of hydraulic conductivity carried out in this study are in good agreement with the model proposed by Tatsuoka. Also in this case the scatter is given by the different dry density values due to the increasing vertical effective stress applied to the specimen. Data have been plotted against the degree of saturation corresponding to the initial water content of the oedometer test.



Permeability n.	1	2	3	4	5	6	7	8	9
Vertical effective stress (kPa)	12.5	25	50	100	200	400	800	1600	3200

Figure 81: Effects of degree of saturation at the end of compaction on the coefficient of hydraulic conductivity for the selected soil type: direct measure (symbols); Tatsuoka relationship (solid line).

The k - S_r trend obtained can be explained considering the micro-structure of compacted soil. For S_r values, lower than a certain threshold (around 70% in this case), a coherent micro-structure is formed with fine particle sticking to coarse particles due to high matric suction resulting from

low S_r . In this case the micro-structure is stable and large voids are present between particles, so that higher values of saturated hydraulic conductivity are measured. On the other hand, when S_r is higher than the optimum value a dispersive micro-structure is present due to lower suction. The voids between the coarse particles are filled with finer particles resulting in a lower value of k (Tatsuoka, 2015).

Figure 82 shows the measured k values plotted against dry density values: it is possible to observe that the general trend is similar to that presented by Tatsuoka. Besides, the hypothesis assumed by Tatsuoka that the slope $a = -5.02$ is applicable to different types of soils is confirmed by the results obtained in this study. The two lines plotted in Figure 82 represent the linear trend between hydraulic conductivity (log scale) and dry density, distinguishing between data obtained for samples on the left side of the optimum and those for the samples on the right side. It is possible to observe that the results for the samples 1, 2 and 4 follow very well the interpolation lines proposed by Tatsuoka. Sample 3 and Sample 5 have more scatter, with this respect, it is important to underline that for the hydraulic conductivity axis a log-scale is used, so the measured hydraulic conductivity for samples 3 and 5 are at least one order of magnitude lower than those for sample 1 and 2. When the values to be measured are very low, the reading on the glass burette is very sensitive to little changes in the position of the water meniscus. Little changes in the measured value are accentuated if reproduced with the log-scale axis.

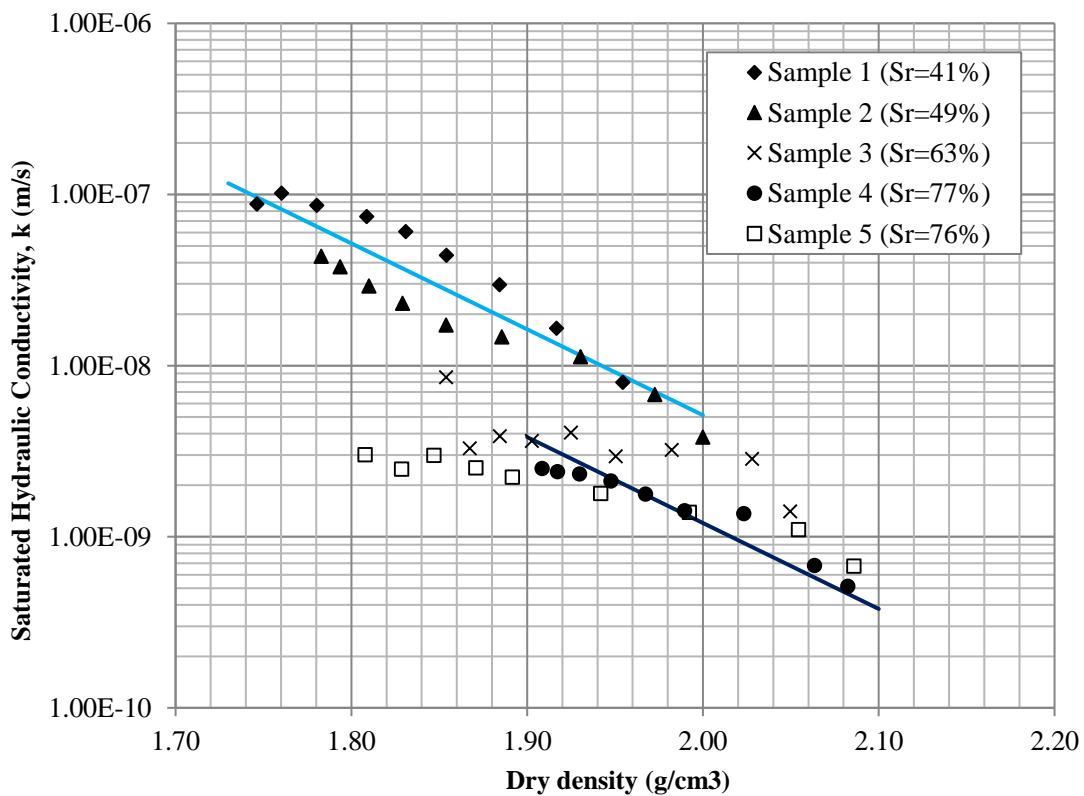


Figure 82: Measured k values vs. dry density. Solid lines refer to Tatsuoka's model (slope $a = -5.02$).

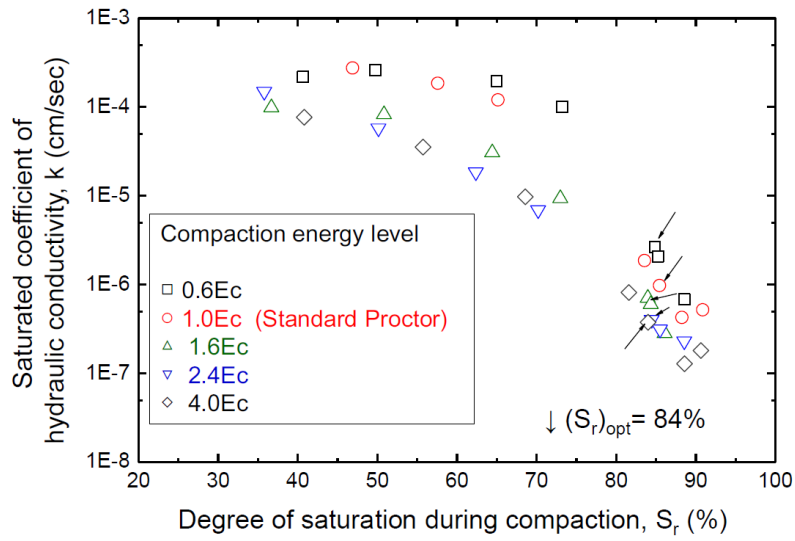


Figure 83: Coefficient of saturated hydraulic conductivity k plotted against S_r at the end of compaction of the data of sieved core material (SCM) for Miboro dam (Tatsuoka, 2015).

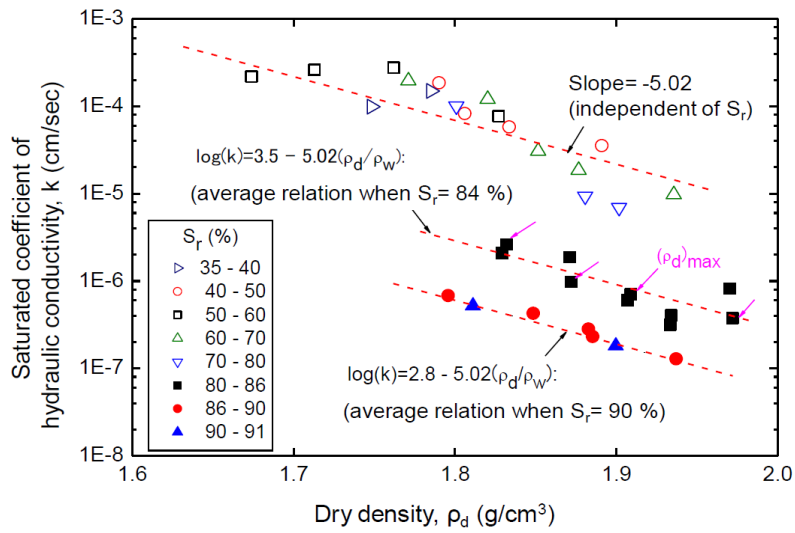


Figure 84: $\log k$ vs. ρ_d relations for different ranges of S_r (Tatsuoka, 2015).

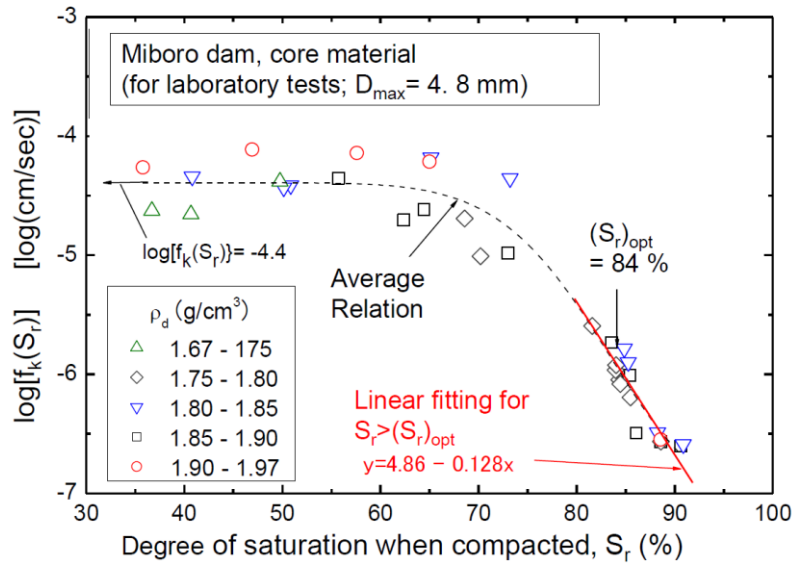


Figure 85 : “logk when $\rho_d = [(\rho_d)_{max}]_{IEc} = 1.872 \text{ g/cm}^3$ ”, $f_k(S_r)$, plotted against S_r (Tatsuoka, 2014a).

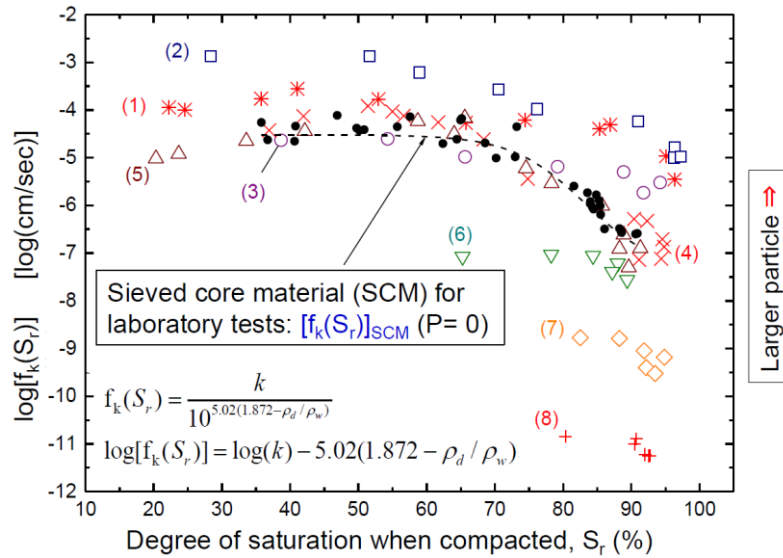


Figure 86: Coefficient of saturated hydraulic conductivity k when $\rho_d = [(\rho_d)_{max}]_{IEc} = 1.872 \text{ g/cm}^3$, $f_k(S_r)$, plotted against S_r at compacted state of eight soil types around Miboro dam site and SCM.

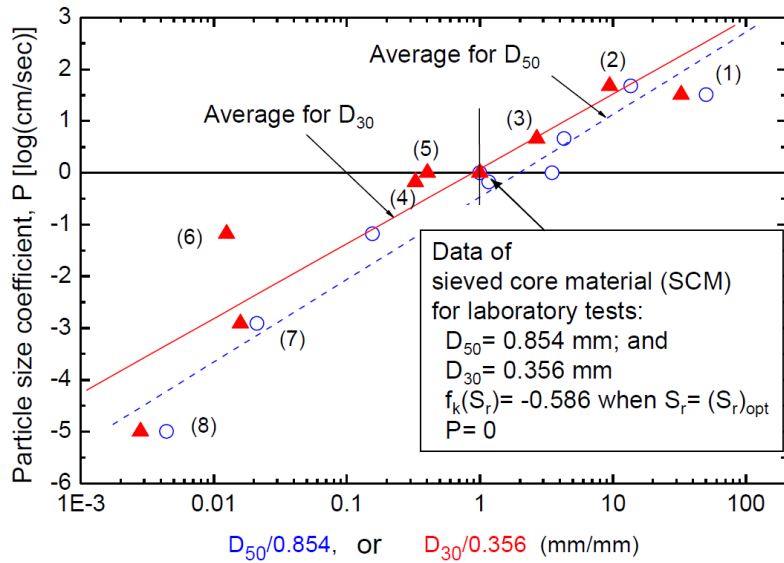
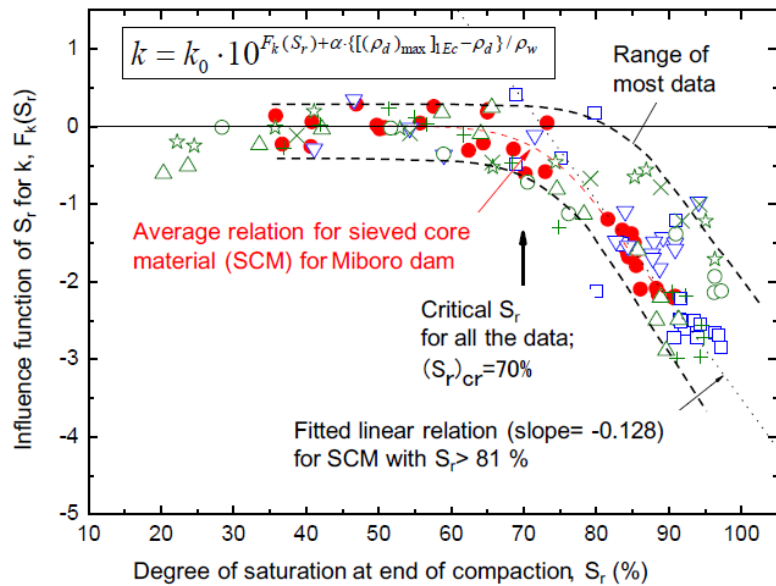


Figure 87: particle size coefficient P plotted against the particle size (Tatsuoka, 2014a)



Symbol	Backfill name	$(S_r)_{opt}$ (%)	k_0 (cm/sec)	α	$[(\rho_d)_{max}]_{1Ec} / \rho_w$
●	SCM	84.0	$10^{-4.40}$	5.02 ⁺	1.872
☆	No.1	84.8	$10^{-3.75}$		1.94
○	No.2	95.4	$10^{-2.86}$		2.12
×	No.3	87.1	$10^{-4.52}$		1.94
+	No.4	92.3	$10^{-4.15}$		1.53
△	No.5	87.7	$10^{-4.41}$		1.70
□	Type A*	91.0	$10^{-4.85}$	3.38	1.47
▽	Type B*	85.0	$10^{-5.8}$	5.675	1.75

+ assumed to be the same as SCM

*Daniel & Benson (1990)

Figure 88: Effects of S_r at the end of compaction on the coefficient of saturated hydraulic conductivity k of a wide variety of soil types (Tatsuoka, 2014b).

The direct estimation of hydraulic conductivity has been carried out in order to evaluate the coefficient of consolidation of the soil and, subsequently, to establish the range of the non-dimensional velocity V available inside the calibration chamber, considering the adopted cone diameter and the possible range of penetration rates.

The following figures show the values of the hydraulic conductivity and the coefficient of consolidation plotted against the vertical effective stress state. The coefficient of consolidation is evaluated employing the measured value of hydraulic conductivity. Furthermore, an estimation of the non-dimensional velocity V is shown. The plotted V values are obtained for penetration rates of 0.006 cm/s and 4.5 cm/s that correspond to the rate range covered during the tests. The diameter of the minipiezocone adopted for the tests is 1.6 cm.

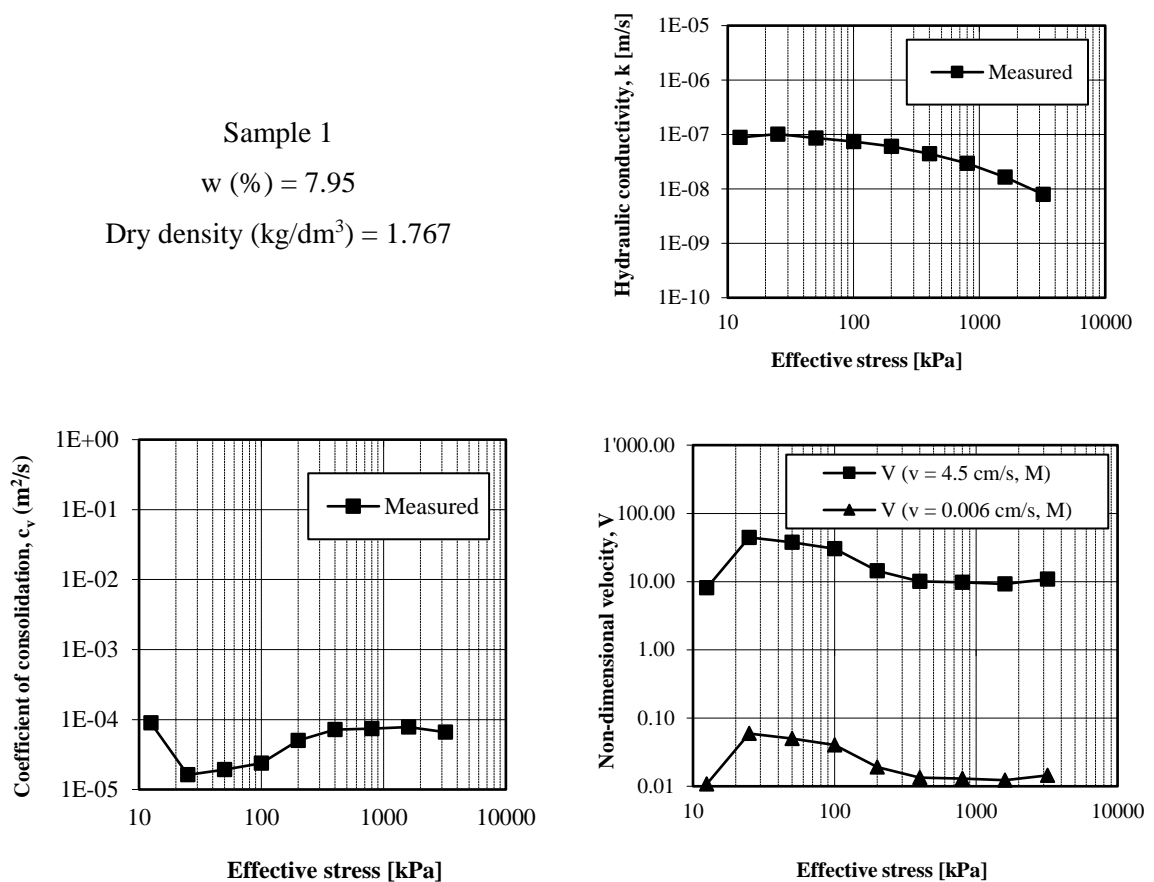


Figure 89: hydraulic conductivity; coefficient of consolidation and non- dimensional velocity V plotted against the vertical effective stress.

To identify the transition points from undrained to partially drained and from partially drained to fully drained conditions, the test conducted at 4.5 cm/s should be under undrained conditions, whereas the test conducted at 0.006 cm/s should be close to fully drained conditions.

From previous studies on the influence of penetration rate on drainage conditions during the piezocone test, the transition value between undrained and partially drained conditions is expected to be between 10 and 30, whereas the transition value between partially drained and

drained conditions should be approximately between 0.01 and 0.1. These results can be used only as a guide to determine the requested V values to cover the range necessary for the present study. Considering that the vertical effective stress applied inside the calibration chamber is between 10 kPa and 20 kPa, test conditions should allow for investigating the transition between the partially drained condition and the completely undrained condition. The obtained V range covers around three orders of magnitude, suggesting that the calibration chamber set up is suitable to investigate drainage boundaries with the available device.

Sample 2
 w (%) = 9.3
 Dry density (kg/dm^3) = 1.847

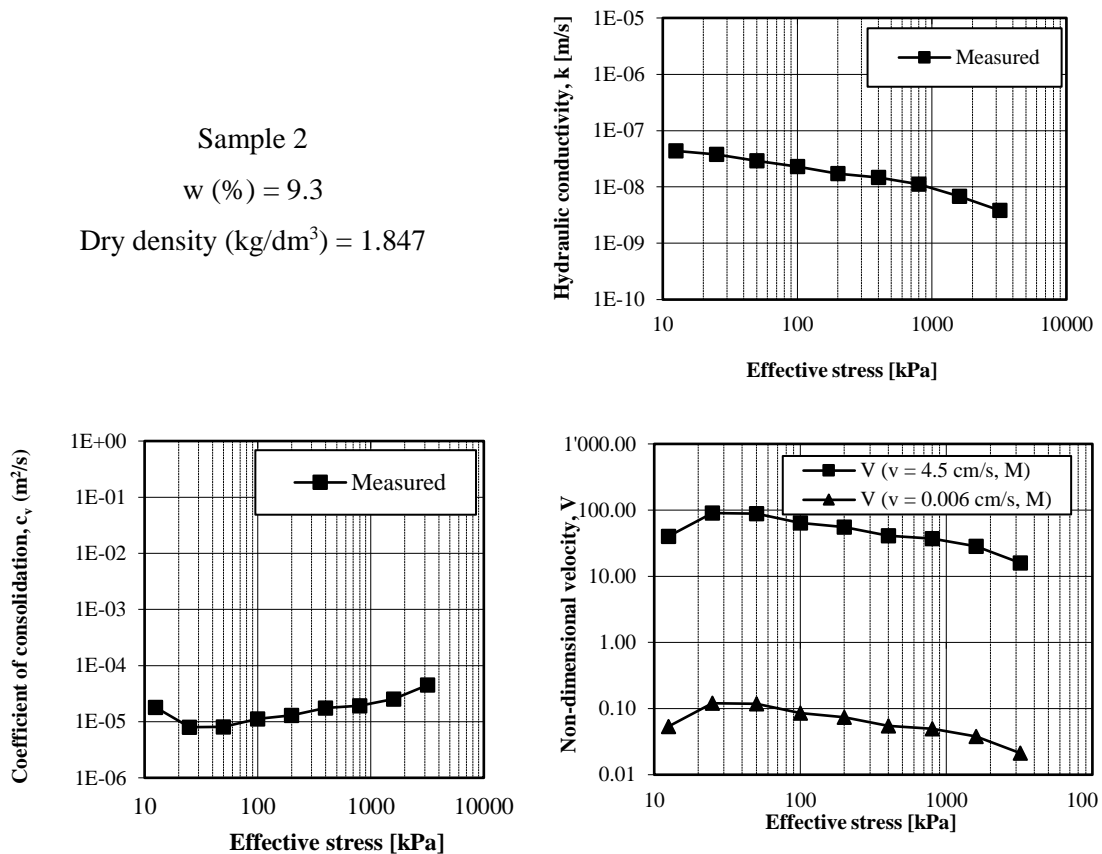


Figure 90: hydraulic conductivity; coefficient of consolidation and non- dimensional velocity V plotted against the vertical effective stress.

Sample 3
 $w (\%) = 10.9$
 Dry density (kg/dm^3) = 1.916

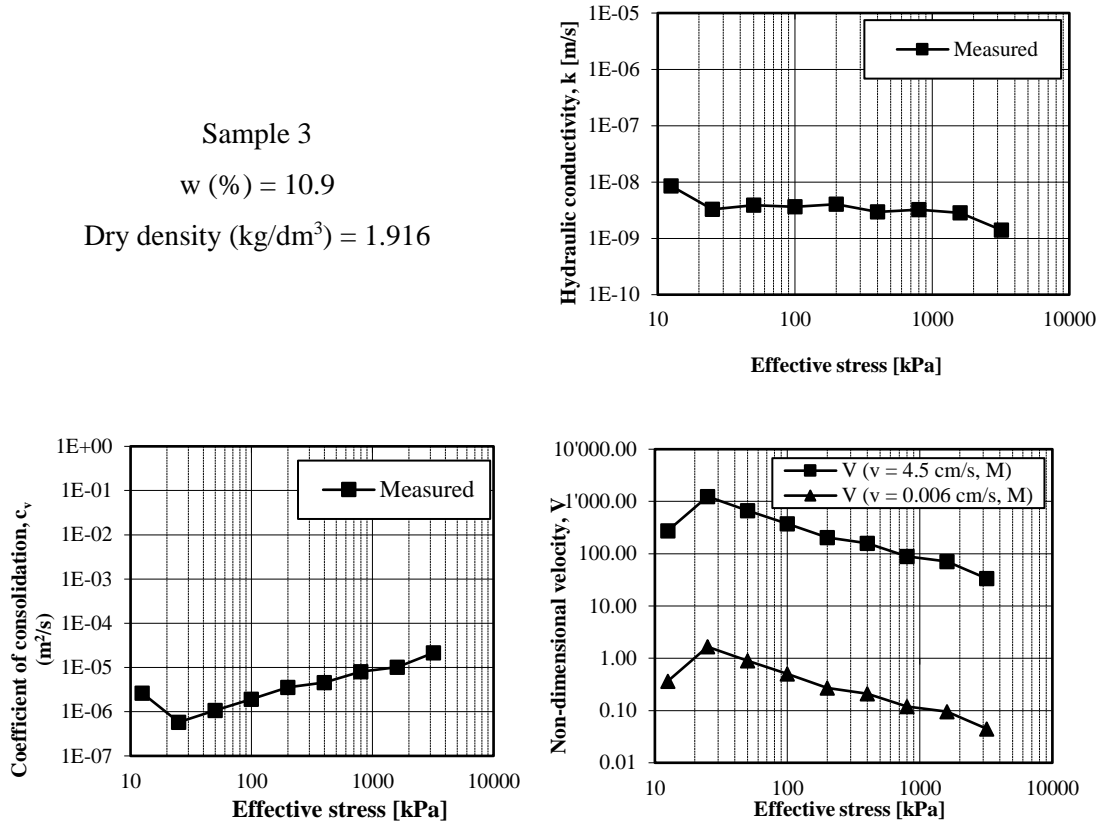


Figure 91: hydraulic conductivity; coefficient of consolidation and non- dimensional velocity V plotted against the vertical effective stress.

Sample 4
 $w (%) = 12.2$
 Dry density (kg/dm^3) = 1.917

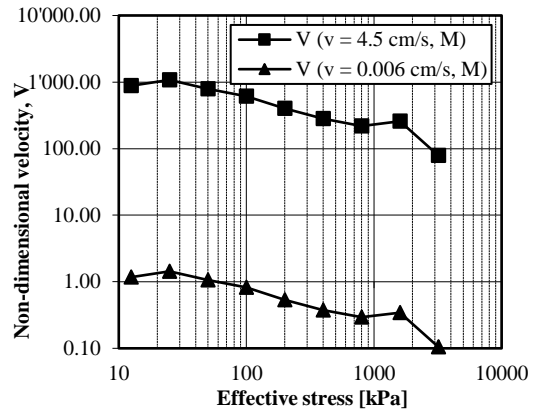
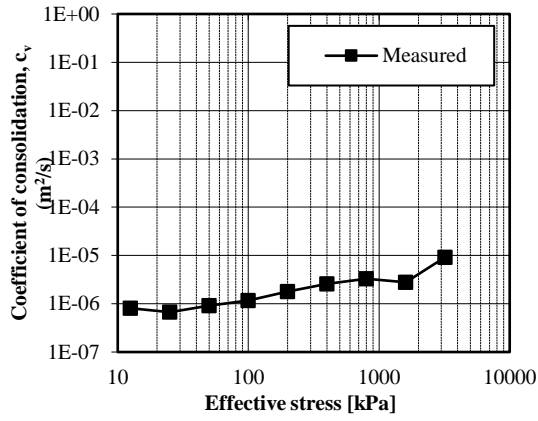
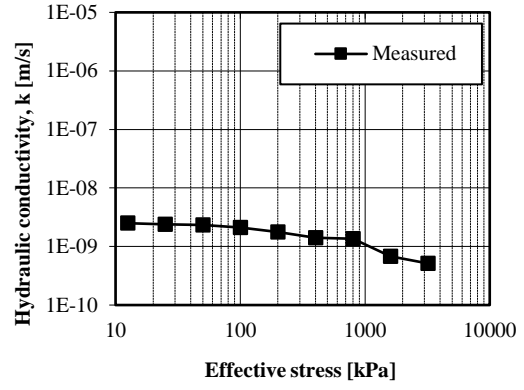


Figure 92: hydraulic conductivity; coefficient of consolidation and non- dimensional velocity V plotted against the vertical effective stress.

Sample 5
 $w (\%) = 14$
 Dry density (kg/dm^3) = 1.787

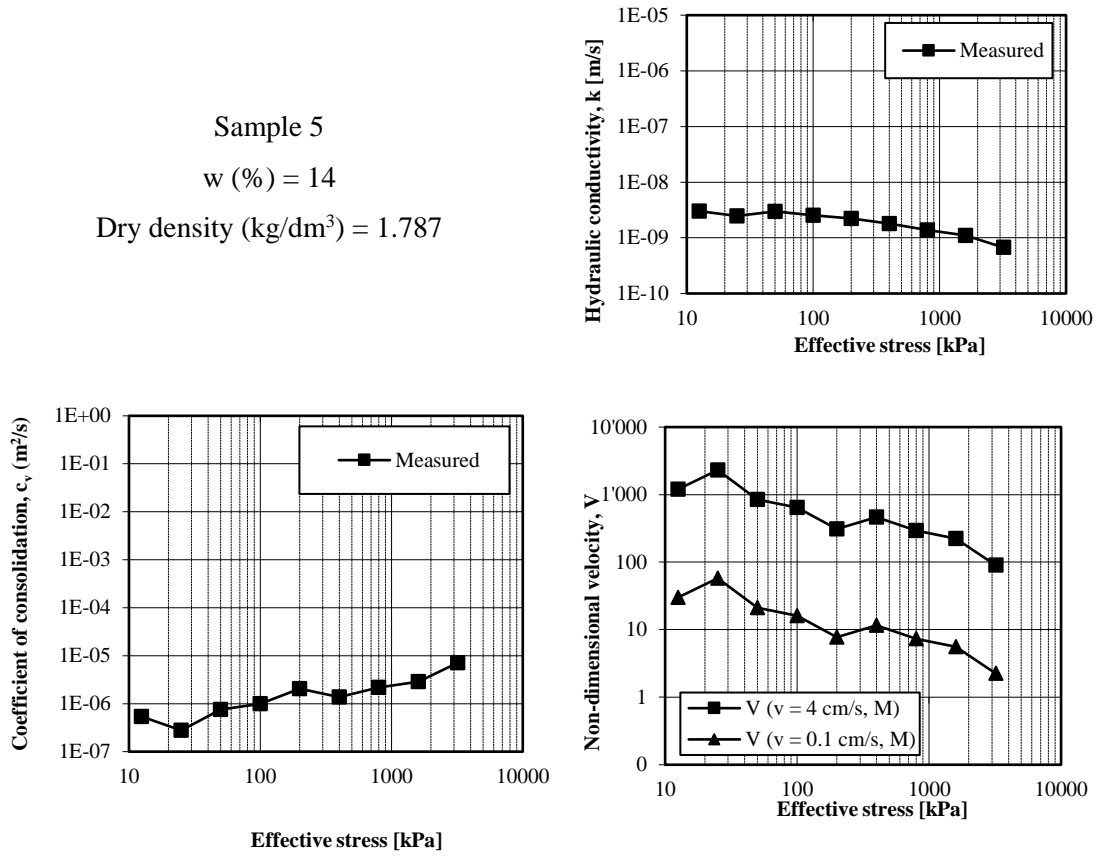


Figure 93: hydraulic conductivity; coefficient of consolidation and non- dimensional velocity V plotted against the vertical effective stress.

7.2.2 Consolidation and mechanical characteristics of the selected soil

As already mentioned, the soil adopted for calibration chamber tests comes from the alluvial deposits of the Po River. The material is composed as follows: 45% of silt, 30% of sand and 25% of clay. The specific gravity value at 20°C, G_s , is 2.72.

Figure 72 shows the compaction curve obtained with the Modified Proctor procedure. The maximum dry density for the applied compaction energy is 1.92 kg/dm³, whereas the optimum water content is around 11.9%. Two different values of dry density have been considered for the compaction of the soil inside the chamber: 1.6 kg/dm³ and 1.9 kg/dm³. Oedometer tests and triaxial tests have been conducted to obtain the main consolidation and mechanical characteristics of the soil at the two different compaction values adopted for the calibration chamber tests. The specimens used for laboratory characterisation have been built up at the laboratory, by extracting a certain amount of material, at the moment of the construction of the calibration chamber specimen. The soil has been subsequently statically compacted inside the Proctor shell, thanks to the use of a mechanical press. The target densities and water content are obtained preparing the specimens with subsequent layers (in particular 5 layers) and applying the pressure required to achieve the desired density inside the Proctor mould. Then the required specimens are extracted from the mould and formed for the specific test (oedometer or triaxial test). The same procedure described in the previous paragraph has been adopted to analyse the consolidation characteristics of the soil effectively present inside the chamber. Direct measurements of hydraulic conductivity have been carried out on both the samples characterised by the dry density and degree of saturation present in the calibration chamber. Measurements of hydraulic conductivity have been plotted against the dry density, the void ratio and the vertical effective stress (Figure 94, Figure 95, Figure 96). Results are analogous to those obtained during the preliminary study showed in the previous section. The linear interpolation of k - S_r data proposed by Tatsuoka is valid also for these set of data, maintaining the same slope of -5.02, but of course different intercept values.

As well described in the following section, the calibration chamber has been divided in two sections (S1 and S2) characterised by two different compaction levels. To quickly refer to one or the other side of the chamber, often in this section the author speaks about the imposed dry density during the compaction process (1.9 and 1.6 kg/dm³, S1 and S2 side respectively). Figure 97 and Figure 99 show the parameters evaluated from the oedometer tests and the estimation of the non-dimensional velocity range achieved with the available device. In particular, k values are those obtained by direct measurements and c_v values are evaluated from k and the constrained modulus obtained from the oedometer test at the respective stress level. The measured void ratios are also included in the tables. As shown in Figure 97, since the specimen is overconsolidated as a consequence of compaction stresses, the constrained modulus initially

decreases with the increase in vertical effective stress, until the preconsolidation stress is reached.

The obtained V range are: 0.1-100 for the S2 side and 1-1000 for the S1 side considering the minimum (0.006 cm/s) and the maximum (4.5 cm/s) penetration rates available for the chamber tests. This implies that, considering the drainage boundaries obtained in previous studies, the soil compacted in the S2 side should go through the entire partially drained range. At lower penetration rates, the fully drained conditions, that usually occurs for V values around 0.1, should be reached. At the same time, the fully undrained conditions, which usually are obtained for V between 30 and 100, should occur during penetration at the maximum velocity. Considering the same limits, the tests conducted inside the S1 side should be more shifted towards the undrained region.

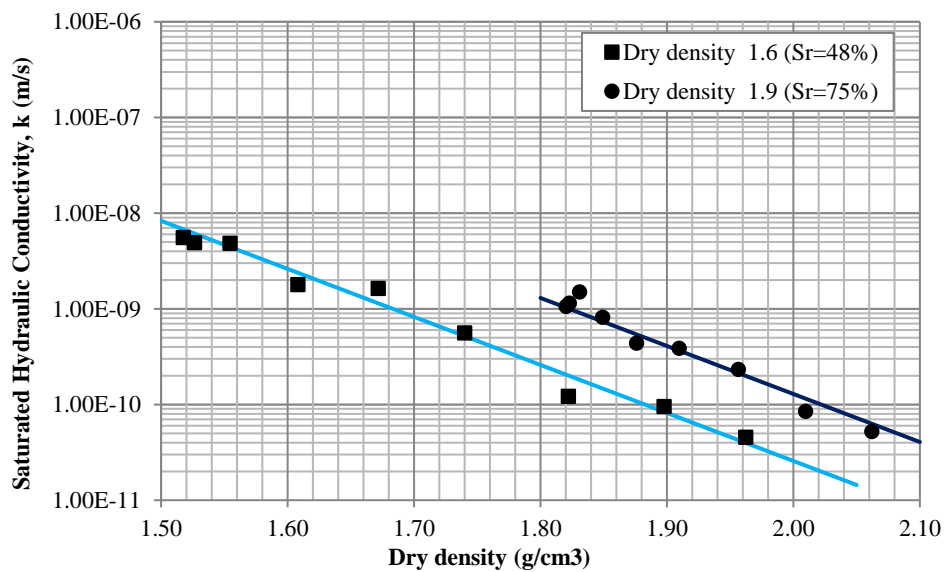


Figure 94: Measured k values vs. dry density. Solid lines refer to Tatsuoka's model (slope $a=-5.02$)

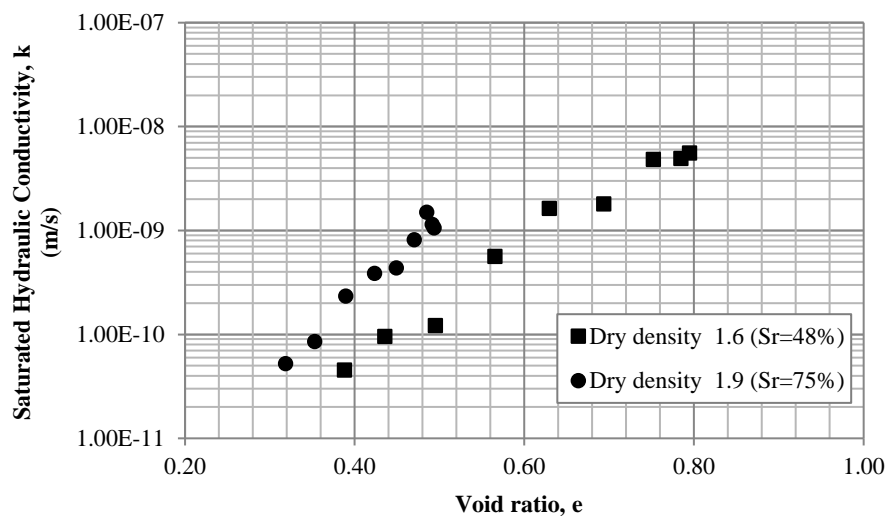


Figure 95: Measured k values vs. void ratio at the beginning of the permeability test.

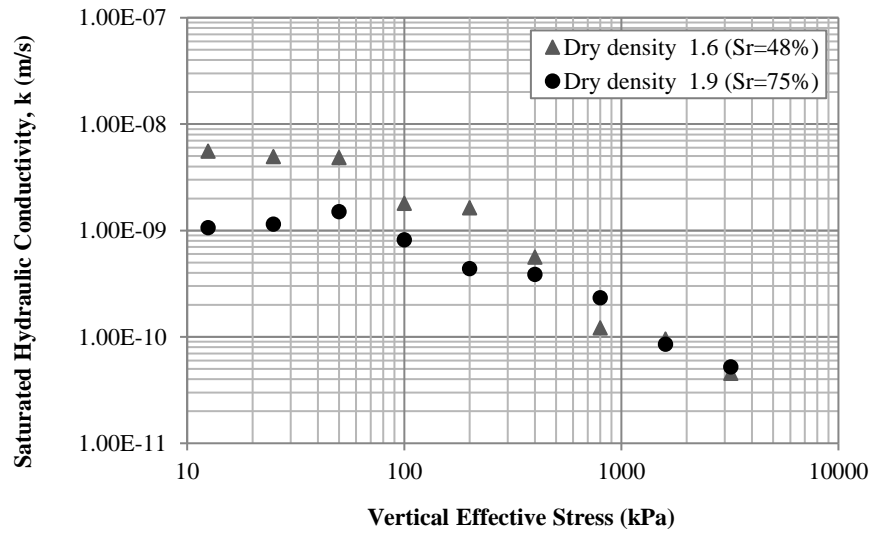
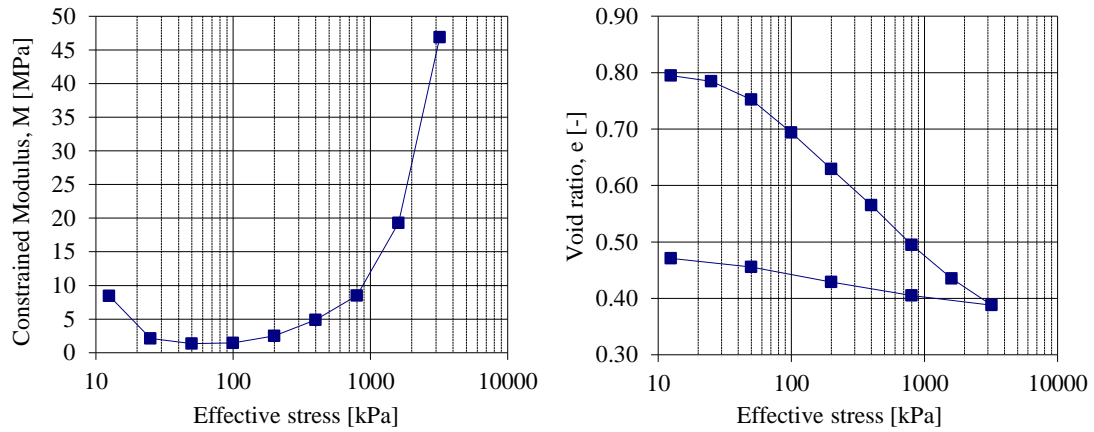


Figure 96: Measured k values versus vertical effective stress during the incremental loading oedometer test.



Vertical Effective stress [kPa]	Void ratio	M (Mpa)	Measured k m/s	c_v (m^2/s)	V ($v = 0.006$ cm/s, M)	V ($v = 4.5$ cm/s, M)
12.5	0.795	8	6E-09	4.8E-06	0.20	149.91
25	0.784	2	5E-09	1.1E-06	0.89	669.87
50	0.752	1	5E-09	6.7E-07	1.44	1079.97
100	0.694	1	2E-09	2.7E-07	3.61	2705.39
200	0.629	3	2E-09	4.2E-07	2.28	1706.93
400	0.565	5	6E-10	2.8E-07	3.43	2571.06
800	0.495	9	1E-10	1.1E-07	9.11	6830.34
1600	0.435	19	1E-10	1.9E-07	5.13	3848.09
3200	0.388	47	5E-11	2.2E-07	4.43	3320.55

Figure 97: Oedometer tests results, direct measurements of hydraulic conductivity and estimation of the coefficient of consolidation for different stress levels for the specimen reproducing the material inside the S2 side of the chamber.

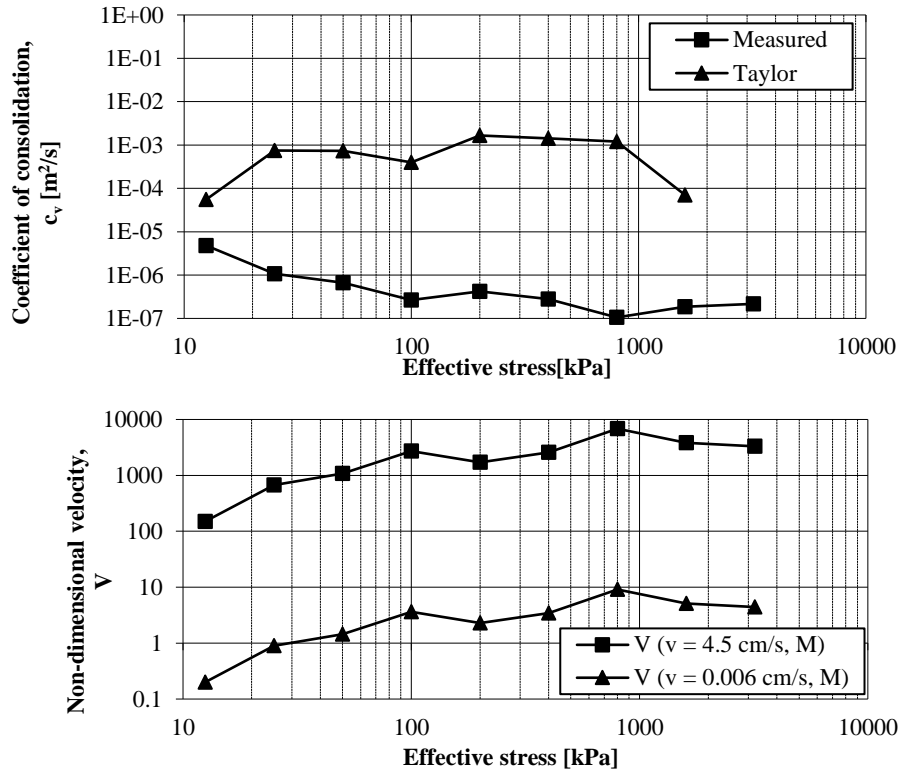
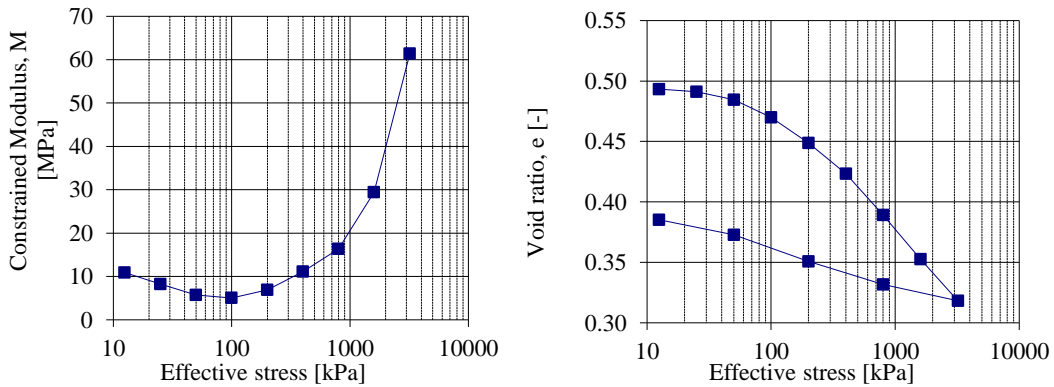


Figure 98: Comparison of direct measurements of hydraulic conductivity with Taylor's estimations. Evaluation of the non-dimensional velocity for the range of penetration rates 0.006-4.5 cm/s available for the chamber tests (S2 side).



Effective stress [kPa]	Void ratio	M (Mpa)	Measured k (m/s)	Cv (m²/s)	V (v = 0.006 cm/s, M)	V (v = 4.5 cm/s, M)
12.5	0.493	11	1E-09	1.2E-06	0.81	609.87
25	0.491	8	1E-09	9.6E-07	1.00	749.72
50	0.485	6	2E-09	8.8E-07	1.09	820.93
100	0.470	5	8E-10	4.2E-07	2.30	1723.59
200	0.449	7	4E-10	3.1E-07	3.13	2347.63
400	0.423	11	4E-10	4.4E-07	2.20	1646.65
800	0.389	16	2E-10	3.9E-07	2.47	1849.86
1600	0.353	29	9E-11	2.6E-07	3.76	2817.21
3200	0.318	61	5E-11	3.3E-07	2.94	2205.18

Figure 99: Oedometer tests results, direct measurements of hydraulic conductivity and estimation of the coefficient of consolidation for different stress levels for the specimen reproducing the material inside the S1 side of the chamber.

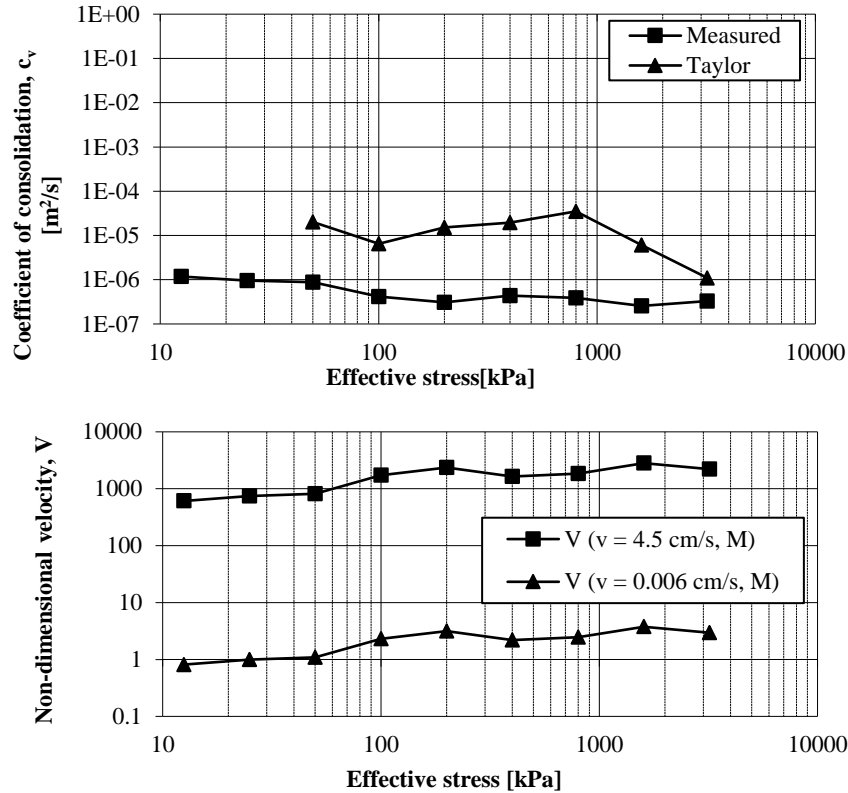


Figure 100: Comparison of direct measurements of hydraulic conductivity with Taylor's estimations. Evaluation of the non-dimensional velocity for the range of penetration rates 0.006-4.5 cm/s available for the chamber tests (S1 side).

Triaxial tests, in particular isotropically consolidated undrained tests (TXCIU) have been carried out to infer strength and large strain stiffness characteristics of the two compacted materials. The specimens have been built up following the procedure previously described and one compacted mould has been prepared under the mechanical press, for each specimen. The specimens have been consolidated at 20 kPa, 60 kPa and 100 kPa for the S2 side soil, and 20 kPa, 50 kPa and 100 kPa for the S1 side soil. Stress strain curves obtained for 20 kPa consolidation stress level, have been analysed to estimate the rigidity index, the ratio between the shear modulus and the undrained resistance. The rigidity index is inferred with respect to the 50% of the shear strength mobilisation. The obtained values have been used to estimate the horizontal coefficient of consolidation from the dissipation test.

Strength envelopes in the t - s' plot, are showed in the following figures. The points illustrated in Figure 101 and Figure 102 represent the Mohr's circle vertex at failure:

$$t' = t = \frac{\sigma'_v - \sigma'_h}{2} ; s' = \frac{\sigma'_v + \sigma'_h}{2}$$

In both cases the strength envelope has an intercept higher than zero. It is not possible to assess if the obtained cohesion is due to the compaction process or if the real envelope is curvilinear with a zero cohesion at the intercept. In fact, given the available device, it has not been possible to carry out triaxial tests at lower consolidation pressures.

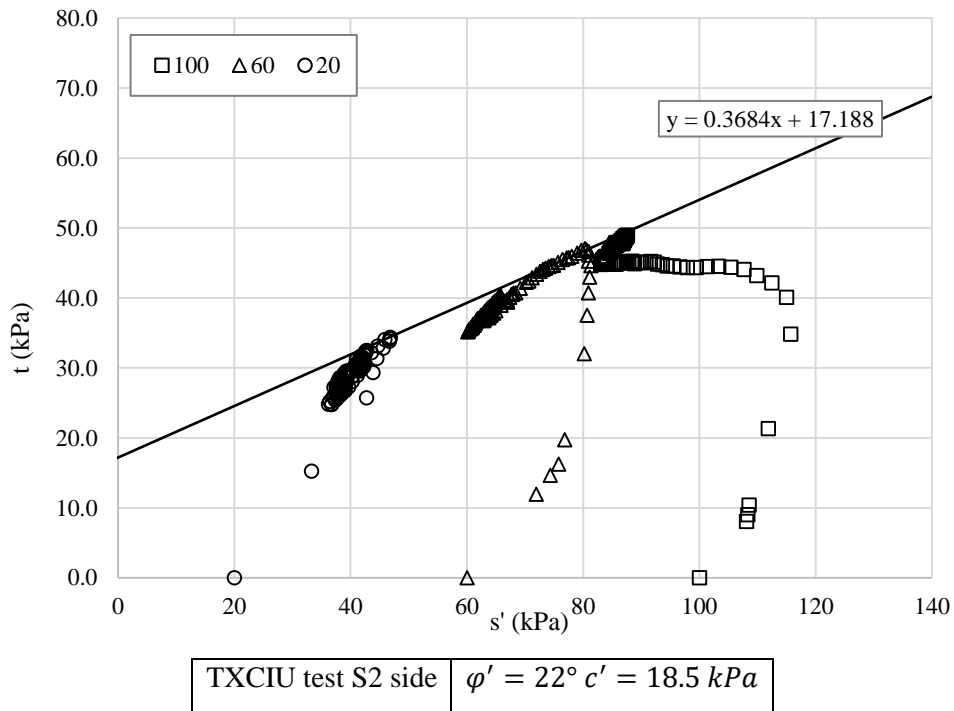


Figure 101: Triaxial tests results (TXCIU) for the S2 side. Consolidation stresses are: 20 kPa, 60 kPa and 100 kPa.

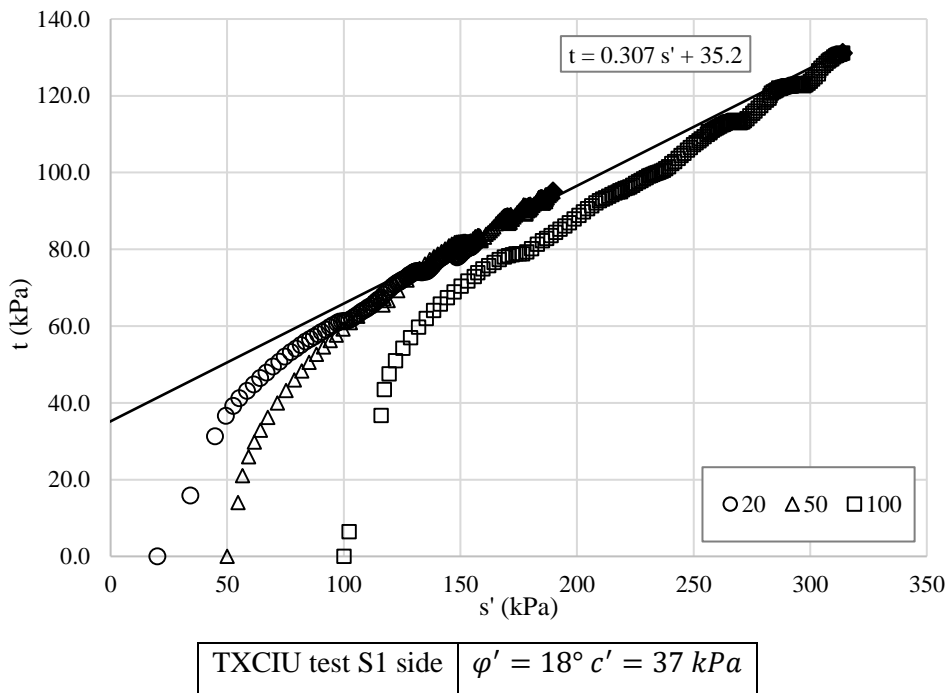


Figure 102: Triaxial tests results (TXCIU) for the S1 side. Consolidation stresses are: 20 kPa, 50 kPa and 100 kPa.

7.3 Specimen preparation procedure

In order to investigate penetration rate effects on the selected soil, two different values of final compaction densities have been selected. The soil inside the left side of the chamber has been compacted at $w = 12\%$ in order to achieve the optimum condition, with a target dry density equal to 1.9 kg/dm^3 (average void ratio = 0.792). The soil inside the right side of the chamber has been compacted at 12% water content and a target dry density of 1.6 kg/dm^3 (average void ratio = 0.492). The compaction energy is given by a manual compactor characterised by a circular plate with a diameter of 30 cm. The compaction process is made layer by layer, for the left side the layers are 10 cm thick, whereas for the right side, layers are 20 cm thick. The total height of the specimen is 120 cm. At the end of the construction process the top layer is covered with geotextile and two steel plates. The plates have several holes to allow access for the cone penetrometer. Each top plate has been made watertight by using gum and silicon in order to prevent lateral water flow during the saturation process.



Figure 103: Construction sequence.

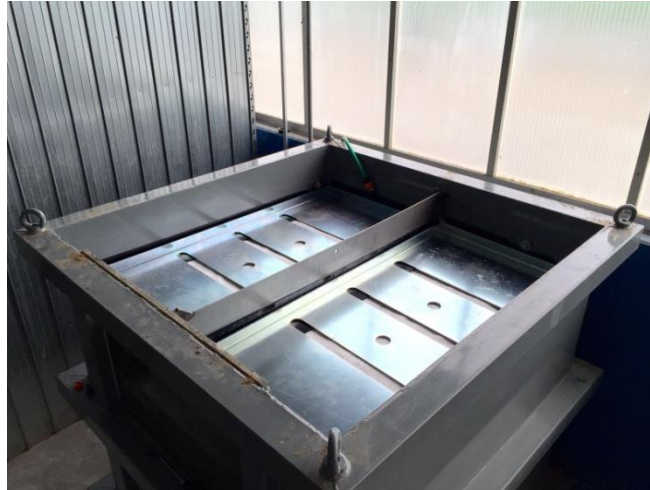


Figure 104: Details of the top layer of the chamber.

After that, the previously described reaction frame has been positioned and fixed to the chamber and the top load has been applied. Four load cells measure the applied load. The described loading system applies a pressure around 10 kPa at the top of the specimen. The vertical stress obtained inside the chamber is therefore the combination of the load applied at the top surface and the self-weight of the material. The top load is maintained constant during the test period. The saturation process is realised by injecting pressured water (0.2 bar) through the irrigation pipe placed at the bottom of the chamber. The saturation process went on for 3 months. The water level at the end of saturation was 5 cm above the upper surface of the specimen.



Figure 105: Water table at the end of the saturation process.

7.4 Cone Penetration tests

A total of 7 tests have been carried out in the left side of the chamber (S1 test series) and 7 tests have been conducted inside the right side of the chamber (S2 test series). The minipiezocone, with a projected tip area of 2 cm² and friction sleeve area of 50 cm², has been used. Penetration tests have been conducted with various velocities ranging between 0.006 cm/s and 4.5 cm/s.

Tests are positioned in the middle area of each side of the chamber (top surface for each side: 20 cm x 80 cm). Tests are displayed following a triangular shaped scheme. The minimum distance between the tests is 20 cm, that more than ten times the cone diameter. The distance between the tests and the front and back sides is 35 cm, the distance between the tests and the lateral sides is 25 cm.

The following table summarises test characteristics.

Test series S1 (left side)		Test series S2 (right side)	
Test N.	Penetration rate [cm/s]	Test N.	Penetration rate [cm/s]
1	0.2	1	0.016
2	0.016	2	2
3	2	3	0.1
4	4.5	4	4.5
5	0.016	5	0.006
6	0.006	6	2
7	0.1	7	0.7

Table 10: Piezocone test characteristics.

7.5 Cone Penetration test results

Test results in terms of profiles of tip resistance, pore water pressure and sleeve friction, are plotted in the following diagrams. Figure 106 and Figure 107 show, respectively, S1 and S2 overlay test series results. The cone resistance has been evaluated as the corrected cone resistance q_t , which has been obtained from the measured cone resistance q_c and the measured pore pressure behind the cone tip. The cone factor area for the minipiezocone is 0.8:

$$q_t = q_c + u_2(1 - a)$$

As far as S1 series is concerned, tip resistance profiles show a first peak value at a depth of 6-10 cm and a second main peak at a depth of 70 - 80 cm. Between these two main peaks, several lower peaks are present. After the second main peak, the penetration resistance gradually decays with depth. This non-homogeneous profile is caused by the sample construction sequence. The sample has been made up compacting manually layers of 10 cm and 20 cm height for S1 and S2 section respectively. In Figure 106 it is possible to observe that the previously described trend is reproduced by all the tests, with differences related to drainage conditions. For S1 series, differences in pore water pressure due to drainage conditions are much more visible. Tests conducted at 0.006 cm/s and 0.016 cm/s are characterised by an almost constant profile with depth, and measured u_2 is between 10 and 20 kPa. As the penetration rate increases, pore water pressure increases significantly. During the tests at 2 cm/s and 4.5 cm/s u_2 reaches values around 300-400 kPa.

As far as S2 series is concerned, tip resistance profiles show several peaks from 50 cm to 85 cm depth. In this case the peak values are more homogeneous. This profile reproduces clearly the construction phases describing the stratified composition. As expected, tip resistance values are lower than those registered during S1 tests.

Despite that many researchers do not consider sleeve friction measurements as reliable as penetration resistance and pore water pressure measurements, in this study an interesting result is obtained for f_s values in both tests series. The penetration rate strongly influences the sleeve friction vertical profile, in particular, f_s increases significantly as the penetration rate increases in both S1 and S2 series.

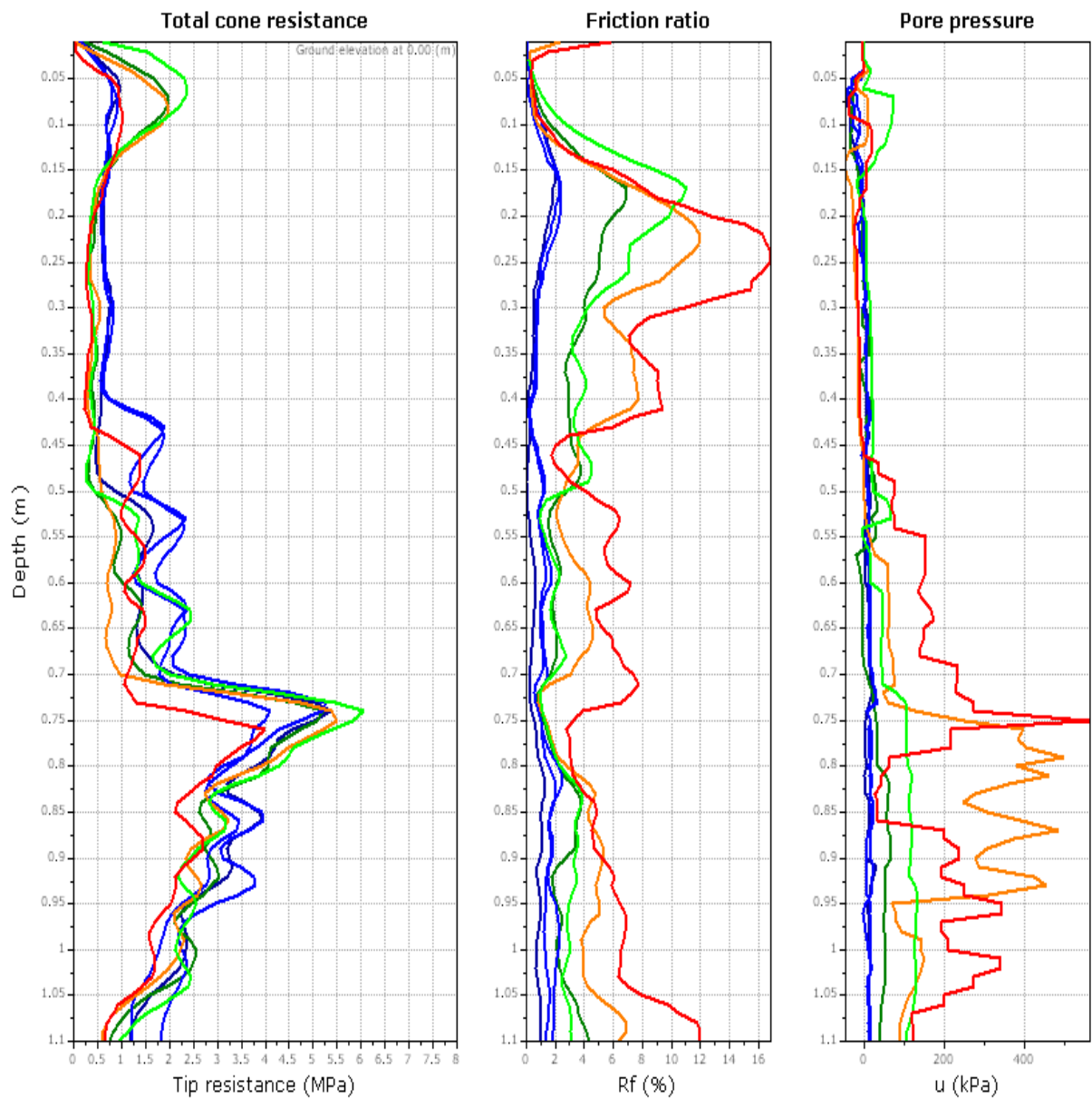


Figure 106: Overlay diagrams of S1 test results. Color legend: dark blue=0.006 cm/s; light blue=0.016 cm/s; dark green=0.1 cm/s; light green=0.2 cm/s; orange=2 cm/s and red=4.5 cm/s (CPeT-IT GeoLogismiki 2007).

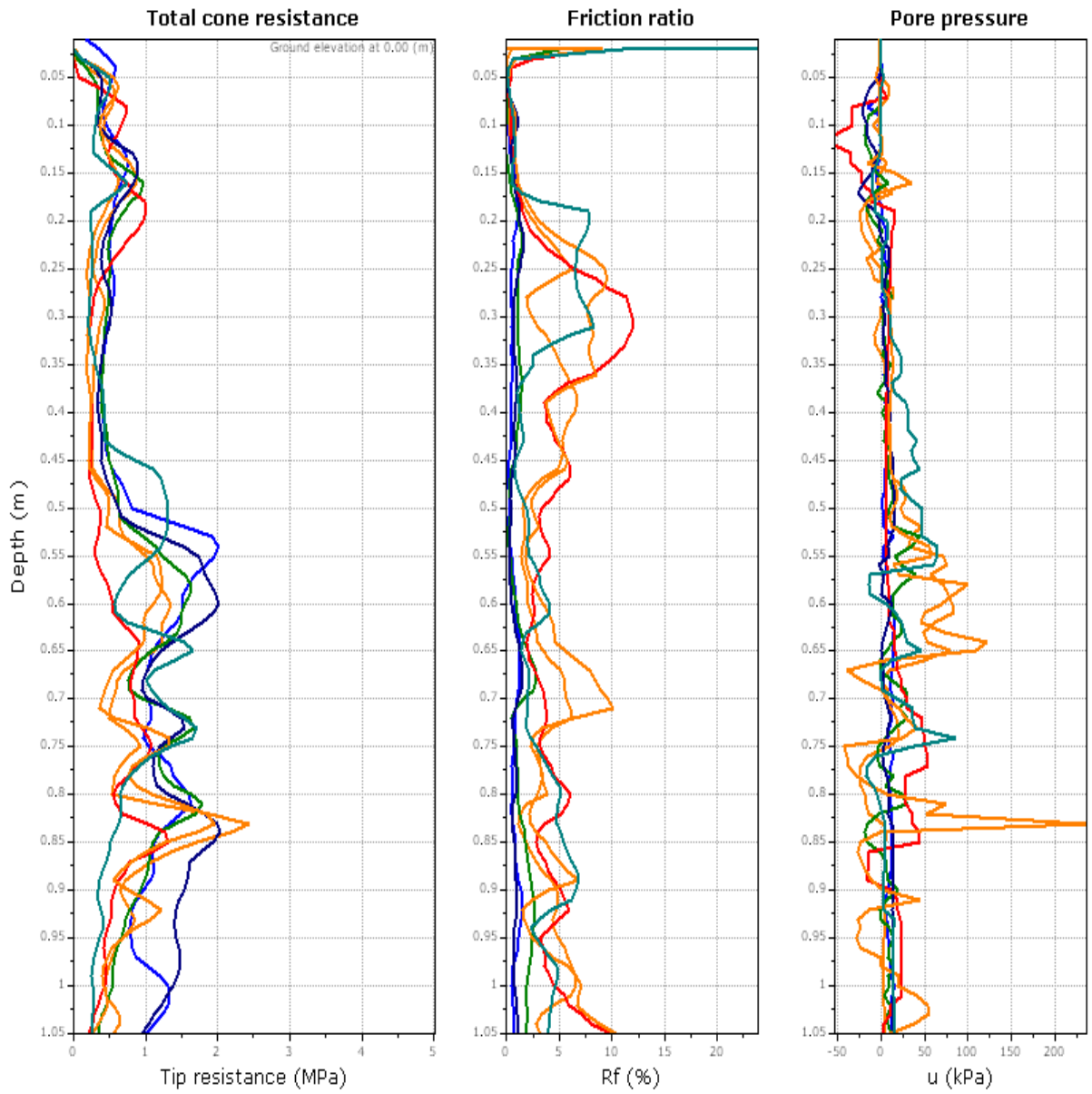


Figure 107: Overlay diagrams of S2 test results. Color legend: dark blue=0.006 cm/s; light blue=0.016 cm/s; dark green=0.1 cm/s; orange=2 cm/s and red=4.5 cm/s (CPeT-IT GeoLogismiki 2007).

7.6 Analysis of Cone Penetration test results

7.6.1 S1 series

In order to study rates effects on test results, average values, of measured cone resistance, pore pressure and sleeve friction have been calculated every ten centimeters. Furthermore, to identify a soil layer where steady state conditions were reached, the gradient of tip resistance with depth, excess pore water pressure and sleeve friction have been evaluated. After that, the soil layer between 50 cm and 70 cm depth has been selected to compare results from different tests. Furthermore, this layer guarantees to avoid disturbances due to surface effects. By evaluating average values (layer between 50 and 60 cm and between 60 and 70 cm), it is possible to compare the results from different tests and study rate effects on piezocone measurements and normalised parameters. The results are summarised in the following figures. Tests have been conducted at: 0.006 cm/s, 0.016 cm/s, 0.1 cm/s, 0.2 cm/s, 2 cm/s and 4.5 cm/s. Tip resistance decreases as the penetration rate increases but the measured data, as expected, do not give the possibility to determine the point where q_t starts decreasing from the fully drainage conditions to the partially drainage conditions. The maximum q_t values are obtained for the range 0.006-0.016 cm/s, average tip resistance in this interval is between 1559 kPa and 2074 kPa (Figure 108). Tip resistance decreasing as the penetration rate increases from 2 to 4.5 cm/s, it dropped from 2074 kPa to 923 kPa. The ratio between the maximum and the minimum tip resistance is around 2.2. Nevertheless, it is not possible to recognise the clear shape of a typical backbone curve.

On the other hand, pore water pressure results show a clearer trend (Figure 109): u_2 increases from 15 kPa to 177 kPa in the range of penetration rates between 0.006 cm/s and 4.5 cm/s. The low u_2 values, measured for the test conducted at the rate of 0.006 cm/s show that the tests are approaching fully drained conditions. The transition between the drained and partially drained conditions can be considered around 0.01 cm/s, whereas the fully undrained conditions are approximated by the results obtained for the test conducted at 4.5 cm/s.

Figure 111 shows the results in terms of sleeve friction measurements. The f_s values increase from 0.87 kPa to 27.66 kPa moving from 0.006 cm/s to 4.5 cm/s. The f_s results can be linearly fitted in the semi-log diagram.

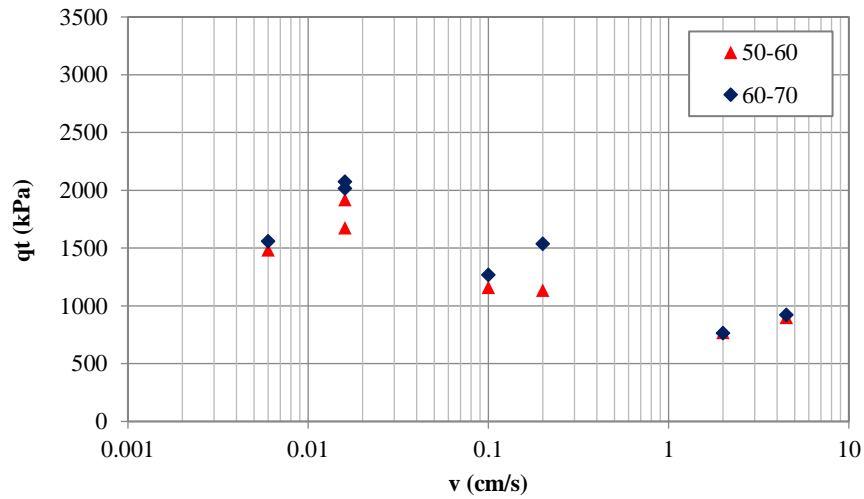


Figure 108: Tip resistance versus penetration rate, S1 series tests. Average results for layers at 50-60 cm depth and 60-70 cm depth.

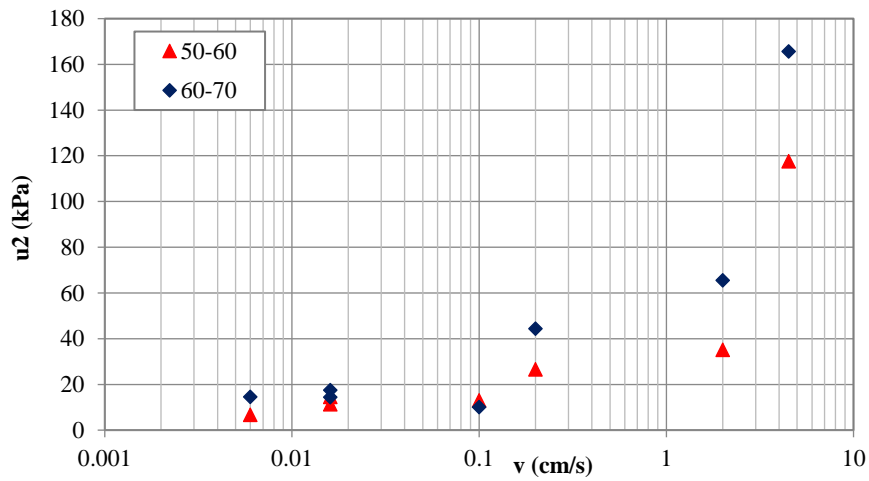


Figure 109: Measured pore water pressure vs penetration rate, S 1 series tests. Average results for layers at 50-60 cm depth and 60-70 cm depth.

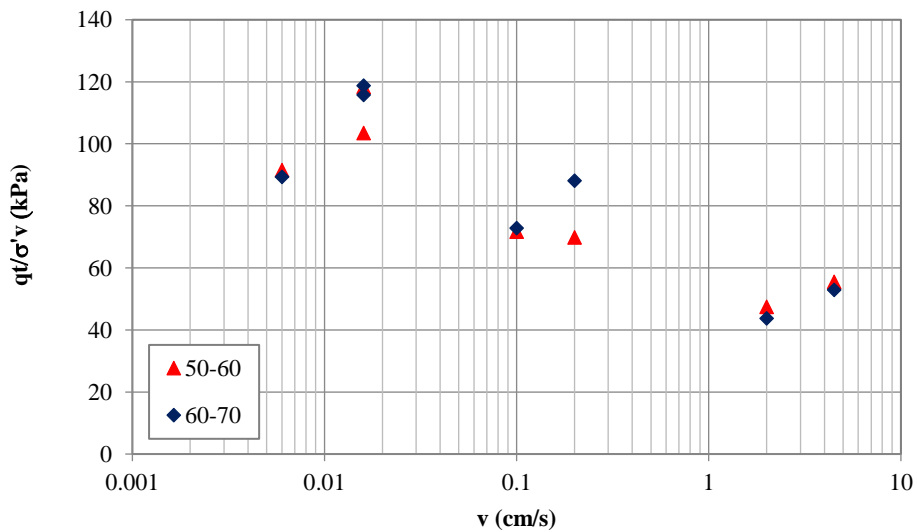


Figure 110: normalised tip resistance with respect to the vertical effective stress, versus penetration rate. Average results for layers at 50-60 cm depth and 60-70 cm depth.

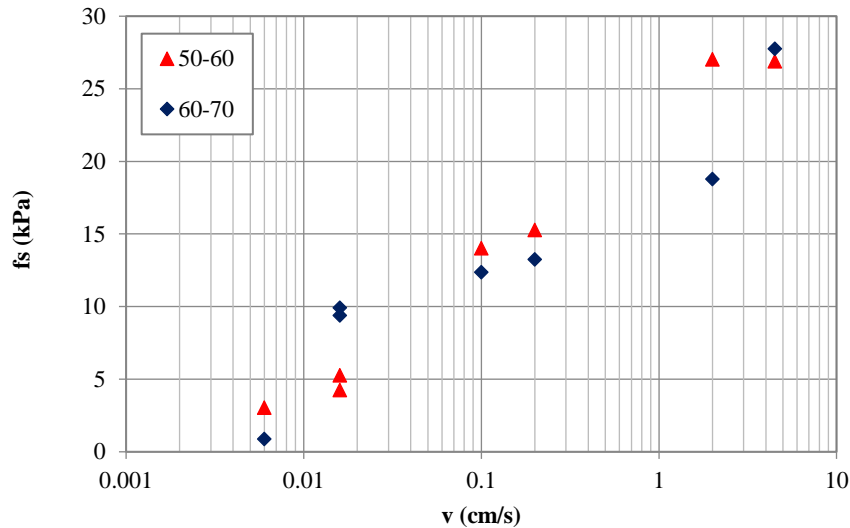


Figure 111: Average sleeve friction vs penetration rate, S1 series tests. Average results for layers at 50-60 cm depth and 60-70 cm depth.

7.6.2 S2 series

The S2 test series has been conducted inside the right side of the chamber with a value of dry density during compaction of 1.6 kg/dm^3 . Tests have been conducted at: 0.006 cm/s, 0.016 cm/s, 0.1 cm/s, 0.7 cm/s, 2 cm/s and 4.5 cm/s. Test results, averaged between 50 cm and 60 cm and between 60 cm and 70 cm depth, are displayed in the following figures.

Figure 112 shows q_t results. Tip resistance results decreases from $q_t=1466 \text{ kPa}$ of the test at lower penetration rate, to $q_t=506 \text{ kPa}$ for the tests at 4.5 cm/s. The same trend is reproduced in the normalised diagram (Figure 113) where q_t/σ'_v is plotted versus the penetration rate.

On the other hand, as expected, pore water pressure increases in the range of penetration rates between 0.006 cm/s and 4.5 cm/s, from 8.84 kPa to 54.6 kPa. Even though the interval of u_2 values is relatively small, the trend of u_2 with penetration rate is evident (Figure 114). Sleeve friction measurements increases as the penetration rate increases, f_s average value is around 3 kPa for the lower penetration rate, and circa 19 kPa for the higher penetration rate (Figure 115). It is possible to notice that in the case of S2 series, measured data in terms of q_t , u_2 and f_s cover a smaller range than that covered from S1 test series results. This is due to the difference in compaction characteristics; in fact, the specimen on the left side of the chamber (S1) has a compaction dry density much higher than that of the specimen inside the right part of the chamber (S2).

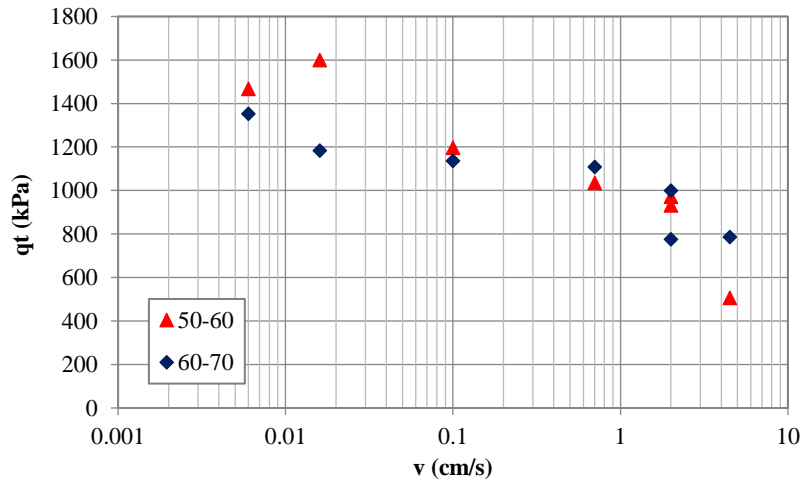


Figure 112: Tip resistance versus penetration rate, S2 series tests. Average results for layers at 50-60 cm depth and 60-70 cm depth.

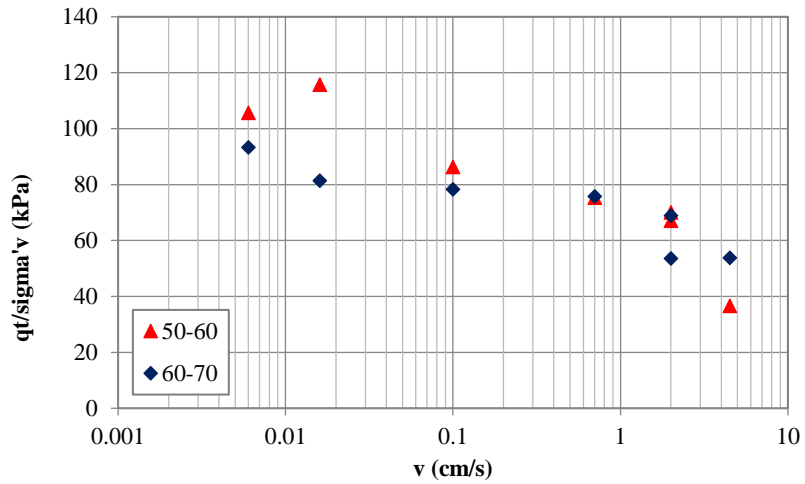


Figure 113: q_t/σ'_v vs penetration rate, S2 series tests. Average results for layers at 50-60 cm depth and 60-70 cm depth.

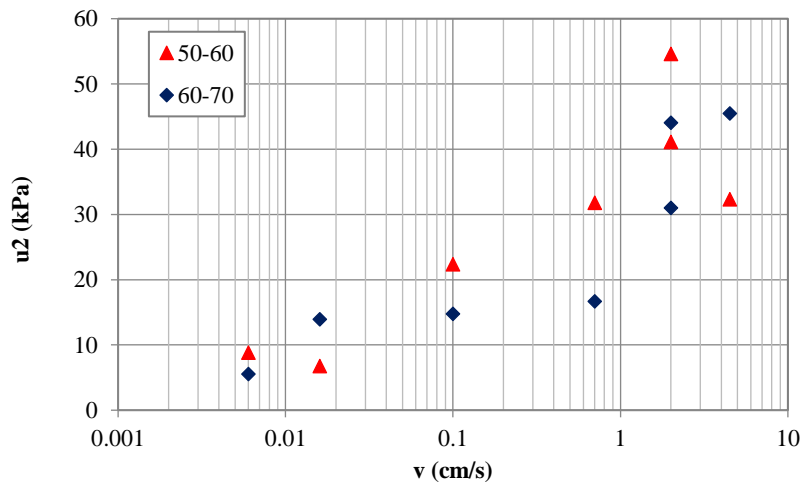


Figure 114: Measured pore water pressure vs penetration rate, S2 series tests. Average results for layers at 50-60 cm depth and 60-70 cm depth.

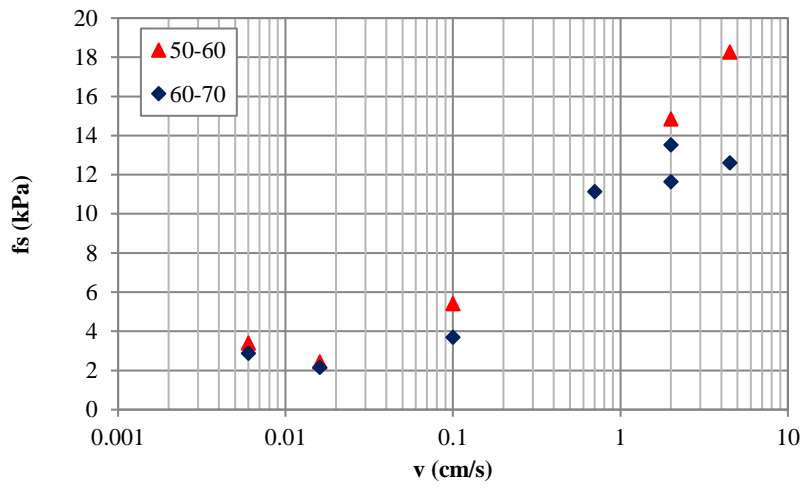


Figure 115: Sleeve friction versus penetration rate, S2 series test. Average results for layers at 50-60 cm depth and 60-70 cm depth.

7.6.3 Dissipation tests

As discussed previously, the non-dimensional velocity V is the proper parameter to assess drainage conditions during penetration. V is given by the penetration rate, the diameter of the cone and the coefficient of consolidation.

In order to have an estimation of the coefficient of consolidation, dissipation tests have been conducted. During a dissipation test the decay with time of the excess pore water pressure, generated during the penetration, is measured. Two dissipation tests have been conducted inside each part of the chamber. Details are summarised in Table 11. Figure 116 and Figure 119 show the excess pore water pressure decay during the dissipation tests in S1 and S2 series. Dissipation tests have been carried out during the test at 2 cm/s and 4.5 cm/s, the maximum penetration rates, during which the phenomenon can be considered closed to the undrained conditions. Unlike the expectation the dissipation curves have a typical monotonic “S” shape without showing an initial increasing and subsequent decreasing of pore water pressure. The interpretation of the results is made through the model proposed by Teh and Houlsby (1991). The values of c_{vh} shown in Table 11 were deduced by the following expression:

$$c_{vh} = \frac{T_{50} \cdot a_c^2 \cdot \sqrt{I_r}}{t_{50}}$$

where: a_c is the probe radius, $I_r = G/s_u$ is the rigidity index of the soil, t_{50} is the elapsed time corresponding to the 50% of excess pore water pressure dissipation and $T_{50} = 0.245$ is the time factor corresponding to the 50% of dissipation for u_2 measurements. The rigidity index has been evaluated from triaxial tests conducted on compacted specimens.

		Depth (cm)	t_{50} (s)	T^*	$a_c (=d/2)$ (cm)	I_r	c_{vh} (m ² /s)
S1	Dissipation test n. 1 (piezocone test at 4.5 cm/s)	71	119	0.245	0.8	83	1.2E-6
	Dissipation test n. 2 (piezocone tests at 2 cm/s)	78	294	0.245	0.8	83	4.8E-7
S2	Dissipation test n. 1 (piezocone test at 2 cm/s)	60	395	0.245	0.8	55	2.9E-7
	Dissipation test n. 2 (piezocone test at 4.5 cm/s)	93	420	0.245	0.8	55	2.9E-7

Table 11: Dissipation test results.

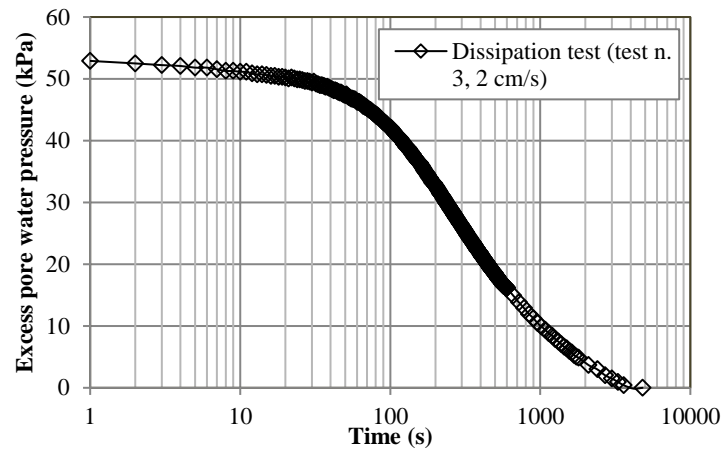
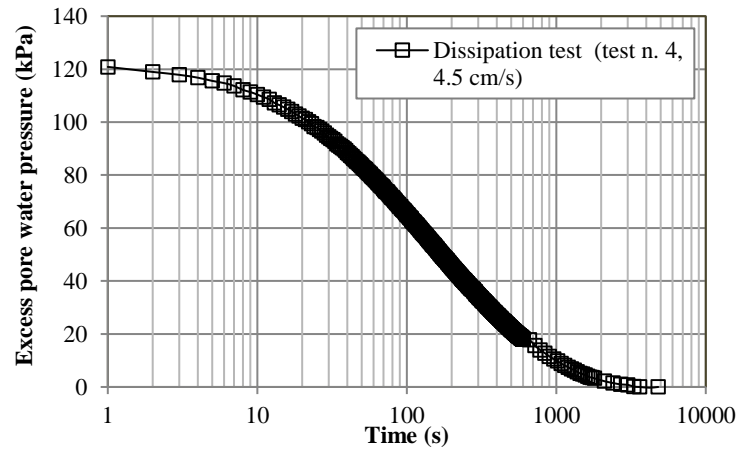


Figure 116: Dissipation tests n. 1 and n. 2 carried out during S1 test series, depth 71 cm and 78 cm respectively.

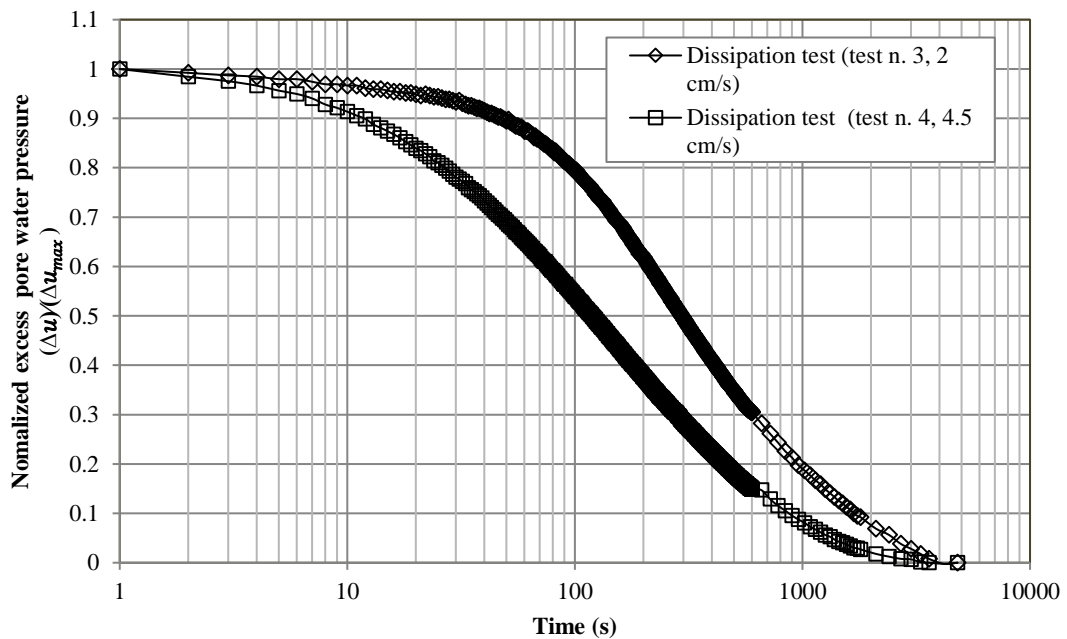


Figure 117: normalised excess pore water pressure dissipation over time. Each curve is normalised using the respective maximum value (S1 side).

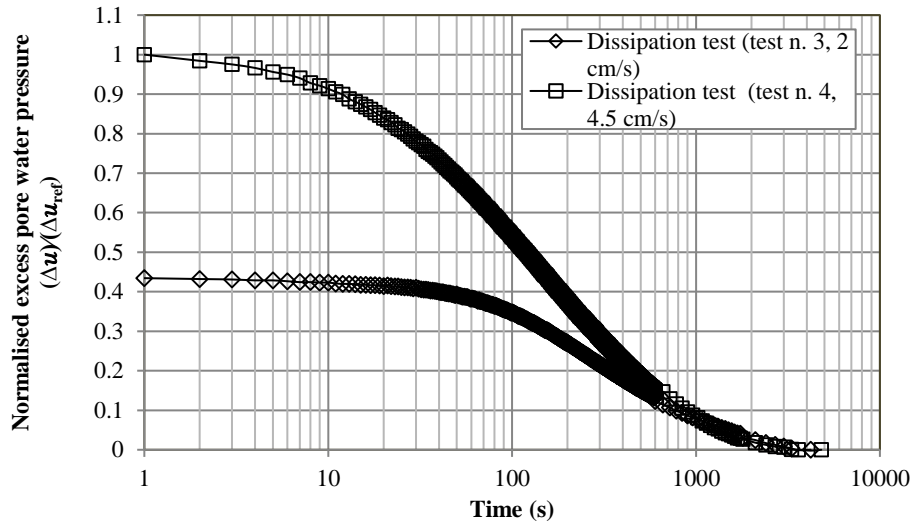


Figure 118 normalised excess pore water pressure dissipation over time. Each curve is normalised using the maximum value obtained for the test n.4 (S1 side).

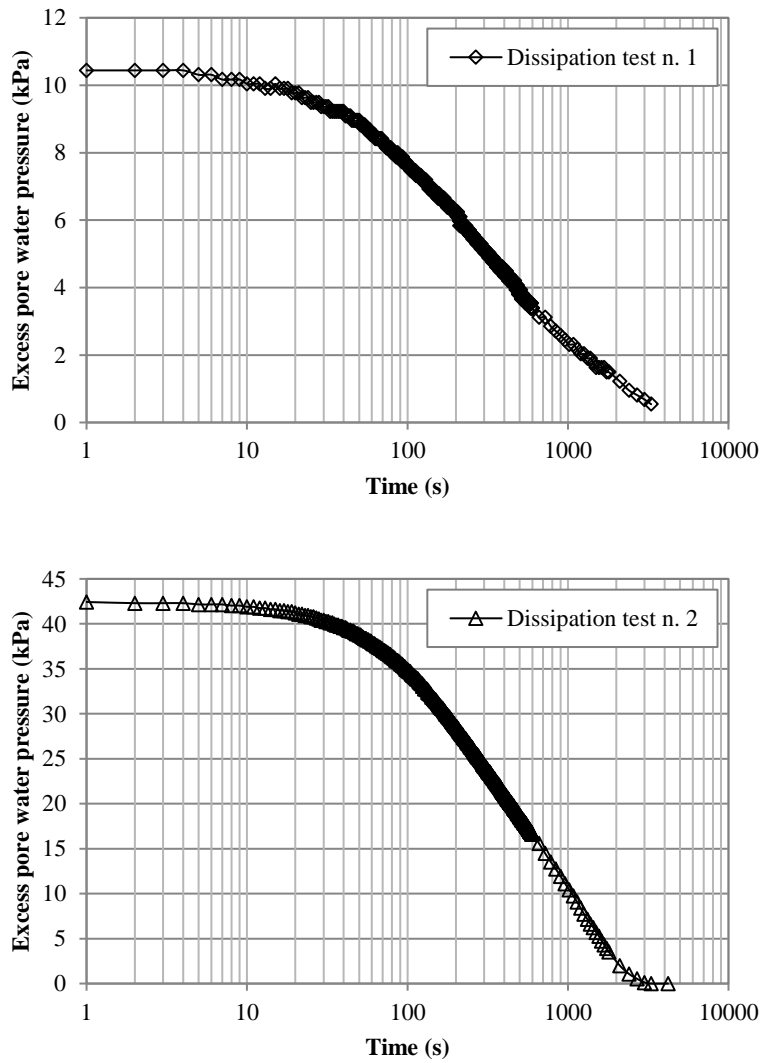


Figure 119: Dissipation tests n. 1 and n. 2 carried out during S2 test series, depth 60 cm and 93 cm respectively.

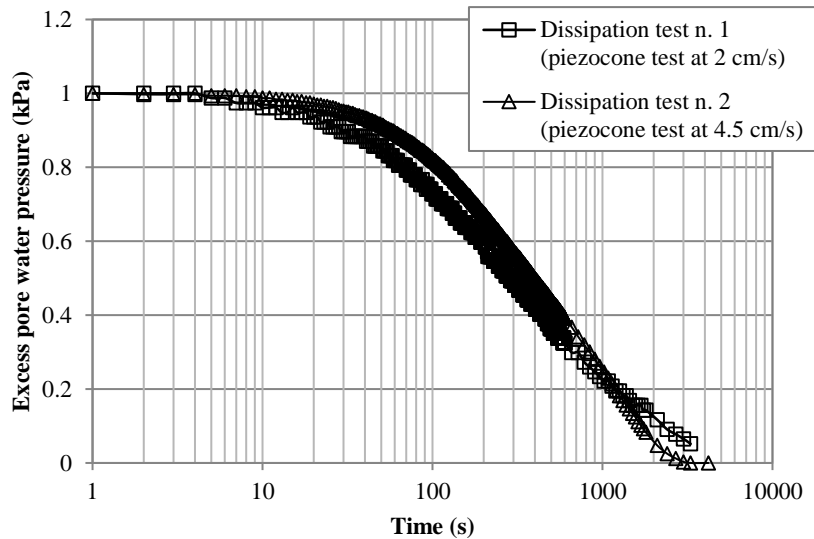


Figure 120: normalised excess pore water pressure dissipation over time. Each curve is normalised using the respective maximum value (S2 side).

As evidenced by DeJong and Randolph (2012), if the excess pore pressure measurements are normalised by the maximum excess pore pressure within the respective dissipation curve, effects of partial consolidation lead to a shift to the right of the dissipation curves resulting in an overestimation of t_{50} values, and therefore in an uncorrected estimation of the coefficient of consolidation. In particular, t_{50} increases as the ratio $\Delta u_2 / \Delta u_{2max}$ decreases (as partial consolidation effects increase). On the other hand, in case of partial consolidation during the penetration test, if dissipation tests measurements are normalised with respect to the reference initial pore pressure measured during undrained penetration, the curves tend to converge to the curve obtained during the undrained condition (Figure 118).

Mahmoodzadeh and Randolph (2012), in their study on dissipation tests on kaolin clay, compared measurements of the vertical coefficient of consolidation inferred from Rowe cell tests with the estimation of the so called horizontal coefficient of consolidation based on dissipation tests interpretation. The ratio between the vertical and the horizontal coefficient of consolidation reaches the value of 4.66. For the present study, results are visible in Table 11 where the measured horizontal coefficient of consolidation is displayed, and in Figure 121 together with Figure 122, which show the vertical coefficient of consolidation inferred from direct measurement of the hydraulic conductivity and oedometer test results. For S1 side soil, c_v and c_h estimated from the dissipation curve, obtain at the maximum penetration rate of 4.5 cm/s, are almost the same (Figure 121). Whilst for the S2 side the estimated horizontal coefficient of consolidation is lower than the vertical value inferred from the oedometer test (as far as the constrained modulus is concerned) and the hydraulic conductivity measurement (Figure 122). As a matter of fact, the dissipation test interpretation is affected by many factors,

as previously said. Since laboratory measurements of hydraulic conductivity of the soil under the conditions adopted for the S2 side of the chamber are lower than those obtained for the S1 side conditions and by considering that the adopted penetration rates are the same, in particular the maximum one, then the c_h underestimation obtained from dissipation tests can be addressed to the more relevant presence of partially drained conditions (as reflected by the shifted non-dimensional velocity intervals between the two materials).

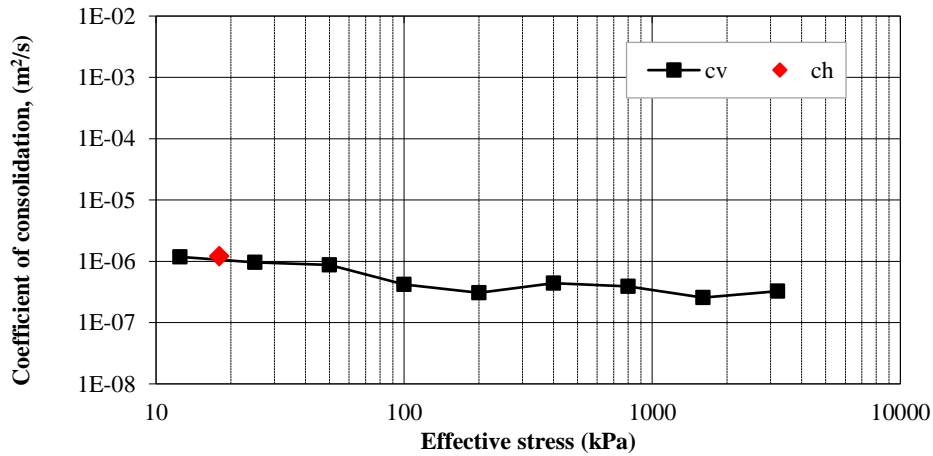


Figure 121: Comparison between vertical and horizontal coefficient of consolidation, S1 side.

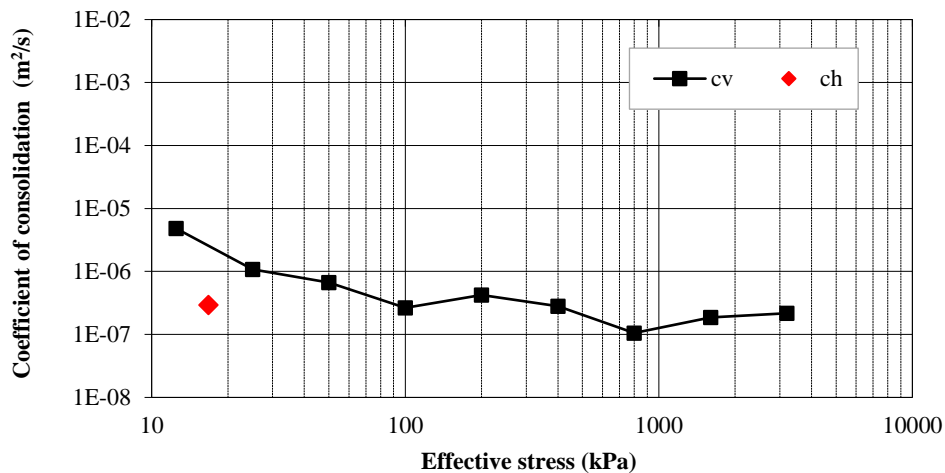


Figure 122: Comparison between vertical and horizontal coefficient of consolidation, S2 side.

Another aspect that has to be considered is the estimation of the Rigidity Index to insert in the formulation proposed by Teh and Houlsby. Usually, and in this study, the value of the shear modulus, is estimated from triaxial tests, considering the 50% of shear strength mobilisation. This procedure may have some limitations, as triaxial test is not properly the best instrument to give reliable estimation of the shear modulus. Regarding this, it would be useful to examine in depth the influence of using in situ shear modulus estimation on the evaluation of the coefficient of consolidation. De Jong and Randolph (2012) suggest that it is more appropriate to base the

evaluation of the rigidity index on the small strain modulus G_0 as determined by seismic cone penetration tests. Unfortunately, these tests are not available for the present study.

7.6.4 Normalised tip resistance and excess pore water pressure versus normalised penetration rate.

The results obtained from the calibration chamber tests have been interpreted in terms of normalised penetration resistance and normalised pore water pressure. Following Randolph and Hope (2004), the normalised tip resistance has been evaluated as the ratio:

$$\frac{q_{net}}{q_{ref}}$$

Where $q_{net} = q_t - \sigma_{v0}$ and $q_{ref} = q_t - \sigma_{v0}$ is the value obtained in undrained conditions. In this case, measured tip resistance during the faster test has been considered as the undrained value, whereas, for the previously made observations, this operation cannot be considered completely correct and in analysing the results has to be taken into account. The normalised tip resistance has been plotted against the non-dimensional velocity V , evaluated considering the coefficient of consolidation inferred from laboratory test, in particular from direct measurement of hydraulic conductivity and the evaluation of the constrained modulus from the oedometer tests. The reason for this choice is the consequence of what observed and discussed in the previous section. The values are those obtained for the vertical effective stress equal to 12.5 kPa.

In Figure 123 it is possible to observe the obtained results for the S1 series. The data have been fitted with the following hyperbolic function (DeJong and Randolph, 2012):

$$\frac{q_{net}}{q_{ref}} = 1 + \frac{\frac{q_{drained}}{q_{ref}} - 1}{1 + \left(\frac{V}{V_{50}}\right)^c}$$

Where $\frac{q_{drained}}{q_{ref}}$ is the normalised drained resistance (equal to 2.8), V_{50} is the normalised velocity corresponding to the penetration rate at which the 50% of drained tip resistance is mobilised (equal to 7), c is the maximum rate of change in tip resistance ratio with V (equal to 1).

Figure 124 shows the results obtained for the S2 chamber. In this case data are fitted with the previous expression, using the following parameters: $\frac{q_{drained}}{q_{ref}} = 2.1$, $V_{50}=7$, $c=1$.

Since measured tip resistance is affected by the characteristics of the soil layers below the advancing tip, it represents the soil characteristics of a soil volume that can have different strength and stiffness characteristics. This phenomenon can cause an additional difficulty to interpret and compare variable rate penetration tests.

Figure 125 shows the normalised excess pore water pressure versus the non-dimensional velocity, for S1 series. Data have been fitted with the following curve (DeJong and Randolph, 2012):

$$\frac{\Delta u}{\Delta u_{ref}} = 1 - \frac{1}{1 + \left(\frac{V}{V_{50}}\right)^f}$$

with $V_{50} = 145$ and $f = 1.5$. The value of V_{50} obtained for kaolin clay and based on c_v (Mahmodzadeh and Randolph, 2014) is around 4-5.5, whereas the coefficient f is 1.4. Figure 126 shows the results for the S2 data, in this case the best-fit curve has the following parameters: $V_{50} = 20$ and $f = 1.2$.

Despite the considerable scatter in test results and the uncertainties in the re-construction of the backbone curve, a general trend can be recognised from the presented plots. Drainage limits are compared with the results obtained by previous researches on this field, for laboratory tests, in situ tests and numerical analyses (among all: Randolph and Hope, 2004; Kim, 2005; Kim et al. 2008; Yi et al., 2012). In particular, the non-dimensional velocity range in which partial drainage is expected to occur for kaolin clay is in the limits 0.1-10/30. As shown by Schneider et al. (2007), the partially drained range is a function of the soil characteristics. In this case the undrained conditions are reached for V values higher than 100, for both sides S1 and S2. This value is confirmed by both normalised tip resistance and pore water pressure measurements. As far as the drained limit is concerned, it can be supposed that normalised tip resistance reached a constant value for V around 0.1, but the scatter in the data does not allow to give a reliable value. Looking at the diagrams of the normalised excess pore water pressure, the drained limit is shifted to the right and can be identified in V equal to around 3 for S1 series, and 1 for S2 series.

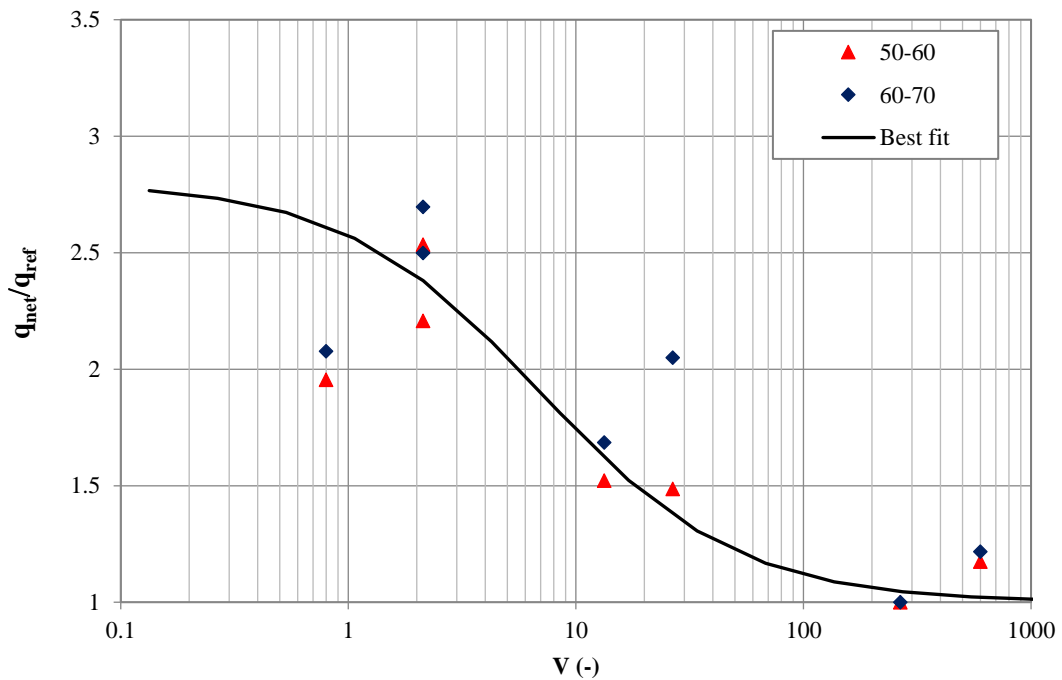


Figure 123: Normalised tip resistance vs non-dimensional velocity V , S1 series.

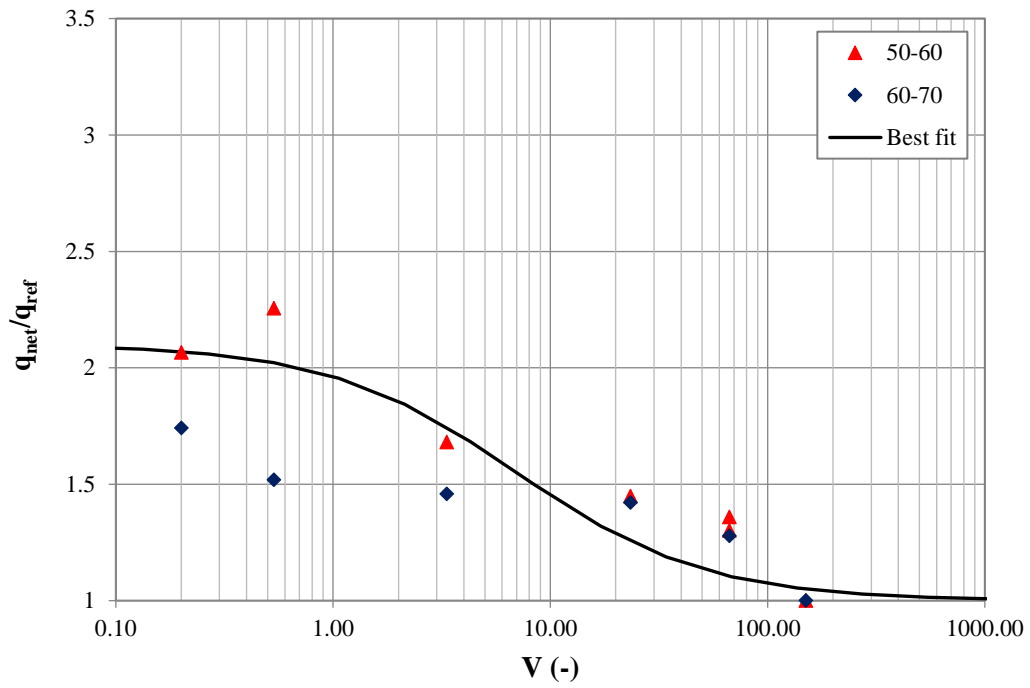


Figure 124: Normalised tip resistance vs non-dimensional velocity V , S2 series.

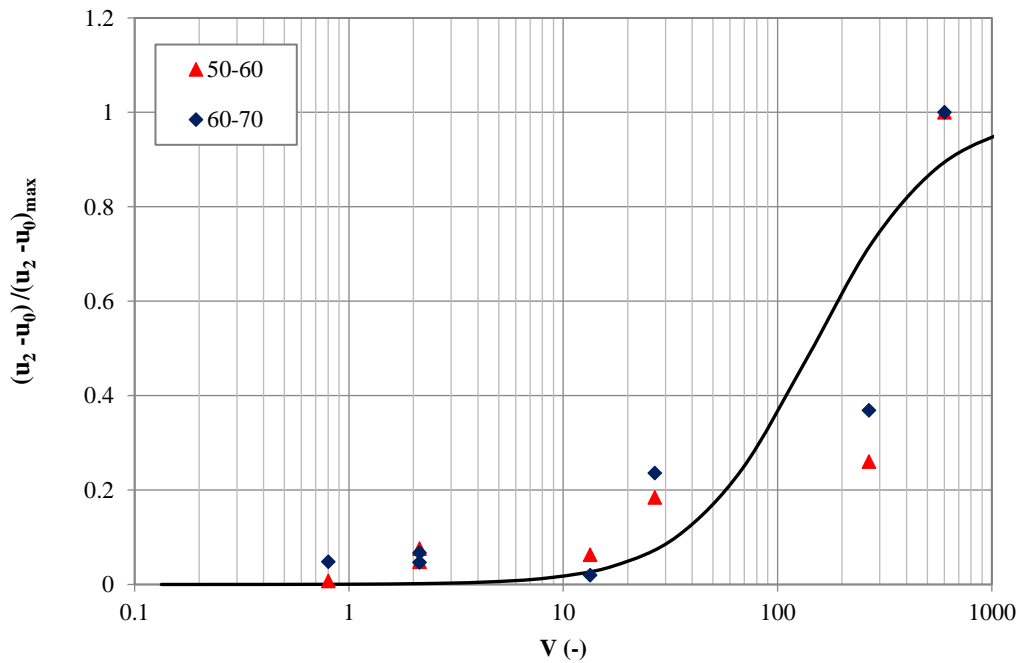


Figure 125: Normalised excess pore water pressure versus non-dimensional velocity V , S1 series.

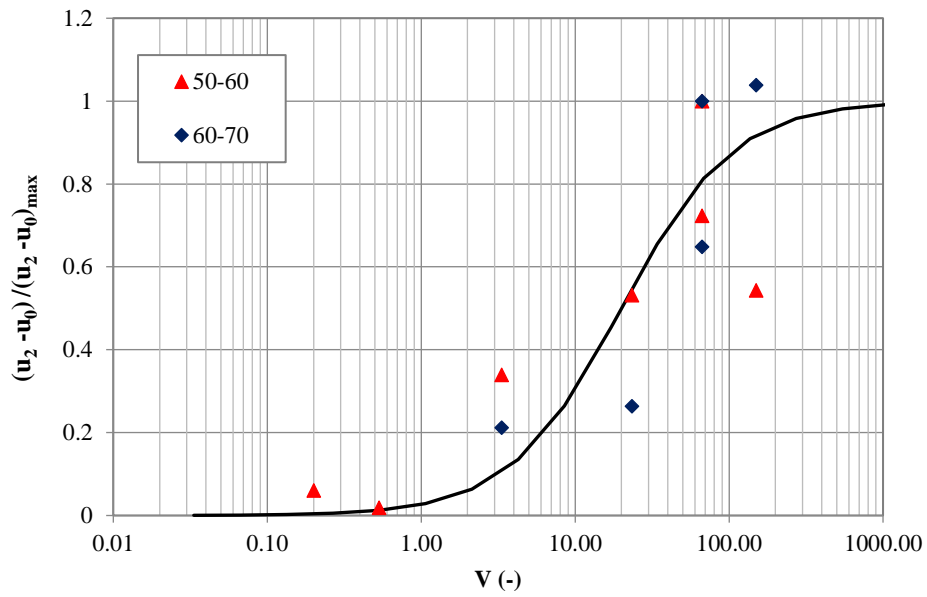


Figure 126: Normalised excess pore water pressure versus non-dimensional velocity V, S2 series.

The most interesting results are obtained from fs measurements. Figure 127 shows the normalised fs value, with respect to the vertical effective stress, versus the penetration rate for S1 results. Figure 128 shows the normalised fs values for the S1 and S2 series: in both cases data can be grouped along a line, in the semi-logarithmic plot, but the slopes are different: fs measurements obtained for the S2 side are lower than those obtained inside the S1 chamber for the same penetration rate (lower slope of the best-fit line).

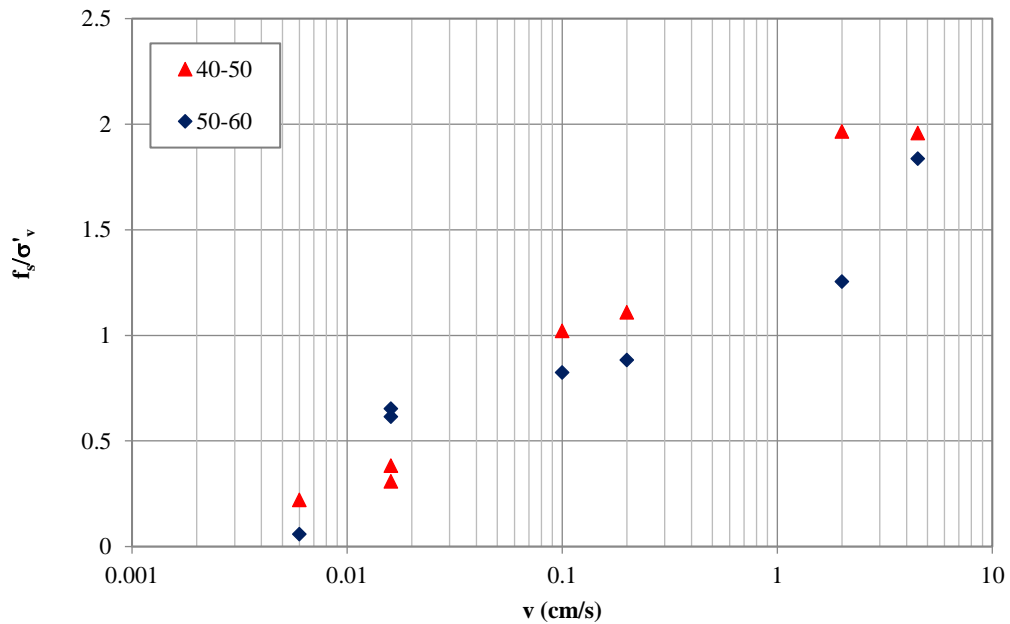


Figure 127: Normalised fs values over penetration rate, S1 series.

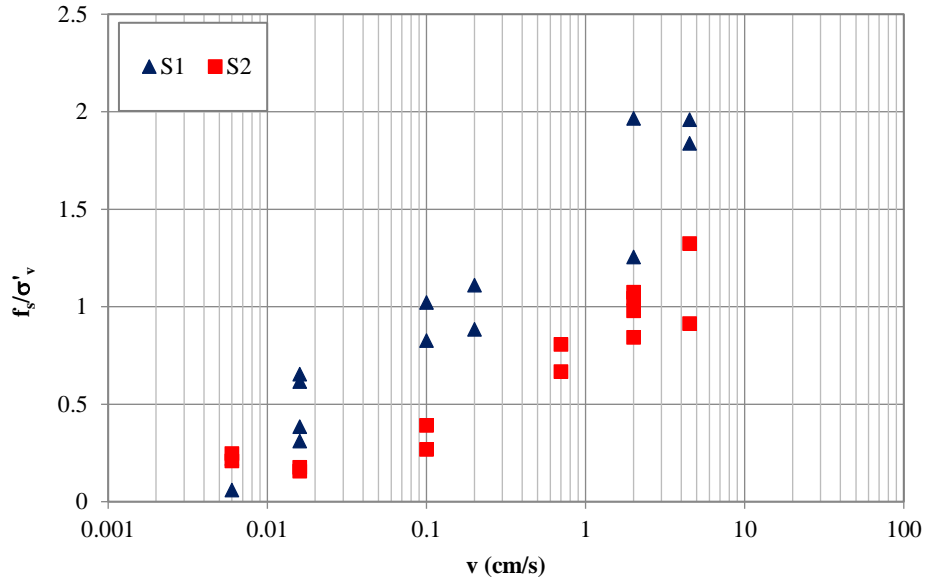


Figure 128: Normalised f_s values for S1 and S2 series versus penetration rate.

Results have been plotted on the classification charts proposed by Schneider et al. (2008 and 2012). The meaning of the chart parameters is the following:

$$Q = \frac{q_t - \sigma_{v0}}{\sigma'_{v0}} = \frac{q_n}{\sigma'_{v0}}; \quad F(\%) = \frac{f_s}{q_t - \sigma_{v0}} \cdot 100 = \frac{f_s}{q_n} \cdot 100$$

Both S1 and S2 results in the $Q - \Delta u/\sigma'v$ chart cover three classification zones, moving from the 1a zone of Silts for higher penetration rates to the zone 3 of transitional soils and finally the zone 2 of sands. The direction of measured data in the plot well-agrees with what expected by the authors if drainage conditions are modified changing the penetration rates. In the $Q - f_s/q_n$ plot, data related to S2 series are shifted to the left, crossing the 1c zone and the 2 zone. Only few dots of the S1 series approaching the 1b zone. In this case too, the direction of movement for increasing drainage is in accordance to what predicted by the authors.

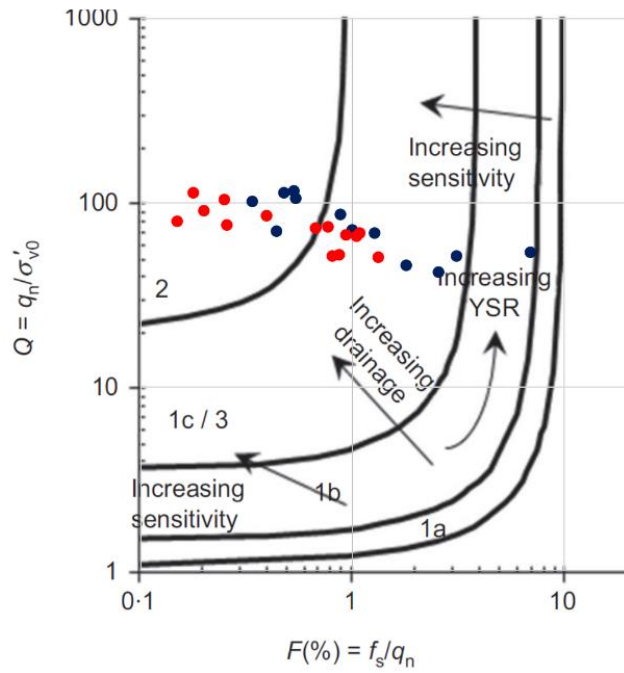
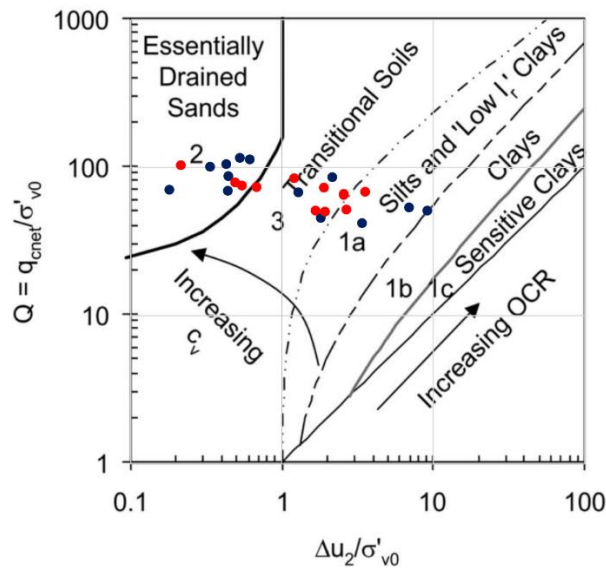


Figure 129: Normalised data (red = S1; blue = S2) plotted on the soil classification chart proposed by Schneider et al. (2012).



Classification zone	Simplified description of soil type
1a	Silts and Low- I_R clays ($I_R = G/s_u$)
1b	Clays
1c	Sensitive clays
3	Silts and transitional soils
2	Essentially drained sands and sand mixtures

Figure 130: Normalised data (red = S1; blue = S2) plotted on the soil classification chart proposed by Schneider et al. (2008)

7.6.5 Proposed f_s/σ'_v versus V expression

Many authors have proposed correlation to express the side friction as a function of the horizontal effective stress and the interface friction between the cone and the soil. The horizontal effective stress can be related then to the vertical effective stress. Correlations are essentially formulated by dividing fully drained conditions in sands from fully undrained conditions in clay. Side friction can be generally expressed as following:

$$f_s = \beta \sigma'_{v0}$$

The aforementioned expression can be used for both drained and undrained conditions, giving different values to the coefficient β . Meyerhof proposed values ranging between 0.4 and 1.2 for sands; 0.15 ± 0.05 for soft clays; 0.25-2.5 for stiff clays. Lower values for crushable calcareous sands have been proposed by Poulos: 0.05-0.1.

Therefore, plotting the obtained f_s results normalised by the vertical effective stress, essentially means to evaluate the effects of penetration rate on the coefficient β .

Since the slopes of the interpolation line of S1 and S2 data in Figure 128 are different, the normalised penetration rate has been introduced instead of the penetration rate. The V values are those used for the tip resistance and pore water pressure, in particular based on the laboratory c_v estimation. The result is plotted in Figure 131: by using the respective non-dimensional velocities the data obtained from S1 and S2 series overlap, giving a unique trend in terms of slope and intercept.

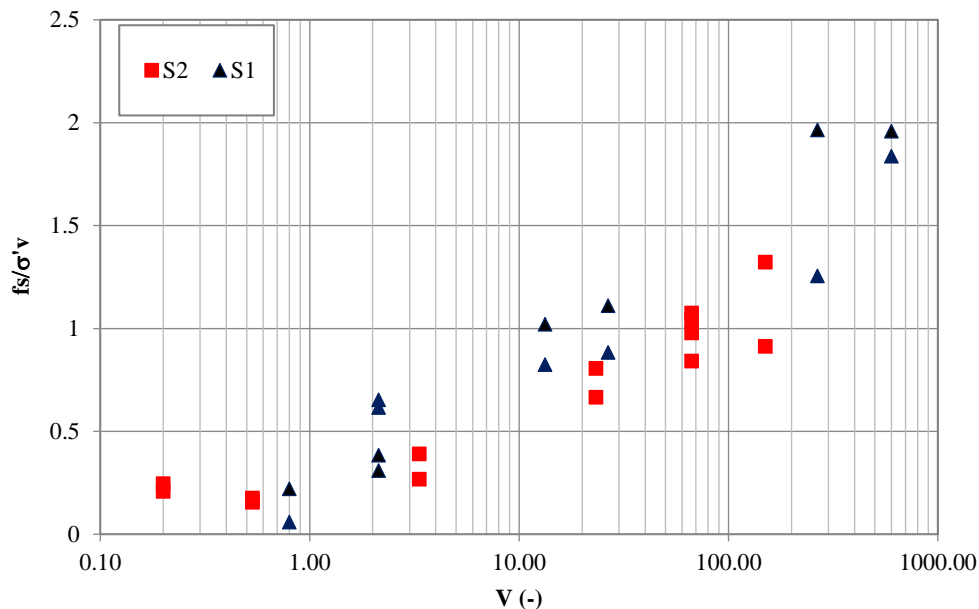


Figure 131: Normalised side friction versus non-dimensional velocity for S1 and S2 series.

This important result has suggested the formulation of the best-fit correlation shown in Figure 132:

$$\frac{f_s}{\sigma'_v} = 0.215 \ln V + 0.2$$

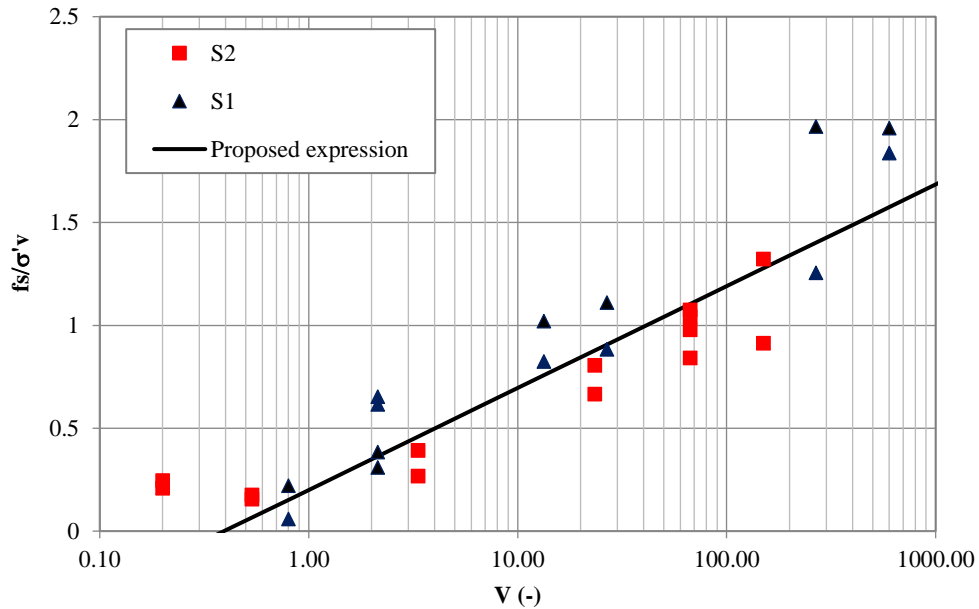


Figure 132: Normalised side friction vs non-dimensional velocity correlation.

7.7 Conclusions

The chapter has described the tests carried out inside the calibration chamber. The material has been selected in order to cover the partial drainage range considering the minipiezcone diameter and the available penetration rate. Results are presented for two different compaction conditions. The previously proposed backbone curves (DeJong and Randolph, 2012) for tip resistance and porewater pressure measurements are evaluated.

Whereas previous experimental studies essentially concentrated the attention on tip resistance and pore water pressure measurements, it is worthwhile to underlie that the present study consists in one of the first experimental studies that explored the effects of penetration rate on sleeve friction measurements. Tip resistance measurement is influenced by the characteristics of the soil layers around the advancing tip, involving a soil volume that depends on the stiffness characteristics. If the deposit is not homogeneous, tip resistance can include information of different materials, and therefore give a trend, less sensitive to differences in penetration rates. On the other hand, friction sleeve is a local measurement and in the case of heterogeneous soil stratification represent a more reliable data from this point of view. For the tests conducted inside the calibration chamber, as the penetration rate is reduced, moving from the undrained conditions to the fully drained conditions, friction sleeve systematically decreases, together with the expected results in terms of increasing tip resistance and decreasing excess porewater

pressure measurements. The clear trend of friction sleeve measurements can be linearly interpolated as a function of penetration rate. Besides, if the normalised f_s values are plotted versus the non-dimensional velocity, data from S1 and S2 series overlap giving a unique linear trend in the semi-logarithmic plot. These results can have many important implications in piezocone interpretation and suggest further investigations. The effects of penetration rate and drainage conditions on side friction are investigated, by suggesting a simple correlation between the normalised friction (i.e. the β coefficient) and the non-dimensional velocity.

The piezocone results, in terms of normalised parameters, are then plotted in the classification charts recently proposed by Schneider et al. (2008, 2012), in order to verify their applicability for the intermediate soils of the present study.

The obtained experimental database of penetration measurements on intermediate soils can be added to the previous worldwide collected data in order to develop a new general interpretation procedure for cone tests in transitional soils, such as clayey silts and silts. In addition to that, since usually the sleeve friction is depicted as the less reliable measurement with respect to the tip resistance and pore water pressure, the present study shows that, for the material investigated, f_s measurements are the most sensitive to the changes in penetration rate and therefore drainage conditions during the tests. Furthermore, the very interesting results in terms of friction sleeve can be the starting point to introduce a new instrument for the characterisation of this kind of materials.

8. Numerical modelling of piezocone penetration

In this section results of the analyses conducted to simulate the penetration process under different drainage conditions are presented. The results are compared with those available in literature (Randolph & Hope, 2004; Schneider et al., 2007) and those obtained in the present study inside the calibration chamber.

The Finite Element method is used with the commercial code Abaqus (2016). The Abaqus finite element system includes Abaqus/Standard and Abaqus/Explicit. Abaqus/Explicit solves dynamic response problems by the use of an explicit direct-integration procedure obtaining values for dynamic quantities at a certain instant based entirely on available values at the previous instant. Abaqus/Standard uses an implicit integration procedure.

8.1.1 Adaptivity technique

It is well known that to model the large displacement penetration process a pure Lagrangian approach is not appropriate. The Arbitrary Lagrangian-Eulerian scheme (ALE) is available both in Abaqus/Standard and Abaqus/Explicit. ALE adaptive meshing consists of two fundamental tasks: creating a new mesh to preserve the quality of the mesh throughout the numerical simulation, and remapping solution variables from the old mesh to the new mesh. The improved mesh quality resulting from adaptive meshing can prevent having severe mesh distortion. In order to study the penetration under partially drained condition it is necessary to introduce coupled pore fluid diffusion/stress analyses. Mixed formulation (“hybrid”) elements are available for porous medium analyses only in Abaqus/Standard. ALE adaptive meshing is available in Abaqus/Standard, but there are significant differences between the ALE adaptive meshing techniques in Abaqus/Explicit and Abaqus/Standard. In fact, the Abaqus/Standard implementation of adaptive meshing has the limitation that “is not intended to be used in general classes of large-deformation problems” (Abaqus Analysis User’s Guide, Simulia 2016). For this reason, the Updated Lagrangian technique has been used to model the penetration process in a bi-phase material. The Updated Lagrangian technique consists in mapping a solution from a deformed mesh, judged too distorted, to another of better quality. The new mesh is created by exploiting the mesh generation capability in Abaqus. The results from the nodes belonging to the old mesh are interpolated to the points of the new mesh. Subsequently the analysis continues as a new problem. The porous medium is modeled by attaching the finite element mesh to the solid phase and the fluid can flow through the mesh.

The Abaqus model has been developed during the visiting period at Massachusetts Institute of Technology. Initially the Updated Lagrangian Procedure availed of Python’s scripts for a limited number of operations, for example, to generate the soil part of the new analysis from

the deformed mesh of the previous one, and to transfer the solution from the distorted mesh to the new mesh. Orazalin (2017) in his PhD thesis developed a complete automated process that allow to execute the entire number of analyses, once the process has been adjusted to the specific model. This procedure has been adopted to carry out the analyses described in this chapter.

8.1.2 Model characteristics

The cone penetrometer is treated as a rigid body (2D analytical surface) and has the standard radius of 18 mm. The shape of the tip is slightly rounded to avoid numerical problems due to the sharp edge between the cone tip and the shaft of the standard piezocone. During the analyses, the cone is pushed down into the soil at a constant rate. The rates adopted cover the entire partial drainage range, in relation to the single case studied, delineating the completely drained and undrained conditions. The total vertical displacement is determined in order to achieve the steady state condition. The soil-tip interaction is modeled with a surface-base contact algorithm (finite sliding). The contact interaction is assumed frictionless.

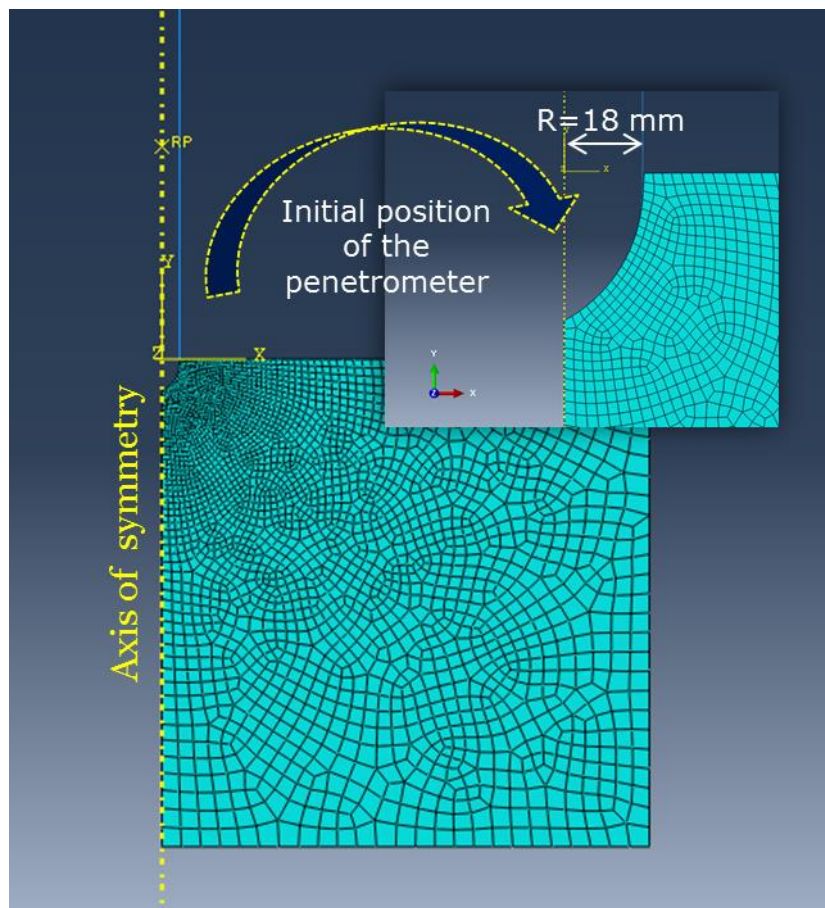


Figure 133: Axisymmetric finite element mesh used for the analysis.

Both the Modified Cam Clay and the Mohr-Coulomb constitutive models are adopted, in particular, the Modified Cam Clay model is exploited to simulate the experimental results obtained on normally consolidated kaolin clay (Randolph & Hope, 2004; Schneider et al., 2007), whereas the Mohr Coulomb model, calibrated on triaxial test results, has been used to simulate the tests conducted inside the calibration chamber.

Taking advantage of the symmetry problem, the soil and the cone are modeled as axisymmetric parts. The model width and height are 28 times the tip radius. The mesh is made up of four-node bilinear displacement and pore pressure elements (CAX4P).

Far field drainage is permitted at the right and bottom boundaries. The left boundary is impermeable because of symmetry constraint. The penetration is simulated at a certain soil depth, for this reason a vertical load is applied on the top of the model representing the vertical stress. For the same reason, the top surface is considered impermeable, forcing the horizontal direction as the main direction of drainage. The soil is considered weightless and an initial stress state is evaluated in equilibrium with the applied vertical and the horizontal loads. The horizontal load reproduces a K_0 condition. The stress state is, therefore, uniform since the gradient of the vertical stress is neglected in comparison with the stress levels involved during the penetration process. The value of the initial excess pore pressure in the soil is equal to zero. Preliminary analyses have been carried out in order to find the best balance between computational time and solution accuracy, in terms of model dimensions as well as mesh element dimensions.

The initial position of the penetrometer is showed in Figure 133. Each analysis consists in pushing down the penetrometer for a distance of 0.2 cm. After that the analysis is interrupted, a new mesh is generated, and the solution from the previous analysis is interpolated to define the initial state of the following analysis. To reach the steady state conditions for the tip resistance-displacement curve, at least 60-80 analyses are necessary for each value of the adopted penetration rate, corresponding to approximately 7-9 times the tip radius.

8.1.3 Modified Cam Clay model results

In this section, the results of piezocone simulation under different drainage conditions are compared with experimental results obtained on kaolin clay in a beam centrifuge. For this purpose, the soil behaviour is simulated with the Modified Cam Clay model (Schofield and Wroth, 1968). The MCC model is an elastoplastic hardening model, based on critical state soil mechanics. Since the input parameters are quite simple to calibrate, in comparison of more sophisticated constitutive models, the model has been widely used to successfully simulate the non-linear behaviour and the main characteristic of real normally consolidated fine-grained

soils. The MCC model parameters adopted to simulate Randolph & Hope (2004) results are displayed in Table 12 (kaolin clay parameters from Stewart and Randolph, 1991). The MCC material model provided in Abaqus has initially showed incompatibility problems with the Updated Lagrangian technique, therefore the UMAT (user-defined mechanical model) subroutine developed by Hashash and Whittle (1993) have been implemented in the analysis procedure.

The soil initially is normally consolidated under K_0 conditions. The value of K_0 is evaluated with the well-known expression (Mayne and Kulhawy, 1982):

$$K_0 = \frac{\sigma'_{h0}}{\sigma'_{v0}} = (1 - \sin \varphi) OCR^{\sin \varphi}$$

Where OCR is the overconsolidation ratio and φ is the internal friction angle.

Modified Cam Clay model – Kaolin Clay	
Angle of internal friction	23°
Slope of normal consolidation line	0.205
Slope of swelling line	0.044
Poisson's ratio	0.25
Critical state friction constant M	0.92
K_0	0.61
Initial vertical pressure	50 kPa
Initial horizontal pressure	30.5 kPa
Initial void ratio ($\sigma'_{v0}=50$ kPa)	1.46
Hydraulic conductivity ($\sigma'_{v0}=50$ kPa)	k = 1.50 E-09 m/s
Vertical coefficient of consolidation ($\sigma'_{v0}=50$ kPa)	$c_v = 9.00$ E-08
Penetration rates –	0.000002 cm/s – V = 0.008
Corresponding non-dimensional velocity V	0.00002 cm/s – V = 0.08
	0.0002 cm/s – V = 0.8
	0.002 cm/s – V = 8
	0.02 cm/s – V = 80
	0.2 cm/s – V = 800

Table 12: Material parameters for MCC Model.

The initial void ratio is then evaluated through the following expression:

$$e = e_{NCL} - \lambda \cdot \ln \left(\frac{1 + 2K_0}{3} \cdot \sigma'_{v0} \right)$$

Where $e_{NCL} = 2.204$ is the void ratio at $p' = 1$ kPa on the Normal Consolidation Line (NCL), σ'_{v0} is the initial vertical effective stress and λ the slope of the normal consolidation line. The cone penetration resistance is related to the rigidity index:

$$I_R = \frac{G}{s_u}$$

The elastic shear modulus, G , is evaluated with the following expression:

$$G = \frac{3 \cdot (1 - 2\nu)p'(1 + e)}{2 \cdot (1 + \nu)\kappa}$$

Where κ is the slope of the swelling line, p' is the mean effective stress and ν is the Poisson ratio.

The coefficient of consolidation has been obtained from the expression proposed by Mahmoodzadeh et al. (2014) based on Rowe cell tests results (Richardson, 2007):

$$c_v = \frac{\sqrt{1 + 0.14\sigma'_{v0}}}{0.003154}$$

Where c_v is expressed in m^2/s and the vertical effective stress is expressed in kPa . Then the hydraulic conductivity, k , is deduced from (Schneider et al.,2007):

$$k = c_v \frac{\lambda\gamma_w}{(1 + e)\sigma'_{v0}}$$

Where γ_w is the unit weight of water.

The penetration rates have been evaluated in order to cover the same range of non-dimensional V values obtained inside the centrifuge. The minimum and the maximum values are 0.000002 cm/s and 0.2 cm/s, respectively. The corresponding non-dimensional velocity are displayed in Table 12. The non-dimensional velocity has been evaluated considering the vertical coefficient of consolidation c_v , in order to compare the results with those published by Randolph & Hope (2004):

$$V = \frac{v \cdot d}{c_v}$$

Where v is the penetration rate and d the con diameter.

Figure 134 shows tip resistance over the normalised penetration distance, distance over tip radius, for several values of non-dimensional velocity. The applied load, and therefore the tip resistance, increases with the vertical displacement until a steady state condition is reached. In this case the penetration is around seven times the tip radius. Further penetration is considered no significant in order to minimise computational costs. The net cone resistance, as expected, increases as the penetration rate decreases and ranges between 118.6 kPa and 240.3 kPa for V values of 800 and 0.008 respectively. For the present analyses, the tip resistance ratio, the ratio between the drained and the undrained tip resistance, is around 2.0. Figure 136 shows the obtained backbone curve, as well as the experimental results and the best-fit curve proposed by Randolph and Hope (2004). The FEM results and the experimental results in the partially and fully drained conditions well-agree, whereas the FEM model underestimates the experimental tip resistance ratio. The experimental data reach a value of around 2.5 for V equal to 0.5, whereas the curve obtained from the FEM simulation reaches lower values. This could be due

to the assumed material properties, in particular the value of the modulus ratio. Yi et al. (2014) show that tip resistance ratio is more sensitive to modulus ratio than friction angle. In their work, the Randolph & Hope experimental data can be well described considering values of the modulus ratio between 35 and 105. The modulus ratio for the present study is around 34. On the other hand, the partial drainage condition boundaries are well reproduced suggesting a transitional V range of two orders of magnitude. The limit of complete undrained penetration can be identified in V equal to 30; this value is confirmed by the previous studies on centrifuge tests and numerical modelling of piezocone penetration in kaolin clay (Randolph & Hope, 2014; Yi et al. (2014)).

Randolph & Hope (2004) proposed the following hyperbolic function to reproduce the backbone curve:

$$\frac{q_{cnet}}{q_{ref}} = \left[1 + \frac{b}{1 + cV^d} \right] = 1 + \frac{b}{1 + (V/V_{50})^d}$$

Where b, c and d are parameter to be evaluated. The parameter b can be evaluated as follows:

$$b = \frac{q_{drained}}{q_{ref}} - 1$$

The backbone curve obtained from FEM analyses is very well described by the previous expression, using the following values (Figure 137):

$$\frac{q_{cnet}}{q_{ref}} = 1 + \frac{1.02}{1 + (V/2)^{1.1}}$$

The obtained tip resistance ratio:

$$\frac{q_{drained}}{q_{ref}} = 2.02$$

It is in very good agreement with the results showed by Yi et al. (2012). They analysed the penetration problem carrying out FEM analyses simulating the soil with the Drucker Prager constitutive model. They proposed the following expression:

$$\frac{q_{drained}}{q_{ref}} = 0.22 \left(\frac{G}{p'} \right) + 1.331$$

That leads to a value of 2.07 considering $\frac{G}{p'} = 33.6$ adopted in the presented analyses.

The results in terms of tip resistance obtained with 0.2 cm/s and 0.02 cm/s are very close each other, suggesting that the undrained condition has been reached. The corresponding tip resistance can be employed to estimate the cone factor. Several expressions are available in literature to estimate the cone factor for undrained conditions. The general expression is the following one:

$$N_{kt} = \frac{q_c - \sigma_{v0}}{s_u} = \frac{q_{cref}}{s_u}$$

The expression proposed by Lu et al. (2004) for the undrained cone factor is:

$$N_{kt} = 3.4 + 1.6 \ln(I_R) - 1.9 \left(\frac{\sigma_{v0} - \sigma_{h0}}{2s_u} \right)$$

It leads to $N_c = 9.28$ substituting the appropriate values.

Teh & Houlsby (1991) have applied the strain path method to evaluate the cone factor. The proposed expression is:

$$N_{kt} = 1.25 + 1.84 \ln(I_R) - 2 \left(\frac{\sigma_{v0} - \sigma_{h0}}{2s_u} \right)$$

For the present study, $N_{kt} = 8.16$. Figure 138 shows that the undrained cone resistance evaluated from the presented FEM analyses are in the between of the values proposed by the authors previously cited.

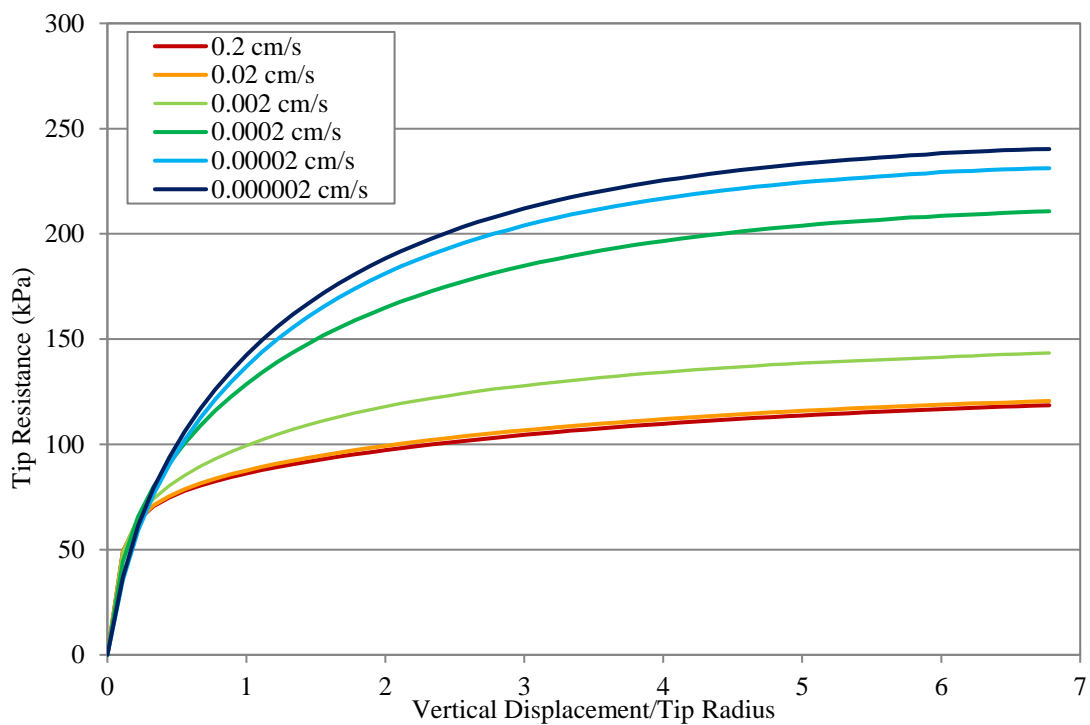


Figure 134: Net cone resistance versus vertical displacement (expressed as number of tip radius).

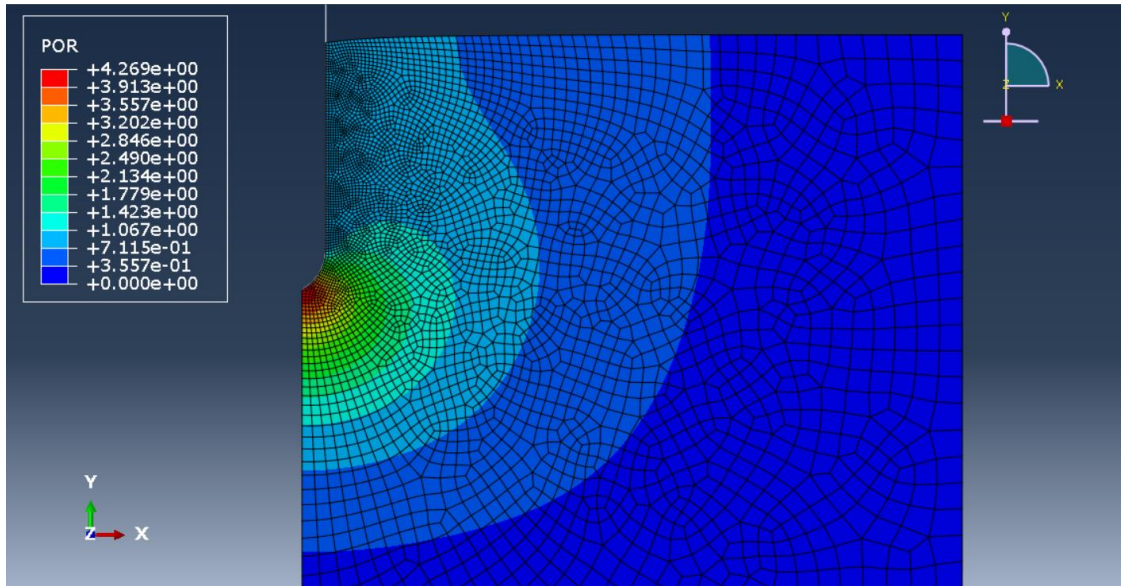


Figure 135: Pore water pressure distribution during the test at 0.000002 cm/s.

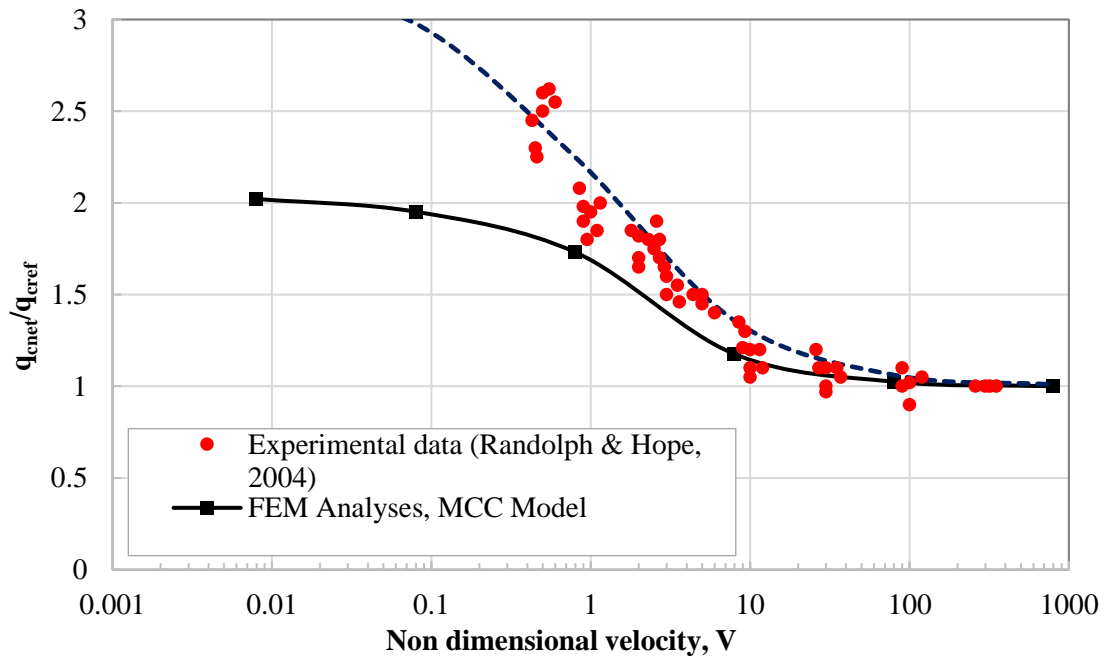


Figure 136: Tip resistance ratio for piezocone simulation in kaolin clay, Randolph & Hope (2004) centrifuge test results.

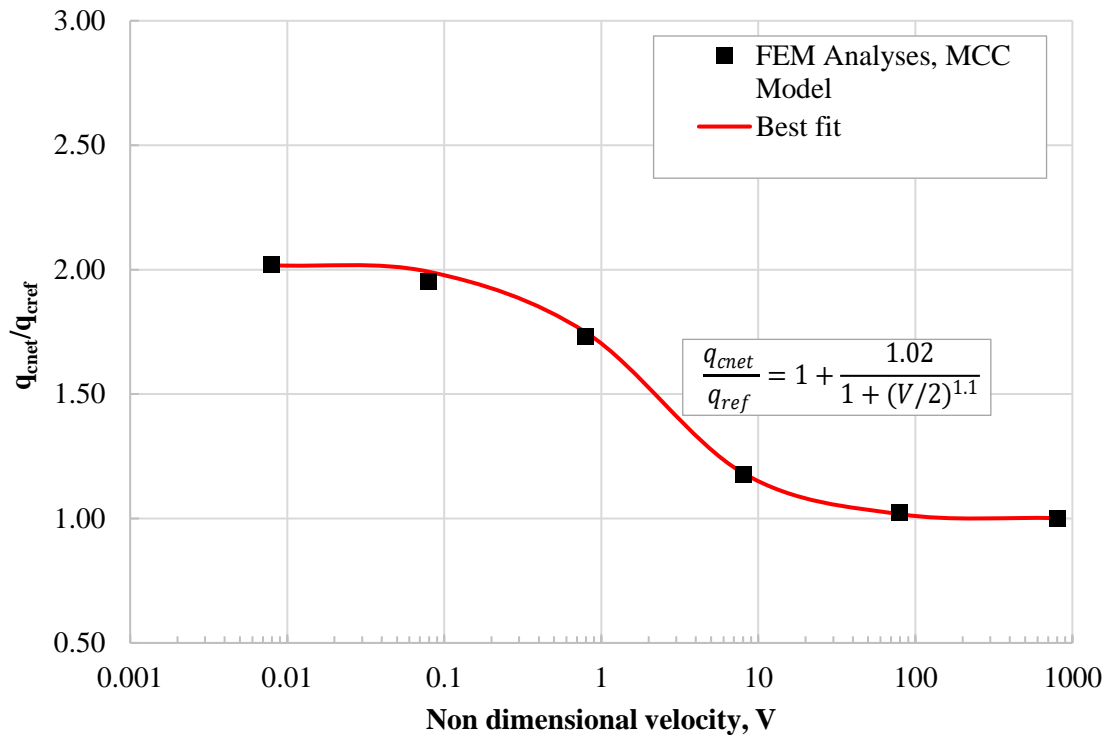


Figure 137: FEM analyses results compared with the expression proposed by Randolph & Hope (2004).

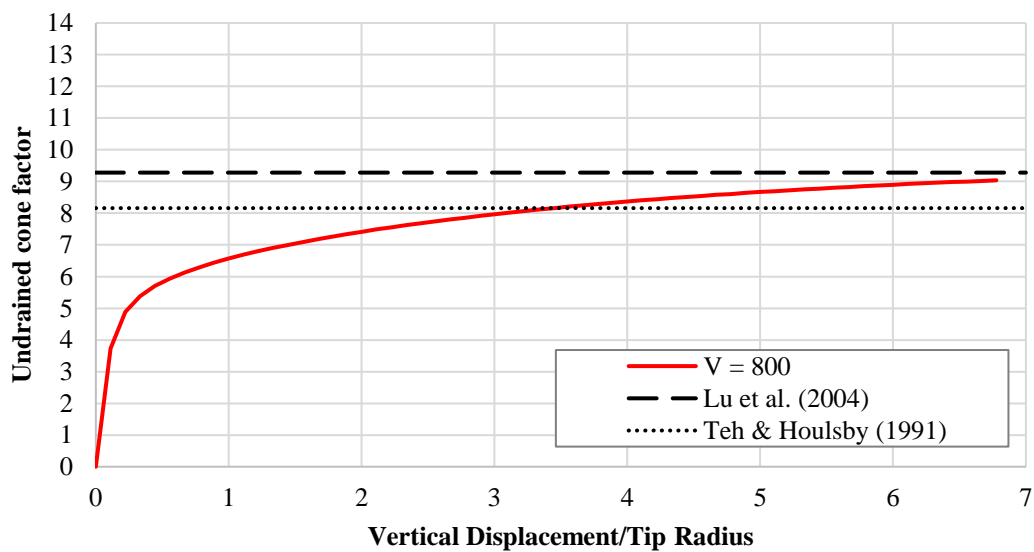


Figure 138: Undrained cone resistance from FEM analyses of the present study.

The analyses have been repeated with the intention to reproduce the result obtained by Schneider et al. (2007) with centrifuge tests on normally consolidated kaolin clay. The material properties are reported in Table 13 (Schneider et al. 2007).

Modified Cam Clay model – Kaolin Clay	
Angle of internal friction, φ'	23°
Slope of normal consolidation line, λ	0.26
Slope of swelling line, κ	0.06
Poisson's ratio, ν	0.25
Critical state friction constant, M	0.92
K_0	0.61
Initial vertical pressure	90 kPa
Initial horizontal pressure	55 kPa
e NCL ($p'=1$ kPa)	2.6
Initial void ratio, e ($\sigma'_{v0}=90$ kPa)	1.51
Hydraulic conductivity, k	1.0 E-09 m/s
Vertical coefficient of consolidation, c_v	6.7 E-08
Penetration rates –	0.000011 cm/s – V = 0.06
Corresponding non-dimensional velocity, V	0.000083 cm/s – V = 0.45
	0.00083 cm/s – V = 5
	0.028 cm/s – V = 150
	0.083 cm/s – V = 451

Table 13: Material parameters for MCC Model.

The tests carried out by Schneider et al. (2007) have been conducted, utilising a tip of 1.0 cm diameter. The penetration rates are: 0.3 cm/s, 0.1 cm/s, 0.03 cm/s, 0.003 cm/s, 0.0003 cm/s and 0.00004 cm/s. The vertical effective stress ranges between 80 and 100 kPa. In order to reproduce the experimental data equivalent penetration rates have been evaluated taking into account the different value of tip diameter, the standard one for FEM analyses (3.6 cm) of the present study and 1.0 cm of the experimental tests.

For the numerical simulation, an average value of vertical effective stress has been used, therefore 90 kPa is the initial vertical stress inside the model. The horizontal effective stress reproduces the K_0 conditions, in particular σ'_{h0} is equal to 55 kPa considering the soil characteristics displayed in Table 13. Data of hydraulic conductivity values, obtained from Rowe cell tests, provided by the authors. The vertical coefficient of consolidation is evaluated with the following expression:

$$c_v = \frac{k(1 + e)\sigma'_{v0}}{\lambda\gamma_w}$$

The non-dimensional velocity has been evaluated by use of the vertical consolidation coefficient.

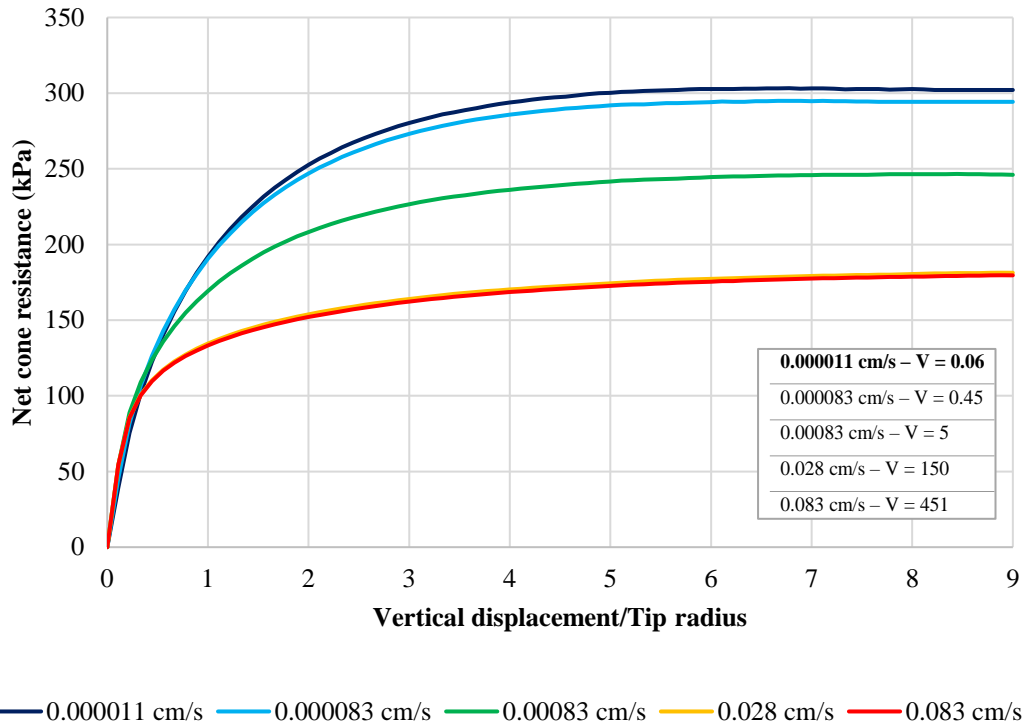


Figure 139: Tip resistance over vertical displacement of the cone, MCC model with Schneider et al. (2007) parameters.

Figure 139 shows the results obtained with FEM simulation of the present study. The adopted penetration rates are displayed in the graph. Starting from the initial position the tip resistance increases as the penetrometer goes down in the soil model. The steady state condition is reached after around 6 times the tip radius; however, the simulation has been continued up to 9R. As expected, the penetration resistance reduces as the penetration rate increases. Tip resistance obtained for V equal to 451 and 150 are equivalent, suggesting that the boundary between partially drained and fully undrained conditions is lower than 150. The ratio between the maximum tip resistance, drained conditions, and the minimum tip resistance, undrained conditions, is 1.68. Looking at the obtained backbone curve showed in Figure 140, it is possible to observe that FEM simulation underestimates the maximum tip resistance ratio, that is, for the experiment results, 2.2.

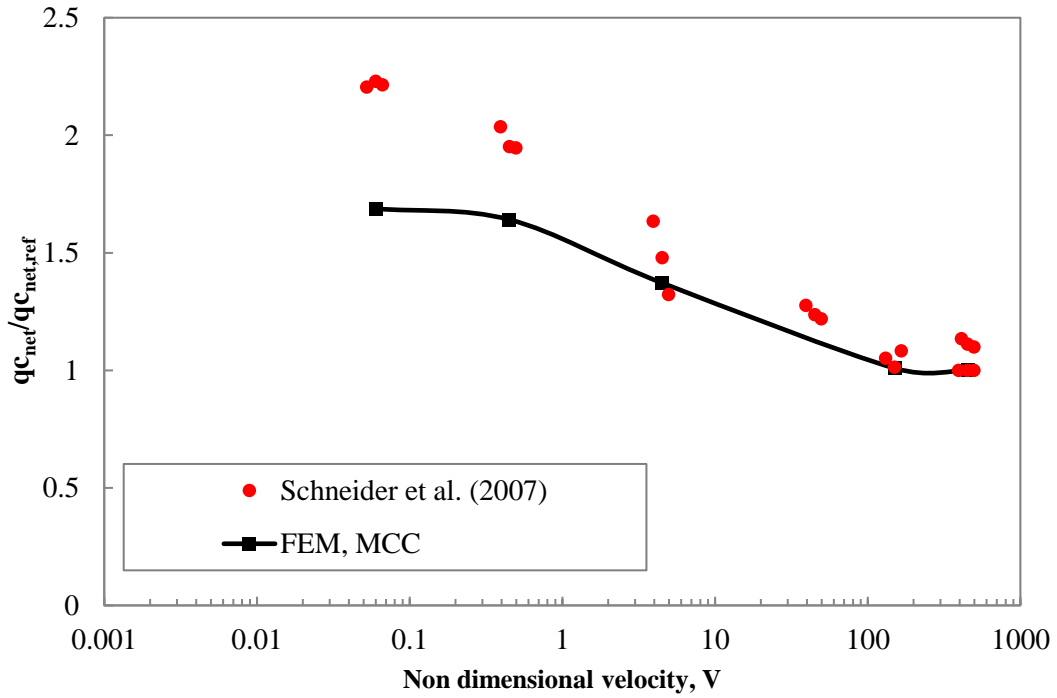


Figure 140: Tip resistance ratio from the present study simulation and the experimental data obtained by Schneider et al. (2007)

Excess pore water ratio is plotted in Figure 141. The pore water pressure is measured at the u_2 position, beyond the rounded tip. The considered values are referred to the last analyses, at 9R penetration depth. The finite element simulation reproduces very well the experimental backbone curve of pore water pressure ratio. Furthermore, Figure 142 shows the normalised pore water pressure versus the non-dimensional velocity:

$$B_q = \frac{\Delta u_2}{q_{cnet}}$$

Where Δu_2 is the excess pore water pressure generated during the penetration, measured at the tip shoulders. It is possible to observe that the experimental data are very well represented by the obtained curve. The transition between the drained and the partially drained conditions is around V values of 0.1, whereas the undrained condition is reached for V value around 100.

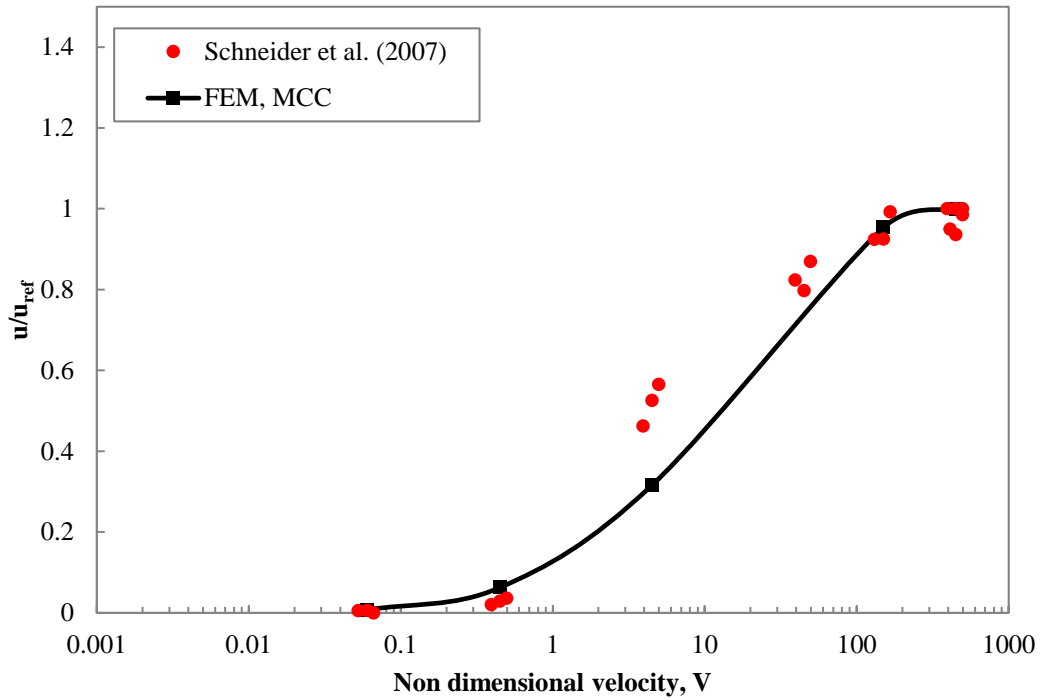


Figure 141: Excess pore water pressure ratio from FEM analyses and experimental data (Schneider et al., 2007)

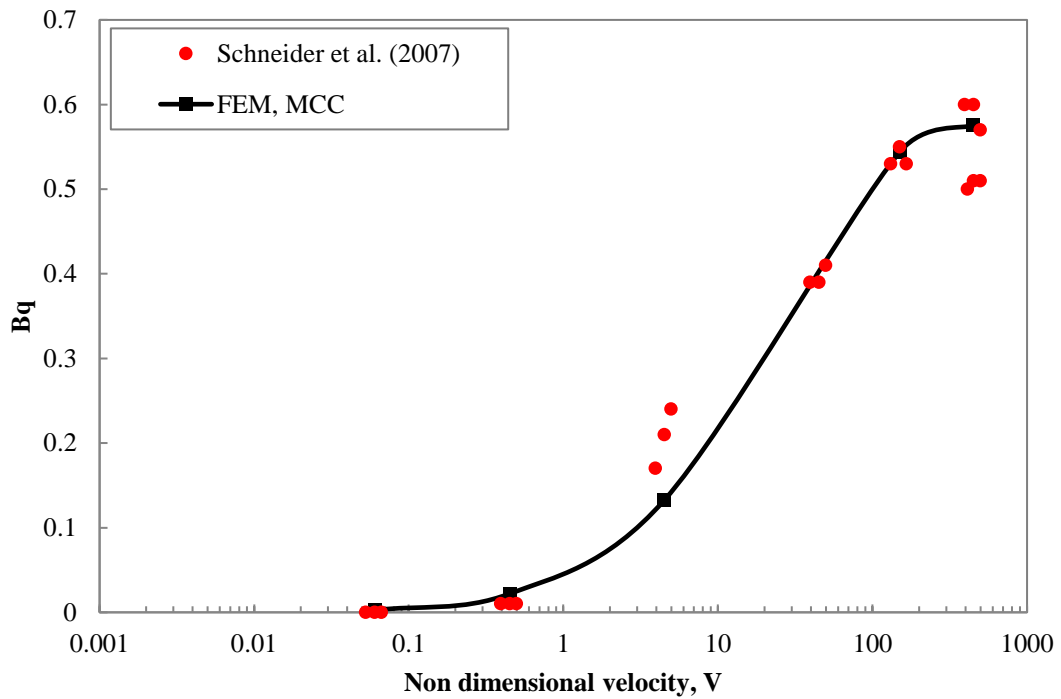


Figure 142: Normalised excess pore pressure obtained with the numerical simulation of the present study compared with experimental results (Schneider at al. 2007).

8.1.4 Numerical simulation of Calibration Chamber tests

In order to reproduce data obtained inside the calibration chamber, an attempt has been made by using the Mohr Coulomb model, in fact the Modified Cam Clay model is not suitable to reproduce the constitutive behaviour of this kind of materials. Yi et al. (2014) executed FEM analyses, with the Mohr Coulomb constitutive model. In their study, the influence of strength and stiffness parameters have been studied. In particular, shear modulus has been varied to obtain rigidity indexes between 17.5 and 140. Friction angle has been varied between 18° and 35° . In their analyses, the c' parameter has been taken always equal to zero. Therefore, their study is not suitable to interpret the result of the calibration chamber tests. In this case, triaxial tests on specimen extracted from the two sides of the chamber show a c' value greater than zero and rigidity index much higher than the maximum value considered by the aforementioned paper.

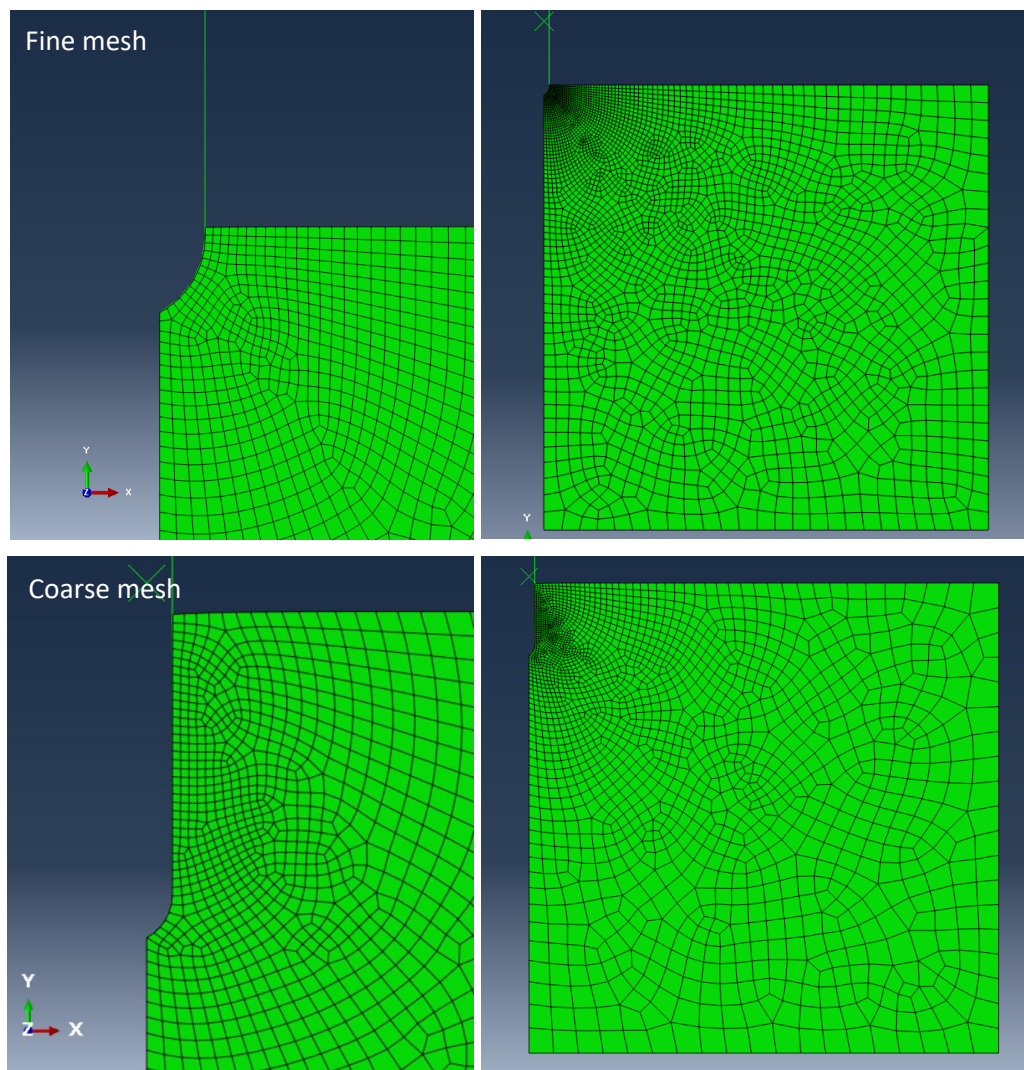


Figure 143: Different sizes of mesh elements, in two different positions of the penetrometer, the last one (100 analyses) and the first one.

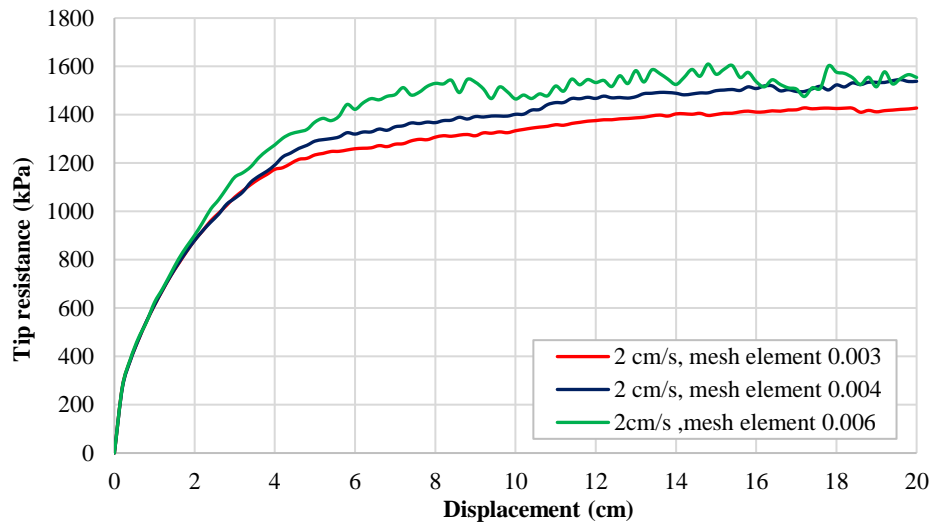


Figure 144: Comparison of tip resistance curve for different values of mesh elements, dimensions of the elements closed to the tip are indicated in the diagram (Friction angle = 45° , Young modulus = 14 MPa, = 35 kPa, dilation angle = 1°).

Model parameters have been inferred from the stress-strain response of triaxial tests (TXCIU) conducted on the selected material. In particular, the curve obtained for the S1 side with a consolidation pressure of 20 kPa has been considered. In order to calibrate the Mohr Coulomb parameters, the simulation of the triaxial test has been done in Abaqus. Calibration process has led to a friction angle of 45° , an elastic stiffness, in particular the Young modulus, of 14 MPa, and c' equal to 35 kPa. Furthermore, in order to reproduce the laboratory test curve, it is necessary to introduce a dilation angle higher than zero.

The use of the Mohr Coulomb model entails the introduction of approximations. In undrained shearing the undrained strength is unbounded, hence the model tends to overestimate the shear resistance close to the penetrometer. During undrained shearing the non-zero dilation angle generates shear induced pore water pressures that may be unbounded at very high strains. However, preliminary analyses have shown that the generation, during penetration, of unrealistic negative porewater pressures close to the tip, has little influence on tip resistance at highest penetration rates.

On the other hand, in drained shearing the Mohr Coulomb model produces an unbounded increase in volume. The following analyses show that dilation angle has, in this case, secondary impact on drained values of tip resistance if compared to soil stiffness characteristics.

The Abaqus model has the same characteristics of the models described in the previous section. A preliminary study has been made in order to evaluate the best mesh and model dimensions. In this case, the tip resistance curve is highly influenced by the shape of the mesh around the tip and in the surrounding soil. An example of differences in tip resistance curves due to different types of mesh is shown in Figure 144. The dimensions, expressed in meters, of the elements closed to the tip, are displayed in the diagram. The shape of the coarser and finer mesh can be seen from Figure 143. The first pictures show the shape of the mesh at the end of the

penetration in the case of the coarser mesh, the second ones show the finer mesh at the beginning of the analyses. The presence of a very high friction angle causes pronounced numerical accuracy issues (Figure 144). The finer mesh has been selected for the present analyses: the size of the elements closed to the tip is equal to 0.003 m, the size of the elements along the bottom and right side of the model is 0.06 m, intermediate dimensions are established by the meshing process.

Hydraulic conductivity k (m/s)	G/p'	$D' = \frac{2G(1-\nu')}{(1-2\nu')}$ (kPa)	Penetration rate v (cm/s)	c_v (m ² /s)	$V = \frac{v d}{c_v}$
1.E-09	270	18846	0.00027	1.9E-06	0.05
			2		375

Table 14: Evaluation of the coefficient of consolidation and the non-dimensional velocity.

Mohr Coulomb model	MC1	MC2	MC3	MC4
Friction angle, ϕ'	45°			
Young modulus, kPa	14000	14000	7000	7000
G/p'	270	270	135	135
Cohesion stress c'	35 kPa			
Dilation angle (°)	1	0.001	1	0.001
Poisson's ratio, ν	0.3			
Initial vertical pressure	20 kPa			
Initial horizontal pressure	20 kPa			
Initial void ratio, e	0.76			
Hydraulic conductivity, k	1.0 E-09 m/s			
Vertical coefficient of consolidation, c_v	1.9 E-06 m ² /s		9.6 E-07 m ² /s	
Penetration rates – Corresponding non-dimensional velocity, V	0.00027 cm/s – $V = 0.05$		0.00027 cm/s – $V = 0.1$	
	2 cm/s – $V = 375$		2 cm/s – $V = 750$	

Table 15: Soil characteristics and model parameters.

With the objective of studying the influence of the dilation angle, several preliminary analyses have been carried out changing the dilation angle and soil elastic stiffness values. Equivalent penetration rates have been evaluated in order to have the same value of the non-dimensional velocity between calibration chamber tests and the respective FEM simulations. In particular in this case, the equivalent penetration rate has been evaluated by assuming the same value of the coefficient of consolidation for Abaqus analyses and calibration chamber data. Table 15 shows the parameters adopted for the soil. Four different models have been used to simulate the penetration at $v=0.00027$ cm/s and $v=2$ cm/s. The non-dimensional velocity, V , is evaluated by

considering the soil model characteristics and the subsequent value of the coefficient of consolidation (Table 14). The coefficient of consolidation has been evaluated as follows:

$$c_v = \frac{k * D'}{\gamma_w}$$

where D' is the constrained modulus of the soil:

$$D' = \frac{2G(1 - \nu')}{(1 - 2\nu')}$$

Figure 145 shows the comparison of the results obtained at the penetration rate of 0.00027 cm/s. In this case, tip resistance is controlled by soil stiffness, with secondary differences due to the presence of a dilation angle greater than zero. In fact, results for MC3 and MC4, models with same stiffness but different dilation angle 1° and 0.001° respectively, are almost the same. At the same time, MC1 and MC2 models exhibit much higher tip resistance values. The differences in tip resistance between MC1 and MC2 are smaller than those with respect to the tip resistance obtained for the soil models with lower Young modulus (MC3 and MC4).

A completely different result is obtained for the higher penetration rate of 2 cm/s (Figure 146). In this case, the analyses obtained for MC2 and MC4 models give the same tip resistance. MC2 and MC4 have the same soil characteristics except of Young modulus that is equal to 14000 kPa for MC2 and 7000 kPa for MC4. On the other hand, when a dilation angle greater than zero is introduced, then, for the penetration rate of 2 cm/s, there are significant differences linked to soil stiffness. MC1 material's analysis gives the higher tip resistance, whereas MC3 qt value is in the middle between MC1 and MC2-MC4 results.

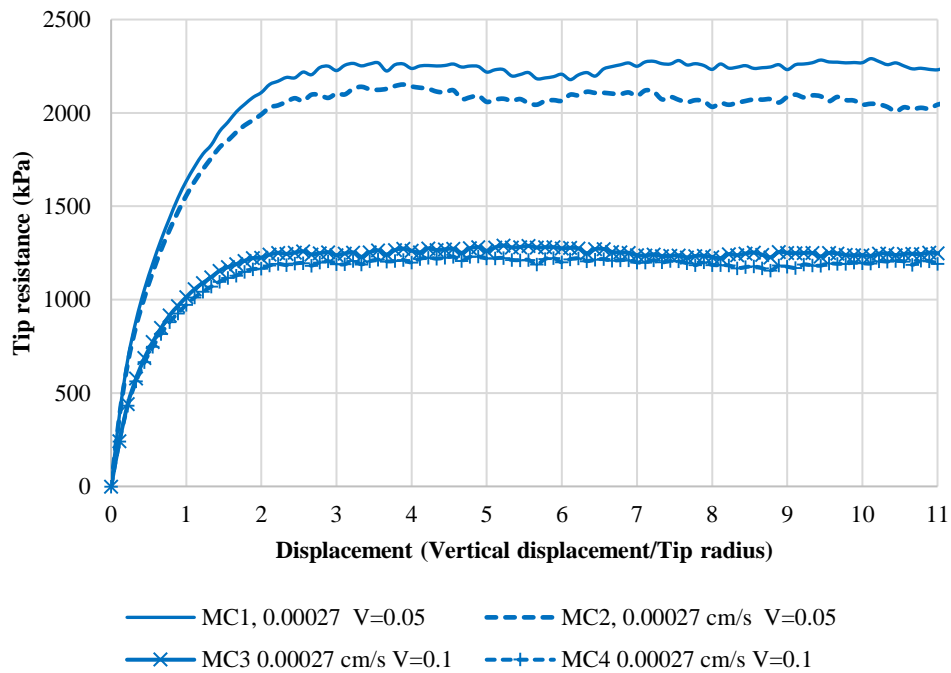


Figure 145: $V=0.05$, fully drained conditions.

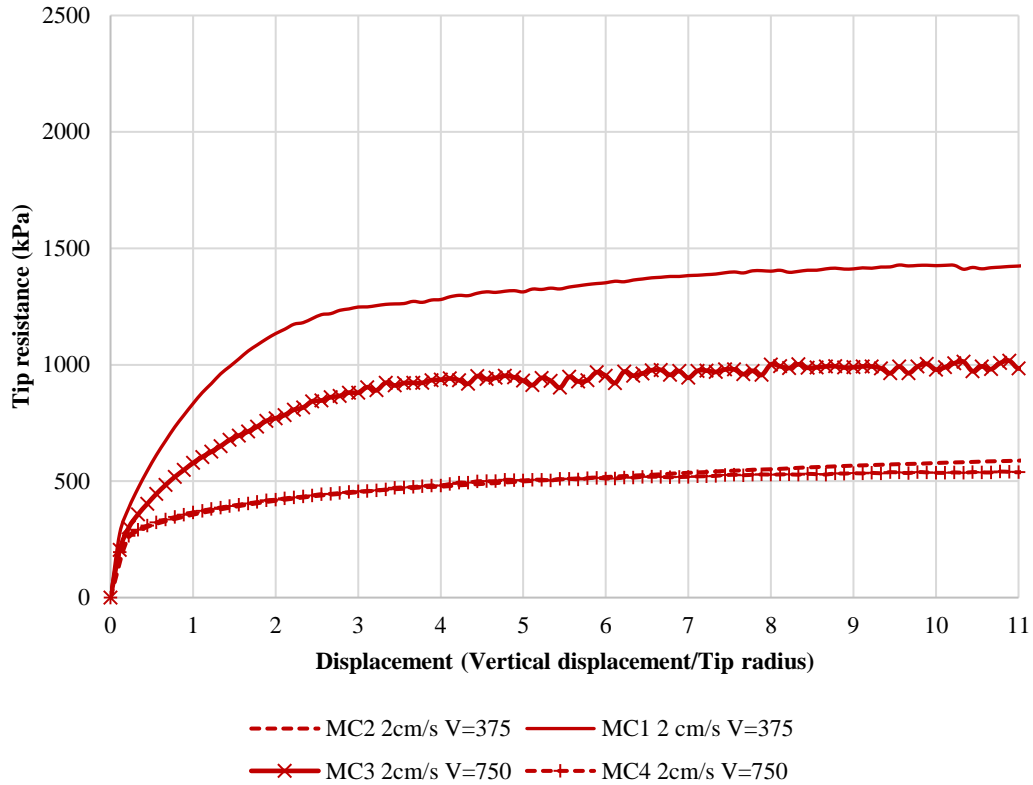


Figure 146: Tip resistance for V=375, undrained conditions.

Figure 147 shows tip resistance versus tip displacement for the analyses conducted at 0.00027 cm/s and 2 cm/s for the MC3 soil model. In this case the ratio between the supposed drained value (V=0.1) and the supposed undrained value (V=750) is around 1.25 (q_{tnet} ratio). The value of 1.25 is the lowest for this series of tests. Table 16 summarises the tip resistance values obtained for $v=0.00027$ cm/s and $v=2$ cm/s and their ratio (q_{tnet} ratio) for the four analysed models. As expected, these values are not in accordance with the results obtained by Yi et al. (2012); on the base of their studies, they proposed the following expression to evaluate the tip resistance ratio:

$$q_{tnetRATIO} = \frac{q_{drained}}{q_{ref}} = 0.22 \left(\frac{G}{p'} \right) + 1.331$$

that leads to 7.25 for the higher stiffness and 4.30 for the lower stiffness. The fact that these values are much higher than the result of the present study is reasonable since the previous expression has been obtained by analysing a cohesionless soil.

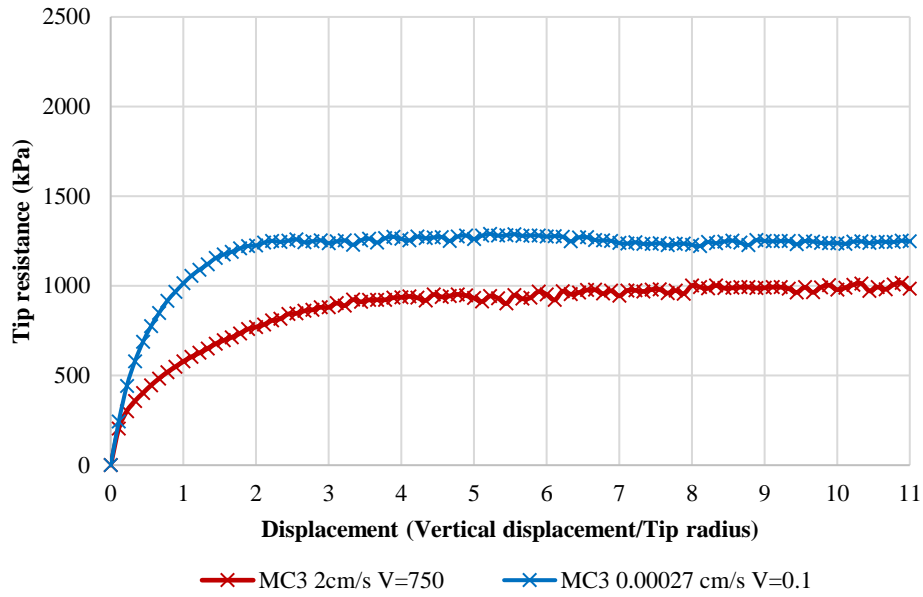


Figure 147: MC3 ($E=7000$ kPa; $\psi=1^\circ$) results, tip resistance versus tip vertical displacement.

		MC1	MC2	MC3	MC4
G/p'		270	270	135	135
Dilation angle ($^\circ$)		1	0.001	1	0.001
q_t (kPa)	V=0.05	2254	2034		
	V=0.1			1245	1202
q_t (kPa)	V=375	1421	633		
	V=750			997	538
q_{tnet} ratio		1.59	3.29	1.25	2.28

Table 16: Drained tip resistance, undrained tip resistance and resistance ratio for different dilation angles and elastic stiffness values.

Previous analyses have shown that the undrained tip resistance is very sensitive to the value of the dilation angle, whereas differences in drained tip resistance are much less pronounced. Therefore, additional analyses have been carried out by varying the dilation angle value in order to fit measured calibration chamber data. Table 17 displays the parameters adopted for the additional soil models MC5, MC6 and MC7. Starting from a value of 1° (MC1), the dilation angle has been halved each time in order to find the target value.

Mohr Coulomb model	MC1	MC2	MC5	MC6	MC7
Friction angle, ϕ'	45°				
Young modulus, kPa	14000				
G/p'	270				
Cohesion yield stress c'	35 kPa				
Dilation angle (°)	1	0.001	0.49	0.25	0.3
Poisson's ratio, ν	0.3				
Initial vertical pressure	20 kPa				
Initial horizontal pressure	20 kPa				
Initial void ratio, e	0.76				
Hydraulic conductivity, k	1.0 E-09 m/s				
Vertical coefficient of consolidation, c_v	1.9 E-06 m ² /s				
Penetration rates – Corresponding non-dimensional velocity, V	0.00027 cm/s – V = 0.05				
	2 cm/s – V = 375				

Table 17: Parameters for the additional soil models MC5, MC6 and MC7.

Figure 148 and Figure 149 show the obtained undrained and drained tip resistance respectively. The undrained tip resistance varies between 633 kPa for the minimum dilation angle (0.001 °) and 1421 kPa for the maximum dilation angle (1°). The undrained value of 918 kPa, obtained for a value of ψ equal to 0.3° is in good agreement with the value measured inside the calibration chamber (Figure 150).

In Figure 150 it is possible to compare measured calibration chamber tip resistances with FEM simulations at the respective calibration chamber penetration rates. As shown in Figure 149, drained values of tip resistance have a lower scatter since the analysed models have the same elastic stiffness characteristics and dilation angle has, in this case, secondary impact. Table 18 shows the tip resistance ratio obtained for the analysed models. Looking at Figure 151 it is possible to observe how the tip resistance ratio decreases with increasing dilation angle values.

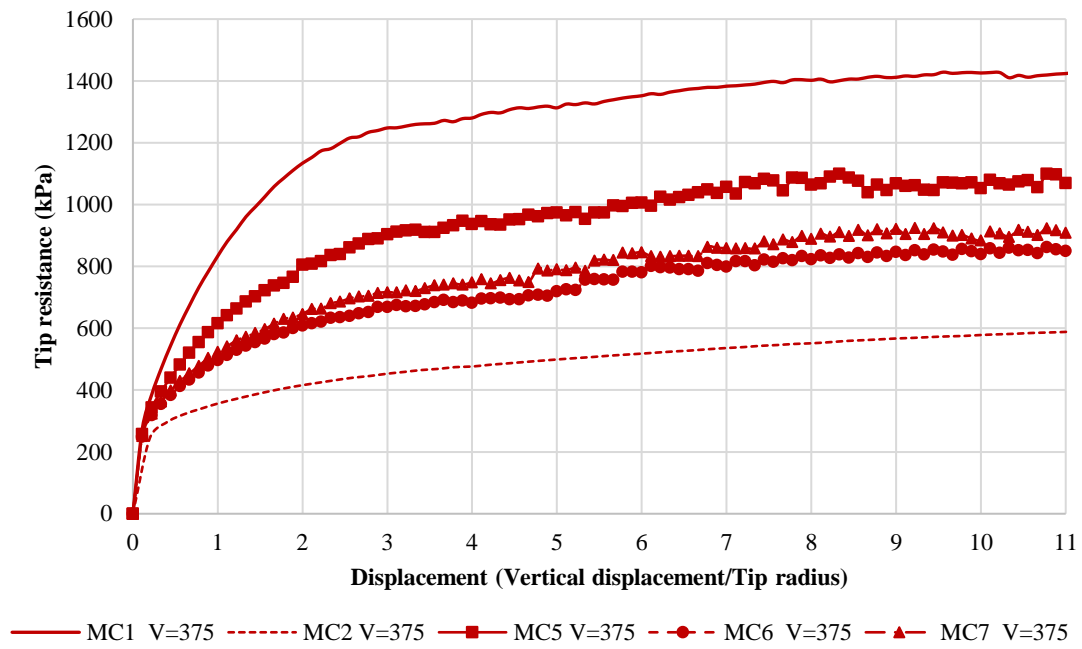


Figure 148: Tip resistance for different dilation angles, maximum penetration rate, non-dimensional velocity $V=375$.

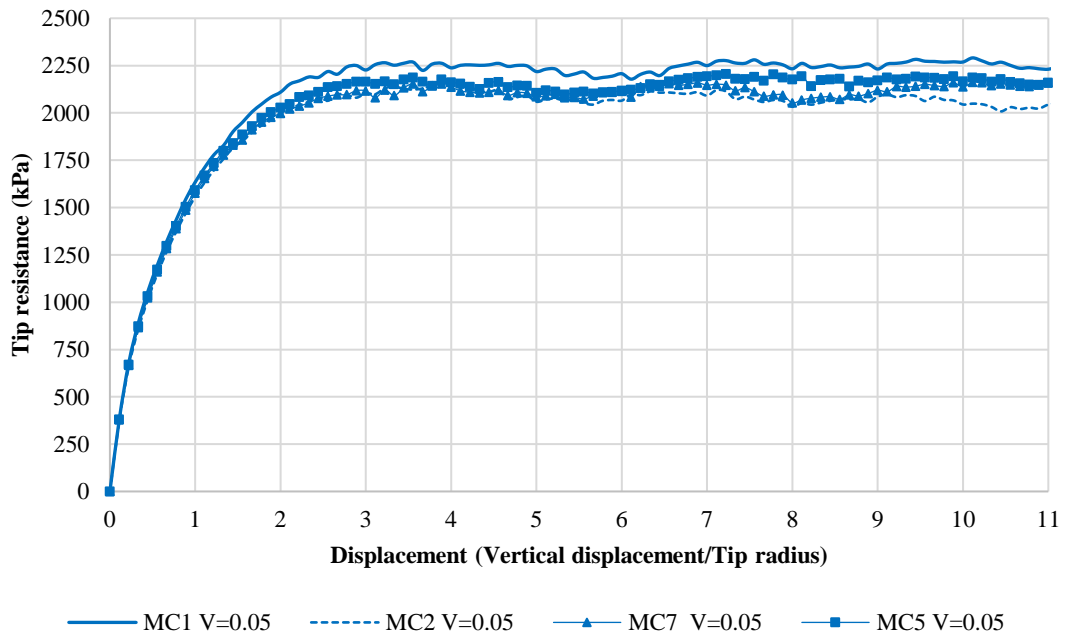


Figure 149: Tip resistance for different dilation angles, minimum penetration rate, $V=0.05$.

	MC1	MC2	MC5	MC7
G/p'	270	270	270	270
Dilation angle (°)	1	0.001	0.49	0.3
qt V=0.05 (kPa)	2254	2034	2156	2158
qt V=375 (kPa)	1421	633	1091	918
q_{tnet} ratio	1.59	3.29	1.99	2.38

Table 18: Undrained tip resistance, drained tip resistance and resistance ratio for different dilation angles.

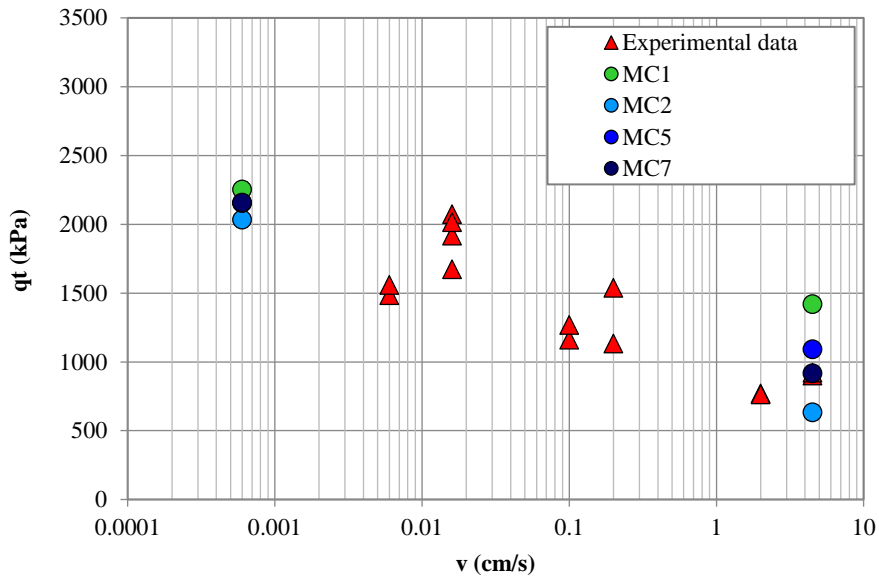


Figure 150: Tip resistance vs penetration rate: numerical analyses and calibration chamber experimental data.

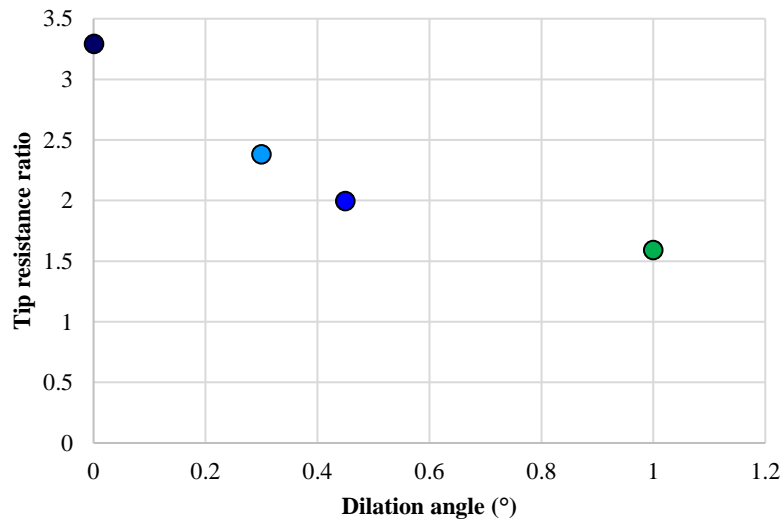


Figure 151: Tip resistance ratio versus dilation angles values.

The soil model MC7 has been considered for additional analyses with intermediate penetration rates, Table 19 summarises model characteristics and adopted penetration rates. In Figure 152 the results in terms of tip resistance versus tip displacement are presented. The drained tip resistance has a value of around 2158 kPa, whereas the tip resistance for the higher penetration rates of 2 and 0.31 cm/s is around 918 kPa. The ratio between the drained and the undrained tip resistance is 2.38. The same analyses have been previously conducted by using the soil model MC1 (Figure 153). In both cases fully drained boundary is reached since, from MC1 analysis results, it is possible to observe that tip resistances for the penetration rate of 0.00027 cm/s ($V = 0.05$) and 0.000027 cm/s ($V = 0.005$) are almost coincident.

MC7 - Mohr Coulomb model	
Friction angle, φ'	45°
Young modulus	14000 kPa
Cohesion yield stress c'	35 kPa
Dilation angle	0.3°
Poisson's ratio, ν	0.3
Initial vertical pressure	20 kPa
Initial horizontal pressure	20 kPa
Initial void ratio, e	0.76
Hydraulic conductivity, k	1.0 E-09 m/s
Vertical coefficient of consolidation, c_v	1.92 E-06 m ² /s
FEM penetration rates –	0.00027 cm/s – $V = 0.05$
Corresponding non-dimensional velocity, V	0.0027 cm/s – $V = 0.51$
	0.0071 cm/s – $V = 1.33$
	0.044 cm/s – $V = 8.25$
	0.31 cm/s – $V = 58.3$
	2 cm/s – $V = 375$

Table 19: Soil constitutive model parameters from TXCIU calibration, MC7 model.

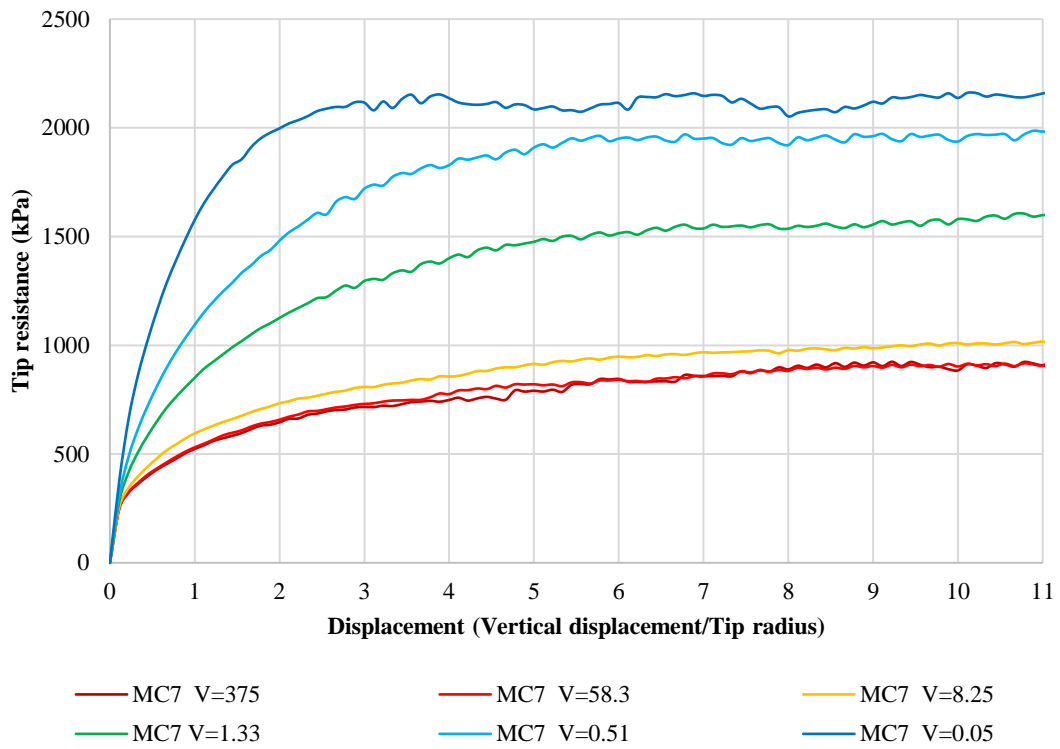


Figure 152: Tip resistance versus tip displacement, MC7 Mohr-Coulomb model.

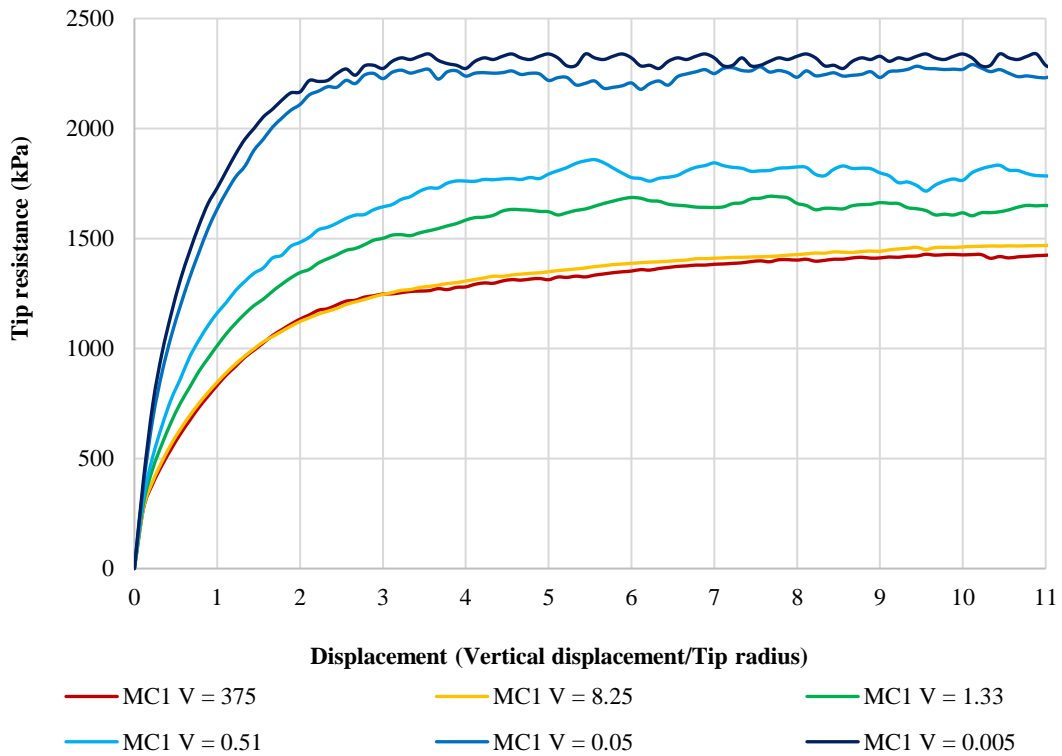


Figure 153: Tip resistance versus tip displacement, MC1 Mohr-Coulomb model.

Analyses with the full range of penetration rates have been repeated, using the MC5 model. Results from MC7 and MC5 results are compared with calibration chamber measurements in Figure 154. The differences between the two models, MC5 and MC7, increase as the penetration rate increases. In this diagram, results are plotted considering an equivalent penetration rate based, in this case, on different values of the coefficient of consolidation, in particular, for calibration chamber data the measured coefficient of consolidation has been used.

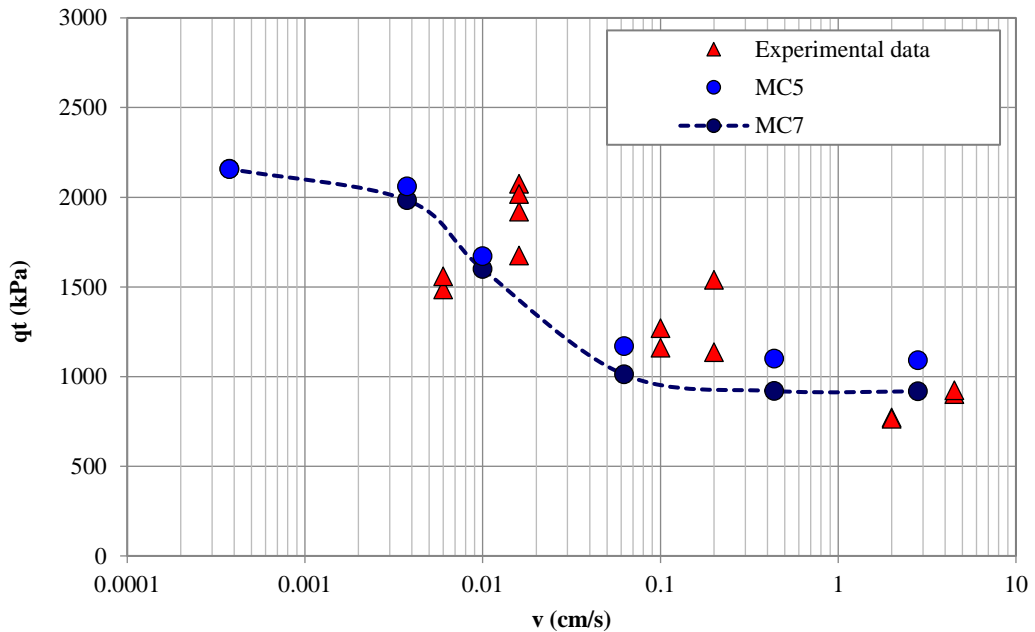


Figure 154: tip resistance ratio versus penetration rate, results are compared with calibration chamber data.

It is possible to observe that the model is able to capture the calibration chamber soil behaviour, giving a good estimation of tip resistance in the entire range covered by the CC tests. The predicted tip resistance using the MC7 model tends to slightly underestimate measured data for the penetration rates between 0.016 cm/s and 0.2 cm/s. The scatter in measured data does not suggest to look for further improvements in the model characterisation.

Appendix: Triaxial test simulation

The specimens used for laboratory characterisation have been built up at the laboratory, by employing a certain amount of material extracted at the moment of the construction of the calibration chamber sample. The soil has been subsequently statically compacted inside a Proctor shell, thanks to the use of a mechanical press. In order to have the desired value of water content, the right amount of water is added before the compaction process. Then the wet material has been subdivided in 5 parts. The target dry densities (1.6 kg/dm^3 and 1.9 kg/dm^3) are obtained by preparing subsequent layers (5 layers) and by applying the pressure required to achieve the desired density inside the Proctor mould. At the end of this process, the required specimen is extracted from the mould and formed for the specific test (oedometer or triaxial test). Each specimen is extracted from one Proctor mould. In order to simulate tip resistance results obtained for the Calibration Chamber, the soil model used for the FEM simulation, has been calibrated on triaxial test results of the specimen reproducing the S1 soil compaction characteristics. The elastic stiffness and cohesion values have been inferred from the stress-strain curve (Figure 156). The consolidation stress is 20 kPa for both cases. As shown in Figure 155, where measured pore water pressure is plotted over axial strain during the TXCIU lab test, the pore water pressure is initially positive and subsequently assumes negative values.

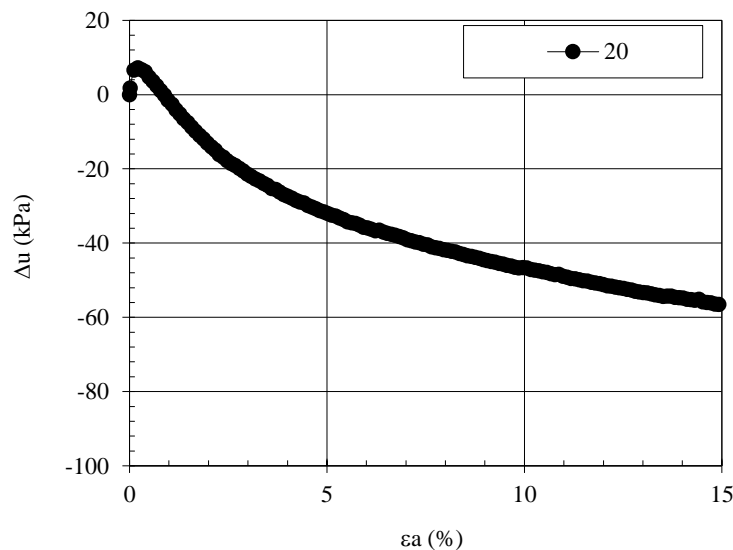


Figure 155: TXCIU test - pore water pressure (S1 side of the calibration chamber).

Figure 156 shows the comparison between the simulation of the triaxial test (TXCIU), using the MC7 soil parameters, and the laboratory triaxial tests in terms of the stress-strain curve, where t is defined as:

$$t' = t = \frac{\sigma'_v - \sigma'_h}{2}$$

and ϵ_a is the axial strain.

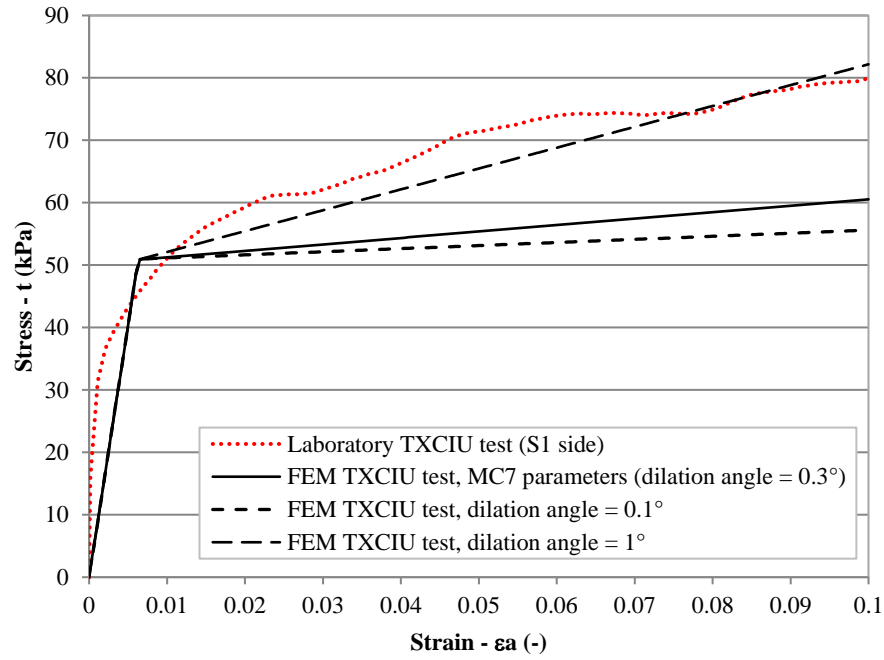


Figure 156: comparison between TXCIU test simulation for MC7 soil parameters and laboratory TXCIU test conducted on a specimen reproducing S1 conditions. TXCIU test simulations for different values of dilation angle, without varying the other MC7 parameters, are also displayed. Consolidation stress is 20 kPa for both numerical simulation and laboratory test.

The discrepancy between the two curves (dotted red line and black line) can be partially due to the differences on the initial compaction states of laboratory tests and calibration chamber model. The MC7 Mohr Coulomb parameters have been calibrated on measured tip resistance inside the calibration chamber, where the soil sample has been compacted by using a dynamic compactor.

8.1.5 Conclusions

Numerical analyses have been carried out by means of the Finite Element Method developed in Abaqus. To the author's knowledge, there are only two researches on partially drained penetration simulated with FEM analyses (Yi et al., 2012; Mahmoodzadeh et al., 2014). For the present study, the Updated Lagrangian technique has been used to simulate the large strain penetration process. The model has been validated on previous experimental results. The Modified Cam Clay constitutive model has been adopted to simulate the results obtained by Randolph & Hope (2004) and Schneider et al. (2007) from piezocone tests on kaolin clay. Besides, the Mohr Coulomb model has been calibrated on triaxial tests conducted on soil specimens extracted from the calibration chamber, and numerical simulations have been done of the tests conducted inside the calibration chamber, adopting equivalent penetration rates in terms of non-dimensional velocity. The soil model adopted presents cohesion and a dilation angle greater than zero. The model is able to reproduce measured tip resistances and in particular the ratio between the drained and the undrained tip resistance, showing very good predictive capabilities. The influence of the dilation angle on tip resistance measurements has been evaluated. Dilation angle has a significant impact on the undrained tip resistance, with important changes in the relatively small range of values analysed. On the other hand, differences in the drained range are more sensitive to the elastic stiffness of the soil, and dilation have secondary importance. The ratio between the net drained tip resistance and the net undrained tip resistance is completely different from the results obtained by Yi et al. (2012) for a cohesion less soil.

9. Use of CPT for soil profiling in transitional soils

The available classification systems (CPTu) do not lead to a correct SBT identification of the loose silt mixtures. More specifically, very loose silt mixtures have been found within the chaotic dredged sediments stored in the artificial basin of the Port of Livorno and in the case of loose silt mixtures of the Serchio River levee – system and its foundation soil. The poorly compacted silt mixtures of the Serchio River levee -system and the loose silt mixtures of the foundation soil of these levees are often classified as clay or even organic clay. A similar systematic type of miss - classification was also observed in the case of dredged sediments of the Livorno Port artificial basin. The term miss – classification here refers to SBT classes and not to the grain size distribution and Atterberg Limits.

Soil layers above the water table may be partially saturated. In this situation, the cone penetration occurs under a partial drainage condition. Whereas the effect of saturation degree appears quite negligible for sands (Schmertmann, 1976; Bellotti *et al.*, 1988; Jamiolkowski *et al.*, 2001), it may become very relevant for fine – grained soils. Jamiolkowski *et al.* (2001) analysed CPTu test results in a Calibration Chamber on dry or fully saturated, reconstituted sand samples. They found that the tip resistance of fully saturated samples was slightly lower than that of dry samples (at the same relative density and boundary stresses) for fine to medium sands. However, even when soil layers are fully saturated by capillarity, the in-situ stress state is controlled by suction, which is usually unknown. The possible effects of suction on soil profiling, in the case of fine-grained soil deposits, can lead to another type of miss – classification, that is overconsolidated clays (because of suction) are sometimes erroneously identified as sands. This is also a consequence of the fact that, for practical reasons, only the pore pressure behind the tip (u_2) is measured.

This chapter proposes two different approaches to improve miss-interpretation of CPTu tests in case of the aforementioned soil types. The first method concerns soil layers above the water table, it consists in a better estimation of the effective stress state in order to take into account the effects of soil suction. To this purpose, the modified Kovacs model (MK) has been applied. The second methodology is purely empirical. It consists in a calibration of the Soil Behaviour Type Index, I_c (Robertson, 1990; Robertson and Wride, 1998), based on direct estimation of soil characteristics from reference boreholes. The methodology has been applied to very loose silt mixture, in particular the foundation soil of the Serchio River levee system and dredged sediments stored inside artificial basins at the Livorno Port.

9.1 Re-interpretation of CPTU at Broni

The methodology, adopted to obtain correct SBTn classes assignation, uses the modified Kovacs model (MK), as described in the original work by Kovacs (1981) and in that by Aubertin et al (2002), to estimate the soil suction from simple physical soil parameters. This methodology requires soil classification, which represents an intrinsic limitation. Such a methodology has been applied to the interpretation of the CPTU carried out at Broni.

Broni is located in the North of Italy in the Po River area near to Pavia. From a geological point of view, it is characterised by alluvial deposits generated by the Po River and its tributaries. Geotechnical investigations have been carried out by the University of Pavia and include geotechnical soundings and CPTu tests conducted at a depth varying between 20m and 30m (Meisina et. al, 2004, Lo Presti et al. 2009). Furthermore, data from around 50 wells are available (Meisina et. al, 2004). Piezometer level monitoring has been done on June 2002 and March 2003 in all the wells installed (Table 20), whereas for some piezometers located in the residential area of Broni, piezometric measurements are available once a month or once a week (Table 21). Well P3 is the closest one to the CPTus and borehole (Figure 157). Almost all the wells reach a depth between 5.4 and 12 meters, hence their levels are controlled by the superficial aquifer. Well number 7 has a depth of 18.5 meters, instead, and more probably reaches the principal and deeper aquifer.

Looking at Figure 158 and Figure 159 it is possible to observe that the water level follows the pluviometric levels. The maximum water level occurs in January. The pluviometric range for the superficial aquifer is approximately 2-2.5 m, whereas it reaches 3.8 meters for the deeper aquifer.

Two CPTUs were carried out, in June 2001 (Figure 162) and September 2001 (Figure 163), at the same location. The observed trend of the water table depth with time confirms the correctness of the measured values that have been considered to interpret CPTu1 and CPTu2 (Figure 162 and Figure 163). In fact, the water table was found at a depth of 3.5 m for the test conducted during the humid season (CPTu1, June 2001) and at a depth of 5 m for the test conducted during the dry season (CPTu2, September 2001).

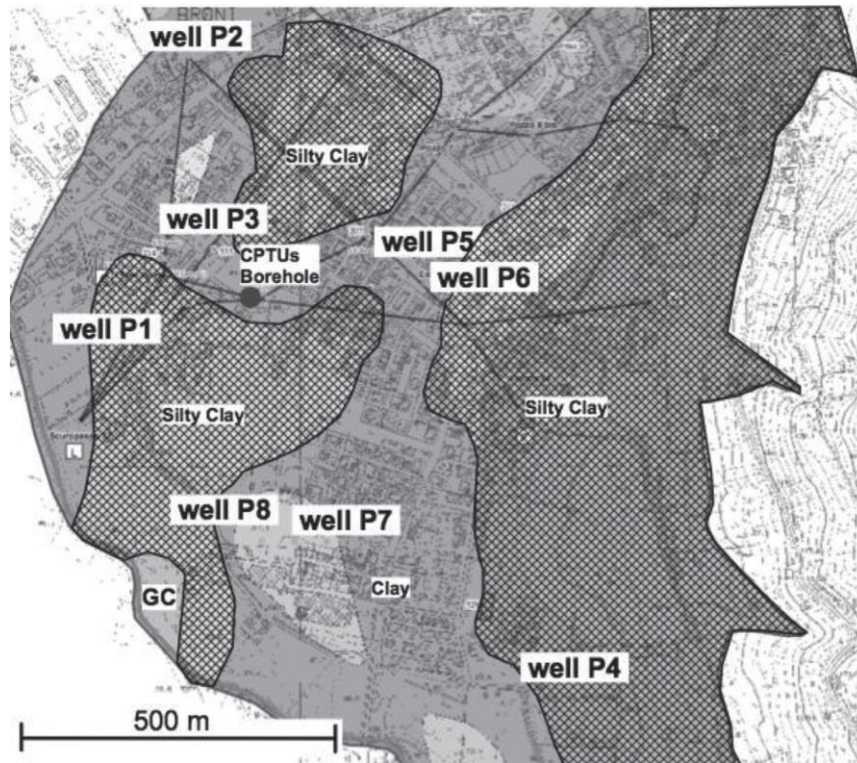


Figure 157: Broni area – Geological map, test and well (P1 to P7) locations.

Well n.	Deep (m)	Surface level (m a.s.l.)	Piezometric level (m a.s.l.) June2002	Distance from surface level June2002	Piezometric level (m a.s.l.) March 2003	Distance from surface level March 2003	Piezometric level (m a.s.l.) August 2003	Distance from surface level August 2003	Piezometric level (m a.s.l.) July 2000	Distance from surface level July 2000	Piezometric level (m a.s.l.) October 2000	Distance from surface level October 2000
7	7.3	62.7	60.7	-2	61.5	-1.2	59.6	-3.1	59.55	-3.15	59.05	-3.65
3		64	60.3	-3.7	61.1	-2.9	59.4	-4.6			60.2	-3.8
5	2.75								62.7		62.66	
7		65.2	61.8	-3.4	63.2	-2	61	-4.2			62.2	-3
8	5.1	65.4	60.5	-4.9	61.7	-3.7	59.6	-5.8	61.35	-4.05	60.91	-4.49
9	15.1	62.3	59.7	-2.6	60.7	-1.6	58.8	-3.5	59.86	-2.44	60.2	-2.1
12	8.97	67.9	66.1	-1.8	67.2	-0.7	64.7	-3.2	59.03	-8.87	64.35	-3.55
18	5.3	71.3	68.9	-2.4	70	-1.3	68	-3.3	68.9	-2.4	68.52	-2.78
19	7.5	71.5	68.2	-3.3	69.7	-1.8	66.8	-4.7	67.2	-4.3	66.59	-4.91
21		71.9	68.9	-3	70.4	-1.5	67.5	-4.4			68.04	-3.86
22	15	75	64.5	-10.5	66.6	-8.4	62.3	-12.7			62.5	-12.5
23	5.15	77.9	73.6	-4.3	74.8	-3.1	dry		74.04	-3.86	73.26	-4.64
24	4.5	76.5	dry		72.7	-3.8	dry		dry		dry	
25	4.65	75.5	71.2	-4.3	72.2	-3.3	dry		70.62	-4.88	dry	
26	5.81	75.8	71.2	-4.6	72.2	-3.6					69.09	-6.71
27		75	71.3	-3.7	72.6	-2.4	70	-5	69.5	-5.5	69.02	-5.98
28	5.37	77.5	dry		dry		dry		dry		dry	
29		83.3	80.2	-3.1	81.4	-1.9	78.8	-4.5		-83.3	80.64	-2.66
31	4.58	78.8	dry		dry		dry		dry		dry	
33		78.9	76.4	-2.5	76.9	-2	dry				70.29	-8.61
34		81.7		-81.7	79.75	-1.95			77.32	-4.38	76.64	-5.06
37	40	87.5	83	-4.5	83.75	-3.75	dry		83	-4.5	69.59	-17.91
38	18	90	79.64	-10.36	82.3	-7.7	79.3	-10.7			76.99	-13.01
39	8.3	100.2	95.6	-4.6	96.4	-3.8	94.7	-5.5			95.43	-4.77
41	3.9	81	77.5	-3.5	78	-3	76.6	-4.4	79.05	-1.95	78.61	-2.39
42	9.4	78.5	73.2	-5.3	73.8	-4.7	70.8	-7.7	73.46	-5.04	69.83	-8.67
43		78.5	69.5	-9	71.8	-6.7	67.8	-10.7		-78.5	69.08	-9.42
44	12.45	80	69.2	-10.8		-80			70.29	-9.71	68.74	-11.26
45	11.6	66.3	63.5	-2.8	64.7	-1.6	62.6	-3.7				
47	6.1	72	65.4	-6.6	68	-4	64.6	-7.4				

Table 20: Piezometric data obtained for all the piezometers in Broni area.

Date	Well n. 1	Well n. 2	Well n. 3	Well n. 4	Well n. 5	Well n. 6	Well n. 7	Well n. 8
7/25/2002	NA	-5,1	-5,3	NA	-4,1	-5,2	-11,3	NA
8/28/2002	NA	-5,1	-5,05	NA	-4	-5,15	-11,15	NA
9/30/2002	NA	-5,2	-5,35	NA	-4,6	-5,75	-11,45	NA
10/23/2002	NA	-5,2	-5,35	NA	-4,65	-5,75	-11,5	NA
11/28/2002	-2,95	-4,3	-3,1	-5,2	-3	-3,5	-9,4	NA
12/06/2002	-3	-3,3	-2,9	-4,9	-2,95	-3,3	-9,25	NA
12/13/2002	-3,4	-3	-3,05	-5,1	-3,2	-3,55	-9,1	NA
1/29/2003	-3,1	-2,25	-2,8	-4,55	-2,15	NA	-7,7	-5,3
2/26/2003	-3,7	-2,35	-3,4	-4,7	-2,3	NA	-7,6	-5,25
03/12/2003	-3,8	-2,4	-3,6	-4,75	-2,4	NA	-7,7	-5,34
3/31/2003	-4	-2,75	-3,8	-4,85	-2,55	NA	-7,7	NA
04/12/2003	-3,95	-2,82	-3,9	-4,9	-2,6	NA	-7,8	NA
4/30/2003	-3,9	-2,9	-3,9	-4,8	-2,55	NA	-7,7	NA
5/15/2003	-4,1	-3,25	-4,1	-4,9	-2,7	NA	-7,8	NA
06/03/2003	-4,3	-3,55	-4,35	-4,9	-2,9	NA	-7,9	NA
6/18/2003	-4,55	-4,05	-4,55	-5	-3,05	NA	-8,65	NA
07/07/2003	NA	-4,45	-5	NA	-3,4	NA	-9,55	NA

Table 21: Water Table Depth from July 2002 to July 2003, residential area of Broni (NA = Not Available, Dry Well).

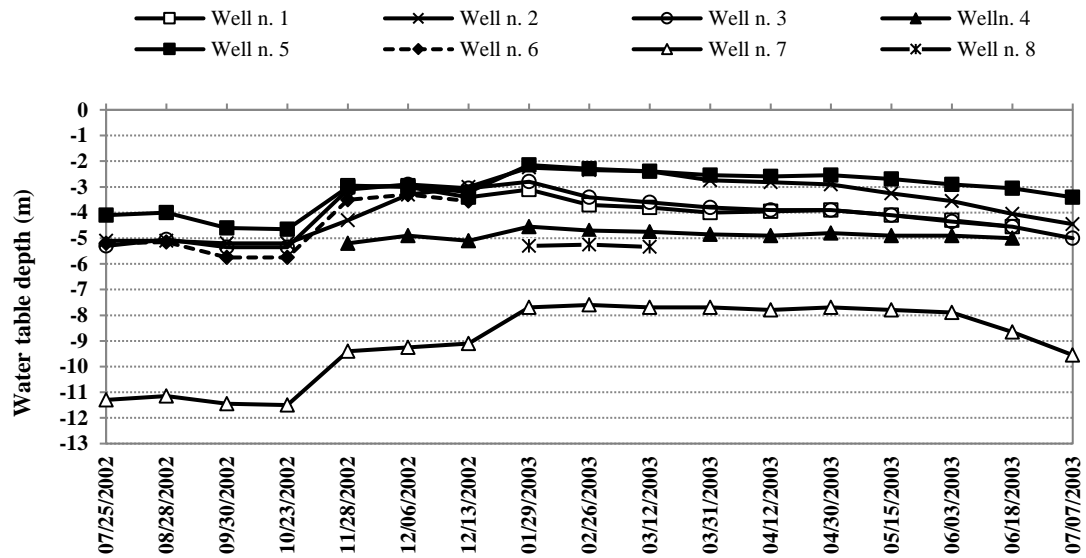


Figure 158: Water table depth during the observation period, residential area of Broni.

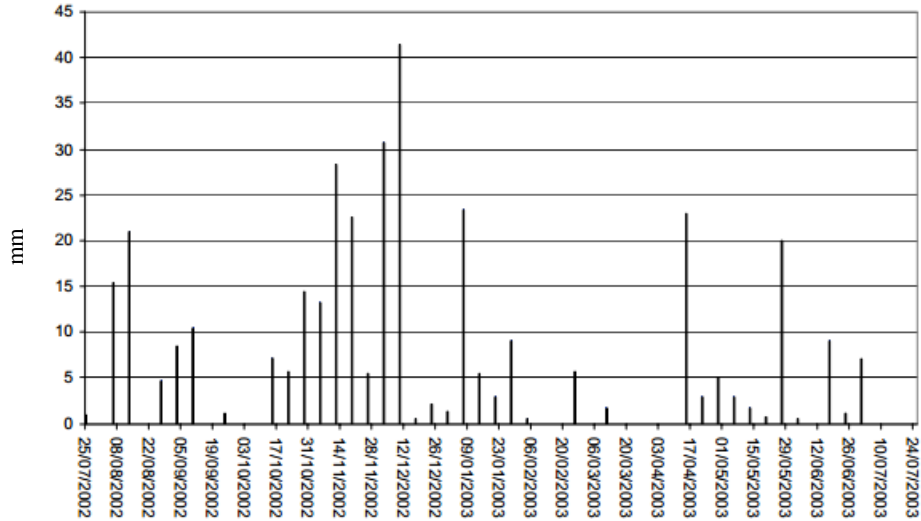


Figure 159: Rainfall levels at Cigognola station (Pavia).

9.1.1 Cone Penetration tests

The results of the two CPTu tests conducted, at the same location during the dry and the humid season, are shown in Figure 162 and Figure 163. A standard piezocone and the standard procedure has been adopted for the tests. The pore water pressure has been measured by using silicone grease (very fluid, NLGI 00) as saturation fluid of the slot filter.

On the basis of laboratory testing on undisturbed samples retrieved from the first three meters (Table 22), the deposit can be considered homogeneous and is mainly classified as CL to CH (USCS, ASTM 2487). The clayey nature of the deposit under consideration, and in particular of its shallower portion (first 3 meters), is shown in Figure 160, Figure 161 and Table 22.

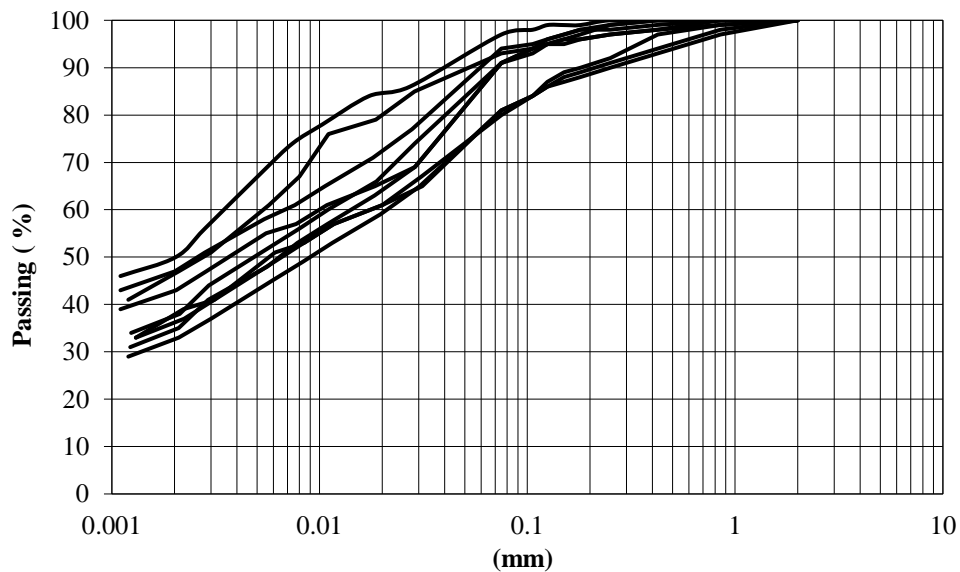


Figure 160: grain size distributions for upper-soil in Broni.

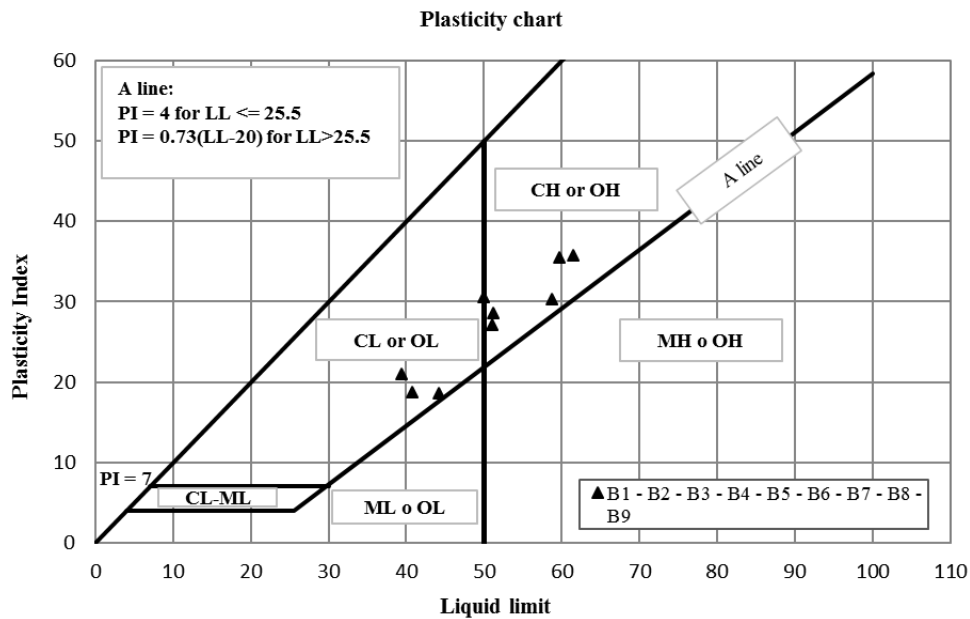


Figure 161: Casagrande classification chart (USCS, ASTM 2487).

Sample	Depth (m)	W _l (%)	W _p (%)	w (%)	γ _d (kN/m ³)	S (%)	e ₀	h _{co} (m)	σ _g (kPa)
B1	0.87	61	26	29.30	14,5	91,00	0,862	2,8	20
B2	1.3	59	28	27.90	15,1	96,00	0,788	2,7	15
B3	1.7	51	24	27.90	15,1	92,00	0,788	3,0	25
B4	2	49	19	27.00	15,4	96,00	0,753	2,6	15
B5	2.15	51	23	29.80	15,5	93,00	0,742	2,5	23
B6	2.3	44	25	30.00	14,7	97,00	0,837	2,6	8
B7	2.5	39	26	28.00	14,7	92,00	0,837	2,3	0
B8	2.63	41	22	26.00	15,5	95,00	0,741	2,5	13
B9	3	60	24	28.80	15,3	97,00	0,765	2,7	10

Table 22: Soil classification (Broni – first three meters) W_l and W_p = Liquid and plastic limit respectively; w = natural water content; S = Saturation degree; e₀ = Void ratio; h_{co} = Capillary rise from lab tests; σ_g = Swelling pressure from lab tests. (Meisina 1996)

The two CPTu tests exhibit the same tip resistance (1.0 – 2.0 MPa) for depths greater than around 3 m. In the vadose zone above the water table, in spite of the deposit homogeneity, the tip resistance (q_c) is strongly influenced by the water table depth, so that q_c increases from 1 – 2 MPa to 3 – 4 MPa (Figure 164). It is worthwhile to notice that such an increase is higher during the dry season. This trend is not confirmed in the very first layer (first 0.5 m). In Figure 164, the layer in which it is possible to observe differences between tip resistances related to suction is highlighted.

The higher values of q_c that have been observed in the vadose zone and the fact that higher q_c values are observed for the test carried out during the dry season could be explained in terms of suction. The differences of q_c concerning the first 0.5 m do not have a definitive explanation. It is possible to assume local granulometric heterogeneities.

As far as pore water pressure measurements are concerned, an almost nil value of u_2 is observed until a depth of around 2 m for CPTu1, then dynamic pore water pressure increases with depth reaching values lower than 25 kPa. These measurements cannot be considered satisfactory because they indicate an initial de-saturation of the filter and subsequent sluggish measurements.

On the other hand, during CPTu2 test, dynamic pore water pressure assumes negative values at depth of between zero and 2.5 meters, after which it increases with depth. The high pore water pressure value observed at 0.5 meters could be explained by considering the extreme stiffness of the shallower man-made soil layer. This could be the cause of filter desaturation.

The unsatisfactory measurement of u_2 during the CPTu1 test does not influence the proposed method, which pertains to the reinterpretation of the first 3 meters using the total tip resistance and friction ratio. The differences between the measured and the total tip resistance are negligible.

Table 23 shows the SBTn classes as defined by Robertson (1990) and the respective intervals of I_c index (Robertson and Wride, 1998).

The effects of suction on SBTn are shown in Figure 165 where I_c values are plotted for the first 5 meters depth, for both tests CPTu1 and CPTu2. In both cases I_c values decrease from the value that assumes at 5 meters depth, to the value of approximately 2 at 0.5 meters depth. I_c values inferred from the CPTu2 test are lower than those obtained with the CPTu1 test. The presence of suction, that is more relevant in the dry season, alter SBTn classification since I_c values diverge from those obtained at the water table level, despite the homogeneity of the soil above and below the water table. This miss-classification is more pronounced for the test carried out during the dry season. The effect of suction in terms of SBTn classes is discussed later, when data are compared to those obtained after the application of the proposed methodology.

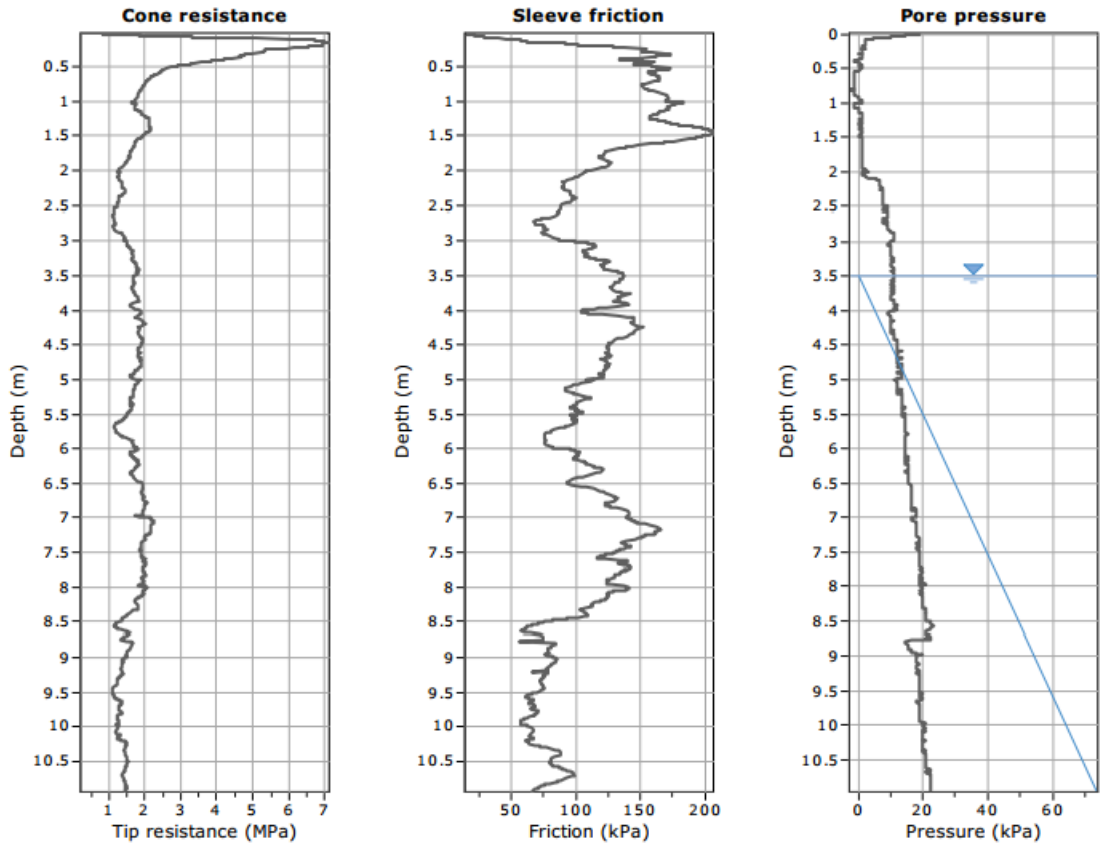


Figure 162: CPTu1 test conducted during the humid season.

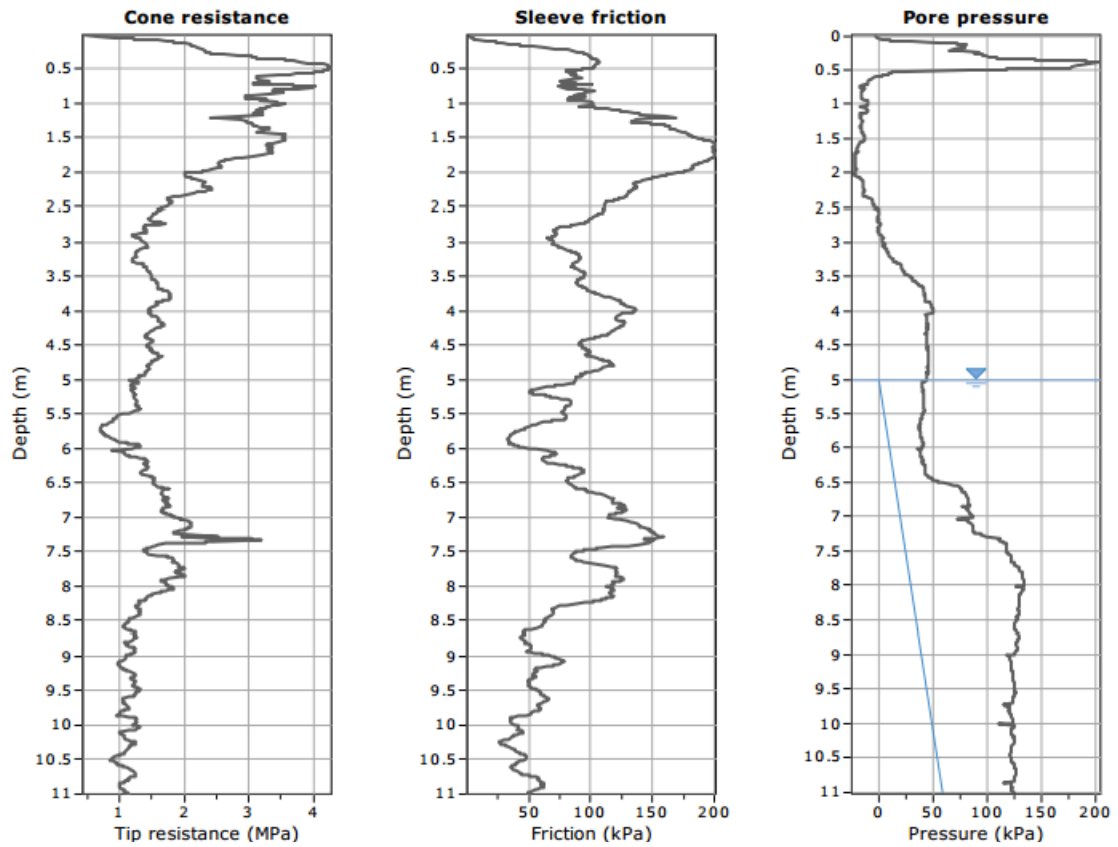


Figure 163: CPTu2 test conducted during the dry season.

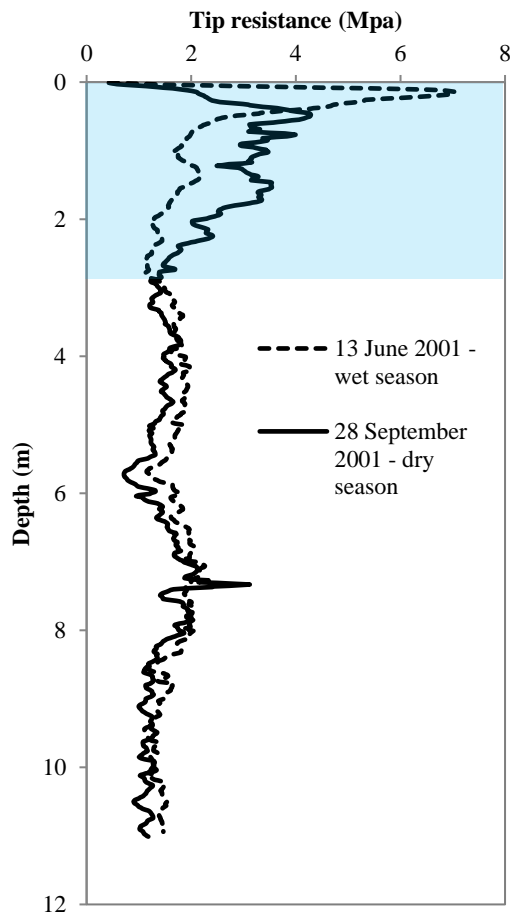


Figure 164: CPTu1 and CPTu2, highlighted is the layer in which we can observe differences in tip resistance.

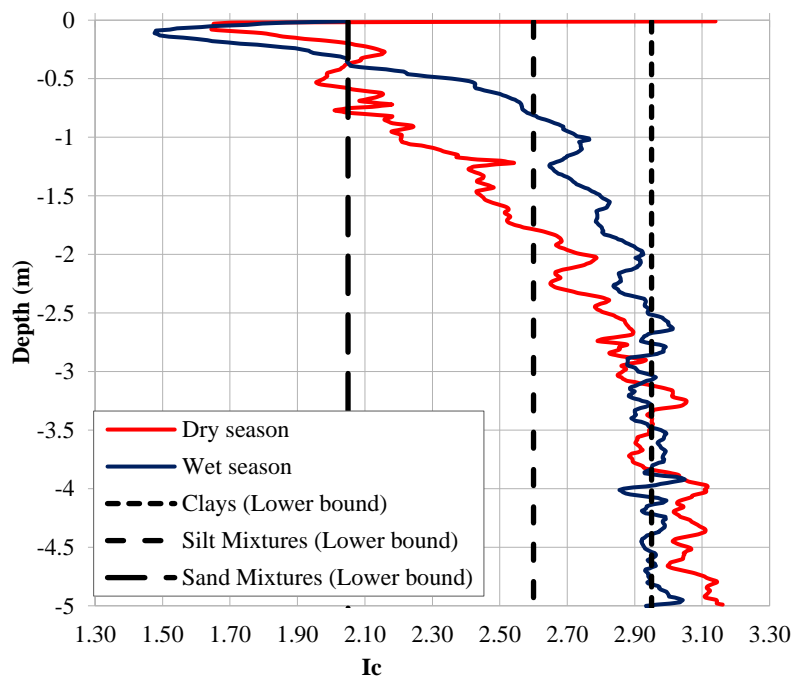


Figure 165: Ic values for CPTu1 test (humid season) and CPTu2 test (dry season).

Soil classification (SBTn)	Zone number (Robertson SBT 1990)	SBT Index values
Organic soils: peats	2	$I_c > 3.60$
Clays: silty clay to clay	3	$2.95 < I_c < 3.60$
Silt Mixtures: clayey silt to silty clay	4	$2.60 < I_c < 2.95$
Sand Mixtures: silty sand to sandy silt	5	$2.05 < I_c < 2.60$
Sands: clean sand to silty sand	6	$1.31 < I_c < 2.05$
Gravelly sand to dense sand	7	$I_c < 1.31$

Table 23: Definition of soil classification (Robertson, 1990) from the Soil Classification Index (Robertson and Wride, 1998)

9.1.2 THE MK MODEL

More information about the model can be found in the works of Kovacs (1981) and Aubertin, et al. (2002). The MK model has been used to evaluate, from simple soil parameters, the matrix suction (ψ_r) at the residual water content and the equivalent capillary height above the water table (h_{co}). The following simplified equations have been used (Aubertin et al. 1998; Mbonimpa et al. 2000, 2002).

For granular soils $h_{co,G}$ (the suffix “G” stands for granular soils) can be considered equivalent to the height of the capillary fringe and can be evaluated with the following expression:

$$h_{co,G} = \frac{b}{eD_{10}} \quad (1)$$

$$b[cm^2] = \frac{0.75}{1.17 \log C_U + 1} \quad (2)$$

Where: e = void ratio, $C_U = \frac{D_{60}}{D_{10}}$ = coefficient of uniformity. Kovacs (1981) defines the following parameter (equivalent particle diameter), embedded in eqs. (1) and (2), for heterogeneous material:

$$D_H = [1 + 1.17 \log C_U]D_{10} \quad (3)$$

For fine grained (plastic, cohesive) materials (the suffix P stands for plastic soils) the following expression is more appropriate:

$$h_{co,P} = \frac{\xi}{e} w_L^{1.45} \quad (4)$$

Where: w_L is the liquid limit, $\xi(cm) \approx 0.15\rho_s$ (kg/m^3), ρ_s = solid density

The MK model uses h_{co} as a reference value to define the relationship between the degree of saturation and the matric suction ψ . In particular the suction at residual water content is defined as following:

$$\psi_r = \frac{0.42}{(eD_H)^{1.26}} \quad (5)$$

where D_H and ψ_r are expressed in cm.

For granular materials:

$$\psi_r = 0.86 h_{c0,G}^{1.2} \quad (6)$$

where $h_{c0,G}$ and ψ_r are expressed in cm.

For clayey soils:

$$\psi_r = 0.86 \left(\frac{\xi}{e}\right)^{1.2} w_L^{1.74} \quad (7)$$

where ψ_r and ξ are expressed in cm.

In order to take into account the influence of suction on the interpretation of test results, a negative pore water pressure has been computed above the water table according to the following equations:

$$u = -\gamma_w \cdot h \quad \text{for } 0 < h < h_{c0} \quad (8)$$

$$u = -\gamma_w \cdot h_{c0} \quad \text{for } h > h_{c0} \quad (9)$$

h = height above the water table.

The adopted hypotheses represent an oversimplification and may still underestimate real the effective stresses.

9.1.3 CPTu interpretation

The effective vertical geostatic stresses have been re-evaluated according to the method explained in the previous section. The pore water pressure has been assumed to be linear from the water table to the capillary height, h_c , calculated with MK model, and then constant to the surface level. It has been assumed that h_c value is equal to ψ_r estimated from equation 7. In this case the h_c values are higher than water level depth, therefore the pore water pressure has been assumed to linearly vary until the ground level. The hypothesis at the basis of this procedure is that the soil above the water table is saturated due to capillarity. It is interesting to note that some measurements of the negative pore pressure in the laboratory, conducted by means of the filter paper method, indicated values of around 2.6 – 3.0 m (Table 22). These values are around half those inferred by means of the M-K model. However, it is important to recall that the soil samples were not retrieved at the same time the CPTu test was conducted. The increased values of σ'_{v0} led to a reduction of the normalised tip resistance, Q , and consequently, an increase of the Soil Classification Index I_c (Robertson, 1990; Robertson and Wride, 1998).

The influence of the proposed correction on I_c is shown in Figure 166 and Figure 167, results are plotted for the soil layers above the water table, therefore from zero to 3.5 meters depth for the test conducted during the humid season, and from zero to 5 meters depth for the test conducted during the dry season. Such a correction moves the I_c parameter toward the target value of 3.0 (*i.e.* the I_c value that the homogeneous clay - deposit exhibits below the water table). In other words, after the correction, the target value of $I_c = 3.0$ is reached below the depth of 1.0 m for CPTu1 and below the depth of 2.0 m for CPTu2.

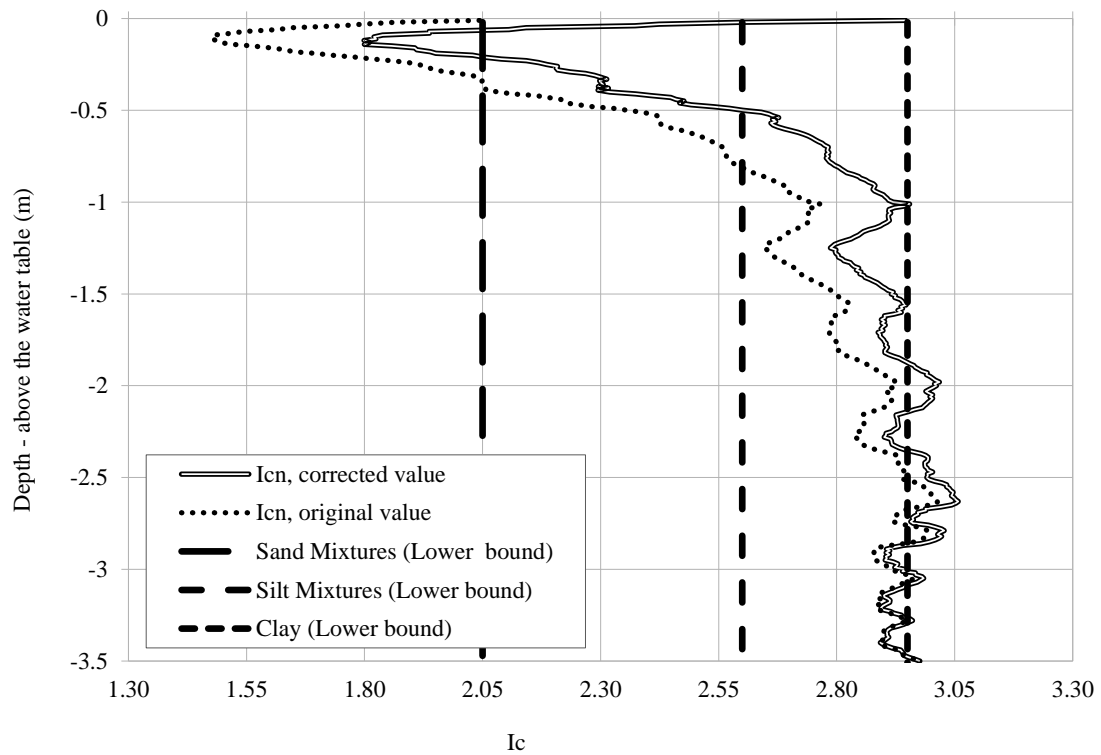


Figure 166: Variation of I_c values for CPTu1 test (humid season).

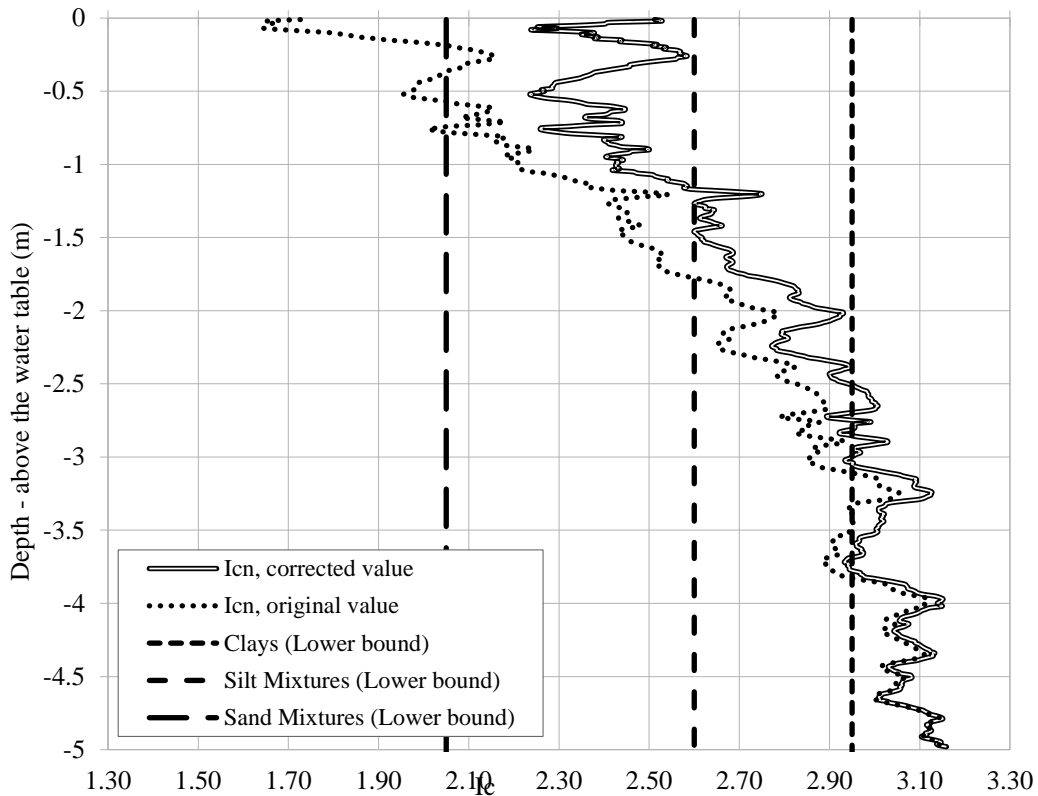


Figure 167: Variation of I_c values for CPTu2 test (dry season).

As shown in Figure 168, the corrected interpretation of data allows the identification of a unique material, belonging to SBTn classes 3 and 4 (clay to clayey silt), below and upon the water table, according to what observed from boreholes soundings and laboratory tests. On the contrary, without considering suction upon the water table, these layers were assigned to SBTn class 9, very stiff fine-grained soils (Figure 168). Therefore, the correction allows for identifying the upper 5 meters of the deposit as fine grained soil (SBTn 3 and 4) and the information of the presence of very stiff fine-grained soils (SBTn class 9) disappears. This is the consequence of the higher values of vertical effective stress obtained once the effects of suction have been taken into account.

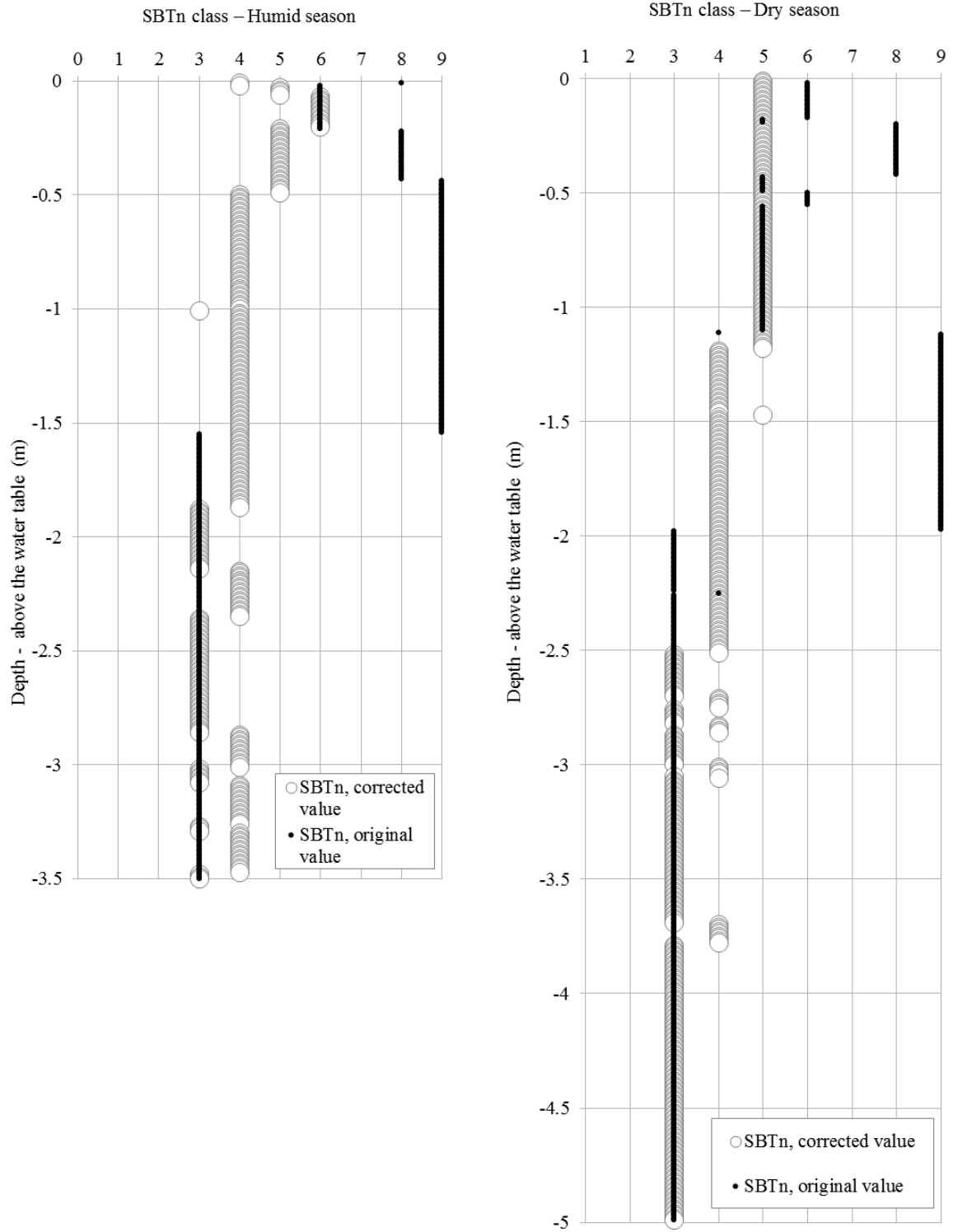


Figure 168: SBTn classes before and after correction for CPTu1 (humid season) and CPTu2 (dry season).

9.2 Specific- empirical calibration of I_c values from borehole evidences

In this chapter, the possibility to implement a site-specific empirical correlation to correct row CPTu data, in order to obtain reliable interpretation results, is analysed. The same technique has been already applied to the interpretation of CPTu tests carried out on Serchio River embankments; this procedure is illustrated in the following chapters.

This methodology is purely empirical and consists of a specific calibration of the I_c values (Robertson 1990, Robertson and Wride 1998) as inferred from CPTu results against the evidences obtained from direct logging (boreholes). This methodology has been applied for the Serchio River levees and foundation soil taking advantage of the large number of CPTu and boreholes.

The proposed calibration is based on the following lines:

- the comparison was only made between the boreholes and CPTus, which were located very close to each other (maximum 1.0 m apart);
- the comparison was only made for those portions of the borehole where the grain size curve was available;
- the grain size curve was obtained and described according to AGI (1997);
- the I_c index from the CPTu was inferred by means of the CPeT-IT software (Geologismiki, 2007);
- the I_c index from the grain size curve was established according to the indications reported in Table 24 and Table 25.

The AGI classification (Italian Geotechnical Society) is based on the following rules:

- the main fraction gives the name to the soil;
- the expression “with” is used for fractions between 5 and 50%;
- the adjective is used for fractions between 10 and 25%;
- fractions less than 5% is not considered.

Fractions between 5 and 10% are shown in brackets in Table 24 and Table 25. An example is given to help understand how a correspondence between I_c and the granulometric curve has been defined. A “silt with clay” soil corresponds to SBTn class 4 with $2.60 < I_c < 2.95$. A more precise value of the index is assumed proportional to the percentage of clay fraction (from 25 to 50%).

It is worth recalling that CPTu-based soil classification mainly refers to the soil behaviour type (SBT), while the proposed borehole-based soil classification refers to the grain size distribution. However, one of the most relevant parameters, in the case of levees and dredged sediments as well, is the permeability, which mainly depends on the grain size and degree of compaction (Tatsuoka, 2015).

Table 24 and Table 25 show the soil classification (according to AGI, 1997) and the selected I_c index for the various soil classes. In addition, I_c index inferred from CPTu and the respective SBTn class number is visible in the tables. In practice, each row in Table 24 and Table 25 shows the soil classification (AGI, 1997), as obtained for a homogeneous portion of borehole, and the “arbitrary” I_c value that was associated to that soil description. The term “arbitrary” I_c value refers to the fact that such an index was introduced to define an SBT and not a soil type. Besides, I_c values and SBTn classes inferred from the corresponding CPTu at the same depth are reported in the same row. Table 24 and Table 25 only consider the soil portion below the water table. The comparison was limited to those portions of boreholes below the water table. The proposed method is intended for a user-defined correction of the classification chart.

Borehole #	Soil classification from borehole (AGI 1997)	Ic from borehole	Ic from CPTu	ΔIc	SBTn	Soil classification
SC3	Silt with sand (5<clay<10%)	2.05	3.28	1.25	3	Clays to silty clay
	Silt with clay (5<sand<10%)	2.70	3.05	0.27	3	Clays to silty clay
SC4	Silt with clay	2.75	2.92	0.13	3	Clays to silty clay
SC7	Silt with clay (5<sand<10%)	2.10	2.30	0.17	5	Sand mixture
	Silt with clay (5<sand<10%) (5<grav-	2.65	3.10	0.40	3	Clays to silty clay
SC8	Sand with silt (5<clay<10%)	1.95	2.20	0.27	5	Sand mixtures
SC14	Sandy silt with clay	2.10	2.36	0.22	5	Sand Mixtures
	Sandy silt with clay	2.10	3.96	1.82	2	Organic soils
	Clayey sand with silt	1.95	2.96	0.96	3	Clays to silty clay
	Clayey sand with silt	1.95	3.12	1.30	3	Clays to silty clay
	Silt with clay (5<sand<10%)	2.10	3.36	1.27	3	Clays to silty clay
	Silt with clay (5<sand<10%)	2.10	3.64	1.55	2	Organic soils

Table 24: Port of Livorno data – Ic and classification from both CPTu and borehole – data interpretation.

Borehole #	Soil classification from borehole (AGI 1997)	Ic from borehole	Ic from CPTu	ΔIc	SBTn	Soil classification from CPTu
1	Clayey and sandy silt	2.60	2.79	0.19	4	SandMixtures
	Silty sand	2.10	2.05	-0.05	6	Sand
	Silty sand	2.10	2.49	0.39	5	SandMixtures
	Sand, gravel and fine gravel	1.30	1.72	0.42	6	Sand
	Silty sand	2.10	2.19	0.09	5	SandMixtures
2	Fine sand with silt	2.40	3.14	0.74	3	Clays
	Silty sand	2.10	2.20	0.10	5	SandMixtures
3	Clayey and sandy silt	2.60	1.63	-0.97	6	Sand
	Clayey and sandy silt	2.60	3.36	0.76	3	Clays
	Silty sand (5<clay<10%)	2.50	3.27	0.77	3	Clays
	Silty sand	2.10	2.85	0.75	4	Silt Mixtures
4	Silty sand	2.10	2.15	0.05	5	SandMixtures
	Sand, gravel and fine gravel	1.30	1.86	0.56	6	Sand
	Sand	1.70	1.93	0.23	6	Sand
	Clayey and sandy silt	2.60	3.70	1.10	2	Clay-Organic Soil
5	Sand with silt	2.50	2.74	0.24	4	Silt Mixtures
	Silt with clay	2.80	2.05	-0.75	6	Sand
	Silty sand	2.10	1.93	-0.17	6	Sand
	Sand	1.60	2.29	0.69	5	SandMixtures
	Silt with clay/clay with silt	3.00	3.23	0.23	3	Clays
6	Sand with silt/silt with sand	2.50	3.23	0.73	3	Clays
	Silt with clay	2.90	3.34	0.44	3	Clays
	Silty sand	2.10	3.18	1.08	3	Clays
	Clayey and sandy silt	2.60	2.99	0.39	3	Clays
	Silty sand	2.10	3.27	1.17	3	Clays
7	Silty sand	2.10	1.94	-0.16	6	Sand
	Medium silty sand	1.90	1.58	-0.32	6	Sand
	Sand, gravel and fine gravel	1.30	1.82	0.52	6	Sand
	Coarse sand (5<clay<10%)	2.00	2.06	0.06	5	SandMixtures
	Clayey and sandy silt	2.60	2.09	-0.51	5	SandMixtures
	Medium sand (5<clay<10%)	2.10	2.26	0.16	5	SandMixtures
	Silty sand	2.10	2.14	0.04	5	SandMixtures
8	Silty sand (5<clay<10%)	2.50	2.50	0.00	5	SandMixtures
	Silty sand	2.10	2.86	0.76	4	Silt Mixtures
	Clayey silt	2.80	3.06	0.26	3	Clays
	Sand (5<silt<10%)	2.00	3.18	1.18	3	Clays
9	Sand with silt	2.35	2.32	-0.03	5	SandMixtures
	Medium sand with gravel	1.40	1.73	0.33	6	Sand
	Sand (5<silt<10%)	2.00	2.95	0.95	3	Silt Mixtures
	Clayey and sandy silt	2.60	3.43	0.83	3	SandMixtures
	Silty sand	2.10	3.34	1.24	3	Clays
	Clayey and sandy silt	2.60	2.24	-0.36	5	SandMixtures
10	Silty sand	2.10	2.16	0.06	5	SandMixtures
	Silty sand (5<clay<10%)	2.50	3.16	0.66	3	Clays
	Silt with sand (5<clay<10%)	2.65	3.34	0.69	3	Clays
	Silty sand (5<clay<10%)	2.50	2.75	0.25	4	Silt Mixtures
	Silty sand	2.10	3.28	1.18	3	Clays
	Clayey silt	2.80	3.48	0.68	3	Clays
	Peat	3.60	3.48	-0.12	3	Clays
	Clayey silt	2.80	3.59	0.79	3	Clays
	Clayey and sandy silt	2.60	3.59	0.99	3	Clays
	Sand with silt/silt with sand	2.50	2.39	-0.11	5	SandMixtures
	Silty sand	2.10	2.75	0.65	4	Silt Mixtures
Clayey silt with sand	2.55	3.73	1.18	2	Clay-Organic Soil	
11	Medium to coarse sand	1.40	2.29	0.89	5	SandMixtures
	Clayey silt	2.80	3.64	0.84	2	Clay-Organic Soil
	Silty sand	2.10	2.79	0.69	4	Silt Mixtures
	Clayey silt	2.80	4.28	1.48	2	Clay-Organic Soil
	Medium sand (5<silt<10%)	2.00	2.73	0.73	4	Silt Mixtures
12	Medium to coarse sand	1.40	2.02	0.62	6	Sand
	Peat	3.60	4.80	1.20	2	Clay-Organic Soil
	Silt with clay	2.90	3.62	0.72	2	Clay-Organic Soil
	Clayey silty sand	2.50	3.77	1.27	2	Clay-Organic Soil
	Silt with clay	2.80	3.88	1.08	2	Clay-Organic Soil
	Silty sand	2.10	1.65	-0.45	6	Sand
	Medium to coarse sand	1.40	1.66	0.26	6	SandMixtures

Table 25: Serchio River data – Ic and classification from both CPTu and borehole – data interpretation.

The Serchio River flood that took place in the Pisa and Lucca Districts (Italy) during December 2009, has led to a huge geotechnical characterisation survey with the aim of studying the safety conditions of the embankments system and the causes that brought to failure. The survey has included: boreholes, Lefranc tests, installation of piezometers for each borehole, piezocone tests, two-dimensional Electric Resistivity Tomography and continuous sampling (4 meters deep). Among these, 149 CPTu tests have been conducted in Pisa area, at a depth varying between 20 and 30 meters.

Since 2000, the Port of Livorno's Authority has realised artificial basins for the storage of dredged sediments. The top surface covers 40 hectare therefore there is a great interest in reusing this areas for the port infrastructures development. To this purpose, the Livorno Port Authority has carried out a huge geotechnical (and environmental) investigation campaign that consists of: 22 boreholes (for a total of 196.5 m); 18 undisturbed samples; 34 remoulded samples; 11 Lefranc (variable head) permeability tests; the installation and reading of 4 piezometers (open pipe); 26 CPTus (for a total of 153 m); 6 DMT (for a total of 29 m); laboratory tests on 50 different samples. A comparison has only been made considering 12 CPTus, and only for those portions of subsoil for which the grain size curve was available.

9.2.1 Empirical I_c correction

The diagram in Figure 169 displays the values of I_c obtained from CPTu tests (Serchio river area) and from the corresponding boreholes for soil layers below the water table. The differences between the two values are especially evident for the SBTn classes 3, 4 and 5 with I_c varying between 1,90 and 3,22. In particular, it is possible to observe an almost systematic bias between the two series of values. The dependence of the Soil Classification Index, I_c , on the total tip resistance, q_t , is shown in Figure 171 (Serchio River area). Figure 171 shows the I_c values obtained from both the CPTu and from borehole data interpretation. The values obtained from the CPTus are generally higher, whereas those inferred from boreholes are lower (Table 25). The differences between the two series become negligible, as the total tip resistance increases, and not very relevant from a practical point of view.

The difference between the two I_c series (ΔI_c) is plotted vs. the total tip resistance in Figure 171 (Serchio River and Port of Livorno areas). The best fit of such data is given by the following equation:

$$\Delta I_c = 0.05 + \frac{0.75}{q_t}$$

Where q_t is in MPa.

The $\Delta I_c(q_t)$ function was used to correct the CPTu interpretation (Serchio river data). The new results, after the correction, are shown in Figure 172. It is possible to observe that the dispersion

of the corrected data is much lower than that of the original values. Furthermore, the I_c values are arranged better around the 45° angle line, thus leading to a much better correspondence between the SBTn classes identified from the CPTu tests and those inferred from the boreholes (based on grain size).

The proposed correction is only applicable to the considered soils and the analysed database. The proposed correction in fact depends on the tip resistance and becomes particularly relevant for resistances below 1 MPa. However, the proposed methodology could be efficiently applied in different contexts.

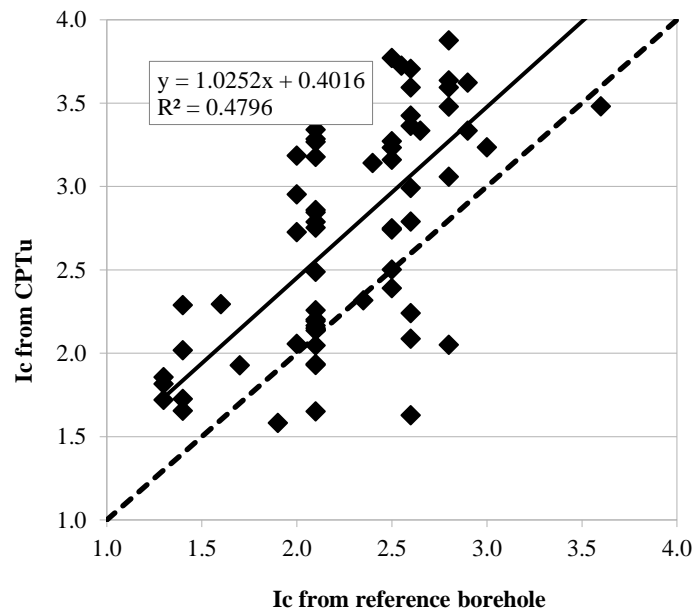


Figure 169: I_c values from boreholes and CPTu test for soil layers below the water table (Serchio river).

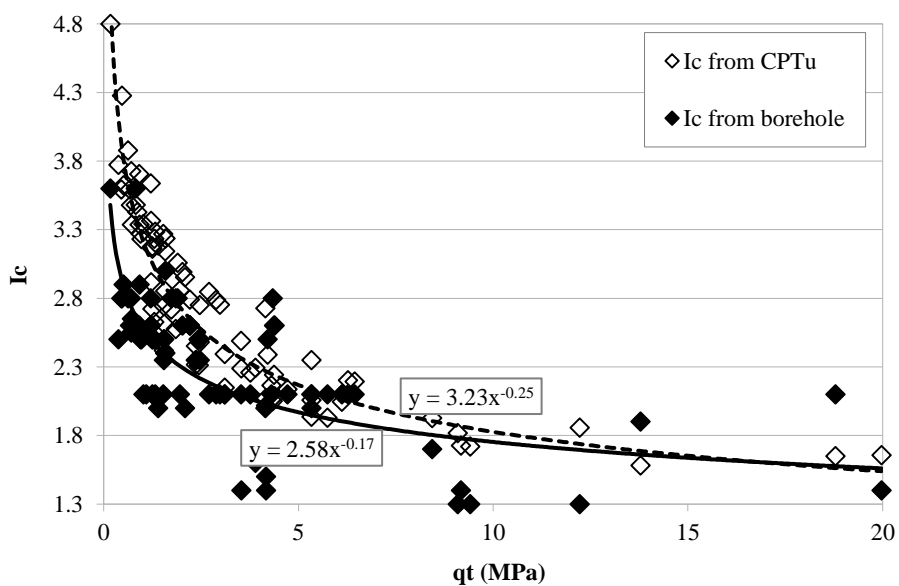


Figure 170: dependency with q_t of both I_c values inferred from CPTu tests and boreholes.

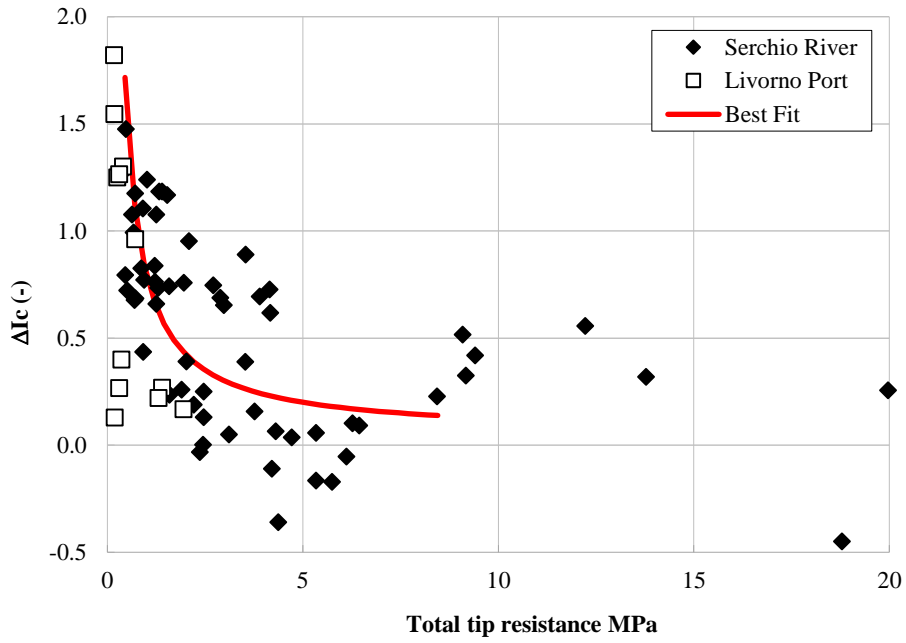


Figure 171: The difference between the two I_c series (ΔI_c) vs. the total tip resistance.

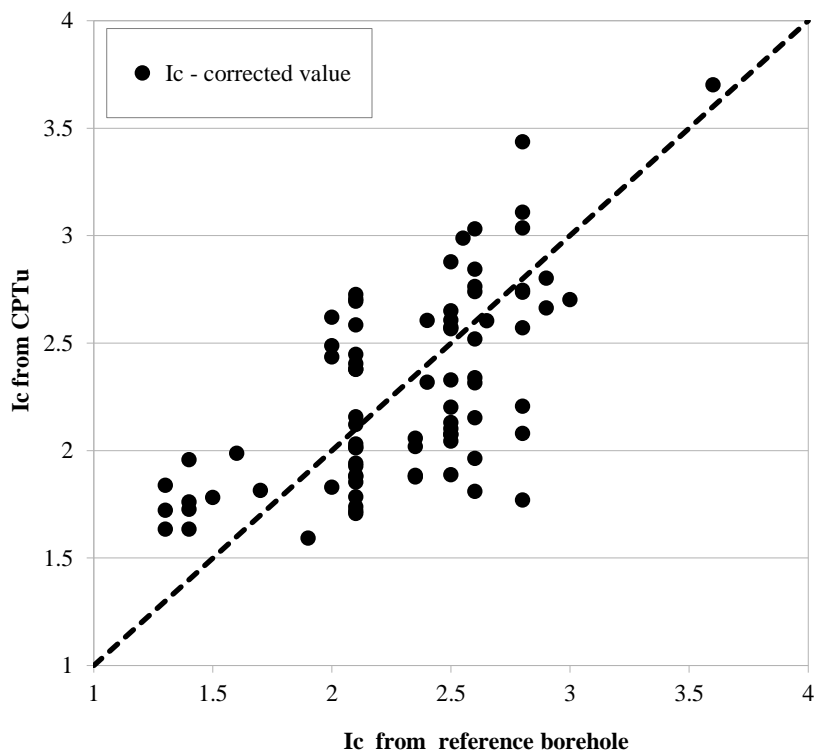


Figure 172: Results obtained after the application of the $\Delta I_c(q_t)$ function.

9.3 Conclusions

The erroneous applicability of currently available classification systems has been shown to be inadequate in the case of effective stress state controlled by suction phenomena. For this kind of conditions, where soil layers above the water table are investigated, it is possible to correct the vertical effective stress in order to take into account of soil suction and obtain a more reliable estimation of the SBTn Index, and therefore, an effective identification of the SBTn class of the soil.

The second correction technique has been applied to the interpretation of piezocone tests in the case of very loose silts and silt mixtures, such as those that characterises the foundation soils of the Serchio River levee system and the dredged sediments stored inside the artificial basins at the Port of Livorno. The procedure is based on the direct calibration of the Soil Behaviour Type Index, thanks to the presence of reference boreholes closed to the position of the analysed piezocone tests. The obtained SBTn Index correction function is specific for the soil investigated and only applicable to the presented cases. Nevertheless, the proposed methodology can be applied to different contexts. This approach allows to continue to use the currently available commercial software to piezocone test interpretation.

The first described methodology suggests the possibility to invert the applied process in order to estimate the real effective stress state using piezocone test results. In particular, in the case of a homogeneous deposit where some layers are subjected to suction phenomena, it is possible to infer the real vertical stress profile, looking for the stress distribution that guarantees to obtain the same value of the SBTn Index above and below the water table. This procedure is shown in the following section, in which are discussed piezocone data interpretation methods to estimate the in-situ preconsolidation stress.

10. Estimation of preconsolidation stress based on piezocone test results

The present chapter deals with the possibility of utilising piezocone test results to infer soil parameters in addition to the stratigraphic profile and Soil Behaviour Type classification. The determination of some soil parameters is well documented in literature and the estimation process is in these cases well consolidated in practice. In other cases, the available correlations are numerous and their applicability outside the specific calibration soil is still not well studied. The evaluation of the preconsolidation pressure and the consequent overconsolidation stress is one of these cases. Therefore, taking advantage of the large number of tests conducted in the alluvial soils in the delta area of Pisa, in the first part of the chapter the possibility to infer the preconsolidation stress profile from piezocone tests is verified by using the most relevant correlations available in literature.

The second part of the chapter describes a new methodology proposed to evaluate the effective stress profile and the preconsolidation stress profile, in the case of soil layers in which suction phenomena are predominant.

10.1.1 Verification of applicability of several empirical correlations available in literature to the over-consolidation ratio estimation

This paragraph does not directly deal with the main topic of the present study, but tackle with a very interesting aspect of practical application of piezocone measurements. Several correlations available in literature to the estimation of the overconsolidation ratio have been evaluated taking advantage of the large number of CPTu tests carried out at the Porta a Mare location and the fact that the OCR profile is well known in this area.

From CPTu test results, it is possible to obtain an estimation of several mechanical properties of the materials passed through during the test. In particular, it is possible to estimate the value of the pre-consolidation stress, and therefore the over consolidation ratio. In literature, many empirical or semi-empirical correlations are available for the estimation of these parameters. In the present study, the following relationships have been taken into account:

For Intact Clays (SBTn classes: 1,2,3,4,9):

- Mayne et al., 1995: $\sigma'_p = 0.33 (q_t - \sigma_{v0})$
- Chen & Mayne, 1996: $\sigma'_p = 0.53 (u_2 - u_0)$
- Mayne, 2005: $\sigma'_p = 0.60 (q_t - u_2)$
- CPeT-IT (Geologismiki): $OCR = \left[\frac{Q_{tn}^{0.20}}{0.25 \cdot (10.50 + 7 \cdot \log(F_r))} \right]^{1.25} \cdot Q_{tn}$

For Sands (SBTn classes: 5, 6, 7, 8), Mayne (2005):
$$OCR = \left[\frac{0.192 \left(\frac{q_t}{\sigma_{atm}} \right)^{0.22}}{(1 - \sin \varphi') \left(\frac{\sigma'_{v0}}{\sigma_{atm}} \right)^{0.31}} \right]^{\left(\frac{1}{\sin \varphi' - 0.27} \right)}$$

For all intact materials (Mayne, 2007):

$$\sigma'_p = 0.101 \sigma_{atm}^{0.102} G_0^{0.478} (\sigma'_{v0})^{0.420} ;$$

Where G_0 is (Robertson P.K., 2009a):

$$G_0 = (q_t - \sigma_{v0}) \cdot 0.0188 \cdot 10^{0.55I_c + 1.68}$$

The present study evaluates the applicability of these correlations to Pisa Porta a Mare (Italy) (16 CPTu tests). As explained in the previous section, the subsoil of Pisa belongs to the alluvial (Holocene-Pleistocene) deposits of the Arno River. The first 60 m are characterised by the following profile (Lo Presti et al., 2003):

- Horizon A: upper variable deposits from 3 to 10 meters, consists of silt, clay and sand of various thickness. The main characteristic of this horizon is that the sediments have been deposit in an estuarine environment, in salty water
- Horizon B: clayey deposits from 10 to 40 m, subdivided in four sub-layers
 - High plasticity marine clay. It is a soft sensitive clay called Pancone clay
 - Intermediate clay and sand layers, similar to the deposit of Horizon A
 - Soft clay similar to Pancone
- Horizon C: lower sand deposits from 40 to 60 m, consists of eolian sands with inter-layers of silt and clay

The CPTu tests have been carried out in Pisa at “Porta a Mare” place up to a depth of 35 meters. It is characterised by a first layer of sandy silt from 1 to 3 meters, a second layer of silty clay from 3 to 5 meters and a third layer of clay from 5 to 7 meters. Below this layer sand is present from 6.8 m to 7.8 meters (Grey sands), lying upon the clay layers of Horizon B.

The following figures show the results related to the correlations adopted to interpret CPTu data obtained in Pisa from 16 tests. Figure 173 shows the typical effective stress and overconsolidation ratio trend in the Pisa area. In particular, the figure is related to the studies made on the subsoil of Pisa Tower (Lo Presti et al., 2003). Figure 174 and Figure 175 show the OCR profile obtained with the analysed correlations.

The correct overall OCR trend is reproduced from all the correlations taken into account, but the most suitable and stable correlation seems to be the Mayne and Brown (2003), applicable to all intact materials and depending on the estimation of the small-strain shear modulus G_0 .

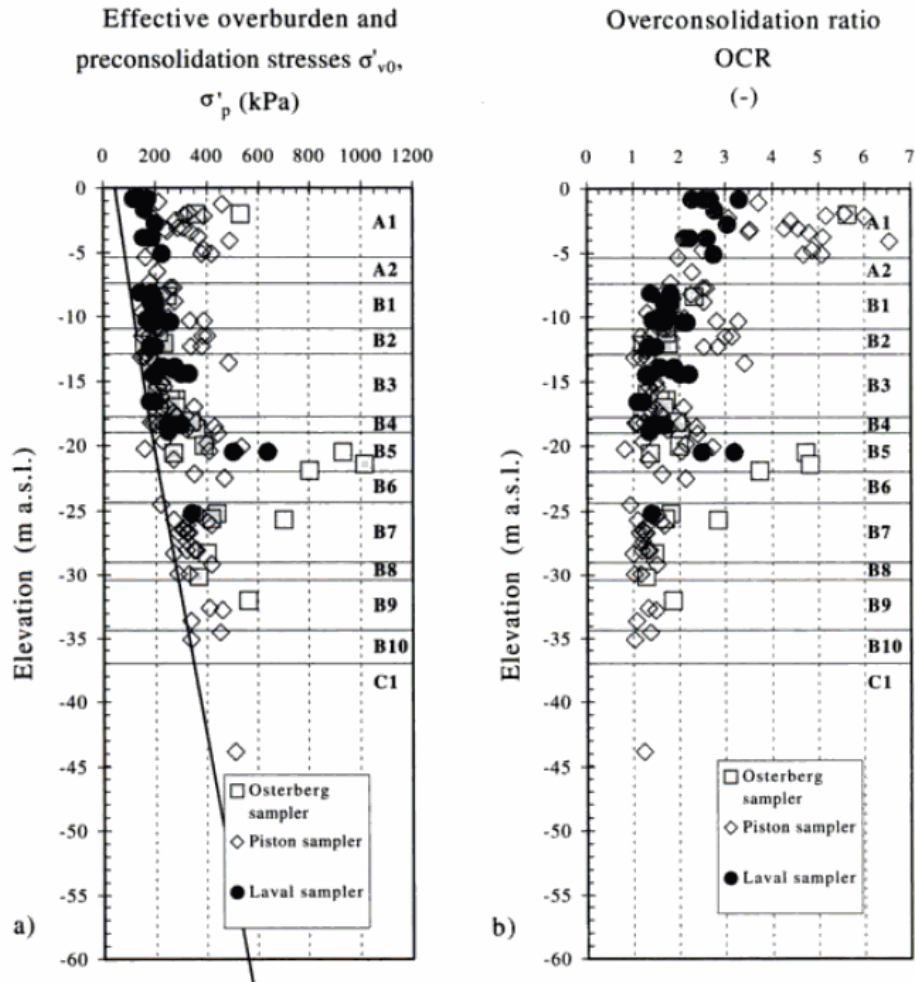


Figure 173: Effective stress and overconsolidation ratio profiles of the soils underlying the Pisa Tower (Lo Presti et al., 2003)

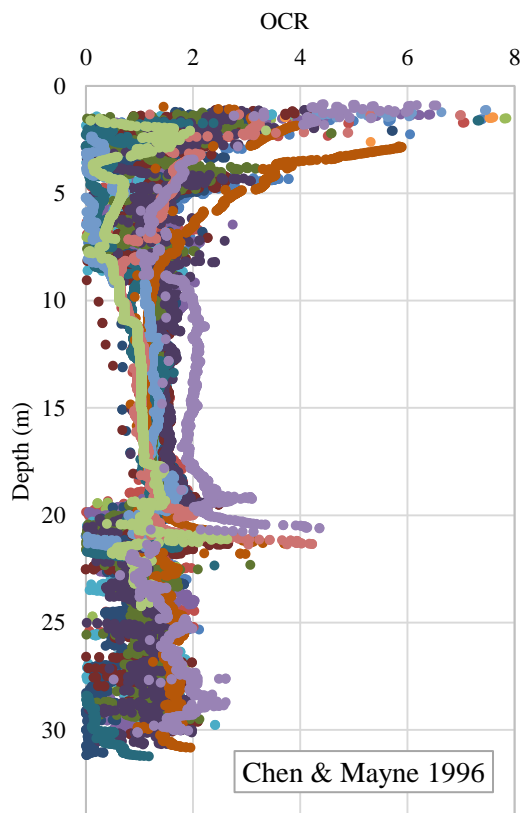
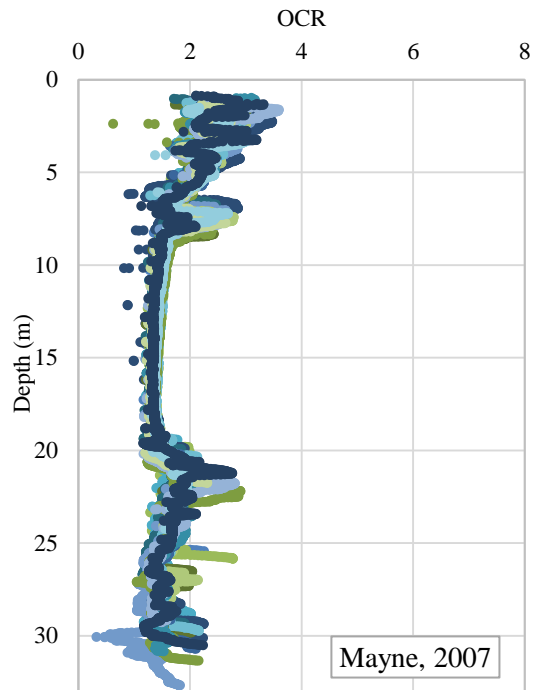


Figure 174: OCR evaluation with Mayne (2007) and Chen & Mayne (1996) correlations.

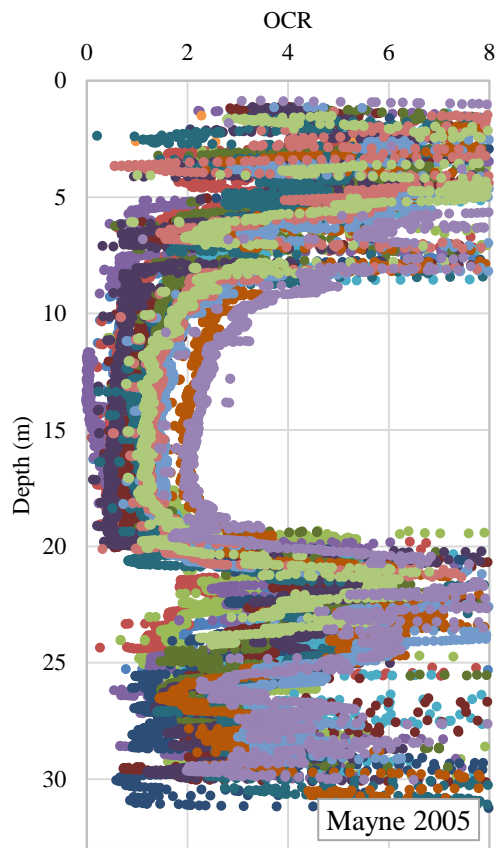
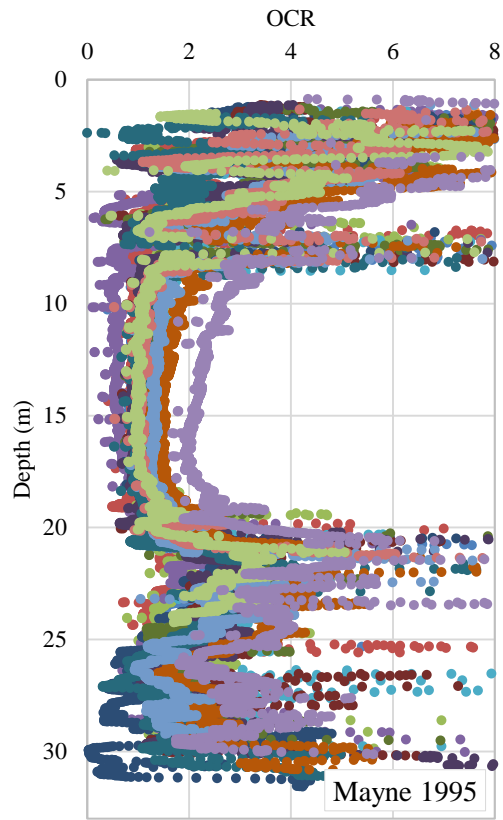


Figure 175:OCR evaluation with Mayne (1995) and Mayne (2005) correlations.

10.1.2 Estimation of the effective in situ stress and preconsolidation stress for soil layers above the water table

On the basis of what shown in chapter 9, it could be possible to use CPTu results to evaluate the effective in situ state for soil layers above the water table, when the soil is homogeneous and the water table is known. In particular, an estimation of the in situ effective stress can be made by finding the corrections to the vertical stress profile that produces a constant I_c value above and below the water table. The comparison between the vertical effective stress profile inferred with this method and the one obtained with the M-K model will give additional information on the history of the deposits. Figure 176 shows the vertical effective stress profile that produces a constant I_c value for the CPTu1 and CPTu2 tests. The curves coincide with those obtained by way of the MK model for depth greater than 1 m and 2 m respectively. The obtained profiles can suggest that the vertical effective stress is the result of a preconsolidation pressure induced in the superficial layers by a desiccation process. This hypothesis cannot be confirmed for Broni area since laboratory tests on undisturbed samples are not available.

Therefore, the working hypothesis was checked by considering additional data (Barsanti, 2016). These data were obtained from Porcari (Lucca, Italy) and refer to a CPTu carried out in a partially saturated fine-grained layer (above the water table) and an oedometer test on an undisturbed sample that had been retrieved at the same location as the CPTu test from a depth of 2.0-2.3 m (Figure 177 and Figure 178). It can be observed that the I_c value increases with depth moving toward the target value of around 2.55, which is reached below the water table, even though in a scattered way. However, when the I_c value at a depth of 2.0 – 2.3 m (circa 2.05) and the I_c target are considered, the application of the proposed method leads to an estimate of the suction of circa 297 kPa. The interpretation of the oedometer test is shown in Figure 178, and leads to an estimate of the preconsolidation pressure of around 320 kPa. Even though a single result cannot be considered sufficient to validate the working hypothesis, the analysed data suggest that the proposed approach deserves further investigations.

It is also worth noting the possible differences between the oedometer preconsolidation pressure and suction. The two values could only coincide when $K_0 = 1$, which is not unrealistic for highly mechanically overconsolidated soils.

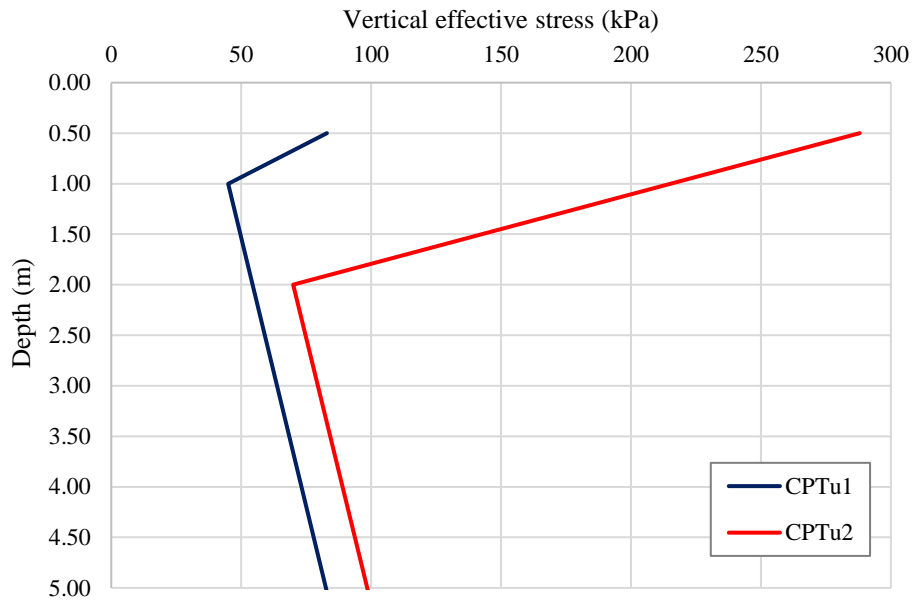


Figure 176: Assessment of in situ vertical effective stress from CPTu1 and CPTu2 tests conducted in Broni.

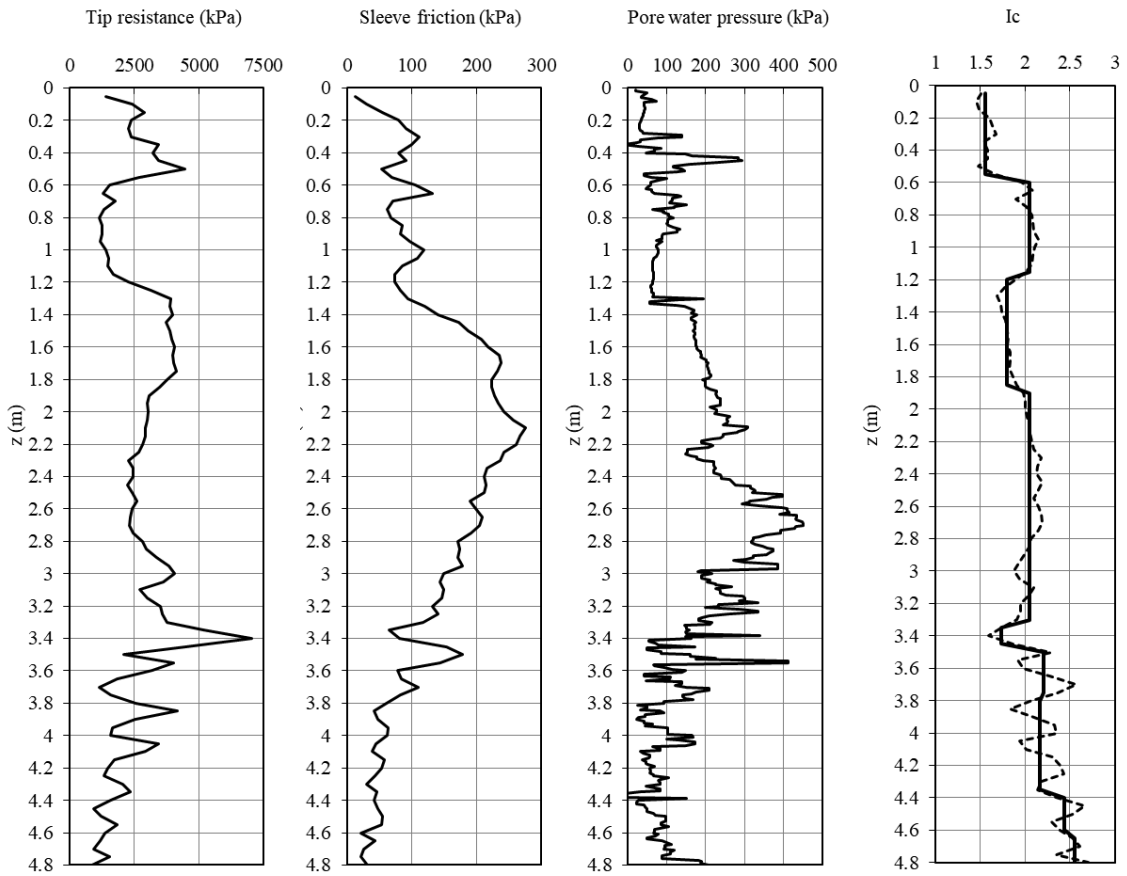


Figure 177: CPTu measurements and Ic index (Porcari, Lucca).

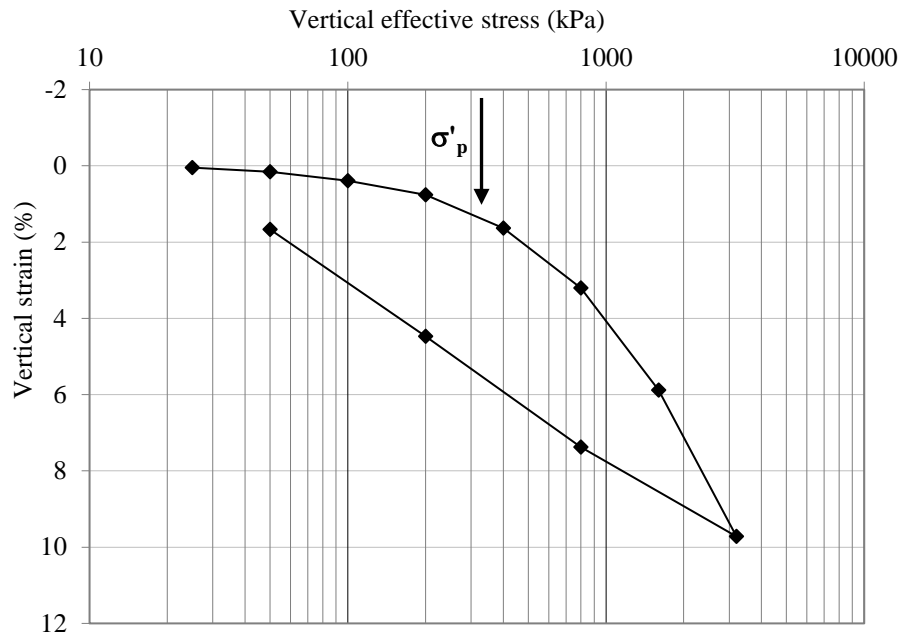


Figure 178: Incremental Loading Oedometer test (Porcari, Lucca).

11. Conclusions

Baligh first proposed the piezocone in 1981 as a means of improving the identification of soil stratigraphy. Today piezocone soundings are widely employed in geotechnical engineering practice using a standardized geometry jacked into the ground at a standard rate of 2 cm/s (ISSMGE IRTP, 1999; ASTM, 2007). These tests are ideal for the identification of the major lithologic variations and the reconstruction of the stratigraphic profile, thanks to measurement reliability, possibility to investigate a soil volume greater than that of a laboratory sample and possibility of getting continuous records. In addition, common applications include the soil engineering parameters evaluation such as stress state, stress history, strength characteristics, and stiffness. While current piezocone test procedures are able to identify sand and clay layers, distinguishing between low permeability clays, which are sheared in an ‘undrained’ mode (i.e., with no migration of pore water within the soil and excess pore pressures develop around the advancing penetrometer), and high permeability sands, where drained shearing occurs (i.e., shearing with no excess pore pressures); interpretation is much more complex in soils of intermediate permeability. In this case, partial drainage of pore water occurs during penetration and affects the shear strength that can be mobilised in the surrounding soil (Lunne et al., 1997). The current interpretation of stratigraphy relies on empirical classification charts (e.g., Robertson et al., 1986; Senneset et al., 1989; Robertson, 1991), and semi-empirical correlations for estimating shear strength, consolidation and permeability properties of the soils (e.g., Wroth, 1984; Baligh, 1986a, b; Teh&Houlsby, 1991). In the case of silts and mixed soils, typically referred as intermediate soils, due to partial drainage during the test, drainage conditions significantly influence tip resistance: for normally consolidated soils, the ratio between drained tip resistance and undrained tip resistance has been reported to vary from two (House et al., 2001; Randolph and Hope, 2004; Schneider et al., 2007) to ten (McNeilan and Bugno, 1985). Therefore, in the case of intermediate soils there is a great uncertainty in the assessment of soil properties and application of design correlations (Schneider et al. 2008). The preliminary identification of partial drainage conditions, during penetration, is a key step, in order to avoid misinterpretation of field measurements and invalid estimates of soil parameters.

Another important aspect to be considered is that standard approaches of piezocone interpretation only consider either fully saturated or completely dry conditions, although, in reality, a vadose zone of unsaturated soils most often exists above the ground water table. The difficulty in applying classification charts in partially saturated soils, especially fine-grained ones, is due to the soil suction, which modifies the effective stress state, thus leading to an overestimate of soil grain size (Lo Presti et al. 2009). The interpretation of piezocone tests in partially saturated soils is still an open issue.

In order to investigate the influence of partial drainage during penetration, the instrument of repeating the tests changing the penetration rate is widely used. However, most of the experimental studies on the influence of penetration rate on piezocone test results have been carried out inside a beam centrifuge on kaolin clay (Finnie and Randolph, 1994, House et al., 2001, Randolph and Hope, 2004, Schneider et al., 2007, Lehane et al., 2009; Mahmoodzadeh and Randolph, 2014). Few studies have been carried out on natural clay (Chung et al., 2006) or mixed soils (Kim et al., 2008; Schneider et al., 2007). The present study shows the results of the experimental analyses of field cone penetration tests as well as the ones of calibration chamber mini-penetrometer tests, on soils of intermediate permeability (silts, clayey silts and sandy-clayey silts). The penetration rate was varied across over three orders of magnitude to provide information on partially drained and undrained tip resistance, excess pore water pressure, and friction sleeve.

Furthermore, numerical analyses have been carried out by the means of the Finite Element Method, developed in Abaqus. To the author's knowledge there are only two researches on partially drained penetration simulated with FEM analyses (Yi et al., 2012; Mahmoodzadeh et al., 2014). For the present study, the Updated Lagrangian technique has been used to simulate the large strain penetration process. The model has been validated on previous experimental results. The Modified Cam Clay constitutive model has been adopted to simulate the results obtained by Randolph & Hope (2004) and Schneider et al. (2007), from piezocone tests on kaolin clay. Moreover, the Mohr Coulomb model has been calibrated on triaxial tests conducted on soil specimens, reproducing the calibration chamber conditions, and numerical simulations of the tests, conducted inside the calibration chamber, have been done, adopting equivalent penetration rates in terms of non-dimensional velocity. A very good agreement has been obtained between experimental results on kaolin clay and numerical simulations. The FEM model of tests conducted inside the calibration chamber, is able to reproduce the measured tip resistance for the entire range of penetration rates adopted.

Piezocone tests, carried out inside the calibration chamber and in the field, have provided to study the effects of the influence of partial drainage, during the penetration in sandy/clayey silts. The investigated penetration rate range allows for delineating the range of partially drained conditions. Whilst previous experimental studies essentially focused on tip resistance and pore water pressure measurements, the present study is one of the first experimental studies that explored the effects of penetration rate on sleeve friction measurements. As the penetration rate is reduced, moving from the undrained conditions to the fully drained conditions, friction sleeve systematically decreases, together with the expected results in terms of increasing tip resistance and decreasing excess porewater pressure measurements. The clear trend of friction sleeve measurements can be linearly interpolated as a function of penetration rate. Furthermore, if

normalised f_s data are plotted versus the non-dimensional velocity, the results from both sides of the calibration chamber overlap, suggesting a unique linear correlation in the semi-logarithmic plot. An interpolation law is proposed. Essentially, the proposed correlation defines the effects of the penetration rate and drainage conditions on the coefficient β (ratio between f_s and effective vertical stress).

In addition to that the obtained results, in terms of normalised parameters, are plotted in the classification charts recently proposed by Schneider et al. (2008, 2012), in order to verify their applicability for the intermediate soils of the present study.

The obtained experimental database of penetration measurements on intermediate soils can be added to the previous worldwide collected data, in order to develop a new general interpretation procedure for cone tests in transitional soils. In addition to that, since usually the sleeve friction is depicted as the less reliable measurement, with respect to the tip resistance and pore water pressure, the present study shows that, for the material investigated, f_s measurements are the most sensitive to the changes in penetration rate and, therefore, in drainage conditions during the tests. Besides, the very interesting results in terms of friction sleeve can be the starting point to introduce a new instrument for the characterisation of this kind of materials.

The problem of piezocone interpretation in soils belonging to vadose zones has been dealt with a new approach. The methodology consists in a better estimate of the effective stress state, in order to take into account the effects of soil suction in the vadose zone above the water table. The Modified Kovacs model has been used for this purpose. This procedure allows for the correction of the Soil Behaviour Type (SBT) index, I_c , in order to correctly allocate the investigated soils inside the SBT classification charts (Robertson, 1990).

Another important aspect of this study is the evidence that currently available classification systems have been found to be inadequate for those cases in which the effective stress state is controlled by suction. The proposed method allows for correctly identifying the soils above the water table, using a very simple correction of the effective stress profile.

Finally, the applied method for the correction of the Soil Behaviour Type Index, has suggested a procedure to estimate the effective stress state from piezocone test, in the case of a homogeneous soil layer in which a vadose zone is present and the stress state is controlled by suction.

Acknowledgments

The author wishes to extend her deepest appreciation to:

The thesis supervisors Prof. Diego Lo Presti, Prof. Joachim Stahlmann and Prof. Andrew Whittle, for providing constant and valuable guidance and assistance during the entire research program, giving precious advices and suggestions;

Pagani Geotechnical Equipment, for contributing to the PhD program in all its aspects, and for giving precious technical support during all the phases of the research work;

The MIT-UNIPI Project, for giving her the possibility to join to Prof. Whittle's research group at the Massachusetts Institute of Technology;

Zhandos Orazalin, for his constant and greatly appreciated support on numerical analyses;

Stefano Giusti (Geotechnical laboratory of the University of Pisa), Massimiliano Siviero and Ervis Uruci (Pagani Geotechnical Equipment), Maurizio Cosco and Francesco Spadaro (Geoservizi), and Girolamo Gervasi, for supporting her in laboratory, calibration chamber and field tests, making these feasible;

The Livorno Port Authority in the person of Enrico Pribaz, for the given possibility to carry out the experimental activities inside the storage basin's area.

12. Appendix

Incremental Loading Oedometer tests and triaxial tests on samples O1, O2, O3, C1 and C2 extracted in Livorno Port Area, within the basin for dredged sediments.

Sample	Depth		Wn (%)	Grain size distribution				MIT Classification
	from (m)	to (m)		Gravel(%)	Sand (%)	Silt (%)	Clay (%)	
C1	1	1.3	29.1	5	37	37	21	Sand with silt
C2	1.2	1.5	47.27	3	41.5	35.5	20	Sand with silt
O1	1.6	2.2	44.68	0	10	57	33	Silt with clay
O2	2	2.5	42.72	0	17	50	33	Silt with clay
O3	2.5	3	40.01	0	15	57	28	Silt with clay

Table 26: MIT Classification for the block samples (C1 and C2) and the Osterberg samples (O1, O2, O3).

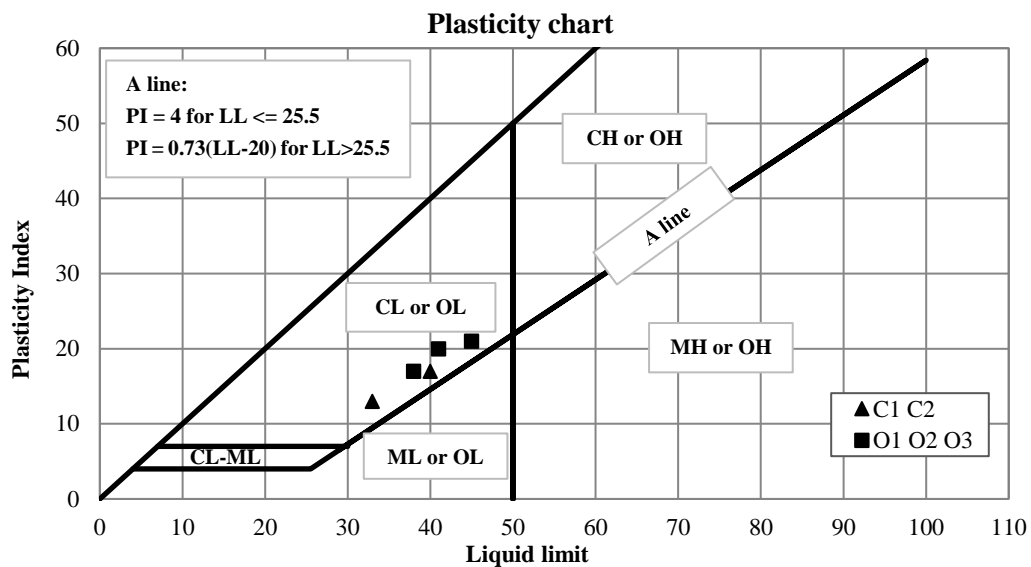
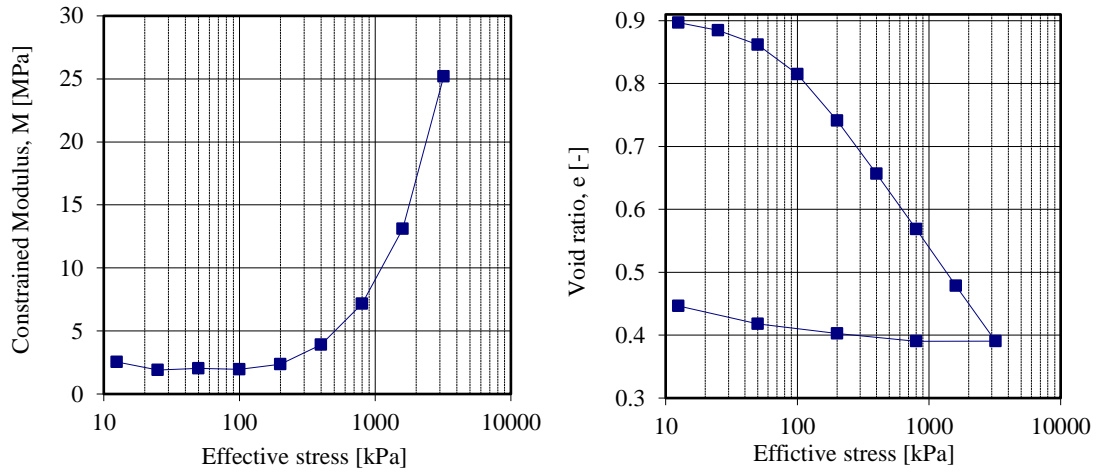
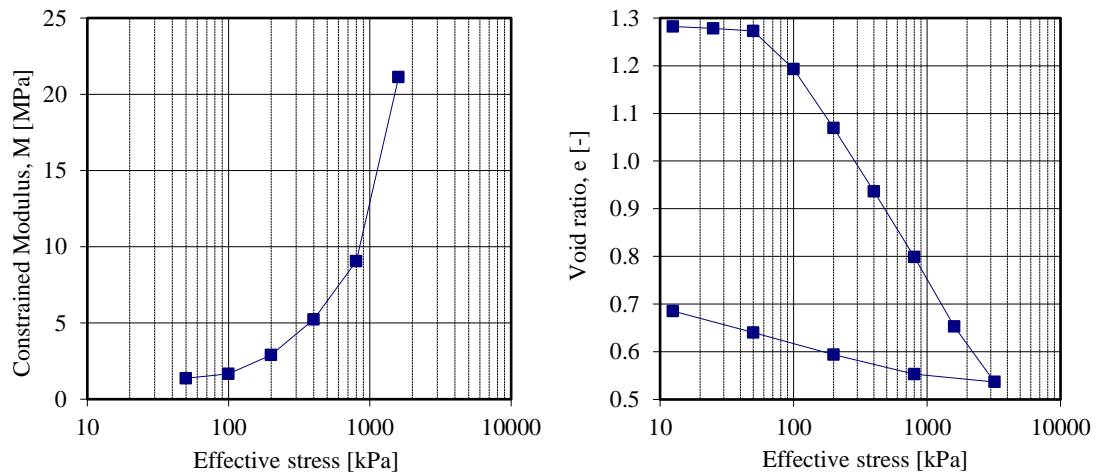


Figure 179: USCS Classification chart, for block samples (C1, C2) and Osterberg samples (O1, O2, O3).



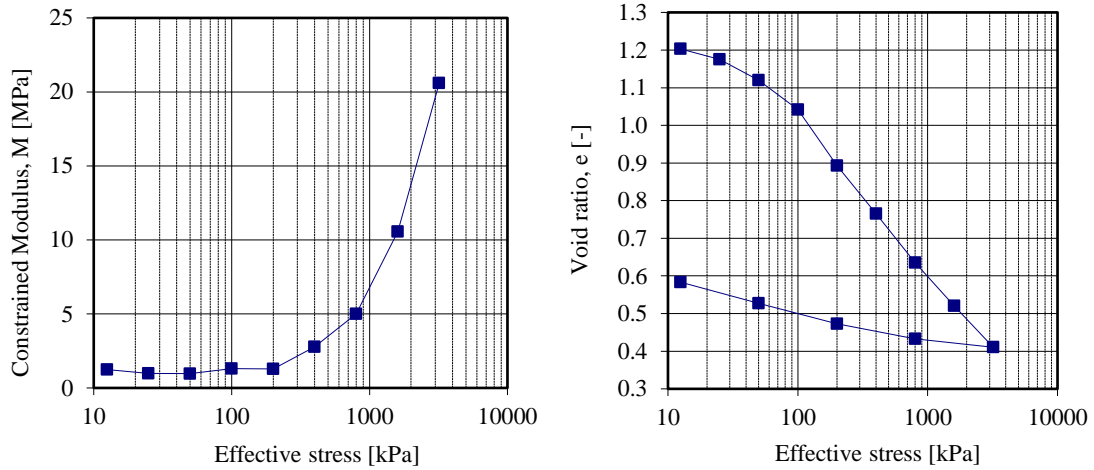
Effective stress	ΔH	H	H_{prog}	e	M	C_v	k
[kPa]	[mm]	[mm]	[mm]	[-]	[MPa]	[m ² /s]	[m/s]
50.0	0.469	19.53	19.65	0.862	2	3.32E-08	1.62E-10
100.0	0.958	19.04	19.29	0.815	2	6.53E-08	3.29E-10
200.0	1.734	18.27	18.65	0.741	2	9.28E-08	3.86E-10
400.0	2.620	17.38	17.82	0.657	4	9.09E-08	2.27E-10
800.0	3.540	16.46	16.92	0.569	7	9.14E-08	1.25E-10
1600.0	4.487	15.51	15.99	0.479	13	8.56E-08	6.41E-11
3200.0	5.413	14.59	15.05	0.390	25	9.79E-08	3.81E-11

Figure 180: Incremental Loading Oedometer test results for sample C1.



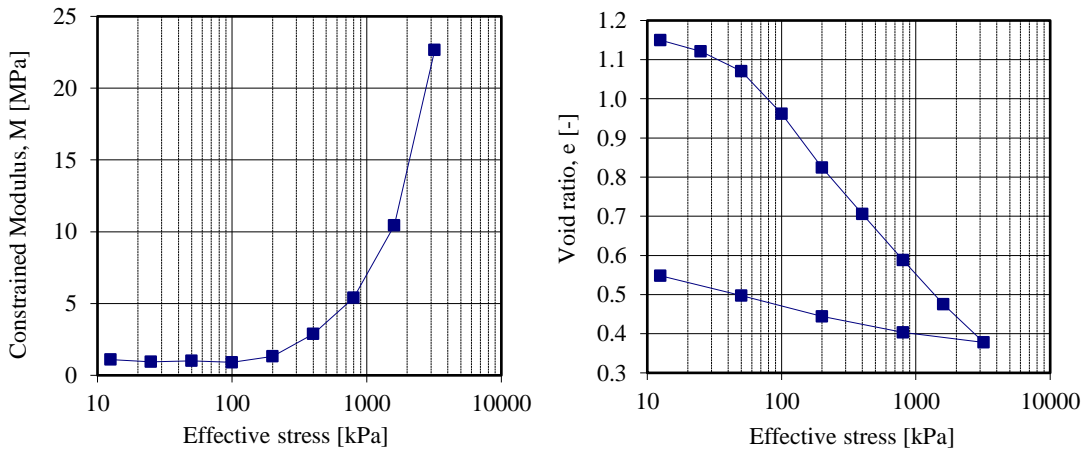
Effective stress	ΔH	H	H_{prog}	e	M	C_v	k
[kPa]	[mm]	[mm]	[mm]	[-]	[MPa]	[m ² /s]	[m/s]
100.0	0.975	19.03	19.37	1.193	1	3.11E-08	2.22E-10
200.0	2.047	17.95	18.49	1.070	2	2.39E-08	1.40E-10
400.0	3.200	16.80	17.38	0.937	3	4.34E-08	1.46E-10
800.0	4.394	15.61	16.20	0.799	5	3.23E-08	6.06E-11
1600.0	5.661	14.34	14.97	0.653	9	2.93E-08	3.17E-11
3200.0	6.670	13.33	13.83	0.537	21	3.62E-08	1.68E-11

Figure 181: Incremental Loading Oedometer test results for sample C2.



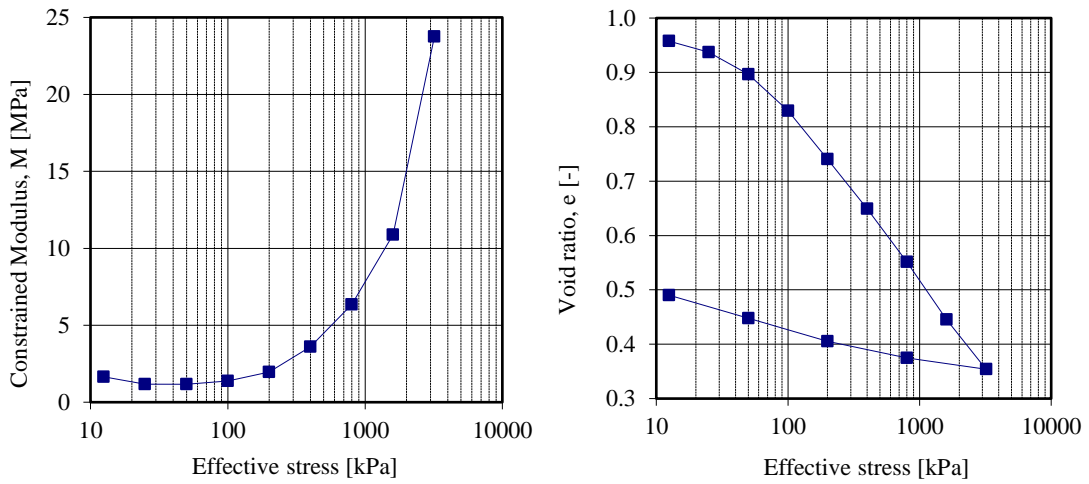
Effective stress [kPa]	ΔH [mm]	H [mm]	H_{prog} [mm]	e [-]	M [MPa]	C_v [m ² /s]	k [m/s]
25.0	0.449	19.55	19.68	1.175	1	8.21E-08	8.24E-10
50.0	0.941	19.06	19.31	1.120	1	5.78E-08	5.86E-10
100.0	1.649	18.35	18.71	1.042	1	3.09E-08	2.33E-10
200.0	2.983	17.02	17.68	0.893	1	2.28E-08	1.75E-10
400.0	4.130	15.87	16.44	0.766	3	3.07E-08	1.09E-10
800.0	5.303	14.70	15.28	0.635	5	7.07E-08	1.38E-10
1600.0	6.337	13.66	14.18	0.520	11	4.03E-08	3.74E-11
3200.0	7.322	12.68	13.17	0.411	21	4.38E-08	2.08E-11

Figure 182: Incremental Loading Oedometer test results for sample O1.



Effective stress [kPa]	ΔH [mm]	H [mm]	H_{prog} [mm]	e [-]	M [MPa]	C_v [m ² /s]	k [m/s]
25.0	0.485	19.52	19.65	1.121	1	4.76E-08	4.99E-10
50.0	0.955	19.05	19.28	1.070	1	4.38E-08	4.24E-10
100.0	1.951	18.05	18.55	0.962	1	7.38E-09	7.99E-11
200.0	3.217	16.78	17.42	0.824	1	2.51E-08	1.86E-10
400.0	4.310	15.69	16.24	0.706	3	3.02E-08	1.03E-10
800.0	5.392	14.61	15.15	0.588	5	3.22E-08	5.85E-11
1600.0	6.432	13.57	14.09	0.475	10	3.85E-08	3.62E-11
3200.0	7.327	12.67	13.12	0.378	23	4.08E-08	1.77E-11

Figure 183: Incremental Loading Oedometer test results for sample O2.



Effective stress [kPa]	ΔH [mm]	H [mm]	H_{prog} [mm]	e [-]	M [MPa]	C_v [m ² /s]	k [m/s]
25.0	0.359	19.64	19.75	0.937	1	7.59E-08	6.34E-10
50.0	0.771	19.23	19.44	0.896	1	7.61E-08	6.40E-10
100.0	1.448	18.55	18.89	0.830	1	6.03E-08	4.32E-10
200.0	2.350	17.65	18.10	0.741	2	6.13E-08	3.07E-10
400.0	3.278	16.72	17.19	0.649	4	7.57E-08	2.06E-10
800.0	4.268	15.73	16.23	0.551	6	7.27E-08	1.12E-10
1600.0	5.345	14.66	15.19	0.445	11	9.02E-08	8.13E-11
3200.0	6.270	13.73	14.19	0.354	24	9.64E-08	3.98E-11

Figure 184: Incremental Loading Oedometer test results for sample O3.

The following diagrams show triaxial tests results (TXCIU) in terms of t and s' :

$$t' = t = \frac{\sigma'_v - \sigma'_h}{2} ; s' = \frac{\sigma'_v + \sigma'_h}{2}$$

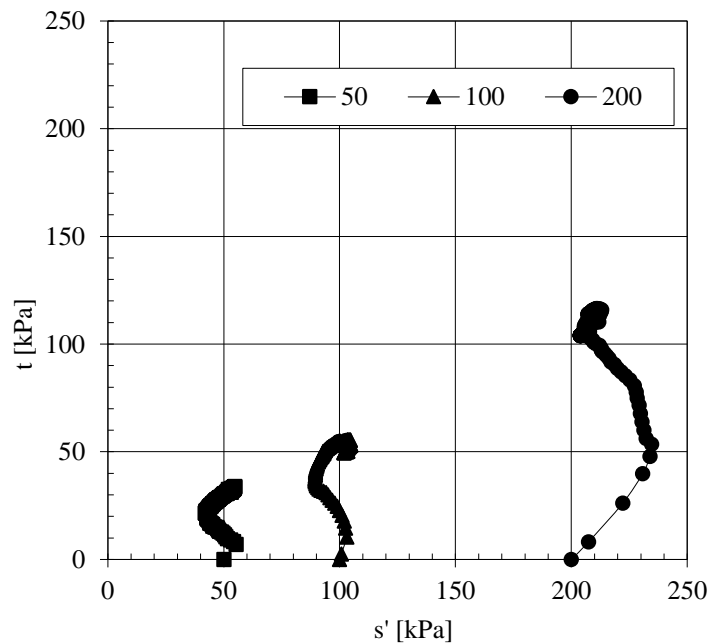


Figure 185: Triaxial test results (TXCIU) for C1 sample. Consolidation stresses are: 50 kPa, 100 kPa and 200 kPa.

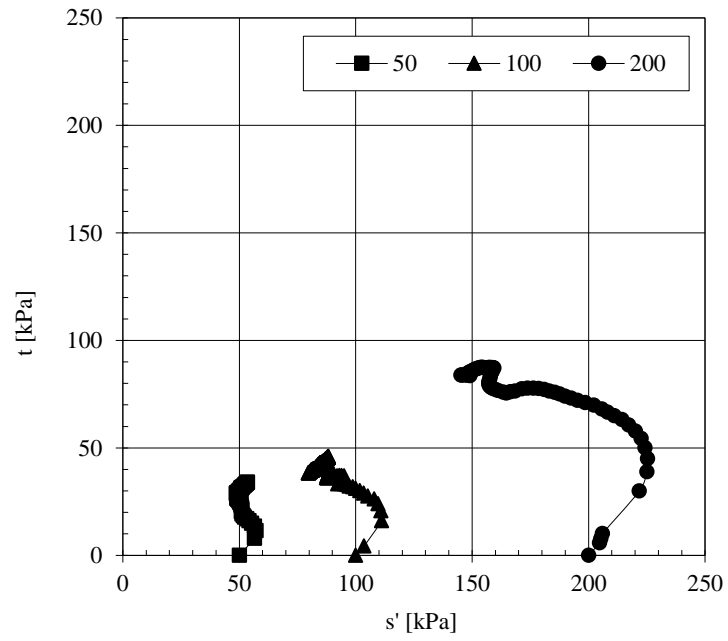


Figure 186: Triaxial test results (TXCIU) for O2 sample. Consolidation stresses are: 50 kPa, 100 kPa and 200 kPa.

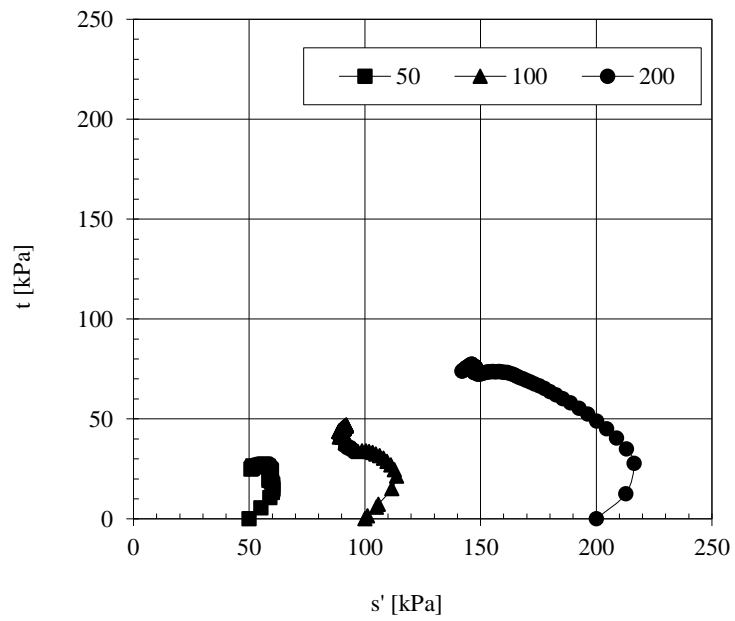


Figure 187: Triaxial test results (TXCIU) for O3 sample. Consolidation stresses are: 50 kPa, 100 kPa and 200 kPa.

13. List of figures

Figure 1: Interpretation of stratigraphy from tip resistance and penetration pore pressures. Piezocone with tip pore pressure transducer (left, Zeeb et al., 1997); Penetration data in layered soil (right)..... 8

Figure 2: Effects of partial drainage on measurements of piezocone tip resistance in silts (McNeilan & Bugno, 1985)..... 11

Figure 3: Normalised cone and T-bar resistance variation with normalised velocity (Randolph & Hope 2004) 13

Figure 4: Variation of excess pore pressures ratio (B_q) with cone velocity (Randolph and Hope, 2004) 14

Figure 5: Variation of tip resistance with cone velocity in kaolin clay: Illustration of form of proposed equation (left); Comparison between T-bar data on normally consolidated kaolin clay and equation data using best-fit parameters $a=0.65$, $b=4.2$, $c=10$ (Lehane et al.,2009)..... 14

Figure 6: Influence of normalised penetration on normalised tip resistance for nearly normally consolidated soils (left) and overconsolidated soils (right). NC Kaolin: normally consolidated Kaolin; LOC SFB: lightly overconsolidated silica flour and bentonite slurry; HOC Kaolin: overconsolidated Kaolin; HOC SFB: heavily overconsolidated silica flour and bentonite slurry (Schneider et al., 2007).16

Figure 7: Influence of normalised velocity on normalised excess pore water pressure and pore pressure parameter B_q . NC Kaolin: normally consolidated Kaolin; LOC SFB: lightly overconsolidated silica flour and bentonite slurry; HOC Kaolin: overconsolidated Kaolin; HOC SFB: heavily overconsolidated silica flour and bentonite slurry (Schneider at al., 2007)..... 16

Figure 8: Classification charts proposed by Schneider et al. (2008) in two different plotting formats... 17

Figure 9: Additional classification chart proposed by Schneider et al. (2012)..... 18

Figure 10: Conceptual pore pressure distribution in saturated clays during CPTu based on field measurements (after Robertson et al. 1986)..... 19

Figure 11: Example of non-standard dissipation curves for overconsolidated clay and sandy silt (Schneider, 2008)..... 20

Figure 12: Shear strains during Simple Pile penetration (Baligh, 1985)..... 22

Figure 13: Symbols - Normalised cone resistance against non-dimensional velocity from numerical simulations for different values of the G/p' ratio (Yi et al., 2012). Dotted lines - Backbone curves obtained with the expression proposed by Randolph and Hope (2004), the respective parameters are shown in the legend. Full dots - Experimental data on normally consolidated kaolin clay (Randolph and Hope, 2004). 24

Figure 14: Basin for the storage of dredged sediments object of this study (Livorno Port). 26

Figure 15: View of the Livorno Port area used for the storage of dredged sediments. 26

Figure 16: Location of the geotechnical soundings and CPTu tests..... 27

Figure 17: Block sample and Osterberg sample (“North” location). 28

Figure 18: Grain size distribution from block samples C1 and C2. 29

Figure 19: Grain size distribution for Osterberg samples P1 (=O1), P2 (=O2) and P3 (=O3). 29

Figure 20: USCS Classification chart, for block samples (C1, C2) and Osterberg samples (O1, O2, O3).	30
Figure 21: Piezocone characteristics (Pagani Geotechnical Equipment).	31
Figure 22: Soil Behaviour Type classification charts proposed by Robertson (1990). CPTu tests conducted at South location ((0.8 cm/s- blue dots, 2 cm/s- green dots, 4.8 cm/s- red dots).	32
Figure 23: Soil Behaviour Type classification charts proposed by Robertson (1990). CPTu tests conducted at North location ((0.8 cm/s- blue dots, 2 cm/s- green dots, 4.8 cm/s- red dots).	32
Figure 24: SBT classification following Robertson (1986), chart on the left, and Robertson (2010), chart on the right. Data from different penetration tests conducted at South location (red dots=4.8 cm/s, green dots=2 cm/s, blue dots= 0.8 cm/s).....	35
Figure 25: SBT classification following Robertson (1986), chart on the left, and Robertson (2010), chart on the right. Data from different penetration tests conducted at North location (red dots=4.8 cm/s, green dots=2 cm/s, blue dots= 0.8 cm/s).....	35
Figure 26: Piezocone test results, site “North”, penetration rate=2 cm/s.	36
Figure 27: Piezocone test results, site “North”, penetration rate=0.8 cm/s	37
Figure 28: Piezocone test results, site “North”, penetration rate=4.8 cm/s.	38
Figure 29: Piezocone test results, site “South”, penetration rate=0.8 cm/s.	39
Figure 30: Piezocone test results, site “South”, penetration rate=2 cm/s.	40
Figure 31: Piezocone test results, site “South”, penetration rate=4.8 cm/s.	41
Figure 32: SBTn Classification (Robertson 1990) and SBT Classification (Robertson, 2010) at site “North” for the standard penetration rate $v=2$ cm/s.	42
Figure 33: SBTn Classification (Robertson 1990) and SBT Classification (Robertson, 2010) at site “South” for the standard penetration rate $v=2$ cm/s.	43
Figure 34: Comparison of CPTu measurements, tip resistance, pore water pressure and friction sleeve, over penetration rate, for the soil layer between 2 and 3.6 meters – south location.....	45
Figure 35: CPTu results at south location for three different rates (0.8 cm/s, 2 cm/s, 4.8 cm/s) and position of dissipation tests.	46
Figure 36: Robertson (1990) SBTn classes for soil layer between 1.8 m and 3.8 m, south location.	47
Figure 37: Robertson (1986) and Robertson (2010) SBT classes for soil layer between 1.8 m and 3.8 m, south location.	47
Figure 38: CPTu results in the north location (depth 1.5 m- 2.4 m) for three different rates (0.8 cm/s - green line, 2 cm/s-blue line, 4 cm/s-red line).	48
Figure 39: Average values of tip resistance, side friction and pore water pressure between 1.6 and 2.3 meters, north location, over penetration rate.	48
Figure 40: CPTu results at north location for three different penetration rates (depth 2.4 m- 3.8 m).	49
Figure 41: Average values of tip resistance, side friction and pore water pressure between 2.4 and 3.2 meters, north location, over penetration rate.	49
Figure 42: Robertson (1990) SBTn classes for soil layer between 1.6 m and 2.3 m, north location.	50
Figure 43: Robertson (1986) and Robertson (2010) SBT classes for soil layer between 1.6 m and 2.3 m, north location.	50

Figure 44: CPT1, minipiezocone at 0.5 cm/s.	52
Figure 45: CPT2, minipiezocone at 0.5 cm/s.	53
Figure 46: CPT9, minipiezocone at 0.5 cm/s.	54
Figure 47: CPT6, minipiezocone at 2 cm/s.	55
Figure 48: CPT8, minipiezocone at 2 cm/s.	56
Figure 49: CPT5, minipiezocone at 2 cm/s.	57
Figure 50: Standard piezocone test at 2 cm/s.	58
Figure 51: Scheme of the tests conducted in Pisa, nine CPTu at two different penetration rates (0.5 and 2 cm/s), and three dissipation tests.	59
Figure 52: CPTu results (in terms of normalised parameters, Robertson 1990) from tests conducted with the minipiezocone at 2 cm/s (red) and 0.5cm/s (blue) in Pisa. The standard cone test is also plotted (black line).	60
Figure 53: CPTu results (in terms of normalised parameters, Robertson 1990) from tests conducted with the minipiezocone at 2 cm/s (red) and 0.5cm/s (blue) in Pisa (1 m - 2 m depth).	60
Figure 54: Normalised CPT soil behaviour type chart, as proposed by Robertson (1990). Soil types: 1, sensitive, fine grained; 2, peats; 3, silty clay to clay; 4, clayey silt to silty clay; 5, silty sand to sandy silt; 6, clean sand to silty sand; 7, gravelly sand to dense sand; 8, very stiff sand to clayey sand (heavily overconsolidated or cemented); 9, very stiff, fine grained (heavily overconsolidated or cemented). OCR, overconsolidation ratio; ϕ' , friction angle.	61
Figure 55 : Tests results from Christchurch (Holtrigter et al., 2014).	62
Figure 56: End resistance effect on oversize friction sleeve (Holtrigter et al., 2014).	63
Figure 57: CPTu1 series, tests with different sleeve diameter along the same line, distance between tests 50 cm (Geologismiki,2007).	64
Figure 58: CPTu2 series, tests with different sleeve diameter along the same line, distance between tests 50 cm (Geologismiki,2007).	64
Figure 59:CPTu3 series, tests with different sleeve diameter along the same line, distance between tests 50 cm (Geologismiki,2007).	65
Figure 60: comparison of tests results for the same sleeve diameter, equal to 35.8 mm, distance between tests 50 cm (Geologismiki,2007).	65
Figure 61: comparison of tests results for the same sleeve diameter, equal to 35.9 mm, distance between tests 50 cm (Geologismiki,2007).	66
Figure 62: comparison of tests results for the same sleeve diameter, equal to 36.0 mm, distance between tests 50 cm (Geologismiki,2007).	66
Figure 63: Comparison of CPTu tests results for the site located in Lucca (color legend: black=standard rate and standard piezocone; orange and red= 2 cm/s; light green and dark green= 0.5 cm/s).	69
Figure 64: Normalised CPT soil behaviour type chart, as proposed by Robertson (1990). Soil types: 1, sensitive, fine grained; 2, peats; 3, silty clay to clay; 4, clayey silt to silty clay; 5, silty sand to sandy silt; 6, clean sand to silty sand; 7, gravelly sand to dense sand; 8, very stiff sand to clayey sand (heavily overconsolidated or cemented); 9, very stiff, fine grained (heavily overconsolidated or cemented). OCR, overconsolidation ratio; ϕ' , friction angle.	69

Figure 65: Frontal view of the steel chamber, particles of the internal partition and the irrigation pipe on the bottom of the chamber.....	72
Figure 66: The pressure on the top layer is applied using four load cells and a reaction frame fixed to the chamber structure.	73
Figure 67: Brushless electric motor (upper part of the image).....	74
Figure 68: The mini-piezocone produced by Pagani Geotechnical Equipment.	74
Figure 69: Calibration test for the slot filter.....	75
Figure 70: Control Panel and Data Acquisition System.....	76
Figure 71: Particle size distribution.	77
Figure 72: Compaction curve (Modified Proctor procedure).	78
Figure 73: Compaction curve of the studied material (Modified Proctor).	78
Figure 74: Vertical displacement vs time for the loading step between 200 kPa and 400 kPa, Sample 1.	80
Figure 75: Variable head test device added to the standard incremental loading oedometer test device.	81
Figure 76: Sample 1 - Comparison between hydraulic conductivity measured data and estimated data from coefficient of consolidation values.	82
Figure 77: Sample 2 - Comparison between hydraulic conductivity measured data and estimated data from coefficient of consolidation values.	82
Figure 78: Sample 3 - Comparison between hydraulic conductivity measured data and estimated data from coefficient of consolidation values.	82
Figure 79: Sample 4 - Comparison between hydraulic conductivity measured data and estimated data from coefficient of consolidation values.	83
Figure 80: Sample 5 - Comparison between hydraulic conductivity measured data and estimated data from coefficient of consolidation values.	83
Figure 81: Effects of degree of saturation at the end of compaction on the coefficient of hydraulic conductivity for the selected soil type: direct measure (symbols); Tatsuoka relationship (solid line). ...	85
Figure 82: Measured k values vs. dry density. Solid lines refer to Tatsuoka's model (slope $a=-5.02$)....	86
Figure 83: Coefficient of saturated hydraulic conductivity k plotted against S_r at the end of compaction of the data of sieved core material (SCM) for Miboro dam (Tatsuoka, 2015).	87
Figure 84: $\log k$ vs. ρ_d relations for different ranges of S_r (Tatsuoka, 2015).	87
Figure 85 : “ $\log k$ when $\rho_d = [(\rho_d)_{\max}]_{IEc=1.872 \text{ g/cm}^3}$ ”, $f_k(S_r)$, plotted against S_r (Tatsuoka, 2014a)...	88
Figure 86: Coefficient of saturated hydraulic conductivity k when $\rho_d = [(\rho_d)_{\max}]_{IEc=1.872 \text{ g/cm}^3}$, $f_k(S_r)$, plotted against S_r at compacted state of eight soil types around Miboro dam site and SCM.	88
Figure 87: particle size coefficient P plotted against the particle size (Tatsuoka, 2014a).....	89
Figure 88: Effects of S_r at the end of compaction on the coefficient of saturated hydraulic conductivity k of a wide variety of soil types (Tatsuoka, 2014b).	89
Figure 89: hydraulic conductivity; coefficient of consolidation and non- dimensional velocity V plotted against the vertical effective stress.	90

Figure 90: hydraulic conductivity; coefficient of consolidation and non- dimensional velocity V plotted against the vertical effective stress.....	91
Figure 91: hydraulic conductivity; coefficient of consolidation and non- dimensional velocity V plotted against the vertical effective stress.....	92
Figure 92: hydraulic conductivity; coefficient of consolidation and non- dimensional velocity V plotted against the vertical effective stress.....	93
Figure 93: hydraulic conductivity; coefficient of consolidation and non- dimensional velocity V plotted against the vertical effective stress.....	94
Figure 94: Measured k values vs. dry density. Solid lines refer to Tatsuoka's model (slope a=-5.02)....	96
Figure 95: Measured k values vs. void ratio at the beginning of the permeability test.	96
Figure 96: Measured k values versus vertical effective stress during the incremental loading oedometer test.	97
Figure 97: Oedometer tests results, direct measurements of hydraulic conductivity and estimation of the coefficient of consolidation for different stress levels for the specimen reproducing the material inside the S2 side of the chamber.	97
Figure 98: Comparison of direct measurements of hydraulic conductivity with Taylor's estimations. Evaluation of the non-dimensional velocity for the range of penetration rates 0.006-4.5 cm/s available for the chamber tests (S2 side).....	98
Figure 99: Oedometer tests results, direct measurements of hydraulic conductivity and estimation of the coefficient of consolidation for different stress levels for the specimen reproducing the material inside the S1 side of the chamber.	98
Figure 100: Comparison of direct measurements of hydraulic conductivity with Taylor's estimations. Evaluation of the non-dimensional velocity for the range of penetration rates 0.006-4.5 cm/s available for the chamber tests (S1 side).....	99
Figure 101: Triaxial tests results (TXCIU) for the S2 side. Consolidation stresses are: 20 kPa, 60 kPa and 100 kPa.	100
Figure 102: Triaxial tests results (TXCIU) for the S1 side. Consolidation stresses are: 20 kPa,50 kPa and 100 kPa.	100
Figure 103: Construction sequence.	101
Figure 104: Details of the top layer of the chamber.	102
Figure 105: Water table at the end of the saturation process.....	102
Figure 106: Overlay diagrams of S1 test results. Color legend: dark blue=0.006 cm/s; light blue=0.016 cm/s; dark green=0.1 cm/s; light green=0.2 cm/s; orange=2 cm/s and red=4.5 cm/s (CPeT-IT GeoLogismiki 2007).	105
Figure 107: Overlay diagrams of S2 test results. Color legend: dark blue=0.006 cm/s; light blue=0.016 cm/s; dark green=0.1 cm/s; orange=2 cm/s and red=4.5 cm/s (CPeT-IT GeoLogismiki 2007).....	106
Figure 108: Tip resistance versus penetration rate, S1 series tests. Average results for layers at 50-60 cm depth and 60-70 cm depth.	108
Figure 109: Measured pore water pressure vs penetration rate, S 1 series tests. Average results for layers at 50-60 cm depth and 60-70 cm depth.	108

Figure 110: normalised tip resistance with respect to the vertical effective stress, versus penetration rate. Average results for layers at 50-60 cm depth and 60-70 cm depth.	108
Figure 111: Average sleeve friction vs penetration rate, S1 series tests. Average results for layers at 50-60 cm depth and 60-70 cm depth.	109
Figure 112: Tip resistance versus penetration rate, S2 series tests. Average results for layers at 50-60 cm depth and 60-70 cm depth.	110
Figure 113: $qt/\sigma'v$ vs penetration rate, S2 series tests. Average results for layers at 50-60 cm depth and 60-70 cm depth.	110
Figure 114: Measured pore water pressure vs penetration rate, S2 series tests. Average results for layers at 50-60 cm depth and 60-70 cm depth.	110
Figure 115: Sleeve friction versus penetration rate, S2 series test. Average results for layers at 50-60 cm depth and 60-70 cm depth.	111
Figure 116: Dissipation tests n. 1 and n. 2 carried out during S1 test series, depth 71 cm and 78 cm respectively.	113
Figure 117: normalised excess pore water pressure dissipation over time. Each curve is normalised using the respective maximum value (S1 side).....	113
Figure 118 normalised excess pore water pressure dissipation over time. Each curve is normalised using the maximum value obtained for the test n.4 (S1 side).	114
Figure 119: Dissipation tests n. 1 and n. 2 carried out during S2 test series, depth 60 cm and 93 cm respectively.	114
Figure 120: normalised excess pore water pressure dissipation over time. Each curve is normalised using the respective maximum value (S2 side).....	115
Figure 121: Comparison between vertical and horizontal coefficient of consolidation, S1 side.	116
Figure 122: Comparison between vertical and horizontal coefficient of consolidation, S2 side.	116
Figure 123: Normalised tip resistance vs non-dimensional velocity V , S1 series.....	119
Figure 124: Normalised tip resistance vs non-dimensional velocity V , S2 series.....	120
Figure 125: Normalised excess pore water pressure versus non-dimensional velocity V , S1 series. ...	120
Figure 126: Normalised excess pore water pressure versus non-dimensional velocity V , S2 series. ...	121
Figure 127: Normalised f_s values over penetration rate, S1 series.	121
Figure 128: Normalised f_s values for S1 and S2 series versus penetration rate.	122
Figure 129: Normalised data (red = S1; blue = S2) plotted on the soil classification chart proposed by Schneider et al. (2012).	123
Figure 130: Normalised data (red = S1; blue = S2) plotted on the soil classification chart proposed by Schneider et al. (2008)	123
Figure 131: Normalised side friction versus non-dimensional velocity for S1 and S2 series.	124
Figure 132: Normalised side friction vs non-dimensional velocity correlation.	125
Figure 133: Axisymmetric finite element mesh used for the analysis.	128
Figure 134: Net cone resistance versus vertical displacement (expressed as number of tip radius).	133
Figure 135: Pore water pressure distribution during the test at 0.000002 cm/s.	134

Figure 136: Tip resistance ratio for piezocone simulation in kaolin clay, Randolph & Hope (2004) centrifuge test results.	134
Figure 137: FEM analyses results compared with the expression proposed by Randolph & Hope (2004).	135
Figure 138: Undrained cone resistance from FEM analyses of the present study.	135
Figure 139: Tip resistance over vertical displacement of the cone, MCC model with Schneider et al. (2007) parameters.	137
Figure 140: Tip resistance ratio from the present study simulation and the experimental data obtained by Schneider et al. (2007)	138
Figure 141: Excess pore water pressure ratio from FEM analyses and experimental data (Schneider et al., 2007)	139
Figure 142: Normalised excess pore pressure obtained with the numerical simulation of the present study compared with experimental results (Schneider et al. 2007).	139
Figure 143: Different sizes of mesh elements, in two different positions of the penetrometer, the last one (100 analyses) and the first one.	140
Figure 144: Comparison of tip resistance curve for different values of mesh elements, dimensions of the elements closed to the tip are indicated in the diagram (Friction angle = 45°, Young modulus = 14 MPa, = 35 kPa, dilation angle = 1°).	141
Figure 145: V=0.05, fully drained conditions.	143
Figure 146: Tip resistance for V=375, undrained conditions.	144
Figure 147: MC3 (E=7000 kPa; $\psi=1^\circ$) results, tip resistance versus tip vertical displacement.	145
Figure 148: Tip resistance for different dilation angles, maximum penetration rate, non-dimensional velocity V=375.	147
Figure 149: Tip resistance for different dilation angles, minimum penetration rate, V=0.05.	147
Figure 150: Tip resistance vs penetration rate: numerical analyses and calibration chamber experimental data.	148
Figure 151: Tip resistance ratio versus dilation angles values.	148
Figure 152: Tip resistance versus tip displacement, MC7 Mohr-Coulomb model.	150
Figure 153: Tip resistance versus tip displacement, MC1 Mohr-Coulomb model.	150
Figure 154: tip resistance ratio versus penetration rate, results are compared with calibration chamber data.	151
Figure 155: TXCIU test - pore water pressure (S1 side of the calibration chamber).	152
Figure 156: comparison between TXCIU test simulation for MC7 soil parameters and laboratory TXCIU test conducted on a specimen reproducing S1 conditions. TXCIU test simulations for different values of dilation angle, without varying the other MC7 parameters, are also displayed. Consolidation stress is 20 kPa for both numerical simulation and laboratory test.	153
Figure 157: Broni area – Geological map, test and well (P1 to P7) locations.	157
Figure 158: Water table depth during the observation period, residential area of Broni.	158
Figure 159: Rainfall levels at Cigognola station (Pavia).	159
Figure 160: grain size distributions for upper-soil in Broni.	159

Figure 161: Casagrande classification chart (USCS, ASTM 2487).	160
Figure 162: CPTu1 test conducted during the humid season.	162
Figure 163: CPTu2 test conducted during the dry season.	162
Figure 164: CPTu1 and CPTu2, highlighted is the layer in which we can observe differences in tip resistance.	163
Figure 165: I_c values for CPTu1 test (humid season) and CPTu2 test (dry season).	163
Figure 166: Variation of I_c values for CPTu1 test (humid season).	166
Figure 167: Variation of I_c values for CPTu2 test (dry season).	167
Figure 168: SBTn classes before and after correction for CPTu1 (humid season) and CPTu2 (dry season).	168
Figure 169: I_c values from boreholes and CPTu test for soil layers below the water table (Serchio river).	173
Figure 170: dependency with q_t of both I_c values inferred from CPTu tests and boreholes.	173
Figure 171: The difference between the two I_c series (ΔI_c) vs. the total tip resistance.	174
Figure 172: Results obtained after the application of the $\Delta I_c q_t$ function.	174
Figure 173: Effective stress and overconsolidation ratio profiles of the soils underlying the Pisa Tower (Lo Presti et al., 2003).	178
Figure 174: OCR evaluation with Mayne (2007) and Chen & Mayne (1996) correlations.	179
Figure 175: OCR evaluation with Mayne (1995) and Mayne (2005) correlations.	180
Figure 176: Assessment of in situ vertical effective stress from CPTu1 and CPTu2 tests conducted in Broni.	182
Figure 177: CPTu measurements and I_c index (Porcari, Lucca).	182
Figure 178: Incremental Loading Oedometer test (Porcari, Lucca).	183
Figure 179: USCS Classification chart, for block samples (C1, C2) and Osterberg samples (O1, O2, O3).	188
Figure 180: Incremental Loading Oedometer test results for sample C1.	189
Figure 181: Incremental Loading Oedometer test results for sample C2.	189
Figure 182: Incremental Loading Oedometer test results for sample O1.	190
Figure 183: Incremental Loading Oedometer test results for sample O2.	190
Figure 184: Incremental Loading Oedometer test results for sample O3.	191
Figure 185: Triaxial test results (TXCIU) for C1 sample. Consolidation stresses are: 50 kPa, 100 kPa and 200 kPa.	191
Figure 186: Triaxial test results (TXCIU) for O2 sample. Consolidation stresses are: 50 kPa, 100 kPa and 200 kPa.	192
Figure 187: Triaxial test results (TXCIU) for O3 sample. Consolidation stresses are: 50 kPa, 100 kPa and 200 kPa.	192

14. List of tables

Table 1: USCS Classification for the block samples (C1 and C2) and the Osterberg samples (O1, O2, O3).	29
Table 2: MIT Classification for the block samples (C1 and C2) and the Osterberg samples (O1, O2, O3).	30
Table 3: Parameters inferred from Oedometer tests (Incremental Loading Oedometer test).	30
Table 4: Strength parameters inferred from triaxial tests, TxCIU tests.	30
Table 5: Soil Behaviour Type classes proposed by Robertson et al. 1986.	34
Table 6: Robertson (1986) SBT classes and respective Robertson (1990) SBTn classes, as proposed by Robertson (2010).	34
Table 7: Definition of soil classification (Robertson, 1990) from the Soil Classification Index (Robertson and Wride,1998).	67
Table 8: Piezocone measurements details.	75
Table 9: Direct measurements of hydraulic conductivity.	83
Table 10: Piezocone test characteristics.	103
Table 11: Dissipation test results.	112
Table 12: Material parameters for MCC Model.	130
Table 13: Material parameters for MCC Model.	136
Table 14: Evaluation of the coefficient of consolidation and the non-dimensional velocity.	142
Table 15: Soil characteristics and model parameters.	142
Table 16: Undrained tip resistance, drained tip resistance and resistance ratio for different dilation angles and elastic stiffness values.	145
Table 17: Parameters for the additional soil models MC5, MC6 and MC7.	146
Table 18: Undrained tip resistance, drained tip resistance and resistance ratio for different dilation angles.	148
Table 19: Soil constitutive model parameters from TXCIU calibration, MC7 model.	149
Table 20: Piezometric data obtained for all the piezometers in Broni area.	157
Table 21: Water Table Depth from July 2002 to July 2003, residential area of Broni (NA = Not Available, Dry Well).	158
Table 22: Soil classification (Broni – first three meters) W_l and W_p = Liquid and plastic limit respectively; w = natural water content; S = Saturation degree; e_o = Void ratio; h_{co} = Capillary rise from lab tests; σ_g = Swelling pressure from lab tests. (Meisina 1996)	160
Table 23: Definition of soil classification (Robertson, 1990) from the Soil Classification Index (Robertson and Wride,1998).	164
Table 24: Port of Livorno data – I_c and classification from both CPTu and borehole – data interpretation.	170
Table 25: Serchio River data – I_c and classification from both CPTu and borehole – data interpretation.	171

15. References

- AGI (1997), “Raccomandazioni sulle Prove Geotecniche di Laboratorio”
<http://www.associazionegeotecnica.it/pubblicazioni/raccomandazioni>
- ASTM D5778-12 (2012) “Standard Test Method for Electronic Friction Cone and Piezocone Penetration Testing of Soils” ASTM International, West Conshohocken, PA
<http://dx.doi.org/10.1520/D5778-12>.
- ASTM D5778-95 (2000) “Standard Test Method for Performing Electronic Friction Cone and Piezocone Penetration Testing of Soils” ASTM International, West Conshohocken, PA
<http://dx.doi.org/10.1520/D5778-95R00>
- Aubertin M., Mbonimpa M., Bussière B., and Chapuis R.P. (2003) “A physically-based model to predict the water retention curve from basic geotechnical properties”. *Canadian Geotechnical Journal*
- Aubertin M., Ricard J.F., Charpuis R.P. (1998), “A predictive model for the water retention curve: application to tailings from hard-rock mines. *Canadian Geotechnical Journal*, 35, pp. 55-69 (with Erratum, 36, 401)
- Baligh, M.M. (1985) “Strain Path Method” *Journal of Geotechnical Engineering*, 111:1108-1136
- Baligh, M.M. (1986a) “Undrained deep penetration I. Shear stresses,” *Géotechnique*, 36 n.4, 471-485
- Baligh, M.M. (1986b) “Undrained deep penetration, II: Pore pressures,” *Géotechnique*, 36(4), 487-501
- Begemann H.K.S. (1965), “The Friction Jacket Cone as an Aid in Determining the Soil Profile. *Proc. 6th ICSMFE*,1, pp. 17-20.
- Begemann, H. K. S., (1953) “Improved method of determining resistance to adhesion by sounding through a loose sleeve placed behind the cone” *Proceedings of the 3rd International Conference on Soil Mechanics and Foundation Engineering, ICSMFE, August 16 - 27, Zurich, Vol. 1, pp. 213 - 217*
- Begemann, H. K. S., (1963) “The use of the static penetrometer in Holland” *New Zealand Engineering, Vol. 18, No. 2, p. 41.*
- Begemann, H. K. S., (1965) “The friction jacket cone as an aid in determining the soil profile. *Proceedings of the 6th International Conference on Soil Mechanics and Foundation Engineering, ICSMFE, Montreal, September 8 - 15, Vol. 2, pp. 17 - 20.*
- Bellotti R., Crippa V., Pedroni S., Ghionna V.N. (1988) “Saturation of Sand Specimen for Calibration Chamber Tests”, *Proc. ISOPT-1, Orlando, 2, pp. 661-672*
- Brown L.J., Weeber J.H. (1992). “Geological Map: Geology of the Christchurch Urban Area. Scale 1:25,000.” *Institute of Geological and Nuclear Sciences*

Burns S.E., Mayne P.W. (1998) "Monotonic and dilatatory pore-pressure decay during piezocone tests in clay" *Canadian Geotechnical Journal* 35: 1063-1073

Burns S.E., Mayne P.W. (2002) "Analytical cavity expansion-critical state model for piezocone dissipation in fine-grained soils" *Soils and Foundations* 42 n. 2:131-137

Chen, B.S.-Y., P.W. Mayne (1996) "Profiling the Overconsolidation Ratio of Clays by Piezocone Tests", Report No. GIT-CEEGEO-94-1 to National Science Foundation by Geosystems Engineering Group, Georgia Institute of Technology, Atlanta, 1994, 280 pp. [Online]. Available:<http://www.ce.gatech.edu/~geosys/Faculty/Mayne/papers/index.html>.

Chen B.S.-Y. and P.W. Mayne (1996) "Statistical Relationships Between Piezocone Measurements and Stress History of Clays," *Canadian Geotechnical Journal*, Vol. 33, No. 3 pp. 488–498

Chung S.F., Randolph M.F., Schneider J.A. (2006) "Effect of Penetration Rate on Penetrometer Resistance in Clay" *J. Geotech. Geoenvironmental. Eng.* 2006.132:1188-1196

Cosranti B., Squeglia N., Lo Presti D.C.F. (2014) "Analysis of existing levee systems: the Serchio river case" *Rivista Italiana di Geotecnica*, n. 4, pp. 47-65

Craig C. (1995) "Advancing in site investigation practice" Proceedings of the international conference held in London on 31-31 March 1995

Craig W.H. (1983) "Strain rate and viscous effects in physical models" *Soil Dynamics and Earthquake Engineering* Vol.2, N. 4: 206-211

DeJong J.T., Randolph M.F. (2012) "Influence of partial consolidation during cone penetration on estimated soil behaviour type and pore pressure dissipation measurements" *Journal of Geotechnical and Geoenvironmental Engineering* 138 n. 7: 777-788

Douglas J.B., Olsen R.S. (1981) "Soil Classification Using Electric Cone Penetrometer" Symposium on Cone Penetration Testing and Experience, Geotechnical Engineering Division, ASCE, St. Louis, pp. 209-227

Elghaib. M. K. (1989) "Prediction and interpretation of piezocone data during undrained, drained and partially drained penetration" PhD Thesis, Massachusetts Institute of Technology

Elmgren K. (1995) "Slot-Type Pore Pressure CPTu Filters" Proc. Int. Symposium on Cone Penetration Testing, Swedish Geotechnical Society Report, n.3, 95, Linköping, Sweden, n.2, pp.9-12.

Eslami A., Fellenius B.H. (1997) "Pile Capacity by Direct CPT and CPTu Methods Applied to 102 Case Histories" *Can. Geotech. J.*, n.34, pp. 886-904

Fellenius H.B., Eslami A. (2000) "Soil Profile Interpreted from Cone Penetration Tests with Porewater Pressure Measurement Data" *Geotechnics, Geotech. Engng. Conf.* Bangkok: Asian Inst. of Technol. Bangkok, Thailand. vol. 1, pp. 163–171.

Facciorusso J., Madiari C., Vannucchi G. (2015) "CPT-Based Liquefaction Case History from the 2012 Emilia Earthquake in Italy" *Journal of Geotechnical and Geoenvironmental Engineering*

Finnie, I.M.S., & Randolph, M.F. (1994) "Punch-through and liquefaction induced failure of shallow foundations on calcareous sediments" *Proc. Int. Conf. on Behavior of Offshore Structures, BOSS '94, Boston: 217-230*

Geologismiki (2007) *Geotechnical Software, CPeTIT v 1.6. CPT interpretation software*, <http://www.geologismiki.gr/Products/CPeT-IT.html>

Forsyth P.J., Barrell D.J.A., Jongens R. (2008) "Geology of the Christchurch area Institute of Geological and Nuclear Sciences 1:250 000 geological map 16." *GNS Science. 1 map plus 67 p. supplement*

Hashash Y.M.A., Whittle A.J. (1993) "Integration of the Modified Cam Clay model in non-linear finite element analysis" *Computers and Geotechnics, 14, 59-83*

House A.R., Oliveira J.R.M.S., Randolph M.F. (2001) "Evaluating the coefficient of consolidation using penetration tests" *International Journal of Physical Modelling in Geotechnics n.3: 17-26*

Holtrigter M., Thorp A. & Hoskin P. W. O. (2014) "The effect of sleeve diameter on fs measurements". *3rd International Symposium on Cone Penetration Testing, Las Vegas, Nevada, USA*

Jamiolkowski M., Lo Presti D. C. F., Manassero M. (2001) "Evaluation of Relative Density and Shear Strength of Sands from CPT and DMT" *Invited Lecture Ladd Symposium, GSP n.119, ASCE, pp.201-238*

Jefferies M.G., Davies M.P. (1993) "Use of CPTu to Estimate Equivalent SPT N60" *Geotechnical Testing Journal, vol. XVI, n. 4, pp. 458-468.*

Kim K., Prezzi M., Salgado R., Lee W. (2008) "Effects of Penetration rate on cone resistance in saturated clayey soils" *Journal of Geotechnical and Geoenvironmental Engineering 134: 1142-1153*

Kim, T. J. _2005_. "Dissipation of pore water pressure due to piezocone penetration in OC clay." *Ph.D. dissertation, Korea Univ., Seoul, Korea*

Kovacs G. (1981) "Seepage Hydraulics" *Elsevier Science Publishers, Amsterdam*

Kulhawy, F.H., P.W. Mayne (1990) "Manual on Estimating Soil Properties for Foundation Design" *Report EPRI EL-6800, Electric Power Research Institute, Palo Alto, Calif., 306 pp.*

Larsson R. (1995) "Use of a Thin Slot as Filter in Piezocone Tests" *Proc. Int. Symposium on Cone Penetration Testing, Swedish Geotechnical Society Report, 3, n. 95, Linköping, Sweden, 2, pp.35-40*

Lehane B.M., O'Loughlin C.D., Gaudin C., Randolph M.F. (2009) "Rate effects on penetrometer resistance in kaolin" *Geotechnique 59 No. 1: 41-52*

Levadoux J.N., Baligh M.M. (1980) "Pore pressure during cone penetration in clays" MIT Res. Rep. No. R80-15, Cambridge, Massachusetts

Lo Presti D., Jamiolkowski M., Pepe M. (2002) Geotechnical characterization of the subsoil of Pisa Tower" Invited Lecture International Workshop on Characterization and Engineering Properties of Natural Characterization and engineering properties of natural soils", (National University of Singapore, Dec. 2002), Balkema, vol. II, pp. 909-946

Lo Presti D., Meisina C., Squeglia N. (2009) "Applicabilità di prove penetrometriche statiche nella ricostruzione del profilo stratigrafico" Rivista Italiana di Geotecnica, n. 2, pp.9-33

Lo Presti D. Squeglia N., Meisina C., Visconti L. (2010) "Use of CPT and CPTu for soil profiling of "intermediate" soils: a new approach"; CPT10 Huntington CA, USA

Long, H., Flemings, P.B., Germaine, J.T. (2007) "Interpreting in situ pressure and hydraulic properties with borehole DVTTP and piezoprobe deployments at southern Hydrate Ridge, Offshore Oregon," JGR Solid Earth, 112(B4), B0-04101

Lunne T. (2001) "In-Situ Testing in Offshore Geotechnical Investigations" Proc., Internat. Conf. on In-Situ Meas. of Soil Properties a Case Histories, Bali, 2001, 61-81

Lunne, T. (2010) "The CPT in offshore soil investigation – a historic perspective" Proc. CPT'10, Los Angeles, May 2010, pp.71-113

Lunne, T. and Anderson, K.H. (2007) "Soft clay shear strength parameters for deepwater geotechnical design" Proc. 6th Int. Conf. Society for Underwater Technology, Offshore Site Investigation and Geotechnics, London, pp.151-176

Lunne, T., Eidsmoen, T. E., Powell, J. J. M., and Quarterman, R. S. T. (1986) "Piezocone testing in overconsolidated clays." Proc., 39th Canadian Geotechnical Conf., CGS, Ontario, Canada, 209–218

Lunne, T., Robertson, P.K. and Powell, J.J.M. (1997) "Cone penetration testing in geotechnical practice" Blackie Academic, EF Spon/Routledge Publ., New York, 1997, 312

Mahmoodzadeh H., Randolph M.F. (2014) "Penetrometer testing: effects of partial consolidation on subsequent dissipation response" Journal of Geoenvironmental Engineering 140 n.6: -1--1

Mahmoodzadeh H., Randolph M.F., Wang D. (2014) "Numerical simulation of piezocone dissipation test in clay" Geotechnique 64 n.8: 657-666

Mahutka, K. P., Konig, F. & Grabe, J. (2006) "Numerical modelling of pile jacking, driving and vibratory driving", Numerical modelling of construction processes in geotechnical engineering for urban environment (ed. Th. Triantafylidis), pp. 235–246.London, UK: Taylor & Francis

Mayne, P.W. (1986): "CPT indexing of in-situ OCR in clays," Use of In Situ Tests in Geotechnical Engineering (GSP6),ASCE, Reston, Virginia, pp. 780-793

Mayne, P.W. (2005) "Integrated Ground Behavior: In-Situ and Lab Tests," Deformation Characteristics of Geomaterials, Vol. 2 (Proc. Lyon, France), Taylor & Francis, London, United Kingdom, pp. 155–177

Mayne, P.W. (1994) "CPT-Based Prediction of Footing Response" Measured and Predicted Behavior of Five Spread Footings on Sand (GSP 41), American Society of Civil Engineers, Reston, Va., pp. 214–218

Mayne, P.W. (2001) "Stress-Strain-Strength-Flow Parameters from Enhanced In-Situ Tests," Proceedings, International Conference on In-Situ Measurement of Soil Properties and Case Histories, Bali, Indonesia, pp. 27–48

Mayne P.W. (2010) "Regional Report for North America" CPT'10 2nd International Symposium on Cone Penetration Testing, Huntington Beach, CA, USA, May 2010

Mayne, P.W. and Bachus, R.C. (1988) "Profiling OCR in clays by piezocone" Penetration Testing 1988, Balkema, Rotterdam, pp. 857-864

Mayne P.W., D.A. Brown (2003) "Site Characterization of Piedmont Residuum of North America," Characterization and Engineering Properties of Natural Soils, Vol. 2, Swets and Zeitlinger, Lisse, The Netherlands, pp.1323–1339

Mayne P.W., Campanella, R.G. (2005) "Versatile Site Characterization by Seismic Piezocone," Proceedings, 16th International Conference on Soil Mechanics and Geotechnical Engineering, Vol. 2 (Osaka), Millpress, Rotterdam, The Netherlands, pp. 721–724

Mayne P.W., Kulhawy F.H. (1982) "K₀-OCR Relationships in soil" Journal of Geotechnical Engineering, Vol. 108 (GT6), 851-872

Mayne P.W., Kulhawy F.H., Kay J.N. (1990) "Observations on the Development of Porewater Pressures During Piezocone Testing in Clays," Canadian Geotechnical Journal, Vol. 27, No. 4, pp. 418–428.

Mayne, P.W., J.K. Mitchell, J.A. Auxt, and R. Yilmaz (1995) "U.S. National Report on CPT," Proceedings, International Symposium on Cone Penetration Testing, Vol. 1, Swedish Geotechnical Society Report 3:95, Linköping, Sweden, Oct. 4–5, pp. 263–276

Mayne, P.W. and G.J. Rix (1995) "Correlations Between Shear Wave Velocity and Cone Tip Resistance in Clays," Soils & Foundations, Vol. 35, No. 2, pp. 107–110

Mayne, P.W., P.K. Robertson, and T. Lunne (1998) "Clay Stress History Evaluated from Seismic Piezocone Tests," Geotechnical Site Characterization, Vol. 2, Balkema, Rotterdam, The Netherlands, pp. 1113–1118

Mayne, P.W, Stewart, H.E. "Pore Pressure Response of K₀ Consolidated Clays," Journal of Geotechnical Engineering, Vol. 114, No. 11, 1988, pp. 1340–1346

Mc Neilan, T. W., and Bugno, W.T. (1985), "Cone Penetration Test Results in Offshore California Silts, Strength Testing of Marine Sediments: Laboratory and In-Situ Measurements", ASTM, San Diego, CA, USA, 55-71

Mbonimpa M., Aubertain M., Chapuis R.P., Bussièrè B. (2000) “Développement de fonctions hydriques utilisant les propriétés géotechniques de base” Proc. 1st Joint IAH-CNC and CGS Groundwater Specialty Conference, 53rd Canadian Geotechnical Conference, Montreal, Quebec, Canada, pp. 343-350

Mbonimpa M., Aubertain M., Chapuis R.P., Bussièrè B. (2002) “Practical pedotransfer functions for estimating the saturated hydraulic conductivity” *Geotechnical and Geological Engineering*

Meisina C. (1996) “Criteri e metodi per la valutazione della capacità di rigonfiamento di alcuni terreni e suoli affioranti nel territorio pavese”. Doctorate thesis, VIII° cycle, University of Pavia

Meyerhof, G. G. (1956) “Penetration tests and bearing capacity of cohesionless soils.” *J. Soil Mech. and Found. Div.*, 82 n.1: 1–19

Orazalin Z. “Analysis of Large Deformation Offshore Geotechnical Problems in Soft Clay” (2017) PhD Thesis, Massachusetts Institute of Technology

Pestana, J.M., Whittle A.J. (1999), “Formulation of a unified constitutive model for clays and sands”, *International Journal for Numerical and Analytical Methods in Geomechanics*, 23, 1215-1243.

Pestana, J.M., Whittle, A.J. & Salvati, L. (2002a), “Evaluation of a constitutive model for clays and sands: Part I – Sand behaviour”, *International Journal for Numerical and Analytical Methods in Geomechanics*, 26, 1097-1121

Pestana, J.M., Whittle, A.J. & Gens, A. (2002b) “Evaluation of a constitutive model for clays and sands: Part II – Clay behaviour,” *International Journal for Numerical and Analytical Methods in Geomechanics*, 26, 1123-1146

Ramsey N. (2010) “Some issues related to applications of the CPT” Proc. of CPT’10, Huntington Beach, CA, USA. Paper No. KN-3.

Randolph, M. F. & Hope, S. (2004) “Effect of cone velocity on cone resistance and excess pore pressures”, *Proceedings of the international symposium on engineering practice and performance of soft deposits*, Osaka, pp. 147–152

Robertson, P.K. (1990) “Soil classification using the cone penetration test”; *Canadian Geotechnical Journal*, 27(1): 151–158

Robertson P.K. (2009) “Interpretation of cone penetration tests – a unified approach” *Canadian Geotechnical Journal*, 46: 1337-1335

Robertson P.K. (2010) “Estimating in-situ soil permeability from CPT & CPTu”; *Proceedings CPT’10 Huntington CA, USA*

Robertson P.K. (2016) “Cone penetration test (CPT)-based soil behaviour type (SBT) classification system — an update” *Canadian Geotechnical Journal*, 53: 1910-1927

Robertson, P.K., R.G. Campanella, D. Gillespie, and J. Greig, (1986) "Use of Piezometer Cone Data," Use of In-Situ Tests in Geotechnical Engineering (GSP 6), American Society of Civil Engineers, Reston, Va., pp. 1263–1280

Robertson P.K., Wride C.E. (1998), "Evaluating cyclic liquefaction potential using the cone penetration test" Canadian Geotechnical Journal 35, N. 3: 442-459

Roscoe K.H., Schofield A.N., Wroth C.P. (1958) "On the yielding of soils" Geotechnique 8 n.1: 22-53

Schmertmann J.H. (1976) "An Updated Correlation between Relative Density DR and Fugro-Type Electric Cone Bearing" qc. Contract Report DACW 39-76 M 6646 WES, Vicksburg, Miss., 1976

Schmertmann J.H. (1978) "Guidelines for cone penetration test performance and design" US Dept. of Transportation, FHWA, R.78-209. Washington D.C.

Schneider J.A., Lehane B.M., Schnaid F. (2007) "Velocity effects on piezocone measurements in normally and overconsolidated calys" International Journal of Physical Modelling in Geotechnics N.2: 23-34

Schneider J.A., Randolph M.F., Mayne P.W. and Ramsey N. R. (2008) "Analysis of Factors Influencing Soil Classification Using Normalized Piezocone Tip Resistance and Pore Pressure Parameters", Journal of Geotechnical and Geoenvironmental Engineering 134:1569-1586

Schneider J. A., Hotstream J. N., Mayne P. W., and Randolph M. F.; (2012) "Comparing CPTU $Q-F$ and $Q-\Delta u_2/\sigma_{v0}$ ' soil classification charts" Géotechnique Letters E-ISSN 2045-2543 Volume 2 Issue 4, October 2012, pp. 209-215

Schofield A.N., Wroth C.P. (1968) "Critical state soil mechanics" McGraw-Hill

Searle J.W. (1979) "The Interpretation of Begemann Friction Jacket Cone Results to Give Soil Types and Design Parameters. Design Parameters in Geotechnical Engineering, BCS London. 2, pp. 265-270

Senneset, K., R. Sandven, and N. Janbu (1989) "Evaluation of Soil Parameters from Piezocone Tests," Transportation Research Record 1235, Transportation Research Board, National Research Council, Washington, D.C, 1989, pp. 24–37

Silva M.F., White D.J., Bolton M.D. "An analytical study of the effect of penetration rate on piezocone tests in clay" Int. J. Numer. Anal. Meth. Geomech. 2006; 30:501–527

Smith T. (2014) "Median water table elevation in Christchurch and surrounding area after the 4 September 2010 Darfield Earthquake" GNS Science Report 2014/18

Suggate RP (1958) "Late Quaternary deposits of the Christchurch metropolitan area". New Zealand Journal of Geology and Geophysics 1: 103–122

Sully J.P., Campanella R.G., Robertson P.K., (1988) "Interpretation of penetration pore pressure to evaluate stress history in clays", Department of Civil Engineering, University of British Columbia, Vancouver, B.C., Canada

Sully J.P., Campanella R.G., Robertson P.K. (1990) "Overconsolidation ratio of clays from penetration pore pressures", Soil Mechanics series N. 138, Department of Civil Engineering, University of British Columbia, Vancouver, B.C., Canada

Sully J.P., P.K. Robertson, R.G. Campanella, D.J. Woeller, (1999) "An approach to evaluation of field CPTU dissipation data in overconsolidated fine-grained soils", Canadian Geotechnical Journal 36: 369-381,

Tatsuoka F. (2015) "Compaction characteristics and physical properties of compacted soil controlled by degree of saturation"

Teh, C-I & Houlsby, G.T. (1991) "An analytical study of the cone penetration test in clay," Géotechnique, 41 n.1: 17-34

Tiggemann, L. and Beukema, H.J. (2008) "Sounding ring investigation" Proc. ISC-3, Taiwan, pp. 757-762

Tonni L., Gottardi G., Berengo V. & Simonini P. (2010) "Classification, overconsolidation and stiffness of Venice lagoon soils from CPTU", CPT10 Huntington CA, USA

van den Berg, P., de Borst, R. & Huétink, H. (1996) "An Eulerian finite element model for penetration in layered soil," Intl. J. for Num. & Anal. Meth. in Geomechs., 20, 865-886

United Nations Conference on Environment & Development (1992) "AGENDA 21" Rio de Janeiro, Brazil, 3 to 14 June 1992

Vesic A.S. "Expansion of cavities in infinite soil mass" Journal of the Soil Mechanics and Foundation Division 98 n.SM3: 265-290

Weeber J.H. (2008) "Christchurch groundwater protection: A hydrogeological basis for zone boundaries, Variation 6 to the Proposed Natural Resources Regional Plan" Environment Canterbury. Report No.U08/21. ISBN 978-1-86937-802-8, 60 p.

Whittle, A.J., Sutabutr, T., Germaine, J.T. & Varney, A. (2001) "Prediction and interpretation of pore pressure dissipation for a tapered piezoprobe," Géotechnique, 51 n.7: 601-617

Wroth, C.P. (1984) "The interpretation of in situ soil tests," Géotechnique, 34, N.4, 449-489

Wroth, C.P., Houlsby G.T. (1985) "Soil mechanics- property characterization and analysis procedures" Proceedings 11th International Conference on soil Mechanics and Foundation engineering San Francisco Vol.1: 1-54

Yi J.T., Goh S.H., Lee F.H., Randolph M.F. (2012) "A numerical study of cone penetration in fine-grained soils allowing for consolidation effects" Geotechnique 62 n. 8: 707-719

Zeeb P., Hemond H., and Germaine, J. (1997) "Design and Performance of a Portable Piezocone Driver for High Resolution Profiling of Wetland Sediments" Geotechnical Testing Journal, Vol. 20, No. 2, pp. 191-198, <https://doi.org/10.1520/GTJ10738J>. ISSN 0149-6115